NASA
Reference
Publication
1090

May 1983

Rate Processes in Gas Phase

C. Frederick Hansen

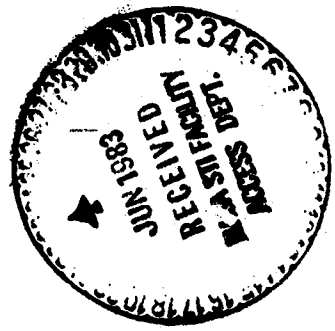

NASA

25th Anniversary
1958-1983

NASA
Reference
Publication
1090

1983

Rate Processes in Gas Phase

C. Frederick Hansen
Ames Research Center
Moffett Field, California

National Aeronautics
and Space Administration.

Scientific and Technical
Information Branch

TABLE OF CONTENTS

PREFACE

Reaction processes are of many kinds and countless approaches have been used to model them. Consequently, the scientific literature on the subject has been almost embarrassingly superfluous. Yet one comes away from the study of this subject with the uneasy feeling that reaction processes aren't really well understood at all. Prof. James Keck of MIT once made the remark to me that, with a couple of disposable parameters that usually occur in the theoretical models, one can fit experimental data equally well to almost any of the models. This is particularly true because most of our experimental data on any one reaction is obtained over a relatively narrow range of absolute temperature while the differences in the theories become apparent only over a broader range of temperature. Thus, a semiempirical fit of data to a theoretical model is a necessary condition, but by no means a sufficient condition to establish some reality in the model.

Many of our current reaction-rate theories are not very helpful in an engineering sense because they are only qualitative and cannot be quantified. Even the so-called "absolute reaction rate theory" includes an undetermined transmission coefficient that gives the probability the system will pass through a saddle point in the potential surface which controls the dynamics of the system, and generally this coefficient is uncertain by many orders of magnitude. Recent work with large, high-speed computers can now quantify some of these coefficients using statistical Monte Carlo techniques, but the computations are long and laborious brute-force approaches that lead to numbers and lack the elegance of analytic methods; nevertheless the numbers we obtain from this approach will certainly be useful. The problem here is that the potential surfaces are not generally known with good precision — though these surfaces will also eventually be calculated with numerical quantum chemistry methods, using our large computers.

Even then, precise knowledge of potential surfaces and the shape of their saddle points will not completely solve the problem. The dynamics of a system are only determined by a single potential surface when the particles involved react as a purely classical system; in many cases quantum effects are important and the transitions between potential surfaces tremendously complicate the computations. When the dynamics of very light weight electrons are involved in a collision process, such as in charge transfer reactions, for example, the model must be a quantum mechanical one to duplicate the full structure of the reaction cross sections — though sometimes a classical approach can be devised that will cut through the mean value of the quantum results. Nevertheless, all classical models of electron collision processes must be regarded as semiempirical at best. Similarly, the reactions of molecular particles with photons are treated as quantum mechanical perturbation problems.

Reactions involving very large molecular systems, as in organic chemical structures or polymers, tend to be in a class by themselves. Generally, the initiation collision process, whether it be a particle or a photon, merely tends to excite some mode of internal energy in the molecule, and after a long, involved process of redistribution of energy among some coupled internal modes, the energy in some critical reaction coordinate takes on a statistical probability of exceeding a threshhold value, and the reaction proceeds long after the causative event. These reactions often appear unimolecular to an experimentalist, that is, they do not depend on the concentration of collision partners as in the usual two- or three-body collision event, and the excited states produced by the collisions can be treated as steady-state species in thermodynamic equilibrium with the lower energy states. Such redistributions of energy in complex structures are very involved, the potential

energy surfaces are multidimensional, and even our best computers are helpless to do the type of numerical statistical computations that could lead to quantitative results.

The wide variety of reaction processes alluded to above cannot be adequately treated in a single small book, even if the author had the breadth of experience and insight to do that job. I will limit this book to the types of reactions of engineering importance that I have encountered in NASA's program of space vehicle development. These have generally been collision-induced rate-processes between low molecular weight particles that occur in hot gases about vehicles entering the earth's and planetary atmospheres and in flow about hypersonic aircraft, also some electron and photon collision processes that occur in flow near intense shock waves and in gasdynamic and electric discharge gas lasers. The reactions are primarily rotational excitation, vibrational excitation, dissociation, atom shuffling, electronic excitation, ionization, and photon absorption. In a few cases, electron-charge transfer processes are important; however, they require a specialized quantum discipline and this will be treated only in a cursory manner here.

Even within the limits set above, the myriad of theoretical models cannot all be adequately treated, and frankly, I have chosen to discuss those models which seem, in my opinion, to be the most useful — either in the sense that they yield quantitative results that can be applied to NASA's engineering needs, or that they provide a good insight into the processes going on in our high temperature gases. Some very simple models are treated here along with some more advanced concepts. The oversimplified theoretical models seem to be the most useful ones, as a matter of fact; most often in engineering applications we use a simple Arrhenius formulation to fit and extrapolate our experimental results. However, some of the more advanced theories do add considerably to the understanding of rate processes, even when they can only be qualitative. Also, they are part of the general background that any scientist or engineer will need to read and absorb research literature on the subject.

Finally, the book makes no attempt to catalog the many calculation results that abound in the literature — particularly in the last few years as a result of the availability of large, fast, digital computers. Rather it concentrates on the fundamental concepts that are needed to understand the meaning and the limitations of the computer numbers. These fundamentals have been well understood for a number of years and there seems to be very little new material of this fundamental type to appear in recent literature; thus, the references will often seem a bit old, though they are in fact valid and up-to-date. The fundamentals have merely been lying dormant until the availability of computers could make use of them to give some useful numerical results. The bulk of the current literature on reaction processes is of the computation type, along with some occasional new experimental data.

The material for this book was first organized for class lectures presented to graduate students in mechanical engineering and in aeronautical engineering at the Massachusetts Institute of Technology (1965-66) as a course entitled, "Atomic and Molecular Kinetic Processes." The material has subsequently been expanded and update for a graduate course in the Aeronautics and Astronautics Department of Stanford University (1975, 1978, and 1981) and also for training seminars attended by research engineers of the Fluid Mechanics Branch, the Magnetoplasmadynamics Branch, and the Physical Gasdynamics and Lasers Branch of the Ames Research Center of NASA. The emphasis in my choice of a small slice of the research material from the vast literature on rate processes has largely been determined in accord with the research needs and goals of these three branches of NASA.

The references cited merely represent a few that have become classic or that I have felt helpful; they fall far short of a full bibliography. However, the basic theoretical foundations of the subject have been relatively stable for a decade or so; consequently, the brevity of the bibliography will hopefully not seriously detract from the purpose of the book. This purpose is basically to help research engineers easily digest and understand the literature on rate processes, so they can efficiently apply this work to their engineering problems, and can then devote their research time to other aspects of these problems as required. Reaction rates are, after all, only a minor part of the problems engineers face in dealing with hot gases and plasmas. Engineers must also give their attention to heat transfer, to aerodynamic design, to boundary layer effects in laminar and turbulent flows, and to many other factors which may or may not be coupled to the rate processes. Thus, the engineer approaches the subject of reaction rates with a willingness to approximate and a need to consider the entire system, which are usually not appropriate for the physicist or the physical chemist devoted to the search for knowledge on reaction processes as an end to itself.

The present text will take a somewhat different approach to reaction kinetics than found in most other texts. The emphasis will be on the formulation of rate processes in terms of inelastic collision cross sections, and the manner in which cross sections of realistic functional shape lead to modified Arrhenius-type available-energy formulas for the rate coefficients. The effects of ladder climbing a series of excited states leading to final reaction will be treated, which will lead to the master equations for chemically reacting gas species. Semiempirical and simple approximate methods will be discussed along with some more advanced mathematical theory, since the practical quantitative needs of the engineer are kept in mind along with the need for basic understanding of the phenomena and the need for comprehension of the literature on the subject. Collision induced vibrational excitation will be treated in depth because this represents the single example of a reasonably well analyzed heavy particle collision reaction that exists at the present time. The more difficult problem of collision-induced rotational excitation is analyzed by approximations that are not very good quantitatively but do provide a useful qualitative insight to this process. Finally, the elementary quantum theory of transitions at potential surface crossings and quantum scattering theory are briefly summarized.

I am particularly indebted to James R. Stallcop and Richard L. Jaffe, of Ames Research Center of NASA, for help with subject matter in chapters VII, VIII, and IX. In addition, students at the Aeronautics and Astronautics Department of Stanford University and at the Department of Aeronautical Engineering of Nagoya University, Japan, helped uncover a myriad of small errors.

CHAPTER I - CRITICAL REVIEW OF REACTION-RATE THEORY AND EXPERIMENT FROM THE VIEWPOINT OF ENGINEERING NEEDS

1.1 SUMMARY

Reaction rate kinetics is an old science, but is nevertheless judged to be very undeveloped in terms of engineering needs. For example, the theory is not yet developed well enough to calculate rates a priori, and is not even very reliable for extrapolating experimental results. Bulk rate experiments are fraught with ambiguity and uncertainties are the order of factors of 3, often more. Molecular beam methods cannot normally measure cross sections for particles of practical interest in the energy range needed. Nevertheless, we are now on the threshold of an era when large, high-speed computers will permit reaction rates to be calculated with accuracy better than experiment and consistent with the accuracy of that of many other physical-chemical properties of matter.

1.2 REVIEW OF REACTION RATE KINETICS

Chemical reaction theory and experiment have received more attention and research study than almost any comparable area of physics and chemistry. The subject has roots reaching back to 1889 when S. Arrhenius (ref. 1) proposed to account for the temperature dependence of the rate of inversion of sucrose by postulating an equilibrium situation between active and inert reactant molecules; this led to the well known Arrhenius equation for a chemical rate coefficient, α

$$\alpha = Ae^{-E^*/kT} \tag{1.1}$$

where E^* is an activation energy representing an amount of internal or kinetic energy required to transform an inert reactant molecule to a chemically active one, and the coefficient A is a constant or a relatively weakly dependent function of temperature. The Arrhenius equation is found to represent the temperature dependence of the specific rate coefficients of most chemical reactions reasonably well. The job of the theorist has been to derive expressions for A and E^*, while the experimentalist determines these quantities by fitting Eq. (1.1) to his observed results. This is the form in which most engineers make use of reaction rate relations — only one of the inputs necessary to solve the varied problems of interest to him, which often involve mixtures of many chemical species in solid, liquid, and gas phases with dynamic motions, heat transfer, mass transfer, viscous dissipation, radiation transfer, etc., all coupled to the reaction rate aspect of the problem.

As a general rule, reaction rate results at normal temperatures (the order of 100 to 1000 K) have been provided by the physical chemistry segment of the scientific community. With the advent of space travel and instrument vehicle probing of the planetary atmospheres, a number of high temperature reactions (at temperatures on the order of 10,000 K) became important in the analysis of gas-dynamic flow over aerodynamic shapes entering the Earth's or planetary atmospheres at very high speeds, of 7 to 20 km/sec. At these speeds the molecular gases vibrate strongly, dissociate, ionize, and eventually recombine in different species with other constituents of the atmosphere, with products of ablation from the vehicle surface, and with products of

the rocket exhaust, if any. These reactions affect the heat transfer to the vehicle structures, the transmission of information through the highly ionized plasma about the vehicle, and the radar and optical signatures provided in the wake flow, for example, all problems of concern to the engineer. As a consequence, aeronautical engineers played an active role in high temperature reaction rate research. In fact much of the presently available high-temperature dissociation rate and ionization rate data, as well as some important shuffle reaction rate data, have been provided by aeronautical engineers using shock tubes (ref. 2). At present, aeronautical engineers are among the most active research scientists in assessing the effects of rocket and aircraft effluents on the upper atmosphere, and they are becoming involved in perfecting the computer modeling of Earth's atmosphere with coupled dynamic flow and photochemical rate processes. For all of these reasons and more, the engineer is now both an active user and supplier of chemical rate data and reaction rate theoretical development.

One might presuppose that reaction rate chemistry is a well matured science by now. Research papers on the subject are legion — they fill much of the space in hundreds of journals published since Arrhenius' time, and literally thousands of chemical rates have been measured. Yet today there is no reliable method of calculating reaction rate coefficients, measurements are usually limited to a narrow region of temperature and pressure where the reaction can be observed in the laboratory, the theory is not yet developed well enough to extrapolate these measurements with any degree of certainty, and in most cases the very interpretation of the experimental measurements is subject to much ambiguity. For example, the experimenter usually observes a complex mixture of competing reactions and by making certain assumptions that some reactions are fast and others are slow, he eventually deduces the Arrhenius coefficients which best fit the assumed model to his data. In this way, many of the reactions of interest to the engineer have been determined within a factor of about two or three, sufficient for many purposes, but hardly matching the precision of other physical chemical data. Extrapolation of the data beyond the range of experiment with the simple Arrhenius equation introduces additional uncertainty; even the most complex and sophisticated theories existent, and there are many, have not been able to do much better in this respect.

Actually, the chemical rate coefficient is not the quantity on which we should be concentrating, anyway. Though this coefficient is the most useful form for many engineering applications, the reaction cross section is a more fundamental quantity. The reaction rate coefficient is merely a suitably weighted average of such cross sections which is a function of the state of the gas; the reaction cross section itself is a fundamental molecular property, dependent only on the collision energy with other molecules. The problem here is that molecular beam research methods are generally limited to very low intensity beams of ionized particles with too large beam energy. Thus, cross sections cannot generally be measured in the important region of collision energy at the threshold of chemical reaction where they are most needed. Also, in almost all cases, the particles which the molecular beam physicist can supply in a well-calibrated, directed beam of usable intensity are not those particles of interest in important chemical reaction. The theory has been just as impotent; the Born approximation (ref. 3) which works well in analysis of high energy collisions breaks down at lower energies where the thresholds of most chemical reactions occur (0.1 to 10 eV collision energy), and at this date some less-than satisfying semi-empirical methods due to Gryzinski (ref. 4) are still about the most useful way to estimate low-energy collision ionization and excitation cross sections for engineering needs. In fact, if one takes a really hard-headed critical view of the field, one can reach the conclusion that only three reactions have been treated in any real depth: first is the collision-induced vibrational excitation of diatomic

molecules (refs. 5 and 6); a second is the simple atom exchange reaction in atom-diatomic collision (refs. 7 and 8), and the third is electron charge transfer (ref. 9). All of these reactions have recently taken on additional importance in engineering problems with the development of gas lasers; vibrational excitation and de-excitation by collision,

$$A_2(v') + M \rightarrow A_2(v'') + M \tag{1.2}$$

is one of the mechanisms establishing the population inversions in diatomic gas infrared lasers, and exchange reactions such as

$$F + H_2 \rightarrow HF + H \tag{1.3}$$

are important in chemical lasers. However, even these well studied reactions have generally been treated only for the collinear collision case, (that is, the collision partners are all constrained to motion along a single line) which is clearly the most atypical collision one can postulate (collinear collisions occur with zero probability), and important effects of rotational coupling have been almost completely ignored. The reader should not infer from these remarks that the reaction rate theory has been useless; the theory has, in fact, provided some very useful functional forms that can be fit to observed data reasonably well. The point is that, reaction rate theory is still very incomplete and has not been suitable for quantitative calculations of cross sections and reaction rate coefficients of the type that would be most useful to engineers.

Perhaps the above comments on the limitations of reaction rate theory and experiment seem unduly pessimistic in an age where scientific achievement has been so extraordinarily successful in many, many ways. Indeed, there are many indications that we are just now reaching the threshold of a new era of high-speed, large-capacity computers that will drastically change the situation with regard to reaction rates. Rice and Teller in a delightful semipopular book (ref. 10) called simply, "The Structure of Matter" pointed out as long ago as 1949 that one could, in principle, determine all the physical-chemical properties of matter, including cross sections and rate coefficients, as accurately as desired, from numerically computed quantum wave functions. The problem is that the labor and expense of accomplishing this has been so large that the only practical way of obtaining these properties of matter has been by experiment, in combination with some rather approximate theory. This situation may now be reversing itself. The advent of large-capacity, high-speed computers has already permitted the calculation of diatomic molecule wave functions with sufficient precision to determine some properties of these molecules as accurately as by experiment (refs. 11 and 12). These calculations can be made more precise yet, merely by expanding the unknown wave functions in terms of a larger set of basis functions, exactly analogous to the process of carrying a series expansion in terms of an orthogonal set of functions to still higher-order terms. This should be possible with still larger and faster computers now being developed, such as the ILLIAC IV with 64 channels of simultaneous parallel data processing (ref. 13). Bigger and faster computer systems being developed for computational fluid mechanics (ref. 14) will also find applications in advanced computational quantum chemistry and will expand the scope and size of the problems that can be attempted. Very likely, the computer will eventually become the fastest and least expensive means of determining many properties of matter, rather than experiment. Polyatomic and solid-state wave functions (refs. 15 and 16) will also be assessed as readily as the diatomic molecule wave functions are assessed now.

To give another example of the impact of large high-speed computers on reaction rate calculations, the problem of pure rotational excitation in collision is now being successfully attacked for the first time. This problem had never been solved correctly because the spacing between rotational states is small compared with kT at the temperatures of interest, and small perturbation methods fail. A rigorous quantum method of solving this problem was formulated some time ago by Takayanagi (refs. 17 and 18), but the solutions expanded in terms of partial waves converged to the answer so slowly that as a practical matter the only numerical estimates were made with rather approximate methods, using the sudden approximation in quantum mechanics or artificially diagonalizing the perturbation matrix obtained in a semi-classical approach (ref. 19). Now Takayanagi and Itikawa (refs. 20 and 21) have succeeded in using the close coupling method to calculate rotational transitions at low temperature in simple He - H_2 and He - HD collision systems, and calculations using their method with larger computers, involving heavier molecules, are presently in progress.

As a final example showing the utility of fast calculators, statistical methods of calculating reaction rates can be used once the interaction potentials are determined. Most atoms and molecules are heavy enough so that classical trajectories can be used with fair precision, and if initial conditions are chosen randomly by a Monte Carlo method, the computer can numerically follow these trajectories and determine whether or not any given set of initial conditions leads to reaction or not. The problem has been that so many trajectories need to be calculated to get a good statistical average over all possible initial conditions, that the necessary computing time becomes exorbitantly long. Recently, however, Shiu (ref. 22) and Jaffe (refs. 23 and 24) have used the method to obtain results for three-dimensional collisions involving simple dissociation and atom exchanges such as

$$H_2 + H \rightarrow H + H + H , \quad H + H_2 \rightarrow H_2 + H ,$$

and

$$H + F_2 \rightarrow HF + F$$

The method is presently being extended to more complex systems using faster computers.

Incidentally, the experimentalist will remain as necessary as before in this new era, only his function will change somewhat. Instead of providing approximate experimental results on properties of matter over as wide a range of conditions as possible, so that they may be available to the engineer as needed, the experimentalist will devise more precise, carefully controlled experiments that are subject to the least possible ambiguity and that will be used as check points on the computer codes which are developed. The computer will then take over the job of extrapolating results to arbitrary values of temperature, pressure, density, etc. as needed. Even with computers that are bigger and faster than those presently available by factors of 100 or so, the job of obtaining precise wave functions is so long that approximate theoretical models will need to be used for reasons of economy. The codes which incorporate these models will thus need to be checked with some firmly anchored experimental points and a few exceedingly long precision calculations. Further improvements in computers by another factor of 100 would be needed before the numerical wave function calculations can be said to be relatively free of approximation. Perhaps this much improvement will be unattainable because of the limiting signal speed of light in computer circuits. However, even if wave functions can

never be computed without some approximation, it is presently becoming clear that they will be obtained with sufficient precision to provide the best numerical evaluation of many of the properties of matter needed by engineers.

Once the wave functions are found, a rather long step remains in the evaluation of cross sections and rate coefficients (ref. 8). First, the potential surface must be obtained for all possible configurations of the reaction species of interest. Then the collision trajectories may be determined by a variety of methods from classical, semi-classical, to full quantum treatments. The latter will always be the standard of precision of course, but in many cases of interest to engineers, the molecular weights are heavy enough and the kinetic motions fast enough so that classical or semiclassical approximations will undoubtedly provide reasonably good results.

With these expectations in mind then, it is the purpose of this book to outline some of the present status of reaction-rate chemistry that is useful to engineers, and also derive some of the concepts that should be useful in the coming era in which machine computations will provide the engineer with more and more of the data he needs, data which has heretofore often been unavailable to him or available only in crude and approximate form.

1.3 ORDER OF CHEMICAL REACTION

The rate of a chemical reaction R is defined as the number of reactions which occur per unit volume per unit time. The rate is generally expressed.

$$-R = \alpha[A][B][C] \ldots \tag{1.4}$$

where α is the reaction rate coefficient and [A], [B], [C], etc. are the concentrations of the reactants involved in the process. The coefficient is a strong function of temperature, but is independent of the density or concentration factors. In much of the literature, the symbol k is used for the rate coefficient; α is used in this text to avoid any ambiguity with the Boltzmann constant.

If only one concentration factor appears, the reaction is first order; if a bimolecular collision process is involved between A and B, then the reaction is second order; if a trimolecular collision between A, B, and C, then the reaction is third order; and so on. In the early days of reaction kinetic studies, much attention was given to the determination of the reaction order because this gave a clue to the rate determining collision process involved. However, the experimentalist typically observes a total reaction process which may consist of many steps or a series of collision-induced reactions. In such cases, the overall reaction can appear to be of fractional order — that is, the rate may be found to be proportional to some fractional power of concentration or density. Thus, the order of reaction is no longer considered to be such a significant parameter. In this text, we take the viewpoint that each step in the reaction is an individual rate process, in which case it generally becomes clear whether the process is a unimolecular decay, a binary collision event, or a three-body collision event. At usual gas phase densities, one never need consider higher-order processes than three-body collisions.

1.4 FIRST ORDER CHEMICAL REACTIONS

The rate of a reaction that proceeds spontaneously is dependent only on the concentration of the reacting species and is said to be first order.

$$A^* \rightarrow A \qquad (1.5)$$

The spontaneous decay of a radioactive material would be one example. The rate R of the first order reaction in terms of the reacting species per unit time per unit volume may be expressed.

$$R = \frac{d[A]}{dt} = -\frac{d[A^*]}{dt} = \alpha[A^*] \qquad (1.6)$$

where [A] and [A*] represent the concentration of species A and A*, respectively, and α is the reaction rate coefficient.

Reactions other than a spontaneous unimolecular reaction may appear to be first order. For example, a photon excited reaction in an equilibrium radiation field may have a steady-state population of the excited molecular state, which may then spontaneously decay back to the ground state or to a new chemical state such as a dissociated state.

$$AB + h\nu \rightleftharpoons AB^* \rightarrow A + B \qquad (1.7)$$

In this case, if the spontaneous optical decay back to the ground state AB is slow, as in quadrupole type radiation decay, the excited molecule AB* may have sufficient lifetime for a reasonable fraction to dissociate, and the corresponding rate process may appear to be first order

$$R = \frac{d[AB]}{dt} = \alpha[AB] = \alpha'[AB^*] \qquad (1.8)$$

even though the initial excitation process is really a two-body collision process between the molecule AB and the photon $h\nu$. The reaction rate coefficients α and α' are both constant if the ratio [AB*]/[AB] is constant, that is, independent of density. These so called constants are typically strong functions of temperature.

What is really occurring in reaction (1.7) involves five separate reactions. Three are second order, giving the rate of absorption excitation, the rate of stimulated deexcitation, and the rate of collision excitation, respectively:

$$AB + h\nu \xrightarrow{\alpha_1} AB^* \qquad (1.7a)$$

$$AB^* + h\nu \xrightarrow{\alpha_2} AB + 2\,h\nu \qquad (1.7b)$$

$$AB + AB \xrightarrow{\alpha_3} AB^* + AB \qquad (1.7c)$$

Two are first-order reactions, giving the rate of spontaneous dissociation and emission, respectively:

$$AB^* \xrightarrow{\alpha_4} A + B \tag{1.7d}$$

$$AB^* \xrightarrow{\alpha_5} AB + h\nu \tag{1.7e}$$

At equilibrium, where the rates of gain and loss in AB and AB* are equal

$$\frac{d[AB]/dt}{d[AB^*]/dt} = \frac{\alpha_1[AB][h\nu] + \alpha_3[AB]^2}{\alpha_2[AB^*][h\nu] + (\alpha_4 + \alpha_5)[AB^*]} = 1 \tag{1.9}$$

and

$$[AB^*] = \frac{\alpha_1[AB][h\nu] + \alpha_3[AB]^2}{\alpha_2[h\nu] + (\alpha_4 + \alpha_5)} \tag{1.9a}$$

If $[h\nu]$ is large enough to that the first terms in both numerator and denominator of Eq. (1.9a) are dominant, then

$$[AB^*] \simeq \frac{\alpha_1}{\alpha_2}[AB] \tag{1.9b}$$

and the total reaction appears to be first order when Eq. (1.9b) is substituted in Eq. (1.8)

$$R = \alpha' \left(\frac{\alpha_1}{\alpha_2}\right)[AB] = \alpha[AB] \tag{1.8a}$$

On the other hand, if the radiation intensity is very low, the spontaneous dissociation and emission are the principal mechanisms depopulating the excited state. Then

$$[AB^*] \simeq \left(\frac{\alpha_3}{\alpha_4 + \alpha_5}\right)[AB]^2 \tag{1.9c}$$

and the overall process tends toward a second-order reaction

$$R = \alpha'\left(\frac{\alpha_3}{\alpha_4 + \alpha_5}\right)[AB]^2 = \alpha[AB]^2 \tag{1.8b}$$

In an actual case, the reaction may appear to the experimentalist to be intermediate between first order and second order. This possibility exists whenever the process observed consists of a series of separate reactions rather than a simple event.

A similar result can occur in a particle collision process with a complex organic molecule. If the time for redistribution of the collision energy among internal modes of the complex molecule (which involve the reaction coordinate; i.e., the weak link of the molecule) is long compared with the time between collisions, then the collisions can establish a pseudosteady equilibrium of the excited state, which then decays in a unimolecular manner to the products

$$A + M \underset{\alpha_1}{\overset{\alpha_2}{\rightleftharpoons}} A^* + M \tag{1.10a}$$

$$A^* \xrightarrow{\alpha_3} A' + A'' \qquad (1.10b)$$

As before, this may look like a first order reaction to the experimentalist.

For these reasons, the order of a reaction is not of primary concern. Non-integer orders of a reaction appear as an artifact because we have grouped several reactions together in one overall reaction, and it is the overall reaction that is observed by the experimentalist. However, on the fundamental level where the reaction is decomposed into its separate rate process, there is no confusion about the order. All of the fundamental reactions considered here will be either second order or third; that is, they will be the result of either two-body collisions, such as

$$A + M \rightleftharpoons A^* + M \qquad (1.11)$$

or three-body collisions, such as

$$A + B + M \rightleftharpoons AB + M \qquad (1.12)$$

In reaction (1.12) the third body M is essential in the forward direction as well as in the reverse direction, because it is needed to carry away the excess kinetic energy of collisions between particles A and B. Otherwise these particles will have more energy than the binding energy of their attraction. Without the third body M, A and B would merely approach one another and accelerate as they entered each other's attractive force field, perhaps orbit one another a time or two, if the angular momentum is just right, and then fly apart again. Only when the third body carries away some of the excess kinetic energy can the particles remain trapped in their attractive potential well.

A similar type of consideration occurs in the chain reactions that are typical of combustion or detonation processes. The reaction is a series of reactions, some of which may be so rapid that experimentally we never observe some of the intermediate products such as free radicals which are responsible for some of the steps in the process (though many free radicals have been identified spectroscopically in reacting gas mixtures). The chain reaction may be a stationary one in which the number of chains starting per unit time equals the number of finishing chains, or it may be an escalating rate process, in which each chain terminates with the production of more than one activating radical. In such cases, the reaction may be explosive, unless the activating radicals can migrate to a wall where they deactivate by collisions at the surface. Then the overall reaction rate depends on the geometry of the container, among other factors.

Let r be the number of active radicals produced on the average in each complete chain cycle of reactions, [A] be the concentration of normal unactivated molecules of the gas, [A*] be the concentration of the activated molecules of A which starts the chain process, and [B] be the concentration of products produced by the chain reaction. For steady state,

$$\frac{d[A^*]}{dt} = -\frac{d[B]}{dt} = 0 \qquad (1.13)$$

The rate of change of [B] can be expressed

$$\frac{d[B]}{dt} = \alpha_1[A^*] - \alpha_2[A][B] = 0 \tag{1.14}$$

where α_1 is the rate constant for spontaneous decay of A* to B and α_2 is the rate constant for deactivation of B by collisions with A. Similarly, the rate of change of [A*] can be expressed.

$$\frac{d[A^*]}{dt} = \alpha_3[A][A] + r\alpha_2[A][B] - \alpha_1[A^*] - \alpha_4[A][A^*] = 0 \tag{1.15}$$

where α_3 is the rate constant for activation of A by collisions with itself, independent of the chain process, $r\alpha_2$ is the rate constant for the production of A* by the active radicals that are products of the chain reaction, and α_4 is the rate constant for deactivation of A* by collisions with the normal molecules A. From Eq. (1.14)

$$[B] = \frac{\alpha_1[A^*]}{\alpha_2[A]} \tag{1.16}$$

Substituting this in Eq. (1.15)

$$\alpha_3[A]^2 + r\alpha_1[A^*] - \alpha_1[A^*] - \alpha_4[A][A^*] = 0 \tag{1.17}$$

Whence, the rate of reaction R is

$$R = \alpha_1[A^*] = \frac{\alpha_1\alpha_3[A]^2}{\alpha_4[A] + \alpha_1(1 - r)} \tag{1.18}$$

If every activated product molecule produces just one reaction, r = 1, the rate becomes

$$R = \frac{\alpha_1\alpha_3[A]}{\alpha_4} \tag{1.19}$$

and the overall reaction can look like a unimolecular first order reaction, even though it does depend in fact upon a series of binary collision processes. Note that if r is greater than one, as often happens in chain reactions, the reaction rate can become very large as $\alpha_1(r - 1)$ approaches $\alpha_4[A]$. In this case the overall reaction appears second order. Once again, however, when the chain process is decomposed into its elemental rate process, each step in the process is clearly defined as to its order.

Exercise 1.1: First order reactions in homogeneous gas phase are rather rare. Among the handful of reactions of this type are thermal dissociations of N_2O_5, N_2O, acetone, various aliphatic ethers, amines, ethyl bromide, and azo compounds. The thermal decomposition of azoisopropane to nitrogen and hexane is typical. The trans configuration of the compound seems to be stable.

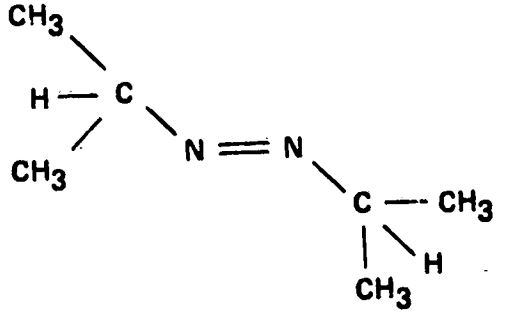

but at elevated temperature the collisions set up an equilibrium distribution between the trans and cis forms, and the latter decomposes spontaneously to nitrogen and hexane

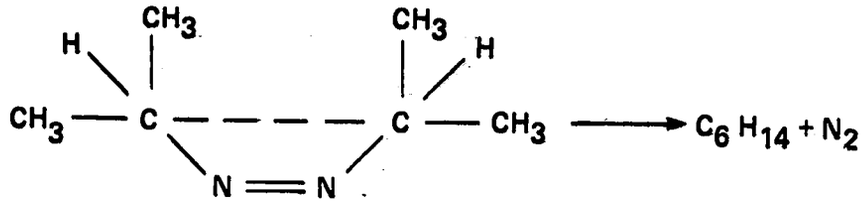

You have measured the rate of this decomposition at 270° C and obtain the following data:

Decomposition of azoisopropane at 270° C

t, sec	P, mm Hg
0	40.0
120	48.8
240	55.4
360	61.0
480	65.3
600	68.4
900	73.7

Knowing that one mole of azoisopropane vapor produces two moles of vapor, calculate the rate coefficient from the above data assuming the vapor is a perfect gas and that the reaction is first order. Is the rate coefficient constant? What are the units of α? Is it justified to assume the reaction is first order? What is the standard deviation from the mean calculated rate coefficient, according to the above data?

1.5 SECOND- AND THIRD-ORDER REACTIONS

Second order reactions are those depending on two body collisions such as the simple dissociation reaction:

$$AB + M \rightarrow A + B + M \tag{1.20}$$

These two-body collisions are very rapid in gases at normal densities, and such reactions can proceed very rapidly if there is an appreciable probability that a collision can produce the reaction.

The reverse reaction is, of course, a three-body or third-order reaction. In the early years of chemical kinetic studies, three-body collisions in gases were believed to be so rare that they were always negligible for any practical purposes. However, we now know that these three-body processes are responsible for establishing the equilibrium condition in cases like the dissociation reaction (1.20). Both forward and reverse reactions occur with rate coefficients α_1 and α_2.

$$AB + M \underset{\alpha_1}{\overset{\alpha_2}{\rightleftharpoons}} A + B + M \tag{1.20a}$$

and the ratio of the forward to reverse rates is:

$$\frac{R_1}{R_2} = \frac{\alpha_1[AB][M]}{\alpha_2[A][B][M]} = K_{eq}\frac{[AB]}{[A][B]} \tag{1.21}$$

where K_{eq} is the equilibrium constant, the ratio of the forward to reverse reaction rate constants.

Four-body collisions are so extremely rare in normal gases that they seem to be truly negligible for all practical purposes. Thus, we shall only need to consider first-, second-, and third-order reactions.

1.6 REACTION RATES IN NONEQUILIBRIUM GASES

Usually experimental rates are available only for one direction of reaction and seldom in the reverse. The usual procedure is to then assume that the forward and reverse rates, α_f and α_r, are related to the equilibrium constant K_{eq}, which can be calculated very precisely from the partition function using spectroscopically determined energy levels (ref. 25).

$$K_{eq} = \frac{\alpha_f}{\alpha_r} \tag{1.22}$$

Then the undetermined rate can be calculated from the measured rate.

The problem here is that the experimentalist never measures a rate at the equilibrium condition. At equilibrium the forward and reverse rates exactly counterbalance and the experimentalist sees only a steady-state population of species. He measures a rate of species production only when the state of the gas is away from equilibrium, such as may occur when two reacting species are suddenly mixed, or when an activating flash lamp is suddenly turned on or off, or when a shock wave suddenly heats and compresses the gas to a nonequilibrium condition. Thus, the measured values of α are not truly the equilibrium values and we cannot be sure that Eq. (1.22) will still be valid for these measured rates. Rice (ref. 26) discusses some of the questions concerning the validity of using Eq. (1.22) with measured nonequilibrium rates and concludes that in many cases, even if the gas is not in equilibrium, the ratio of the observable rates should still equal the equilibrium constant. One illustrative mechanism that suggests this is as follows: Suppose there are substances A and B existing in a total of four states and that transitions take place only between adjacent states

$$A_1 \rightleftharpoons A_2 \rightleftharpoons B_3 \rightleftharpoons B_4 \tag{1.23}$$

This model simulates the situation where multiple excited transition states occur, as in the vibration-rotation states leading to molecular dissociation or the excited electronic states leading to ionization for example; then A_2 and B_3 represent a sort of average of all the intermediate states from which the reaction actually takes place following a collision event. These activated states are typically present only in small numbers. The experimenter usually measures only the rate of change in A_1 or B_4, however, and may be quite unaware of A_2 and B_3. If the system is not in equilibrium, the concentrations of A_2 and B_3 will not be their equilibrium values; however, we shall later see that in typical cases the system quickly reaches a pseudosteady state in which these transition states are relatively constant and close to their equilibrium value.

If the entire system were in equilibrium $\alpha_{12}[A_1] = \alpha_{21}[A_2]$, $\alpha_{23}[A_2] = \alpha_{32}[B_3]$, and $\alpha_{34}[B_3] = \alpha_{43}[B_4]$, where α_{ij} is the rate constant for state i to state j. The equilibrium constant is thus

$$K_{eq} = \frac{[B_4]}{[A_1]} = \frac{[B_4]}{[B_3]} \cdot \frac{[B_3]}{[A_2]} \cdot \frac{[A_2]}{[A_1]} = \frac{\alpha_{12}}{\alpha_{21}} \frac{\alpha_{23}}{\alpha_{32}} \frac{\alpha_{34}}{\alpha_{43}} \tag{1.24}$$

Now assume the most nonequilibrium possible initial condition, $[B_4] = 0$. For this case, the observed forward-rate constant is

$$\alpha_{eff} = \frac{-1}{[A_1]} \frac{d[A_1]}{dt} = \frac{1}{[A_1]} \frac{[dB_4]}{dt} \tag{1.25}$$

Incidentally, a plot of α_{eff} as a function of time, made from the observed $[\dot{B}]$ and $[A]$ as functions of time, is found to be relatively constant for many reactions, like dissociation and ionization. The reaction scheme for this nonequilibrium extreme is now

$$A_1 \underset{\alpha_{12}}{\overset{\alpha_{21}}{\rightleftharpoons}} A_2 \underset{\alpha_{23}}{\overset{\alpha_{32}}{\rightleftharpoons}} B_3 \xrightarrow{\alpha_{34}} B_4 \tag{1.23a}$$

and the rate of reaction R is

$$R = \frac{d[B_4]}{dt} = \alpha_{34}[B_3] \tag{1.26}$$

If B_3 is assumed to be in pseudosteady state

$$\alpha_{23}[A_2] - \alpha_{32}[B_3] - \alpha_{34}[B_3] \simeq 0 \tag{1.27a}$$

$$[B_3] \simeq \frac{\alpha_{23}}{\alpha_{32} + \alpha_{34}} [A_2] \tag{1.27b}$$

Similarly, if A_2 is assumed to be in pseudosteady state

$$\alpha_{12}[A_1] - \alpha_{21}[A_2] - \alpha_{23}[A_2] + \alpha_{32}[B_3] \simeq 0 \tag{1.28a}$$

$$[A_2] \simeq \frac{\alpha_{12}[A_1]}{\alpha_{21} + \alpha_{23}} + \frac{\alpha_{32}[B_3]}{\alpha_{21} + \alpha_{23}} \tag{1.28b}$$

Substituting (1.28b) in (1.27b), one obtains

$$[B_3] \simeq \frac{\alpha_{23}\alpha_{12}[A_1]}{(\alpha_{32} + \alpha_{34})(\alpha_{21} + \alpha_{23})} + \frac{\alpha_{32}\alpha_{23}[B_3]}{(\alpha_{32} + \alpha_{34})(\alpha_{21} + \alpha_{23})} \tag{1.29a}$$

or

$$B_3(\alpha_{21}\alpha_{32} + \alpha_{21}\alpha_{34} + \alpha_{23}\alpha_{34}) \simeq \alpha_{23}\alpha_{12}[A_1] \tag{1.29b}$$

Then from Eqs. (1.29b) and (1.26) the reaction rate R is given by

$$R = \alpha_{eff}[A_1] \simeq \frac{\alpha_{12}\alpha_{23}\alpha_{34}}{\alpha_{21}\alpha_{32} + \alpha_{21}\alpha_{34} + \alpha_{23}\alpha_{34}} [A_1] \tag{1.30}$$

Now consider the opposite extreme, where $[A_1] = 0$

$$A_1 \xleftarrow{\alpha_{21}} A_2 \underset{\alpha_{23}}{\overset{\alpha_{32}}{\rightleftharpoons}} B_3 \xrightarrow[\alpha_{34}]{\alpha_{43}} B_4 \tag{1.23b}$$

In an exactly similar way, assuming A_2 and B_3 to be again in pseudosteady state, the reverse rate R' and the effective reverse reaction rate α'_{eff} are given by

$$R' = \frac{\alpha_{43}\alpha_{32}\alpha_{21}}{\alpha_{23}\alpha_{34} + \alpha_{21}\alpha_{34} + \alpha_{21}\alpha_{32}}[B_4] = \alpha'_{eff}[B_4] \qquad (1.31)$$

Then the ratio of the effective observed forward and backward rates is

$$\frac{\alpha_{eff}}{\alpha'_{eff}} \simeq \frac{\alpha_{12}\alpha_{23}\alpha_{34}}{\alpha_{21}\alpha_{32}\alpha_{43}} = K_{eq} \qquad (1.32)$$

which is just the same as the equilibrium constant given by Eq. (1.24).

The simple derivation above is by no means a proof that the ratio of observed forward and backward rates will equal the equilibrium constant for all reactions. We have, after all, assumed that a pseudosteady state exists among the activated states that are the bridge between reactants and products, and this means than there needs to be a very rapid exchange between the activated states and a rather rapid deactivation from the excited states to the ground state compared with the rate of activation of the ground state to the excited state. In chapter V we shall see that some reactions do indeed more or less satisfy this condition; for example, the excitation of diatomic molecules to a ladder of close lying rotation-vibration states that eventually lead to dissociation; similarly, the excitation of excited electronic states that eventually lead to ionization. The activated species A_2 and B_3 in Eq. (1.23) may actually represent an entire group of close lying states in such reactions.

In many real reactions, the deactivation from B_3 to B_4 will be so rapid that the concentration $[B_3]$ will also be essentially zero as well as $[B_4]$ in Eq. (1.23a). In this case, one simply analyzes the problem as a three-state system, but as long as the intermediate state between reactant and product is in pseudosteady state, the same result as Eq. (1.32) follows. This is left as exercise (1.2) for the reader to solve.

Exercise 1.2: Consider a three-state system

$$A_1 \underset{\alpha_{12}}{\overset{\alpha_{21}}{\rightleftharpoons}} A_2^* \underset{\alpha_{23}}{\overset{\alpha_{32}}{\rightleftharpoons}} A_3$$

First let $[A_3] = 0$ and derive the expression for the observed forward rate constant under this nonequilibrium condition with steady state A_2^*

$$\alpha_{eff} = \frac{[\dot{A}_3]}{[A_1]}$$

then let $[A_1] = 0$ and derive the expression for the observed reverse rate constant under this nonequilibrium condition, again with steady state A_2^*

$$\alpha'_{eff} = \frac{[\dot{A}_1]}{[A_3]}$$

and show that the ratio of these two rate constants is the equilibrium constant K_e.

In chapter V we shall find that when an entire ladder of close lying states exist between the ground state reactants and the products, the states having energy within kT of the final product state will also be depleted by thermal collisions so they are nearly zero when the concentration of products is zero, while the lower lying states will be close to their equilibrium concentrations and all in pseudosteady state. Such reaction systems will again approximately obey the relation of Eq. (1.32). However, we should keep in mind that this is not necessarily a general relation for all reactions. Some caution must be observed in deriving reverse rates using the equilibrium constant with forward rates observed under nonequilibrium conditions.

Exercise 1.3: Second order reactions are the most frequently encountered in homogeneous gas phase. This includes thermal dissociation of HI, NO_2, O_3, ClO, HCHO, CH_3, CHO, etc., and also many combination reactions such as $H_2 + I_2 \rightarrow 2HI$, polymerization of ethylene, hydrogenation of ethylene, etc.

You have measured the thermal decomposition of acetaldehyde, CH_3CHO, at 520° C and obtain the following data:

Decomposition of acetaldehyde at 520° C

t, sec	P, mm Hg
0	400
60	455
120	495
180	530
240	560
360	602
600	645

You have determined that the products are methane and CO. Assume the decomposition reaction is first order as in Exercise 1.1.

$$CH_3CHO \rightarrow CH_4 + CO$$

Is the rate coefficient constant? Now assume a second-order reaction requiring the collision between two acetaldehyde molecules.

$$2CH_3CHO \rightarrow 2CH_4 + 2CO$$

Find the relation between the rate coefficient α and the measured pressure P and the initial pressure P_o and calculate α from the above data. Is α constant with this assumption? What are the units of α? Is it justified to assume this reaction is second order? What is the standard deviation from the mean calculated rate coefficient, according to the above data? What about collisions between acetaldehyde and the products CH_4 and CO? Would these give the same rate coefficient? How would you experimentally determine what these rate coefficients were? Why didn't we need to include corrections for these alternate collisions in reducing the above data?

1.7 REACTION RATE LITERATURE

Although the archive journal literature on reaction rates and rate theories is voluminous, not many books have been written on the subject. This is probably a reflection of the fact that the subject is not really developed in a totally satisfying and consistent way yet — at least not for all types of reactions. Books that do exist are written primarily from the physical chemist's viewpoint or a quantum scattering viewpoint; engineering texts usually treat reaction kinetics in a very simple and cursory manner — for example, texts on combustion and detonation or on flow about high-speed vehicles. Nevertheless, a number of books on reaction processes are useful to engineers; just a few of these will be suggested here. Hinshelwood's "The Kinetics of Chemical Change" (ref. 27) covers the concepts of the old, but still useful, physical chemistry viewpoints up to 1940. A classical work representing the beginnings of a new viewpoint is "The Theory of Rate Processes" by Glasstone, Laidler, and Eyring (ref. 28). A more recent book by Benson, "Thermochemical Kinetics" (ref. 29) gives some methods for estimating rate parameters, particularly for reactions involving complex organic molecules, and also gives useful methods for estimating the thermochemical data for these molecules so that the equilibrium constants and reverse rates can be calculated. Perhaps the most widely used books in Russian literature are by Kondratiev, and one of these is available in English translation (ref. 30).

Most books on reaction rates seem to be edited collections (refs. 31-34). They provide useful updates but generally lack the coherency desirable in a text. Some of the most useful books to the engineer are collections of reaction rate data; these save the engineer from the tedious task of sifting through the literature for this data. Perhaps the most useful of these collections is the "Defense Nuclear Agency Reaction Rate Handbook" (ref. 35). Several other such collections exist, such as a

collection of data by Kondratiev (ref. 36) and some kinetic rate data for H_2-O_2-N_2 systems (ref. 37). Specialist reports by The Chemical Society (ref. 38) summarize much of gas-kinetic literature up to 1976.

A number of good texts exist on the subject of quantum scattering theory. They are not usually directly usable to the engineer because they are not quantitative theories; nevertheless they are essential background for understanding much of the literature and the physical significance of reaction processes. The classic text is by Mott and Massey, "The Theory of Atomic Collisions" (ref. 39), and it's still as valid as when first published. A couple of more recent good books on this subject are by Levine (ref. 40) and by Rodberg and Thaler (ref. 41). The theory of quantum scattering becomes particularly necessary and useful when applied to electron collisions. Two very good texts that give the experimentalist's viewpoint along with some theory are by Hasted (ref. 42) and by McDaniel (ref. 43); these texts are also still reasonably up to date on the subject of electron collision processes, more than 15 years after their publication.

REFERENCES

1. Arrhenius, S.: Uber die Reaktionsgeschwindigkeit bei der Inversion von Rohrzucker durch Säuren. Z. Physik. Chem., vol. 4, no. 226, 1889.

2. Wray, K. L.: Chemical Kinetics of High Temperature Air. AVCO Research Rep. 104, June 1961.

3. Massey, H. S. W.: Theory of Atomic Collisions. In Atoms II, Handbuch der Physik, vol. XXXVI, Springer Verlag, Berlin, 1956, pp. 232-306.

4. Gryzinski, M.: Classical Theory of Electronic and Ionic Inelastic Collisions. Phys. Rev., vol. 115, July 15, 1959, pp. 374-383; ibid vol. 138, 1965, p. A336

5. Bethe, H. A.; and Teller, E.: Deviations from Thermal Equilibrium in Shock Waves. Aberdeen Proving Ground Report X-117, 1945.

6. Schwartz, R. N.; Slawsky, Z. I.; and Herzfield, K. F.: Calculation of Vibrational Relaxation Times in Gases. J. Chem. Phys., vol. 20, no. 1591-9, 1952.

7. Gladstone, S.; Laidler, K. J.; and Eyring, H.: The Theory of Rate Processes. McGraw Hill, 1941.

8. Karplus, M.; Porter, R. N.; and Sharma, R. D.: Exchange Reactions with Activation Energy. I. Simple Barrier Potential for (H, H_2). J. Chem. Phys., vol. 43, Nov. 1965, pp. 3259-3287.

9. Delos, John B.: Theory of Electronic Transitions in Slow Atomic Collisions. Rev. Mod. Phys., vol. 53, 1981, pp. 287-355.

10. Rice, F. O.; and Teller, E.: The Structure of Matter. John Wiley, 1949, New York.

11. Das, G.: Multiconfiguration Self-Consistent Field (MCSCF) Theory for Excited States. J. Chem. Phys., vol. 58, June 1973, pp. 5104-5110.

12. Arnold, J. O.; Whiting, E. E.; Garber, J. A.; Lyle, G. C.; and Burnett, K.: A New Program to Apply the MCSCF Method to the ILLIAC IV and CDC 7600 Computers at NASA Ames Research Center. 29th Molecular Spectroscopy Symposium, Ohio State University, Columbus, Ohio, June 1974.

13. Slotnick, D. L.: The Fastest Computer, Illiac IV. Sci. Am., vol. 224, Feb. 1971, pp. 76-87.

14. Chapman, D. R.; Mark, H.; and Pirtle, M. W.: Computers vs Wind Tunnels. Astronautics and Aeronautics, vol. 13, April 1975, pp. 22-30.

15. Chapman, D. R.: Computational Aerodynamics Development and Outlook. Dryden Lectureship in Research, 17th Aerospace Sciences Meeting, New Orleans, La., June 15-17, 1979.

16. Slater, J. C.: Quantum Theory of Molecules and Solids. McGraw Hill, 1965.

17. Takayanagi, K.: Vibrational and Rotational Transitions in Molecular Collisions. Prog. Theo. Phys. Suppl., vol. 25, 1963, pp. 1-98.

18. Takayanagi, K.: The Production of Rotational and Vibrational Transitions in Encounters Between Molecules. Adv. Atom. Mol. Phys., vol. 1, D. R. Bates and I. Estermann, eds., Academic Press, N.Y., 1965, pp. 149-194.

19. Pearson, W. E.; and Hansen, C. F.: Collision Induced Rotational Transition Probabilities in Diatomic Molecules. In Rarefied Gasdynamics, K. Karamcheti, ed., Academic Press, 1974, pp. 167-175.

20. Takayanagi, K.: Rotational Relaxation of HD. Inst. Space and Aero. Sci., University of Tokyo, Report 467, vol. 36, July 1971, pp. 229-237.

21. Itikawa, Y.; and Takayanagi, K.: Rotational Transitions in the HD Molecule in Low Energy HD-He Collisions. J. Phys. Soc. Japan, vol. 32, June 1972, pp. 1605-1611.

22. Shui, V. H: Thermal Dissociation and Recombination of Hydrogen According to the Reactions $H_2 + H \rightleftarrows H + H + H$. J. Chem. Phys., vol. 58, June 1973, pp. 4868-4879.

23. Jaffe, R. L.; and Anderson, J. B.: Classical Trajectory Analysis of the Reaction $F + H_2 \rightarrow HF + H$. J. Chem. Phys., vol. 54, Mar. 1, 1971, pp. 2224-2236.

24. Jaffe, R. L.; Henry, J. M.; and Anderson, J. B.: Variational Theory of Reaction Rates: Application to $F + H_2 \rightleftarrows HF + H$. J. Chem. Phys., vol. 59, August 1, 1973, pp. 1128-1141.

25. Hansen, C. F.: Molecular Physics of Equilibrium Gases. NASA SP-3096, 1976.

26. Rice, O. K.: On the Relation Between an Equilibrium Constant and the Nonequilibrium Rate Constants of Direct and Reverse Reactions. J. Phys. Chem., vol. 65, Nov. 1961, pp. 1972-1976.

27. Hinshelwood, C. N.: The Kinetics of Chemical Change. Oxford Press, Oxford, 1940.

28. Glasstone, S.; Laidler, K. J.; and Eyring, H.: The Theory of Rate Processes. McGraw Hill, N.Y., 1941.

29. Benson, S. W.: Thermochemical Kinetics. Second ed. John Wiley and Sons, N.Y., 1976.

30. Kondrat'ev, V. N.: Chemical Kinetics of Gas Reactions. J. M. Crabtree and S. N. Carruthers, transl., and N. B. Slater, ed. Pergamon Press, London, 1964.

31. Bamford, C. H.; and Tipper, C. F. H., eds.: Comprehensive Chemical Kinetics. Vols. 1-22. Elsevier Publishing Co., Amsterdam, 1969-80.

32. Klopman, G., ed.: Chemical Reactivity and Reaction Paths. John Wiley and Sons, New York, 1974.

33. Porter, G., ed.: Progress in Reaction Kinetics. Vol. 1-5, Pergamon Press, London, 1961-70.

34. Jennings, K. R.; and Cundall, R. B., eds.: Progress in Reaction Kinetics. Vols. 6-7, Pergamon Press, London, 1972-73.

35. Bortner, M. H.; and Baurer, T., eds.: U.S. Defense Nuclear Agency Reaction Rate Handbook. Second ed. Published by DASIAC, DOD Nuclear Information and Analysis Center, General Electric, TEMPO, Santa Barbara, Calif., 1972.

36. Kondrat'ev, V. N.: Rate Constants of Gas Phase Reactions. L. J. Holtschlag, transl., and R. M. Fristrom, ed. NBS U.S. Dept. of Commerce, Washington, D.C., 1972.

37. Baulch, D. L.; Drysdale, D. D.; Horne, D. G.; and Lloyd, A. C.: Evaluated Kinetic Data for High Temperature Reactions. Vols. 1 and 2, Chemical Rubber Co. Press, Cleveland, Ohio, 1972 and 1973.

38. The Chemical Society: Vol. 1 - Reaction Kinetics, Vol. 2 - Gas Kinetics and Energy Transfer, Burlington House, London, 1977.

39. Mott, N. F.; and Massey, H. S. W.: The Theory of Atomic Collisions. Second ed., Oxford Press, 1949.

40. Levine, R. D.: Quantum Mechanics of Molecular-Rate Processes. Clarendon Press, Oxford, 1969.

41. Rodberg, L. S.; and Thaler, R. M.: Introduction to the Quantum Theory of Scattering. Academic Press, N.Y., 1967.

42. Hasted, J. B.: Physics of Atomic Collisions. Butterworths, Washington, 1964.

43. McDaniel, E. W.: Collision Phenomena in Ionized Gases. John Wiley & Sons, N.Y., 1964.

CHAPTER II CROSS SECTIONS, REACTION RATES, AND ACTIVATION ENERGIES

2.1 SUMMARY

Reaction is described in terms of transition at a crossing of potential surfaces reached in the collision process. The increase in potential up to the crossing point is identified as the activation energy. The energy available to the system in reaching this barrier is the kinetic energy of relative motion in center of mass coordinates. The collision cross section and reaction rate coefficient are formulated in terms of velocity distribution functions, and in particular the Maxwell-Boltzmann distribution functions. The known form of the cross section leads to the Arrhenius form for the rate coefficient. The apparent activation energy (that is the negative slope of an Arrhenius plot) is found to depend on the shape of the cross-section function at high temperature, but at low temperature it reduces to the true activation energy, independent of the cross section. The dissociative recombination of $NO^+ + e$ is used as an example of the analysis of experimental data in terms of cross sections and activation energies.

2.2 INTRODUCTION

We consider two particles in gas phase, with masses m_1 and m_2 and velocities $\vec{u}_1$ and $\vec{u}_2$, respectively, that have a collision encounter with one another (fig. 2.1). A potential exists between the two, principally due to interactions between the electronic and nuclear charges of the particles. At long range the potential may be either attractive or repulsive, depending upon how the electronic spin functions pair up, but at short range the potential is always strongly repulsive. The range of the potential is about the range of the outer electron wave functions of the particles involved; when these wave functions overlap, the forces that result in attraction or repulsion are created. Outer electron wave functions for atoms and most simple molecules all extend about a few Angstroms in their ground electronic state, so the size of the total scattering cross sections are usually about 10^{-15} cm^2 or so.

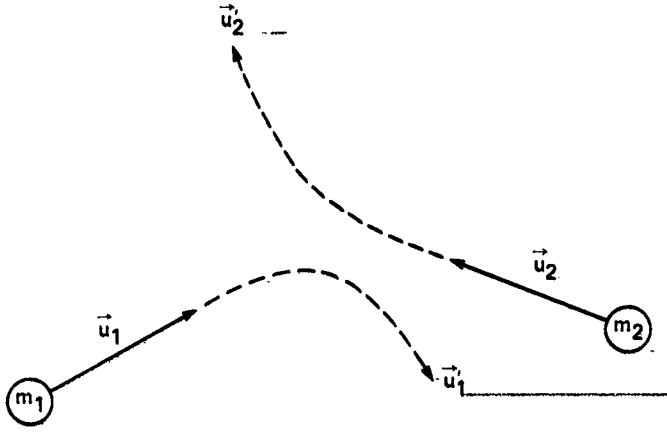

Figure 2.1- Collision between two particles in gas phase with masses m_1 and m_2, initial velocities $\vec{u}_1$ and $\vec{u}_2$, and final velocities $\vec{u}_1'$ and $\vec{u}_2'$.

2.3 ELASTIC AND INELASTIC COLLISIONS

Some of the kinetic energy of collision may be converted to a change in internal energy, ΔE_i, of one or both of the collision partners

$$\frac{m_1 u_1^2}{2} + \frac{m_2 u_2^2}{2} = \frac{m_1 (u_1')^2}{2} + \frac{m_2 (u_2')^2}{2} + \Delta E_i \tag{2.1}$$

If $\Delta E_i = 0$, the collision is said to be elastic; if $\Delta E_i \neq 0$, the collision is said to be inelastic; if $\Delta E_i < 0$, the collision is sometimes termed superelastic. The change in internal energy could be due to a change in (1) rotational state, (2) in vibrational state, or (3) in electronic state of either one or both of the particles, or it might be the difference between the heats of formation of the molecules, if an atom exchange takes place between the particles during the collision, or the reaction may be any combination of these changes of internal state. In the limit as very high rotational and/or vibrational states are excited, the molecules become dissociated; or if very high electronic energy states are excited, the particles are ionized. In these cases the reaction produces more particles than enter the collision. All of these changes in internal state may be encompassed in a simple general definition of the term reaction, namely, reaction is the process produced in inelastic collision. A reaction which leads to new chemical species (such as atom exchange, dissociation, or ionization) is merely a special case of the above. If ΔE_i is positive the reaction is said to be endothermic (i.e., it abstracts kinetic energy from the gas); if ΔE_i is negative the reaction is said to be exothermic (i.e., it adds to the kinetic energy of the gas).

2.4 REACTION POTENTIAL SURFACES

The total energy of the collision process shown in figure 2.1 may be expressed in terms of laboratory coordinates of the two particles

$$E = \frac{m_1}{2}(\dot{x}_1^2 + \dot{y}_1^2 + \dot{z}_1^2) + E_1 + \frac{m_2}{2}(\dot{x}_2^2 + \dot{y}_2^2 + \dot{z}_2^2) + E_2 + V(x_1, y_1, z_1, x_2, y_2, z_2, \ldots) \tag{2.2}$$

where E_1 and E_2 are the initial internal energy levels of the two particles, and the potential V is the transient change in internal energy of the particles during the collision process. The interaction potential may be taken to include the initial internal energies E_1 and E_2 as the reference base level. In general it will include a dependence on internal structure and orientation coordinates as well as the particle collision coordinates shown. If the collision is inelastic, $E_1 + E_2 \neq E_1' + E_2'$ and the particles may be considered to have made a transition to a new potential surface with a different reference energy. The situation is diagrammed for a simple one-dimensional form of reaction path in figure 2.2. This would be the case for a perfectly spherically symmetric interaction potential, for example, but in the most general case the reaction path would need to be described with additional coordinates involving the internal configurations of the colliding particles. Such a case will be discussed later when we consider three-dimensional collisions leading to coupled vibration-rotation transitions. However, for the present we are interested in the general concepts of a reactive collision which may be treated symbolically, at least, with the one-dimensional reaction coordinate model. At

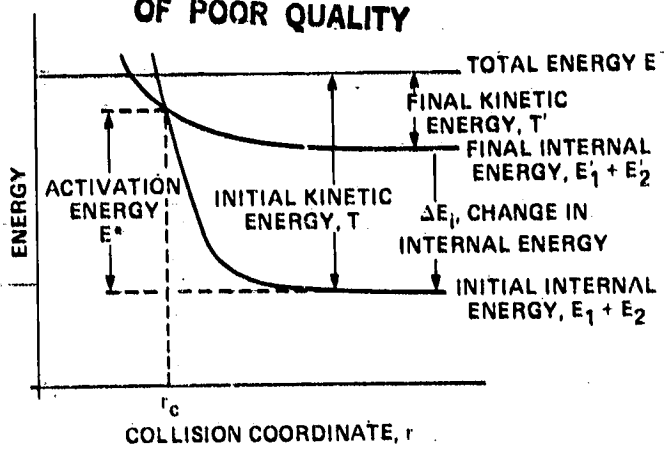

Figure 2.2- Energy diagram for simplified one-dimensional reaction path.

infinite distance apart, the potential is a constant, $E_1 + E_2$, the sum of the initial internal energies of the two particles; the kinetic energy is T, and the total energy is $E = T + E_1 + E_2$. As the particles come together the internal energies (which may be rotational, vibrational, or electronic) are perturbed and the potential and kinetic energies interchange such that the total is conserved. Another potential surface may be defined for a different set of internal states E_1' and E_2'. If this surface intersects, or comes very close to the first surface at some value of the collision coordinate r_c, and the total energy E is sufficiently large for the particles to approach one another as close as r_c or closer, a transition to the new potential surface may occur. The energy difference E^* between the transition region and the initial potential $E_1 + E_2$ will be identified with the Arrhenius activation energy. If the transition does not occur, the particles recede from one another along the same potential surface as the one on which they approached, the collision is elastic, and the total effect of the collision has been to produce scattering. This scattering changes the components of momentum and energy of the two particles and gives rise to the phenomena of mass flux, viscosity, and heat transfer whenever gradients in number density, mass velocity, or temperature occur in the gas, respectively. If, on the other hand, a transition to the new potential surface occurs with a certain probability P, which will be unity or less, the collision is inelastic and the particles recede from one another at large separation with a different kinetic energy T' and new steady-state internal energy levels E_1' and E_2'. In general, a multiplicity of such potential surfaces occur with different crossing points r_c and different activation energies E^*. Also, some of the potentials may have attractive regions as well as the purely repulsive shapes shown symbolically on figure 2.2. Thus, a single collision event between two simple gas molecules can lead to a complex multiplicity of reaction channels. Although reaction processes need not always be treated as potential surface transitions (indeed other methods may be preferable in many cases) one can in principle always define potential surfaces with which to describe the reaction in conceptual terms at least.

2.5 CENTER OF MASS COORDINATES

The most elementary question we must first answer is: What portion of the total kinetic energy is available along the reaction coordinate? The interaction potential V. of Eq. (2.2) will in general be a function of the distance r between the two particles and the internal orientation coordinates of the colliding molecules (such as bond lengths and direction cosines). However, the latter coordinates do not relate to the position of the molecules and for present purposes we need concern ourselves only with dependence of V on the intermolecular distance r. Thus, we wish to transform the laboratory coordinates $\vec{r}_1$ and $\vec{r}_2$ used in Eq. (2.2) to describe the particle positions in laboratory space, to the coordinate $\vec{r}$, the vector distance between the two particles, and whatever additional coordinate $\vec{R}$ which is

needed to diagonalize the kinetic energy expression such that only squared terms in the velocities appear with no cross product terms. This is the coordinate of the center of mass of the two particles, of course. This transformation allows us to separate the equations of motion into two independent equations, one a function only of R, the other a function only of r.

$$\vec{r} = \vec{i}r_x + \vec{j}r_y + \vec{k}r_z = \vec{i}(x_2 - x_1) + \vec{j}(y_2 - y_1) + \vec{k}(z_2 - z_1) \tag{2.3}$$

$$(m_1 + m_2)\vec{R} = (m_1 + m_2)(\vec{i}X + \vec{j}Y + \vec{k}Z) = \vec{i}(m_1x_1 + m_2x_2) + \vec{j}(m_1y_1 + m_2y_2) + \vec{k}(m_1z_1 + m_2z_2) \tag{2.4}$$

The inverse transformation given by Eqs. (2.3) and (2.4) leads to the expressions for the components of $\vec{r}_1$ and $\vec{r}_2$

$$\left.\begin{aligned} x_1 &= X - \frac{m_2}{m_1 + m_2} r_x, & x_2 &= X + \frac{m_1}{m_1 + m_2} r_x \\ y_1 &= Y - \frac{m_2}{m_1 + m_2} r_y, & y_2 &= Y + \frac{m_1}{m_1 + m_2} r_y \\ z_1 &= Z - \frac{m_2}{m_1 + m_2} r_z, & z_2 &= Z + \frac{m_1}{m_1 + m_2} r_z \end{aligned}\right\} \tag{2.5}$$

When these are substituted in the expression for total energy, Eq. (2.2), one obtains

$$E = \frac{M}{2}(\dot{X}^2 + \dot{Y}^2 + \dot{Z}^2) + \frac{\mu}{2}(\dot{r}_x^2 + \dot{r}_y^2 + \dot{r}_z^2) + V(r) \tag{2.6}$$

where M is the total mass $(m_1 + m_2)$ and μ is the reduced mass $m_1m_2/(m_1 + m_2)$. The internal energies E_1 and E_2 have been incorporated in the potential V(r) as discussed in relation to figure 2.2.

The kinetic energy associated with the center of mass is a constant of the motion inasmuch as the potential V, no matter how complex it may be or how nonspherical it may be, does not involve the center of mass coordinates X, Y, and Z. This is just the kinetic energy of a free particle of mass M and velocity $\vec{i}\dot{X} + \vec{j}\dot{Y} + \vec{k}\dot{Z}$. This energy is thus unavailable for reaction purposes; only the kinetic energy associated with the relative velocity between the two particles may interchange with the internal energy of the particle. Moreover, the reaction path may be described as though it were the motion of a single particle of mass μ moving in the potential V(r). Accordingly, figure 2.1 illustrating the reaction paths in laboratory coordinates is redrawn as figure 2.3 illustrating the reaction path in the relative distance coordinate r. The position of the hypothetical "single particle" with mass μ may be described relative to an origin that is fixed at the center of mass and an axis AA' parallel to the initial relative velocity vector $\vec{u}$. Another independent coordinate is needed to unambiguously fix the collision geometry; this is the miss distance or impact parameter b shown in figure 2.3. If the interaction potential is aspherical, then a third coordinate, the cylindrical angle ϕ is needed to describe the orientation of the collision relative to the potential geometry. As the particles approach one another, the trajectory is deflected by the interaction potential, of course, but if the particles were to continue undeflected on their

initial path, they would then miss one another by the distance b. Sometimes it is more convenient to consider one of the collision partners fixed at the origin with fictitious infinite mass and the other molecule approaching with the fictitious mass μ. In either case, r represents the relative distance between the molecules at any instant of time, and b represents the miss distance if the particles were not interactive. Other time dependent parameters may be useful in describing the collision process, for example, the angle ψ between the vector $\vec{r}$ and the reference axis AA'. In scattering problems it is usual to define a different reference axis, the line between the two particles at the point of closest approach, and then define the scattering angles relative to this axis. However, for our present purposes it will be sufficient to concentrate on the cylindrical coordinates of the initial configuration relative to the reference axis AA'; these are the radial distance b and the angle ϕ about the reference axis.

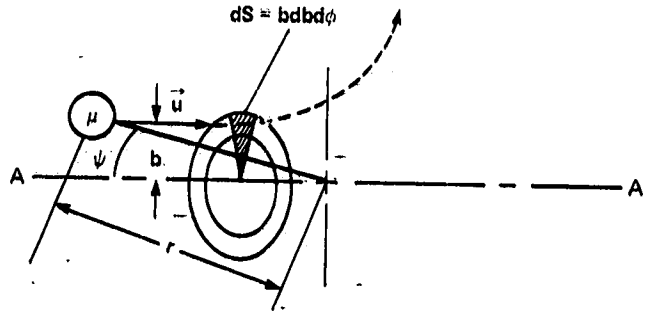

Figure 2.3- Collision between two particles represented by the motion of a single particle with reduced mass $\mu = m_1m_2/(m_1 + m_2)$ moving in a potential field V(r) with origin fixed on the center of mass.

2.6 COLLISION CROSS SECTIONS AND REACTION RATE COEFFICIENTS

In the sample of gas many encounters occur simultaneously with a distribution over all possible velocities u and impact parameters b and ϕ. All values of b and ϕ are assumed equally probable, and the velocities are given by some distribution function f(u). The velocity distribution function is normally a Maxwell-Boltzmann distribution. Quantum effects of gas degeneration are normally negligible at conditions where reactive collisions are important, and the Maxwell-Boltzmann distribution establishes itself so quickly in a gas at conditions of usual interest, even where internal energies are far out of equilibrium with the kinetic energies, that nonequilibrium velocity distributions need not normally be considered. However, one could easily account for a nonequilibrium velocity distribution in the formulations which follow, if that distribution is known.

The number of encounters that occur in a unit volume of gas within a range of velocities du, of miss distance db, and angular parameter $d\phi$ may be expressed (refs. 1 and 2)

$$dN = \frac{un_1n_2}{s} f_1(u_1)f_2(u_2)d\vec{u}_1\ d\vec{u}_2 b\ db\ d\phi \qquad (2.7)$$

where u is the magnitude of the relative velocity $|\vec{u}_2 - \vec{u}_1|$, n_1 is the number density of molecules of type 1, n_2 is the number density of molecules of type 2, f_1 and f_2 are the velocity distribution functions for molecules of type 1 and type 2, respectively, and $bdbd\phi$ is the element of cross section area shown in figure 2.3. The factor s is called the symmetry number; it is unity if the two particles are different but equals two if the two particles are identical. The symmetry number must be included to avoid counting systems twice in the latter case; the number of

all different combinations of two particles in a unit volume is the product $n_1 n_2$ if the particles are different, it is $n_1^2/2$ if the particles are identical.

Normally we need consider only distribution functions that are isotropic in space, in which case it is convenient to express the velocity volume elements in terms of spherical coordinates

$$d\vec{u}_i = d\dot{x}_i\, d\dot{y}_i\, d\dot{z}_i = \sin\theta_i\, d\theta_i\, d\phi_i\, u_i^2\, du_i \tag{2.8}$$

and integrate over all angular orientations. Equation (2.7) then becomes

$$dN = (4\pi)^2 \frac{n_1 n_2}{s} u f_1(u_1) f_2(u_2) u_1^2\, du_1 u_2^2\, du_2 b\, db\, d\phi \tag{2.9}$$

At this point we want to transform the laboratory velocities $\vec{u}_1$ and $\vec{u}_2$ shown in figure 2.1 to the center of mass velocity $\vec{U} = (\overrightarrow{dR/dt})$ and the relative velocity $\vec{u} = \dot{\vec{r}}$, so that it will be convenient to integrate Eq. (2.9) with respect to the relative velocity magnitude, u. The volume elements are simply related (see Eq. 2.5)

$$d\dot{x}_1 d\dot{x}_2 = \begin{vmatrix} \dfrac{\partial \dot{x}_1}{\partial \dot{X}} & \dfrac{\partial x_1}{\partial \dot{r}_x} \\ \dfrac{\partial \dot{x}_2}{\partial \dot{X}} & \dfrac{\partial x_2}{\partial \dot{r}_x} \end{vmatrix} d\dot{X}\, d\dot{r}_x$$

$$= \begin{vmatrix} 1 & \dfrac{-m_2}{m_1 + m_2} \\ 1 & \dfrac{m_1}{m_1 + m_2} \end{vmatrix} d\dot{X}\, d\dot{r}_x = d\dot{r}_x\, d\dot{X} \tag{2.10}$$

so the Jacobian for the entire transformation is unity

$$d\dot{x}_1\, d\dot{x}_2\, d\dot{y}_1\, d\dot{y}_2\, d\dot{z}_1\, d\dot{z}_2 = d\dot{r}_x\, d\dot{r}_y\, d\dot{r}_z\, d\dot{X}\, d\dot{Y}\, d\dot{Z}$$

$$= (4\pi)^2 u_1^2\, du_1 u_2^2\, du_2 = (4\pi)^2 u^2\, du U^2\, dU \tag{2.11}$$

The total number of encounters in a unit volume of gas in unit time may thus be expressed in an integration of Eq. (2.7)

$$N = \frac{(4\pi)^2 n_1 n_2}{s} \int_0^{2\pi} \int_0^{\infty} \int_0^{\infty} \left[\int_0^{\infty} f_1 f_2 U^2\, dU \right] u^3\, du\, b\, db\, d\phi \tag{2.12}$$

The inner integral in Eq. (2.12) is a function only of u. We can define a function f(u)

$$f(u) = (4\pi u)^2 \int_0^{\infty} f_1 f_2 U^2\, dU \tag{2.13}$$

which represents the fraction of the collision encounters which have a relative velocity magnitude between u and $u + du$. With this definition, the number of collision encounters may be expressed

$$N = \frac{n_1 n_2}{s} \int_0^{2\pi} \int_0^{\infty} \int_0^{\infty} f(u) u \, du \, b \, db \, d\phi \qquad (2.14)$$

Only a fraction of the collision encounters results in a given change of internal state or reaction. Let $P(\phi,b,u)$ be the probability that a collision, with cylindrical angular orientation ϕ, miss distance b, and relative velocity u, results in reaction. The rate of reaction is defined as the total number of reactions produced in unit volume in unit time

$$R = n_1 n_2 s \left[\int_0^{2\pi} \int_0^{\infty} \int_0^{\infty} P(\phi,b,u) f(u) u \, du \, b \, db \, d\phi \right] \qquad (2.15)$$

The quantity in brackets is, by definition, the rate coefficient α for the reaction in question. The integration over the parameters b and ϕ yields the reaction cross section $S(u)$

$$S(u) = \int_0^{2\pi} \int_0^{\infty} P(\phi,b,u) b \, db \, d\phi \qquad (2.16)$$

which is a function only of the relative velocity u. In terms of this parameter the rate coefficient is

$$\alpha = s \int_0^{\infty} S(u) u f(u) du \qquad (2.17)$$

Thus, the rate coefficient α physically represents the volume swept out in unit time by a disc of cross section $S(u)$ moving with the velocity u, all weighted with the velocity distribution function $f(u)$ and averaged over all velocities; its dimensions are cm^3/sec.

The definitions above have been left as general as possible so that the procedures for evaluating the cross sections and rate coefficients can be visualized even for nonequilibrium velocity distribution functions. The only assumption which has been made is that the distribution functions are isotropic, that is, that the gas phase in which reaction occurs is without appreciable gradients. In practice, it is usually safe to assume that the kinetic motions are in an equilibrium Maxwell-Boltzmann distribution at a given temperature T, since this distribution normally establishes itself much faster than the reactions of interest. In cases where the internal energy establishes equilibrium on the same time scale as the kinetic motions, which is often the case with rotational energy of molecules, for example, the reaction can merely be considered as infinitely fast for most practical engineering needs. For Maxwell-Boltzmann velocity distributions (refs. 1 and 2) then, we have

$$f_1 f_2 d\vec{u}_1 d\vec{u}_2 = \frac{(m_1 m_2)^{3/2}}{(2\pi kT)^3} \exp\left[\frac{-m_1(\dot{x}_1^2 + \dot{y}_1^2 + \dot{z}_1^2) - m_2(\dot{x}_2^2 + \dot{y}_2^2 + \dot{z}_2^2)}{2kT}\right] d\dot{x}_1 d\dot{y}_1 d\dot{z}_1 d\dot{x}_2 d\dot{y}_2 d\dot{z}_2$$

$$= \frac{(m_1 m_2)^{3/2}}{(2\pi kT)^3} \exp\left[\frac{-M(\dot{X}^2 + \dot{Y}^2 + \dot{Z}^2) - \mu(\dot{r}_x^2 + \dot{r}_y^2 + \dot{r}_z^2)}{2kT}\right] d\dot{X}\, d\dot{Y}\, d\dot{Z}\, d\dot{r}_x d\dot{r}_y d\dot{r}_z \qquad (2.18)$$

Integrating Eq. (2.18) over all center-of-mass velocity components and multiplying by $(4\pi u)^2$, as defined in Eq. (2.13), we obtain

$$f(u) = 4\pi u^2 \left(\frac{\mu}{2\pi kT}\right)^{3/2} \exp(-\mu u^2/2kT) \qquad (2.19)$$

for the distribution function of the encounters between two particles with relative velocity magnitude u. This distribution is of course normalized; the integration over all u yields unity.

The reaction rate coefficient of Eq. (2.17) may now be expressed

$$\alpha(T) = \frac{4\pi}{s}\left(\frac{\mu}{2\pi kT}\right)^{3/2} \int_0^\infty S(u) \exp(-\mu u^2/2kT) u^3 du$$

$$= \frac{1}{s}\left(\frac{8kT}{\pi\mu}\right)^{1/2} \int_0^\infty S(x) \exp(-x) x\, dx \qquad (2.20)$$

The second expression in Eq. (2.20) has been transformed to the dimensionless kinetic energy variable $x = \mu u^2/2kT$. The radical in front of the integral is just the mean velocity $\bar{u}$

$$\bar{u} = \int u f(u) du = 4\pi \left(\frac{\mu}{2\pi kT}\right)^{3/2} \int_0^\infty u^3 \exp(-\mu u^2/2kT) du$$

$$= \left(\frac{8kT}{\pi\mu}\right)^{1/2} \qquad (2.21)$$

so the rate coefficient may be expressed

$$\alpha(T) = \frac{\bar{u}}{s} \int_0^\infty S(x) \exp(-x) x\, dx \qquad (2.22)$$

The integral in Eq. (2.22) represents the average cross section weighted by the Maxwell-Boltzmann distribution function. The rate coefficient $\alpha(T)$ will vary as the product of $T^{1/2}$, due to the factor $\bar{u}$, and another function of temperature representing the functional dependence of this average cross section. To proceed further than this we must know the form of the cross section function, either experimentally or theoretically.

2.7 DEPENDENCE OF APPARENT ACTIVATION ENERGY ON CROSS SECTION FUNCTION

Unfortunately, very little is known about cross sections at low collision energies where they contribute most to the integral of Eq. (2.22). From our concept of an activation energy leading to a potential crossing where the transition can take place with reasonable probability, we know that the cross section must vanish until the kinetic energy of collision at least reaches the activation energy E^*. All our experimental experience indicates that the cross sections increase very rapidly above E^* until they reach some maximum value, which is less than the total cross section for all processes, including elastic scattering. As discussed previously, this total cross section is the order of 10^{-15} cm^2 for most atoms and simple molecules, and for cases where a single highly probable reaction is involved, the maximum in the reaction cross section may approach this total. At still higher energies the cross sections decrease again, generally as the inverse square root of collision energy, and become vanishingly small at collision energies that are two or three orders of magnitude greater than the threshold activation energy. The form of a typical reaction cross section function is sketched in figure 2.4.

The simplest functional form we can use to empirically approximate the behavior of real cross sections is a step function

$$\begin{aligned} S &= 0 , \quad E < E^* \\ &= S_o , \quad E^* < E \end{aligned} \tag{2.23}$$

where S_o is some constant value. The rate coefficient for such a cross section is, from Eq. (2.22)

$$\begin{aligned} \alpha(T) &= \frac{\bar{u} S_o}{s} \int_{x^*}^{\infty} e^{-x} x \, dx \\ &= \frac{S_o}{s} \bar{u}(x^* + 1) e^{-x^*} \end{aligned} \tag{2.24}$$

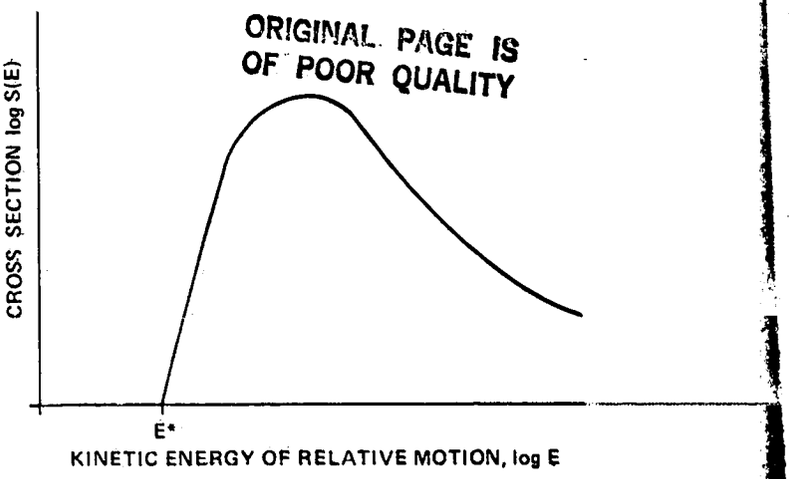

Figure 2.4- Typical form for reaction cross section as a function of collision energy.

where x^* is the dimensionless activation energy E^*/kT. The variation of $\bar{u}(x^*+1)$ with temperature is so weak compared with the variation of the exponential term e^{-x^*}, that for many practical purposes Eq. (2.24) is the same as the Arrhenius function, where the coefficient in front of the exponential is taken to be constant. Expressing Eq. (2.24) in terms of the parameter $\beta = (kT)^{-1}$

$$\alpha = \frac{S_o}{s} \left(\frac{8}{\pi \mu \beta} \right)^{1/2} (\beta E^* + 1) e^{-\beta E^*} \tag{2.25}$$

one finds the slope of the logarithm of α as a function of β

$$\frac{d \ln \alpha}{d\beta} = -E^* + \frac{E^*}{\beta E^* + 1} - \frac{1}{2\beta} = -E^* \left[1 - \frac{1}{2\beta E^*} + \left(\frac{1}{\beta E^*} \right)^2 - \left(\frac{1}{\beta E^*} \right)^3 + \ldots \right] \tag{2.26}$$

For many chemical reactions E^* is the order of 1 eV or more, while the thermal energy kT at normal temperatures is the order of (1/40) eV; for such cases the factor $(2\beta E^*)^{-1}$ is the order of 10^{-2}, small compared with unity. Thus, the slope of an Arrhenius plot (a plot of $\ln \alpha$ vs β) for the step-function cross section, Eq. (2.23), would very closely be equal to $(-E^*)$, except at rather high temperatures where it would become somewhat less negative.

From this point on we shall treat the interaction potential as spherically symmetric, as this greatly simplifies the analysis. Strictly speaking, the potential is spherically symmetric only for a single electron in collision with an atom or ion having outer electrons all in the s state; atomic or molecular wave functions having finite angular momentum have lobes, and molecular wave functions are also elongated about the interatomic bond directions. Aspherical effects may be particularly important where strong dipole moments exist. Nevertheless, it is common practice to average the potential over all angular configurations to obtain an effective average spherical potential for use in quantitative calculations. The rationale for this procedure is that the effective potential represents an average for a multitude of collisions in which all possible initial angular orientations are equally probable. In practice the average potential gives reasonably good results for many simple molecules for which the permanent dipole moments are not too strong.

The cross section is not really a step function as assumed in Eq. (2.23), of course, but varies as sketched in figure 2.4. Because of the strong exponential weighting of the cross section at thermal collision energies near kT by the Maxwell-Boltzmann kinetic energy distribution (see Eq. (2.20)), the important part of the function for our purposes is the region just above the threshold E^*. In this region the cross sections for all reactions are observed to increase as a simple power of collision energy. Part of this increase is due to the requirement that angular momentum be conserved during collision, the remaining increase is due to the variation in transition probability at the potential crossing as the collision velocity changes.

The conservation of angular momentum in collision may be expressed in terms of the angle ψ of figure 2.3

$$\mu r^2 \dot{\psi} = \mu u b \tag{2.27}$$

The energy is also conserved during collision, of course

$$\frac{\mu}{2}\left(\dot{r}^2 + r^2\dot{\psi}^2\right) + V(r) = \frac{\mu u^2}{2} \tag{2.28}$$

Substituting $\dot{\psi}$ from Eq. (2.27) into Eq. (2.28), one obtains an expression for $\dot{r}$

$$\dot{r} = \left[u^2 - \frac{2V(r)}{\mu} - \frac{u^2 b^2}{r^2}\right]^{1/2} \tag{2.29}$$

At the point of closest approach in the trajectory, r_o, the derivative $\dot{r}$ vanishes and we have a relation between the impact parameter and r_o

$$\left(\frac{b}{r_o}\right)^2 = 1 - \frac{2V(r_o)}{\mu u^2} = 1 - \frac{V(r_o)}{E} \tag{2.30}$$

where E is the initial kinetic energy. Now if the reaction is to occur, r_o must be less than or equal to r_c, the potential crossing point. At this point the

potential V is just the activation energy E*. Thus, the maximum value which the impact parameter can have if the point of closest approach is to be less than or equal to r_c is

$$\left(\frac{b_m}{r_c}\right)^2 = 1 - \frac{E^*}{E} \qquad (2.30a)$$

All larger values of the impact parameter will result in a deflection of the collision partners at distances greater than r_c. Thus, we may express the effective spherical symmetric cross section

$$S = \pi r_c^2 p\left(1 - \frac{E^*}{E}\right), \quad E^* < E \qquad (2.31)$$

where the factor $(1 - E^*/E)$ is the fraction of systems with initial miss distance less than r_c which reach the transition point according to conservation of angular momentum, and p is the probability of transition at the configuration r_c. The latter is analyzed by the Landau-Zener theory which predicts a rapid increase of p with collision energy near threshold (ref. 3). This theory will be considered in some detail later; for the moment we will account for this factor empirically by adding another factor $((E/E^*) - 1)^{m-1}$ to the cross section function (ref. 4)

$$S = S_o\left(1 - \frac{E^*}{E}\right)\left(\frac{E}{E^*} - 1\right)^{m-1} \qquad (2.32)$$

where S_o is some constant and m is the observed slope of the logarithm of the cross section as a function of the logarithm of excess collision energy near the threshold. This slope is typically between 1 and 3 for cross sections that are observed.

The cross section of Eq. (2.32) can be integrated exactly in Eq. (2.22) to give

$$\alpha = \bar{u} S_o \, e^{-\beta E^*} \frac{\Gamma(m+1)}{(\beta E^*)^{m-1}}, \quad \beta E^* \gg 1 . \qquad (2.33)$$

As indicated, the approximation is useful where $\beta E^* \gg 1$. It may be noted that an additional factor $1 + (m + 1)/\beta E^*$ is often given in the literature, but the second term in this factor is meaningless; it results from the unrealistic divergence of the cross section at high collision energies when the cross section is assumed to have the form $S = S_o[(E/E^*) - 1]^m$. The second order term in $(\beta E^*)^{-1}$ is always negative, not positive, when cross sections are used that approach a proper asymptotic limit, or decrease, at high-collision energy. These higher order terms are of little consequence anyway for $\beta E^* > 10$, an inequality that is easily satisfied for many reactions.

However, reactions do exist where E* may be small compared with kT at the temperatures of interest, for example the ionization of highly excited electronic species. In such cases it is necessary to choose a cross-section function that has a more realistic asymptotic behavior than Eq. (2.32). The transition probability p cannot exceed unity, so the cross section at high collision energies has an upper bound with the functional form

$$S = S_o\left(1 - \frac{E^*}{E}\right) \qquad (2.34)$$

Using this upper bound in Eq. (2.22) one obtains the rate coefficient

$$\alpha = \bar{u} S_o \, e^{-\beta E^*} , \qquad \beta E^* \ll 1 \tag{2.35}$$

The apparent activation energy will be defined as the negative slope of an Arrhenius plot (the plot of $\ln \alpha$ vs β), and in the limiting cases considered this quantity approaches

$$-\frac{d \ln \alpha}{d\beta} \xrightarrow[\beta E^* \gg 1]{} E^* + \frac{2m - 1}{2\beta}$$

$$\xrightarrow[\beta E^* \ll 1]{} E^* + \frac{1}{2\beta} \tag{2.36}$$

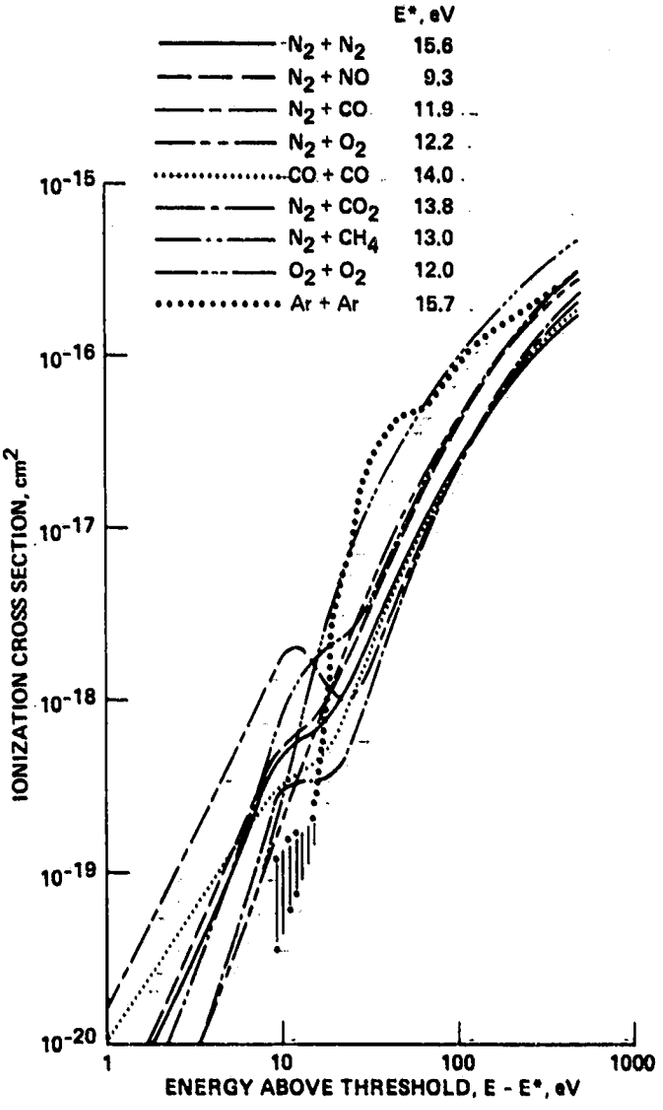

Figure 2.5- Measured ionization cross sections for various collision partners as a function of kinetic energy in excess of threshold.

Near room temperature $\beta \simeq 40$ eV^{-1} and the correction terms are a few hundredths electron volt. Thus, where the activation energy is the order of 1 eV, it is perfectly justified to equate the slope of the Arrhenius plot with the true activation energy, as is usually done by chemists. However, at high temperatures the correction term becomes appreciable. For temperatures near 10^4 K, for example, $\beta \simeq 1$ eV^{-1}, and the corrections are between 0.5 eV and 1.5 eV (for $m = 2$) according to the above limits. These are not at all negligible corrections. Note that the curvature of the Arrhenius plot is not in question here; the curvature will usually be negligible over the temperature range involved in a typical experiment and the data may plot as a very nice straight line. What is not generally appreciated is that the true activation energy cannot be evaluated from the slope of this line if the data are taken at high temperature, without some knowledge of the form of the cross-section function. Normally α is not measured over a wide enough range of temperature and with sufficient reproducibility in shock tube experiments to determine a reliable value for m. Molecular beam experiments have been of limited help because accurate measurements are difficult to make near threshold. A number of heavy particle impact ionization cross sections have been measured by Utterback (ref. 5) within an electron volt or so of threshold. These are summarized in figure 2.5 on a plot of log S vs log (E - E*).

The values of the slope m generally range between 2 and 3 for this class of reaction. Kieffer and Dunn (ref. 6) summarized a number of measured electron impact ionization cross sections, shown in figure 2.6, and for this class of reaction the slope m is characterized by values between 1 and 2. Measured cross sections for other classes of reaction are not generally available near threshold, but it is likely that these will fit the same general type of functional dependence, with slopes the order of 2.

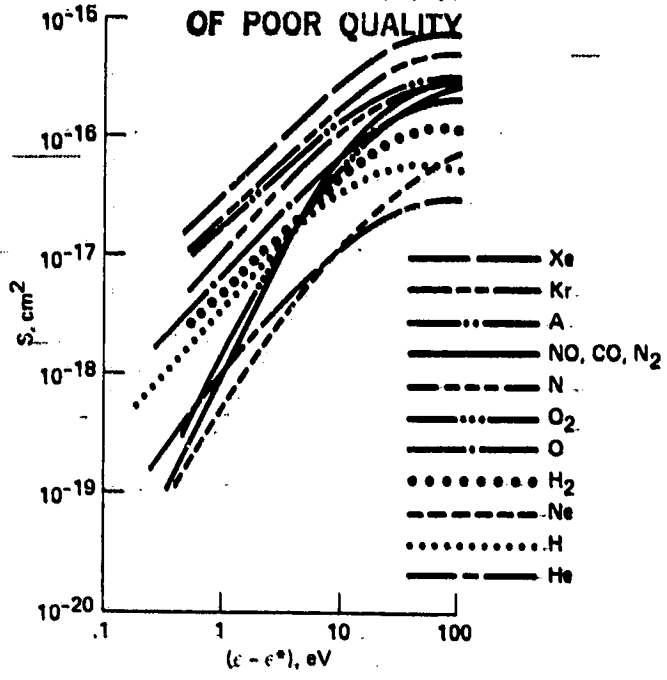

Figure 2.6- Cross sections for ionization by electron impact.

Exercise 2.1: A cross section often used in reaction-rate literature is

$$S = S_0 \left(\frac{x}{x^*} - 1\right)^m$$

where

$$x = \frac{\mu u^2}{2kT} = \beta E$$

Evaluate the rate coefficient α and the apparent activation energy $-(d\ \ell n\ \alpha/d\beta)$ for this cross section. Show that the first order terms are the same as obtained for $S = S_0(1 - x^*/x)(x/x^* - 1)^{m-1}$, but that the next order terms in $(\beta E^*)^{-1}$ give an increase in α and a decrease in $-(d\ \ell n\ \alpha/d\beta)$. Don't forget that $\bar{u}$ is proportional to $\beta^{-1/2}$.

Exercise 2.2: The cross section above diverges unrealistically at large collision energy. Consider the cross section

$$S = S_0\left(1 - \frac{x^*}{x}\right)^m$$

which approaches the limit S_0 at large x. Evaluate α and $-(d\ \ell n\ \alpha/d\beta)$ for this cross section and show that the leading term is the same as above, but that the next order terms in $(\beta E^*)^{-1}$ decrease the rate coefficient α and decrease the apparent activation energy.

Hint: expand x^{-m} about x^*.

2.8 DISSOCIATIVE RECOMBINATION OF $NO^+ + e$

To give a concrete example of an application of some of the preceding concepts, consider the dissociative recombination reaction

$$NO^+ + e \underset{\alpha_f}{\overset{\alpha_r}{\rightleftharpoons}} N + O \qquad (2.37)$$

This reaction is one of the dominant mechanisms leading to ionization and electron recombination in hypersonic airflow. The forward rate for this reaction was first measured by Lin, Neal, and Fyfe (ref. 7). Lin and Tear (ref. 8) proposed the dissociative recombination rate coefficient

$$\alpha_f = 0.003T^{-3/2} \text{ cm}^3/\text{sec} \qquad (2.38)$$

to fit their experimental data. This value has been widely used in calculations of flow about high-speed vehicles and of the electron densities in wake flow following such vehicles.

Subsequent experiments indicated that while Eq. (2.38) may be correct at normal temperatures, the rate should be somewhat higher at high temperatures as shown in figure 2.7. The high temperature experiments yield the reverse rate coefficient α_r, and at equilibrium, this is related to the forward rate with the equilibrium constant K_e

$$\alpha_f = \alpha_r K_e \qquad (2.39)$$

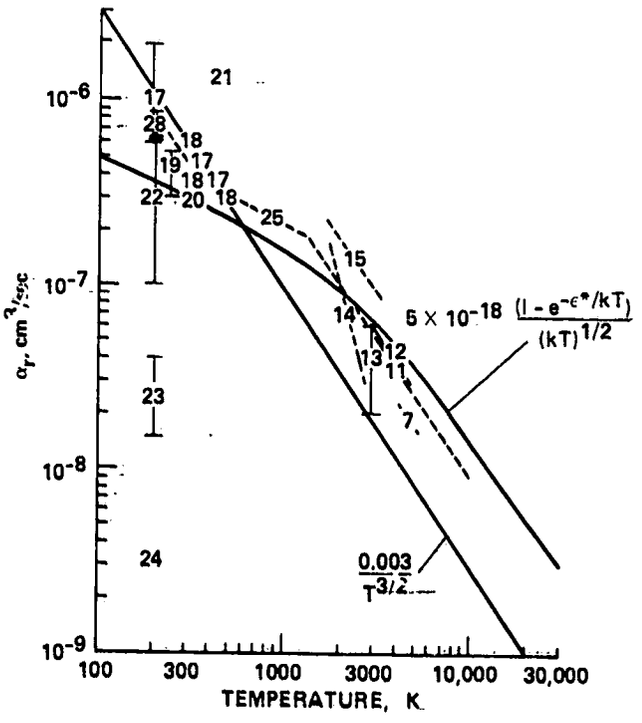

Figure 2.7- Dissociative recombination rate for $NO^+ + e \rightarrow N + O$. Data numbered by reference number.

Some speculation has persisted about the validity of this relation at the nonequilibrium conditions where the measurements are made (the experimenter cannot measure a change in species concentration at equilibrium, of course), but Rice (ref. 9) has long argued that the equilibrium constant is still the ratio of forward to reverse rates under most nonequilibrium conditions where reactions are measured, as long as the Boltzmann distribution of velocities is present. McLaren and Appleton (ref. 10) have confirmed these ideas with measurements of both forward and reverse rates of vibrational excitation of CO over a range of temperature. Accordingly we assume that Eq. (2.39) is valid for the reaction of present interest also, and that the trends shown by the data in figure 2.7 are valid. Thompson (ref. 11), and Frohm and DeBoer (ref. 12) suggest that the constant 0.003 in Eq. (2.38) should be increased by a factor of 3; Frohm and DeBoer point out that an increase by a factor of 2 actually fits the original data of reference 8 better. The mean value given by Stein et al. (ref. 13)

is twice as large as that given by Eq. (2.38), and Eckerman and Stern (ref. 14) and Eschenroeder and Chen (ref. 15) both observed that increasing the rates by factors up to 5 are consistent with measured electron decay in the wake of high speed models. Dunn and Lordi (ref. 16) also verified the correctness of higher values at the higher temperatures. However, a number of low temperature measurements (refs. 17-22) agree with Eq. (2.38) (except for some estimates of upper atmosphere electron recombination (refs. 23 and 24); these latter should probably be weighted lightly compared with the other evidence). This anomaly led Sutton (ref. 25) to use values for wake calculations that are empirically faired between the high and low temperature as shown on figure 2.7.

Hansen (ref. 26) pointed out that theoretical grounds exist for predicting a smooth variation of α_f from a $T^{-1/2}$ to a $T^{-3/2}$ dependence as the temperature increases. The ionization is presumed to occur when the N + O atoms interact along a potential that intersects the minimum of $NO^+(^1\Sigma^+)$ potential, figure 2.8 (ref. 27). Of the many possible interactions at least one crossing will probably occur near this minimum. If this is the case, then the threshold or activation energy E* is about the heat of formation, which is from 0.4 to 2.8 eV depending upon which of the low lying electronic states of the atoms are involved in the collision.

$$\left.\begin{aligned} N(^4S) + O(^3P) &\rightarrow NO^+(^1\Sigma^+) - 2.8\ eV \\ N(^4S) + O(^1D) &\rightarrow NO^+(^1\Sigma^+) - 0.8\ eV \\ N(^2D) + O(^3P) &\rightarrow NO^+(^1\Sigma^+) - 0.4\ eV \end{aligned}\right\} \quad (2.40)$$

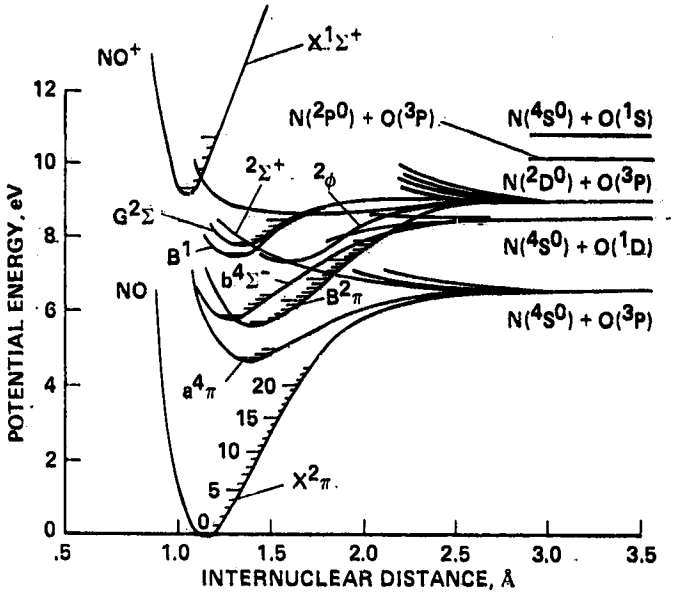

Figure 2.8- N + O and NO^+ interaction potentials.

Higher lying atomic states are ignored because the reaction becomes exothermic and the population in these states will normally decrease exponentially without a corresponding increase in reaction probability.

Let r_c be the equilibrium interatomic distance of the NO^+ ion and assume that a fixed fraction p of the colliding atoms which reach this crossing point will form NO^+, and that the potentials are spherically symmetric. The reaction cross section for the reverse reaction of Eq. (2.37) is then written as in Eq. (2.32). The fraction p will be a function of collision energy according to the Landau-Zener theory (ref. 3), but we will merely choose some constant value, the order of 10^{-2}, which fits the function to the observed data. With this assumption the rate coefficient is given by Eq. (2.35)

$$\alpha_r = \bar{u} S_o \, e^{-E^*/kT} \quad (2.41)$$

where S_o is a constant to be fit to experimental data and E* is the activation energy, in this case 2.8 eV. If excited species are present in their equilibrium concentrations and have the same cross section function as Eq. (2.32), but with

appropriately shifted threshold energy E^*, the same expression is obtained for α as Eq. (2.33), with the same activation energy, 2.8 eV, except that the constant S_o is multiplied by the sum

$$\frac{g(N^4S)g(O^3P) + g(N^4S)g(O^1D) + g(N^2D)g(O^3P)}{g(N^4S)g(O^3P)} = \frac{4\times9 + 4\times5 + 10\times9}{4\times9} = 4.06 \qquad (2.42)$$

where the symbols g are the degeneracies of the atomic electronic states indicated. This effect of excited electronic states will be considered later in chapter IV. For the present, it is pointed out that the effect produces a constant factor which can be merely absorbed in the empirical constant S_o, and the reverse rate coefficient α varies as the product of $T^{1/2}$ and $\exp(-2.8\ \text{eV}/kT)$.

Now the equilibrium constant for the reaction in the forward direction is the product of the partition functions of the products divided by the product of the partition functions of the reactants, all multiplied by the exponential of the factor E^*/kT

$$K_e = \frac{Q_N Q_O}{Q_e Q_{NO^+}} e^{E^*/kT} \qquad (2.43)$$

To a reasonably good approximation we may take the electronic partition functions as the ground state degeneracies and treat NO^+ as a harmonic oscillator with characteristic vibrational energy $\hbar\omega = 0.27$ eV. The temperature factors in the translational partition functions all cancel, and the temperature dependence of the NO^+ rotational and vibrational partition function remains. Thus, an approximate expression for K_e is

$$K_e = \left(\frac{714\ \text{eV}}{kT}\right)\left(1 - e^{-0.27\ \text{eV}/kT}\right)e^{2.8\ \text{eV}/kT} \qquad (2.44)$$

Accordingly the forward rate coefficient is, with $S_o = p\pi r_c^2 = 3\times10^{-18}\ \text{cm}^2$

$$\alpha_f = \alpha_r K_e = \frac{4.8\times10^{-8}}{(kT)^{1/2}}\ (\text{eV})^{1/2}\left(1 - e^{-0.27\ \text{eV}/kT}\right)\ \text{cm}^3/\text{sec} \qquad (2.45)$$

Equation (2.45) is shown on figure 2.7 and is seen to follow the same trends as shown by the data. At high temperatures where $kT \gg 0.27$ eV, α_f varies as $T^{-3/2}$, essentially the variation in $\bar{u}$ divided by the rotational and vibrational partition functions of NO^+. At lower temperature the vibrational partition function approaches unity and α_f then varies as $T^{-1/2}$. The latter variation agrees very well with the measurements of Weller and Biondi (ref. 28) at 450 K and 300 K which are the most recent data shown in that temperature range. However, Weller and Biondi's data at 200 K is abnormally high in comparison with the theory, which suggests that some additional experimental or theoretical effect may yet be unaccounted for at very low temperatures.

2.9 CONCLUDING REMARKS

In conclusion, the reaction-rate mechanism can be interpreted as a potential curve crossing transition, and the known form of reaction cross sections leads to the Arrhenius form of reaction-rate coefficient. At low temperatures where kT is considerably less than the activation energy E^*, the latter can be accurately equated to the negative slope of an Arrhenius plot (the plot of $\ln\alpha$ vs $1/kT$). However, at

high temperatures where kT is the order of E^* or greater, the negative slope of this plot is greater than the activation energy by a sizable amount, and the activation energy can only be deduced in this way if the form of the cross-section function near the threshold collision energy is known.

The dissociative recombination of NO^+ and e, which was used to illustrate the concepts discussed, is an example of the approximate nature of current rate theory and experiment as discussed in chapter 1. The experimental data are widely scattered, inconsistencies between high temperature and low temperature data exist, and the theoretical interpretation of the functional trends is very elementary. Yet this reaction, because of its importance, is at present one of the best studied and measured reactions; the results are mute testimony to the need for more rigorous quantitative treatment of reaction rates for engineering purposes.

REFERENCES

1. Kennard, E. H.: Kinetic Theory of Gases. McGraw Hill, New York, 1938.

2. Beckner, R.; and Leibfried, G.: Theory of Heat. Second ref. ed., Springer-Verlag, Berlin, 1967.

3. Eyring, H.; Walter, J.; and Kimball, G. E.: Quantum Chemistry. John Wiley & Sons, New York, 1944.

4. Hansen, C. F.: Apparent Activation Energy of Chemical Reaction at High Temperature. Phys. Fluids, vol. 12, May 1969, pp. 1127-1128.

5. Utterback, N. G.: Inelastic Molecular Collisions. Rarefied Gas Dynamics, Proc. 6th Int'l. Symposium on Rarefied Gas Dynamics, MIT, July 1968. Academic Press, New York, 1969.

6. Kieffer, L. J.; and Dunn, G. H.: Electron Impact Ionization Cross Section Data for Atoms, Atomic Ions, and Diatomic Molecules: I. Experimental Data. Rev. Mod. Phys., vol. 38, Jan. 1966, pp. 1-35.

7. Lin, S. C.; Neal, R. A.; and Fyte, W. I.: Rate of Ionization Behind Shock Waves in Air. I. Experimental Results. Phys. Fluids, vol. 5, Dec. 1962, pp. 1633-1648.

8. Lin, S. C.; and Teare, J. D.: Rate of Ionization Behind Shock Waves in Air. II. Theoretical Interpretations. Phys. Fluids, vol. 6, Mar. 1963, pp. 355-375.

9. Rice, O. K.: On the Relation Between the Equilibrium Constant and the Nonequilibrium Rate Constants of Direct and Reverse Reactions. J. Phys. Chem., vol. 65, Nov. 1961, pp. 1972-1976.

10. McLaren, T. I.; and Appleton, J. P.: Vibrational Relaxation Measurements of Carbon Monoxide in a Shock-Tube Expansion Wave. J. Chem. Phys., vol. 53, Oct. 1, 1970, pp. 2850-2857.

11. Thompson, W. P.: Ionization and NO Production in Air at 3000-5000°K. Bull. Am. Phys. Soc., vol. 10, 1965, p. 727.

12. Frohm, A.; and DeBoer, P. C. T.: Ion Density Profiles Behind Shock Waves in Air. AIAA J., vol. 5, Feb. 1967, pp. 261-264.

13. Stein, R. P.; Scheibe, M.; Syverson, M. W.; Shaw, T. M.; and Gunton, R. C.: Recombination Coefficients of Electrons with NO^+ Ions in Shock-Heated Air. Phys. Fluids, vol. 7, Oct. 1964, pp. 1641-1650.

14. Eckerman, J.; and Stern, R. G.: Electron-Ion Recombination in High Temperature Air. Paper 63-445, AIAA Conference on Physics of Entry Into Planetary Atmospheres, MIT, 1963.

15. Eschenroeder, A. Q.; and Chen, T.: Ionization Behind a Sphere in Hypersonic Flight. I. Near-Wake Theory. AIAA J., vol. 4, Dec. 1966, pp. 2149-2154.

16. Dunn, M. G.; and Lordi, J. A.: Measurement of Electron Temperature and Number Density in Shock Tunnel Flows. Part II: NO^+ + e Dissociative-Recombination Rate in Air. AIAA J., vol. 7, Nov. 1969, pp. 2099-2104.

17. Gunton, R. C.; and Shaw, T. M.: Electron-Ion Recombination in Nitric Oxide in the Temperature Range 196 to 358°K. Phys. Rev., vol. 140, Nov. 1, 1965, pp. A756-A763.

18. Weller, C. S.; and Biondi, M. A.: Ambipolar Diffusion, Electron Attachment, and Electron-Ion Recombination in Nitric Oxide. Bull. Am. Phys. Soc., vol. 11, 1966, p. 495.

19. Yeung, R. A.; and St. John, G.: The Recombination Coefficient of NO^+ with e. Bull. Am. Phys. Soc., vol. 12, 1967, p. 218.

20. Doering, J. P.; and Mahan, B. H.: Photoionization of Nitric Oxide. J. Chem. Phys., vol. 36, Feb. 1, 1962, pp. 669-674.

21. Gunton, R. C.; and Inn, E. C. Y.: Rates of Electron Removal by Recombination, Attachment, and Ambipolar Diffusion in Nitric Oxide Plasmas. J. Chem. Phys., vol. 35, Nov. 1961, p. 1896.

22. Whitten, R. C.; and Poppoff, I. G.: A Model of Solar-Flare-Induced Ionization in the D Region. J. Geophys. Res., vol. 66, Sept. 1961, pp. 2779-2786; D. Region Ionization by Solar X-Rays, ibid, vol. 67, July 1962, pp. 2986-2988.

23. McElhinny, M. W.: Some Further Analyses of E-Layer Measurements in South Africa During the Solar Eclipse of 25 December 1954. J. Atmos. Terrest. Phys., vol. 14, June 1959, pp. 273-286.

24. Bates, D. R.; and Nicolet, M.: Ion-Atom Interchange. J. Atmos. Terrest. Phys., vol. 18, April 1960, pp. 65-70.

25. Sutton, E. A.: Chemistry of Electrons in Pure-Air Hypersonic Wakes. AIAA J., vol. 6, Oct. 1968, pp. 1873-1882.

26. Hansen, C. F.: Temperature Dependence of the NO^+ + e Dissociative-Recombination Rate Coefficient, Phys. Fluids, vol. 11, April 1968, pp. 904-906.

27. Gilmore, F. R.: Potential Energy for N_2, NO, O_2 and Corresponding Ions. Rand Memo RM-4034-PR, June 1964.

28. Weller, C. S.; and Biondi, M. A.: Temperature Dependence of Recombination of NO^+ Ions and Electrons. Paper B-4, 20th Annual Gaseous Electronics Conference, San Francisco, 18-20 Oct. 1967. (Also abstract, pg. 199, Bulletin of Am. Phys. Soc., vol. 13, no. 1, Jan. 29, 1968.)

CHAPTER III SIMPLE AVAILABLE ENERGY THEORY OF DISSOCIATION RATES

3.1 SUMMARY

A simple, available-energy theory is developed which provides numerical estimates of dissociation rates for diatomic and triatomic molecules, which generally agree with experimental data within a factor of 3, over a wide range of temperature and a variety of collision partners. Since other theories, even though often rather complex, are unable to provide better results, the available energy theory will probably remain a useful model for many engineering purposes until rigorous computer calculations of rate coefficients become economically and routinely available.

3.2 INTRODUCTION

A sizable number of theoretical models have been proposed for analysis of simple reactions such as atom exchange and dissociation. One widely studied model is the activated complex theory developed by Glasstone, Laidler, and Eyring (ref. 1). While this theory has been very useful conceptually, describing a short-lived molecular complex existing at the saddle point of a potential surface in equilibrium with the normally stable molecular species of which it is composed, the theory has not been very useful quantitatively. The reaction is described as a vibration-like motion along a trajectory crossing the saddlepoint, and the functional form of the crossing rate is derivable in part, but one is left with an undetermined transmission coefficient representing the fraction of systems which approach the saddlepoint that actually cross the barrier into the domain of the reaction products, the remainder is reflected back into the domain of the initial collision partners. This transmission coefficient is uncertain by many orders of magnitude and its functional form is undetermined, in general. It has been evaluated numerically only in a few special cases such as a collinear $H + H_2 \rightarrow H_2 + H$ type atom exchange reaction. Thus, for engineering purposes we seek a model that can be used for estimating dissociation rates with greater quantitative certainty.

Another theoretical approach that seems helpful is to calculate the flux of three-body recombination systems across a given surface S in phase space, which is chosen to separate the product domain from the reactant domain. In principle, this method is appropriate wherever classical mechanics is adequate to describe the motions involved. This flux F may be expressed

$$F = \int \rho \frac{dS/dt}{|\text{grad } S|} d\vec{\sigma} \tag{3.1}$$

where ρ is the density of points in phase space, usually chosen to be the equilibrium distribution density, S is the given surface defined as a function of the coordinates and their conjugate momenta, and $d\vec{\sigma}$ is the vector surface element. The concept "surface" means here a $(2m - 1)$ dimensional subspace in $2m$ dimensional phase space, where m is the appropriate number of sets of coordinates and their conjugate momenta. The derivative dS/dt divided by $|\text{grad } S|$ is the velocity with which the phase points cross this surface. Wigner (ref. 2) shows that if such a surface is properly chosen, namely so that the flux across the surface is minimized, then the recombination rate is rigorously determined. Keck (ref. 3) developed the method

further by using variational methods to find minimum values for surfaces having plausible functional forms. However, the calculations become increasingly intricate as one attempts to define this surface more rigorously, and the extension of the method to even triatomic molecule dissociation is discouragingly formidable. A related classical approach has been taken by Light and Arnstein (refs. 4 and 5), who solve the Liouville equation for diatomic molecule dissociation with the somewhat unrealistic assumption that collisions are adiabatic. Once again, the solutions become so intricate that they must be done numerically, and the extension to polyatomic molecule dissociation does not appear tractable. A very simple model for dissociation of diatomic molecules was proposed by Rice (ref. 6), in which he assumed that only molecules with vibrational energy within kT of the dissociation limit are capable of being dissociated by collision. This simple concept was extended by Benson and Fueno (ref. 7), who consider the recombination process as a cascade sequence of single vibrational quantum jumps from the top vibrational levels. However, this model overlooks the equally important role of rotational transitions in the cascade de-excitation process, as well as the strongly anharmonic effects which occur in the closely spaced vibrational levels near the dissociation limit, which promote multiple quantum transitions that are difficult to include.

All of the above models, and others not mentioned, provide certain conceptual insights into the dissociation mechanism, but when the quantitative results are considered, one is left with the conclusion that none of them, no matter how intricate the theory or the calculations performed, are superior for engineering purposes to a simple available energy theory described many years ago by Fowler and Guggenheim (ref. 8). This model has been found to reproduce observed dissociation rates generally within a factor of ten (ref. 9), which even to the present day is reasonably consistent with the uncertainties in experimental data. In spite of its obvious deficiencies as a modern scientific theory of reaction rates, it is still widely used for making engineering estimates of rates in connection with fluid-flow problems, and will probably continue to be used in this way until precise numerical computer quantum solutions of rates become routinely and economically available. Therefore, a brief analysis of the model is appropriate for our purposes here.

The available energy theory is similar in a way to the Wigner theory mentioned above; the principal difference is that the surface S is now taken to be a surface in phase space which all collision systems must cross, whether reactive or unreactive, rather than a surface which divides the two as in the Wigner approach. The fraction of the flux F in Eq. (3.1) which leads to reaction is simply taken to be that fraction with energy in a given number of degrees of freedom n, which equals or exceeds the activation energy of the reaction. This fraction is the reaction probability used in Eq. (2.16).

3.3 AVAILABLE ENERGY DISSOCIATION RATE MODEL

Consider the general collision induced dissociation reaction

$$AB + M \rightarrow A + B + M \tag{3.2}$$

with the rate coefficient α defined

$$\frac{d[AB]}{dt} = -\alpha[AB][M] \tag{3.3}$$

where the brackets signify concentrations. The rate coefficient is expressed as a collision rate θ and the probability P that dissociation results from a single collision

$$\alpha = \frac{\theta P}{s} \qquad (3.4)$$

the symmetry number s is the same as discussed in chap. II; s equals unity unless the molecules AB and M are identical, in which case it equals 2.

For a gas in equilibrium, θ is given by

$$\theta = (2\pi\mu kT)^{-3/2} \int_0^\infty \frac{p}{\mu} S(p) e^{-p^2/2\mu kT} 4\pi p^2 dp \qquad (3.5)$$

where p is the momentum of the colliding partners in center-of-mass coordinates, μ is the reduced mass of AB and M, and $S(p)$ is the total collision cross section for both favorable and unfavorable events.

The total cross section is not precisely known, but it is not difficult to estimate within a factor of about 2, sufficient for present purposes. The wave functions of outer electrons extend about the same range for all atoms and only slightly more for diatomic molecules, such that all total cross sections are the order of 30×10^{-16} cm^2. As a next approximation, the cross section can be considered a weak function of momentum p, namely the cross section appropriate for calculation of viscosity:

$$S = S_\infty\left(1 + \frac{8k\mu C}{\pi p^2}\right) \qquad (3.6)$$

where C is Sutherland's constant, a quantity the order of a few hundred degrees Kelvin for most atoms and molecules, and S_∞ is the constant cross section derived from viscosity measurements at high temperatures compared with the Sutherland constant. In this case, the collision rate given by Eq. (3.5) becomes

$$\theta = \left(\frac{8kT}{\pi\mu}\right)^{1/2} S_\infty\left(1 + \frac{4C}{\pi T}\right) \qquad (3.7)$$

The crucial problem is to evaluate the probability factor P in Eq. (3.4). Fowler and Guggenheim (ref. 8) consider the surface S to be any surface normal to the component of momentum between centers of the colliding particles, which the system crosses prior to collision. The flux of systems across this surface given by Eq. (3.1) is just

$$F = \int \cdots \int \frac{p_1}{\mu} e^{-E/kT} \, dp_1 \cdots dp_k dq_k \qquad (3.8)$$

where the phase density ρ has been taken as the exponential Boltzmann distribution, the velocity across the surface is p_1/μ, and the surface element $dp_k dq_k$ involves all the momenta and their conjugate coordinates except q_1, the coordinate that is held constant over the surface S. Then, assuming that the energy which contributes to the dissociation of AB involves just n terms with only momenta or coordinates

squared, and that the equilibrium distribution of energy exists among those modes, one finds that the fraction of this flux where the energy in these n degrees of freedom is greater than the dissociation energy D is given by

$$P = \frac{\int_D^\infty E^{(n-1)/2} \exp(-E/kT)dE}{(kT)^{(n+1)/2}\,\Gamma[(n+1)/2]} \tag{3.9}$$

The momenta and coordinates involved have been transformed to the energy variable E, which is the total energy in the n modes considered and includes the kinetic energy along the collision path. The factors in the denominator are just the normalization constants required so that the total probability goes to unity when both favorable and unfavorable events are considered.

The problem remaining is that the number of degrees of freedom which should contribute to dissociation is undefined. If only one degree of freedom is considered, that is the kinetic energy associated with the momentum of the collision partners along the direction between centers, the probability P is generally too small. On the other hand, if the total number of degrees of freedom involved in the two particles AB and M is used, P is invariably much too large. In this dilemma, the concepts provided by the activated complex theory are helpful. The energy which causes dissociation appears, at least momentarily, in the internal energy modes of this complex. Since energy is conserved, we assume that n is the number of internal degrees of freedom which disappear when the complex breaks up, and that the remaining degrees of freedom carry away their full share of the energy distributed among these degrees of freedom at equilibrium.

In general, the activated complex may include the collision partner, but for the present we consider this partner inert. The interaction potential in this case is normally approximated by a very steep, short range, repulsive potential which is spherically symmetric with respect to the closest atom of the molecule. The collision process is then conceived as a sudden discontinuity in one component of the molecule internal momentum modes, without change in the other momentum component or in the atomic position coordinates. This model is sometimes referred to as the sudden approximation. The activated complex is just the original molecule in which one component of internal momentum has suddenly taken a new distribution independent of the energy residing in the other modes. As in the Eyring theory (ref. 1), the activated molecule is taken to have a Boltzmann-like distribution of internal energies, except that we take the distribution to be bounded by the requirement that the molecule be stable before the collision event.

Now we choose the surface S, over which the flux of systems is calculated, orthogonal to the coordinate conjugate to the excited component of momentum — the component which has suffered the sudden discontinuity as a result of collision. (The momentum coordinates can always be transformed by rotation to bring one component parallel to the direction between atomic line of centers at impact). Then the fraction of the flux crossing S with energy in the excited mode between ε^* and $\varepsilon^* + d\varepsilon$ and with residual energy in the reamining (n - 1) modes between ε and $\varepsilon + d\varepsilon$ is given by

$$dP = \frac{\exp(-\varepsilon^*/kT)d\varepsilon^*}{kT} \cdot \frac{\varepsilon^{(n-3)/2}\exp(-\varepsilon/kT)d\varepsilon}{\Gamma[(n-1)/2](kT)^{(n-1)/2}} \tag{3.10}$$

The denominators in Eq. (3.10) are just the normalization constants required.

A somewhat subtle difference exists between the procedure above and the original ersion of the available energy theory expounded by Fowler and Guggenheim. Fowler nd Guggenheim chose a surface S which the systems cross prior to collision in valuating the flux of systems with sufficient energy to promote reaction; the problem n this approach is that we do not know a priori how many modes of energy will conribute to the activation process. In the present development, a surface has been hosen which the excited molecule crosses subsequent to collision; in this case the umber of degrees of freedom which contribute to the dissociation process is clear, ut we were forced to make an assumption about the distribution of energy in one of hese modes just after the collision event, specifically we chose the distribution to e Boltzmann. This is probably not a bad approximation for about 2/3 of the collision vents, where from the geometry of collision one expects a rotational mode to be the xcited one; a few collisions are known to be sufficient to promote a full Boltzmann istribution in rotational states, for example. However, objections to this assumption have been raised in connection with the remaining collisions which promote ibrational transitions; the vibrational transition probabilities are very small at sual collision velocities in gases and many collisions are required before a full oltzmann distribution is reached in this case. Perhaps the reason the assumption orks as well as it does is because the dissociation process normally proceeds only at emperatures rather higher than the characteristic vibrational temperatures involved. his means, first of all, that multiple quantum jumps are produced and the process ecomes classical like, in which the entire continuum spectrum of energy can be xcited in a single collision event. More important yet, high lying vibrational tates are available in the initial state before the collision event, and the dissociation reactions occur primarily from the upper states within kT of the dissociation limit, as postulated by Rice (ref. 6). These states lie close together, with trong anharmonic coupling, and the classical type impulse approximation becomes a easonable model in this case. Finally, the corrections for nonBoltzmann excitation f vibrational modes by the collision would be applicable only in about 1/3 of the ollision events anyway, which is well within the order of the approximation being onsidered with the available energy theory here.

Exercise 3.1: Show that if a portion of a molecule's energy ε depends on n squared coordinates q (which may be either momenta or position coordinates)

$$\varepsilon = \sum_{i=1}^{n} a_i q_i^2$$

the transformation from coordinate variables to the energy variable, transforms the integration volume element

$$\prod_{i=1}^{n} dq_i \to \varepsilon^{(n-2)/2} d\varepsilon$$

Further show that the normalization to unity of a Boltzmann distribution of energy in these n modes leads to

$$f(\varepsilon) = \frac{\exp(-\varepsilon/kT)\varepsilon^{(n-2)/2}}{\Gamma\left(\frac{n}{2}\right)(kT)^{n/2}}$$

In Eq. (3.10) the energy ε has an upper bound the order of the dissociation nergy D, whereas the normalization constant $\Gamma[(n-1)/2](kT)^{(n-1)/2}$ is for an nbounded Boltzmann distribution. However, for the temperatures of usual interest the atio D/kT is considerably greater than unity, in which case the correction required ls small. It will be neglected here for simplicity.

Integrating Eq. (3.10) over all combinations of internal energy greater than D, with ε^* unbounded and with $\varepsilon \leq D$, one obtains

$$P = \frac{\int_0^D \varepsilon^{(n-3)/2} \exp(-\varepsilon/kT)\left[\int_{D-\varepsilon}^{\infty} \exp(-\varepsilon^*/kT)\,d\varepsilon^*\right] d\varepsilon}{\Gamma[(n-1)/2](kT)^{(n+1)/2}} = \frac{(D/kT)^{(n-1)/2}\exp(-D/kT)}{\Gamma[(n+1)/2]} \qquad (3.11)$$

This is the same result obtained by Fowler and Guggenheim (ref. 8), except that higher order terms in kT/D are missing, terms which appear when the energy in each mode is considered unbounded and independent.

In the dissociation of diatomic molecules, for example, four internal energy degrees of freedom disappear when the molecule breaks apart: two rotational and two vibrational degrees of freedom. (Recall that a single vibrational mode has two degrees of freedom, one associated with the kinetic energy of vibrational motion and the other with the potential energy term. On the other hand, each rotational mode has a single degree of freedom associated with kinetic energy of rotational motion; a potential is not involved in these modes). Thus $n = 4$ in this case, and the probability factor to be used in Eq. (3.4) for the rate coefficient is

$$P_{n=4} = \left(\frac{16}{9\pi}\right)^{1/2}\left(\frac{D}{kT}\right)^{3/2} e^{-D/kT} \qquad (3.12)$$

Two corrections to the preceding model for diatomic molecule dissociation can be included rather simply. The rotation of the diatomic molecule contributes a term $\ell^2/2\mu r^2$ to the effective interatomic potential (ref. 3), where ℓ is the angular momentum; thus, instead of integrating throughout a domain bounded by a simple surface of constant energy D, one should integrate throughout an ellipsoid-like domain in energy space depending upon the rotational state. In addition, the upper limit of the outer integral in Eq. (3.11) should be reduced by the initial energy in the excited mode, and the result averaged over this distribution of initial energy. For purposes of approximation one can simply add an average rotational barrier equal to kT ($kT/2$ for each of the two rotational modes involved), and take the initial energy in the excited momentum mode as the average value $kT/2$. Then the probability factor for diatomic molecule dissociation becomes

$$P_{n=4} = \frac{\int_0^{D+kT/2} \varepsilon^{1/2} \exp(-\varepsilon/kT)\left[\int_{D+kT-\varepsilon}^{\infty} \exp(-\varepsilon^*/kT)\,d\varepsilon^*\right] d\varepsilon}{\Gamma(3/2)(kT)^{5/2}} = \left(\frac{16}{9\pi}\right)^{1/2}\left(\frac{D}{kT}+\frac{1}{2}\right)^{3/2} \exp(-D/kT - 1) \qquad (3.13)$$

The factor $1/2$ introduced into the pre-exponential term by these corrections is rather negligible, but the factor -1 in the exponent is significant; it represents the correction for the rotational barrier, that is the increase in dissociation energy that occurs when the molecule is rotating.

Other corrections could be considered. For example anharmonic effects are important at high temperature and the energy is no longer well approximated by a simple

quadratic sum. At low temperatures quantum effects become noticeable, and the integrations should all become summations. However, the approximate nature of the available energy model is inconsistent with a detailed analysis of higher order effects. We expect the model to provide only some numerical estimates of rate coefficients; precise effects of anharmonicities and quantization should be assessed with more rigorous theoretical models.

Consider next a linear, triatomic molecule with a total of 10 degrees of internal freedom (2 rotational degrees of freedom, 4 degrees of freedom associated with the two vibrational stretch modes, and 4 more associated with the two vibrational bending modes). The diatomic fraction formed in dissociation preserves 4 degrees of internal energy, so the number of active degrees of freedom which disappear and contribute to the dissociation process is taken to be 6. Once again the two rotational modes will be considered to increase the effective potential along any of the stretching or bending coordinates by kT and $D + kT/2$ will be taken as the bound on the five active modes unexcited by the collision. Then the probability factor becomes

$$P_{n=6} = \frac{\int_0^{D+kT/2} \varepsilon^{3/2} \exp(-\varepsilon/kT) \left[\int_{D+kT-\varepsilon}^{\infty} \exp(-\varepsilon^*/kT) d\varepsilon^* \right] d\varepsilon}{\Gamma(5/2)(kT)^{7/2}} \qquad (3.14)$$

$$= \frac{8}{15\pi^{1/2}} \left(\frac{D}{kT} + \frac{1}{2} \right)^{5/2} \exp(-D/kT - 1)$$

A nonlinear triatomic molecule has 9 degrees of internal freedom (one more rotational mode than the linear triatomic molecule, but one less vibrational bending mode with its 2 degrees of freedom). Thus $n = 5$ for this case. The three rotational modes are considered to increase the effective potential barrier along any stretching coordinate by $3kT/2$, and the four active modes which remain unexcited are accordingly bounded by $D + kT$. In this case the probability factor used in Eq. (3.4) becomes

$$P_{n=5} = \frac{\int_0^{D+kT} \varepsilon \exp(-\varepsilon/kT) \left[\int_{D+3kT/2-\varepsilon}^{\infty} \exp(-\varepsilon^*/kT) d\varepsilon^* \right] d\varepsilon}{\Gamma(2)(kT)^3} \qquad (3.15)$$

$$= \frac{1}{2} \left(\frac{D}{kT} + 1 \right)^2 \exp(-D/kT - 3/2)$$

In the case of triatomic molecules, the collisions might be expected to excite at least two modes of internal energy. For example, an end on collision with the linear triatomic molecule would excite a component of momentum feeding both the symmetrical and asymmetrical stretch vibrational modes. Similarly, a collision normal to the molecular axis would simultaneously excite one of the bending vibrational modes and one of the rotational modes. Two modes can be assumed to be excited merely by shifting one mode from the integration over ε (the energy in the unexcited modes) into the integration over ε^* (the energy in the excited modes). When this is done, the results obtained are the same except for some small higher-order terms. These are negligible at temperatures of usual interest ($kT \ll D$) as found in the following exercise. Thus, the above model is considered adequate for purposes of estimating numerical values for dissociation rate constants.

Exercise 3.2: Assume that collisions excite exactly two degrees of freedom, in both linear triatomic molecules and nonlinear triatomic molecules, in unbounded Boltzmann energy distributions. Calculate the probability that collision leads to dissociation. Show that the results are the same as when the collision was assumed to excite just 1 degree of freedom in the molecule, except for correction terms the order of $(D/kT)^{-1/2}$ smaller than the leading term.

3.4 COMPARISONS OF AVAILABLE ENERGY THEORY OF DISSOCIATION RATES WITH EXPERIMENT

Experimental values of dissociation rates are available for a number of diatomic molecules and a few triatomic molecules. Up to 1965 these are summarized by Hansen (ref. 9); some more recent measurements have appeared, but as far as the author is aware none of these have to date significantly changed the situation, either in terms of numerical values or experimental scatter. The totality of all these results is given in figure 3.1, where the logarithm of the ratio of the theoretical dissociation rate coefficient (given by the available energy theory) to the measured rate coefficients is shown as a function of the dimensionless temperature kT/D. The effective cross sections have been taken three times smaller than the viscosity cross sections when inert atoms are the collision partners, equal to the viscosity cross sections when stable molecules are the collision partners, and three times larger than the viscosity cross sections when the collisions are with reactive atoms such as O or N. This is in accord with the observed variation of O_2 dissociation with different collision partners, for example. With this assumption, a large majority of the data scatters within a factor of 3 about the predicted values. The single points represent mean values for sets of data measured under identical conditions by a single experimental team; often the scatter in such data sets is the same order as the range of discrepancy between theory and experiment. The figure includes dissociation rates for both triatomic molecules such as O_3, CO_2, N_2O, NO_2, and H_2O and a wide variety of diatomic gases such as O_2, N_2, NO, and the halogens. Collision partners include inert gases such as Ar and Xe, the same or other diatomic molecules, and O atoms. The various sources of data are cited in reference 9. Without going into all the details of each specific case, the main point to be emphasized is that the available energy theory can be useful in estimating numerical values of dissociation rates for a wide variety of collision partners and over a wide range of temperature. Very likely the model would be equally useful for some other types of reaction such as atom exchange, though detailed comparisons between the model and data have apparently not been carried out for such cases.

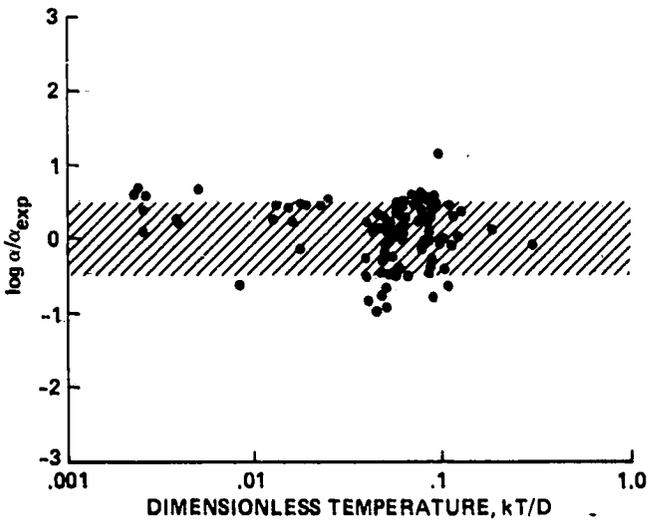

Figure 3.1- Ratio of predicted to measured dissociation rates as a function of dimensionless temperature.

Exercise 3.3: You have run experiments in a shock tube using dilute mixtures of O_2 in Ar, so that you can assume the gas kinetic collisions with O_2 are only with an Ar atom partner. Various strength shock waves are produced in this mixture at temperatures which dissociate the O_2, and the O_2 concentration and rate of change of concentration are measured using UV absorption at 1470 Å, following the method pioneered by Camac and Vaughan (ref. 10). The shock-excited gas temperature and density are determined by measuring the shock velocity, using well-known relations between shock properties and the shock wave speed (ref. 11). In this way the following data have been obtained:

T, °K	cc/mol sec	T, °K	cc/mol sec	T, °K	cc/mol sec
7635	2.0×10^{11}	5495	8.0×10^{9}	4485	2.0×10^{9}
7635	1.9×10^{11}	5235	4.2×10^{9}	4330	1.2×10^{9}
6945	9.5×10^{10}	5180	3.9×10^{9}	4330	8.4×10^{8}
6535	7.0×10^{10}	5180	8.0×10^{9}	4185	5.6×10^{8}
6330	5.5×10^{10}	5000	6.0×10^{9}	4165	7.6×10^{8}
6330	5.0×10^{10}	5000	3.8×10^{9}	4100	4.0×10^{8}
6175	2.5×10^{10}	4545	5.8×10^{9}	3705	1.3×10^{8}
5880	3.2×10^{10}	4545	3.0×10^{9}	3570	6.0×10^{7}
5555	1.4×10^{10}	4715	2.4×10^{9}	3450	4.0×10^{7}
5465	1.2×10^{10}	4610	2.0×10^{9}	3460	3.9×10^{7}

a) Graphically fit this data to a simple Arrhenius formula $\alpha = \alpha_o \exp(-E/kT)$, find the values of the constants α_o and E which provide a best fit.

b) Now fit a formula for the simple available-energy theory to this data

$$\alpha = \alpha_o (D/kT) \exp(-D/kT) \tag{3.16}$$

where the characteristic dissociation temperature, D/k, is 58,970 K. How does α_o compare with the values found above?

c) Calculate the mean square deviation of the data from the two formulas above. Is the difference significant?

In figure 3.2 the data from exercise 3.3 above are plotted

$$\ln \alpha - \frac{3}{2} \ln\left(\frac{D}{kT} + \frac{1}{2}\right) + \frac{1}{2} \ln \frac{D}{kT} \text{ vs } \left(\frac{D}{kT} + 1\right)$$

in order to find a good fit of the data to the modified available energy formula of Eq. (3.13), which was derived to fit this case of collision-induced dissociation of a diatomic molecule.

$$\alpha = \alpha_o \frac{[(D/kT) + (1/2)]^{3/2}}{(D/kT)^{1/2}} e^{-(D/kT+1)} \tag{3.17}$$

$$\alpha = 1.59\times10^{14} \frac{[(58{,}970/T) + (1/2)]^{3/2}}{(58{,}970/T)^{1/2}} e^{-(D/kT+1)} \text{ cc/mol sec} \tag{3.17a}$$

The factor 1/2 in the pre-exponential term of Eqs. (3.17) and (3.17a) is rather unimportant; however, the factor 1 in the exponent does make a noticeable difference in the value of α_o. Nevertheless, either equations 3.16 or 3.17 will fit the data about equally well.

Exercise 3.4: Calculate the root mean square deviation of the data from the formula of Eq. (3.17a) and also from the fit to the formula of Eq. (3.16). Is there a significant difference? What would need to be accomplished experimentally to differentiate between the various formulas?

The problem encountered in fitting theoretical expressions to reaction rate data is that all reactions span a finite range of temperature over which they can be measured. If the reaction is very slow, the shock tube experimenter will not detect any reaction; if the reaction is very fast, the reaction will appear to be instantaneous in terms of the spatial or temporal resolution of the instrumentation – in the present example, the finite width of the UV absorption beam through which the reacting flow is streaming. A correction factor like 1/2 in the factor (D/kT + 1/2) is not going to be noticed as significant until the temperature T becomes the same order as the characteristic reaction temperature D/k; at these temperatures the reaction becomes instantaneous for most practical purposes.

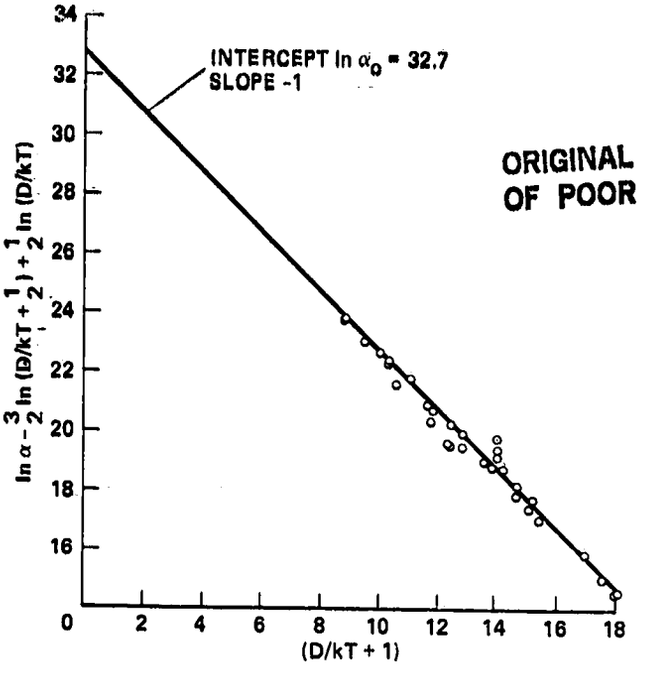

Figure 3.2- Dissociation rates of O_2 produced by collisions with Ar.

3.5 CONCLUDING REMARKS

The somewhat surprising thing about dissociation rate theories is that very different models yield approximately the same sort of correlation with experiment, upon judicious adjustment of some of the semi-empirical factors that appear. These models incorporate a range of assumptions such as the applicability of optical selection rules (ref. 7), of purely classical behavior (ref. 2), of adiabatic type collisions (ref. 4), of impulsive type collisions, etc. Sometimes the more rigorous the model attempts to be, the worse the correlation becomes (ref. 5). Thus, agreement with experimental data is not a sufficient test to differentiate between the merits of one approach over another, though it is certainly a necessary condition that must be satisfied by any model deserving serious consideration. All of this again points to the elemental stage of development of reaction rate theory, and the current need for more rigorous approaches such as may be provided by modern computer methods. In the meantime, the available energy model is as good or better than most other models, it is simpler and analytic, and it provides numerical approximations that are useful for some engineering purposes, at least, if not fully satisfying from a rigorous scientific point of view.

The available-energy theory cannot be expected to fill the need for a scientific theory of reaction rates; it is too simplified and tied to purely classical concepts. For example, it cannot be expected to work well for processes such as impact ionization and electronic excitation where quantum transitions at a potential crossing are important; however, for processes such as dissociation of molecules composed of heavy atoms, whose motions are classical, the simple available energy theory seems to give reasonably reliable results.

REFERENCES

1. Glasstone, S.; Laidler, K. J.; and Eyring, H.: The Theory of Rate Processes. McGraw Hill, N. Y., 1941.

2. Wigner, E.: Calculations of the Rate of Elementary Association Reactions. J. Chem. Phys., vol. 5, Sept. 1937, pp. 720-725.

3. Keck, J. C.: Variational Theory of Chemical Reaction Rates Applied to Three Body Recombinations. J. Chem. Phys., vol. 32, April 1960, pp. 1035-1050.

4. Light, J. C.: Dissociation of Gaseous Diatomic Molecules: Classical Adiabatic Scattering Approach. J. Chem. Phys., vol. 36, Feb. 1962, pp. 1016-1030.

5. Light, J. C.; and Arnstein, R.: Dissociation of Diatomic Molecules. II. Effect of Anharmonicities. J. Chem. Phys., vol. 37, Nov. 1962, pp. 2240-2246.

6. Rice, O. K.: On the Recombination of Iodine and Bromine Atoms. J. Chem. Phys., vol. 9, March 1941, pp. 258-262.

7. Benson, S. W.; and Fueno, T.: Mechanism of Atom Recombination by Consecutive Vibrational Deactivations. J. Chem. Phys., vol. 36, Mar. 1962, pp. 1597-1607.

8. Fowler, R. H.; and Guggenheim, E. A.: Statistical Thermodynamics, Chapt. XII. Cambridge U. Press, 1952.

9. Hansen, C. F.: Estimates for Collision-Induced Dissociation Rates. AIAA J., vol. 3, Jan. 1965, pp. 61-66.

10. Camac, M.; and Vaughan, A.: O_2 Dissociation Rates in O_2-Ar Mixtures. J. Chem. Phys., vol. 34, Feb. 1961, pp. 460-470.

11. Hansen, C. F.: Molecular Physics of Equilibrium Gases. NASA SP-3096, 1976.

CHAPTER IV EFFECTS OF EXCITED STATES ON REACTION RATES

4.1 SUMMARY

Reaction cross sections are observed to have the same type of functional dependence on excess collision energy for the excited states as they do for the ground states of molecular gas species. Approximate expressions for the total rate coefficient including the effects of excited species are derived, and the effects on the rates and on the apparent activation energy of reaction are assessed.

4.2 INTRODUCTION

Usually, chemical reactions are expressed by equations such as

$$A + B \rightleftharpoons C + D \tag{4.1}$$

with corresponding forward and reverse rate expressions in terms of a reaction rate coefficient α_f and α_r and total species concentrations [A], [B], [C], and [D]

$$R_f = \alpha_f[A][B] \ , \qquad R_r = \alpha_r[C][D] \tag{4.2}$$

Such an equation tacitly implies that the reaction takes place between ground state species. This can be misleading, for most reactions proceed predominantly from collisions involving excited states such as

$$A + B^* \rightarrow C + D \tag{4.3}$$

The cross sections for such collisions are generally so much larger than for collisions involving ground state species, that this more than compensates for the effect of the lower species concentrations of excited states that exist in the usual Boltzmann distribution among states. In discussing this problem we will focus attention on impact ionization reactions such as

$$A + B^* \rightarrow A + B^+ + e \tag{4.3a}$$

where A may be an atom or molecule or another electron, and B may be either an atom or molecule. This will allow us to make use of some direct cross-section measurements which are available for this type of reaction, but which are not as generally available for other reactions such as rotational and vibrational excitation, atom exchange, and dissociation.

A number of cross sections for heavy particle-impact ionization have been measured within an electron volt or so of threshold; these are summarized in figure 2.5. Similarly, the electron impact ionization cross sections are summarized in figure 2.6. Although some structure appears on some of the curves and not on others, and quantitative differences the order of 10 to 100 appear, all the measured ionization cross sections have a similar form when shown as functions of impact energy above threshold, $E - E^*$. Near threshold the logarithm of the cross section increases linearly with $\log(E - E^*)$ with a nearly constant slope, m, which is typically between 2 and 3 for heavy particle-impact ionization and between 1 and 2 for electron-impact ionization.

The cross-section functions then level off at about 10^{-15} to 10^{-16} cm^2 at impact energies about 100 eV above threshold. The above measurements are all for ground state molecular species, and the cross-section function for excited state species will also be needed in order to assess the effect of excited states on a reaction of this type. Utterback and Van Zyl (ref. 1) found that the form of the cross section for ionization of N_2 by impact with $Ar(^1S)$ was essentially the same whether the N_2 was in the ground state $N_2(X^1\Sigma)$ or the excited state $N_2(A^3\Sigma)$ as shown in figure 4.1. This equivalence of ground state and excited state cross-section functions is not necessarily universal; one expects transition probabilities to depend on the degeneracies of the potential surfaces and the gradients of the surfaces at the transition point. Moreover, colliding molecules usually enter a network of transition points involving a number of excited state potentials, as in figure 2.8. Thus, the total transition probability can be a rather complex function, which undoubtedly accounts for some of the structure and variation in cross-section magnitudes shown in figures 2.5 and 2.6. Nevertheless, on the average we expect all cross sections to have a similar functional dependence on the excess collision energy, $E - E^*$, and for purposes of approximating the effects of excited states in reaction processes we will assume that all cross sections for the same species have the same slope, m, near threshold, regardless of the state of excitation, but will allow the constant S to increase as the size of the outer electron wave function increases in excited states.

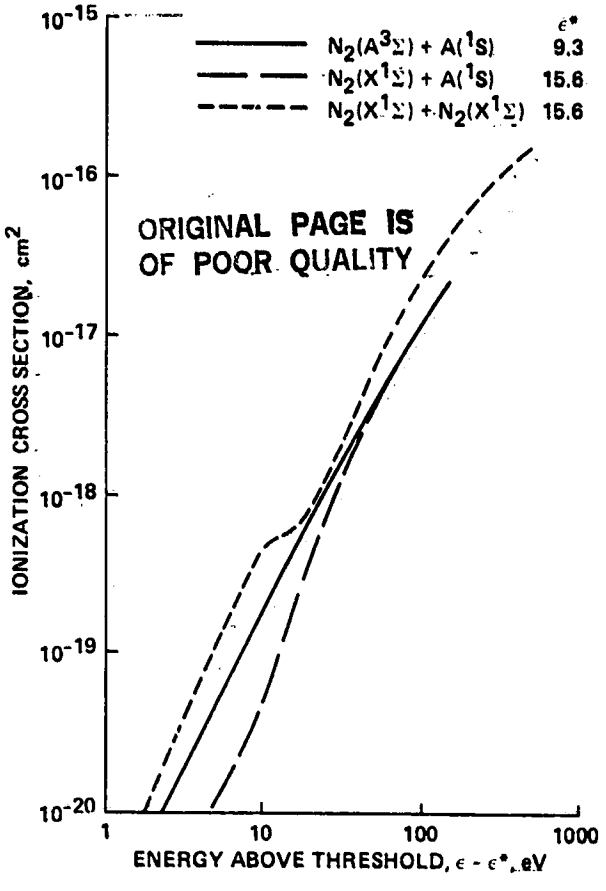

Figure 4.1- Effect of electronic excitation on cross section.

In accord with the above considerations, we assume that all cross sections for the same atom or molecule have a universal form of the following type:

$$S = S_o\left(1 - \frac{E^*}{E}\right)\left(\frac{E}{E^*} - 1\right)^{m-1}, \quad E^* < E < 2E^*$$
$$= S_o\left(1 - \frac{E^*}{E}\right), \quad 2E^* < E \qquad (4.4)$$

The factor $(1 - E^*/E)$ is just that required by conservation of angular momentum and the factor $(E/E^* - 1)^{m-1}$ represents a probability that transition occurs between the reactant and product potential surface once the collision system reaches the reaction configuration, as discussed in chapter II. The slope, m, is taken to be the same constant for all states, and S_o will be chosen as a different constant for each state, increasing with the size of the outer electron wave function. Although the function given by Eq. (4.4) does not decrease at very large impact energy E as it should, this discrepancy will usually occur so far beyond the peak of the Boltzmann

energy distribution that the error is negligible as far as the rate coefficient is concerned.

Integrating the cross section of Eq. (4.4) in Eq. (2.22) one obtains

$$\alpha = \frac{\bar{u}S_0\, e^{-\beta E^*}}{g} H_m(\beta E^*) \tag{4.5}$$

where $H_m(\beta E^*)$ is given by the solid lines of figure 4.2. Provided the slope of the ln of the cross section as a function of $\ln(E - E^*)$ is not greater than 3, a good approximation for $H_m(\beta E^*)$ is obtained by joining the asymptotic limits

$$\left.\begin{aligned} H_m(\beta E^*) &= m!/(\beta E^*)^{m-1}, \quad \beta E^* \gg 1 \\ &= 1, \quad \beta E^* \ll 1 \end{aligned}\right\} \tag{4.6}$$

these limits are the dashed curves in figure 4.2.

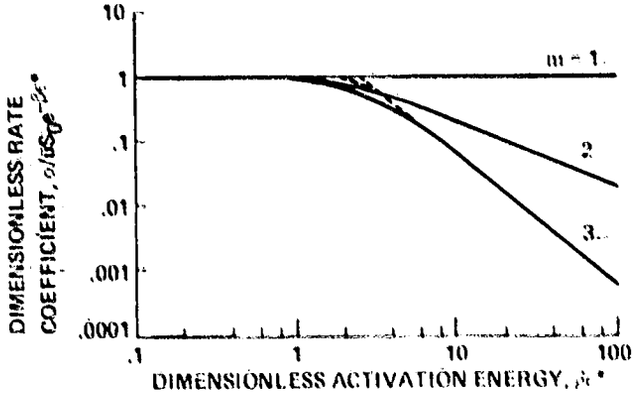

Figure 4.2- Effect of cross-section shape on the Arrhenius form of the rate coefficient.

Exercise 4.1: Assume the reaction cross section has the form

$$s = s_0\left(1 - \frac{x^*}{x}\right)^m$$

where $x = \beta E = E/kT$ and $x^* = \beta E^* = E^*/kT$, the value of x at the reaction threshold. Calculate the probability factor $H_m(x^*)$ as defined in the relation

$$\alpha = \bar{u}S_0\, e^{-x^*} H_m(x^*)$$

for the limiting cases $x^* \ll 1$ and $x^* \gg 1$. Expand in powers of x^* and $1/x^*$, respectively, and find the first three terms in the expansion. Show that the first order terms are the relations given by Eq. (4.6).

Exercise 4.2: Derive the result of Eq. (4.15). Assume that the collision partners are primarily ground state argon atoms.

For exothermic reactions the rate coefficient will have the same form as the reverse rate coefficient α_r for endothermic reactions. By detailed balancing

$$\frac{\alpha}{\alpha_r} = \frac{g^*}{g} e^{-\beta E^*} \tag{4.7}$$

where g and g* are the products of the degeneracies of reactant and resultant species, respectively. Thus

$$\alpha_r = \frac{\bar{u}}{s}\left(S_o \frac{g}{g^*}\right) H_m(\beta E^*) \qquad (4.8)$$

the constant factor $(S_o g/g^*)$ may be interpreted as a total cross section for the reverse reaction, with probability of de-excitation equal to $H_m(\beta E^*)$.

4.3 EFFECT OF EXCITED STATES ON RATES

The total rate for reaction between two molecular species with a multiplicity of excited states is given by

$$R = \alpha n n' = \sum_{i,j} \alpha_{ij} n_i n'_j \qquad (4.9)$$

where n is the total concentration (that is, $\Sigma\, n_i$), n_i is the concentration of excited species in level i, and the primes designate the second species involved. The coefficients α_{ij} are given by equations such as (4.5). Although the concentrations of excited species fall off as a Boltzmann distribution, the cross sections and the rate coefficients increase rapidly as the state of excitation increases, due to the decrease in the activation energy E* for the upper states. This more than compensates for the decrease in population density, so that the rate coefficient is dominated by the contribution from upper states.

Equation (4.9) can be rearranged to yield an explicit expression for the total rate coefficient α, normalized to the rate coefficient for the ground state species α_{oo}.

$$\frac{\alpha}{\alpha_{oo}} = \frac{g_o g'_o}{QQ'} \sum_{i,j} \left(\frac{\alpha_{ij}}{\alpha_{oo}}\right)\left(\frac{n_i}{n_o}\right)\left(\frac{n'_j}{n'_o}\right) \qquad (4.10)$$

The index zero designates the ground state, Q is the partition function, g_o is the ground-state degeneracy, and n has been replaced by $n_o Q/g_o$. For the assumed form of the cross sections and Boltzmann populations of excited states, Eq. (4.10) becomes

$$\frac{\alpha}{\alpha_{oo}} = \frac{g_o g'_o}{QQ'} \sum_{i,j} \left(\frac{S_{ij}}{S_{oo}}\right)\left(\frac{g_i g'_j}{g_o g'_o}\right)\left(\frac{H_m(\beta E^*_{ij})}{H_m(\beta E^*_{oo})}\right) \qquad (4.11)$$

The constants S_{ij} represent the appropriate asymptotic cross-section limits, and E^*_{ij} is the appropriate activation energy, in this case $I - E_i - E'_j$, where I is the ground-state ionization energy and E_i and E'_j are the electronic excitation energy of states i and j for the two species, respectively.

A reaction is observed only when the products are out of equilibrium with the reactants. Then the populations are not strictly Boltzmann as assumed in Eq. (4.11) but are given by solutions to a set of master equations, such as formulated by Keck and Carrier (ref. 2). These solutions will be discussed later; for the time being we

merely use the result that the rate coefficients are approximately duplicated if the Boltzmann distributions are simply truncated about kT below the ionization limit.

The principal result to note from Eq. (4.11) is that the exponential factors in the population densities and in the rate coefficients have cancelled. Thus, terms become increasingly larger as the internal energy of the reactants increases. The factor $g_o g_o'/QQ'$ is near unity, except at very high temperature, and can be disregarded. The ratio S_{ij}/S_{oo} is expected to be about the ratio of total scattering cross sections, other factors being assumed equal. The mean size of atoms or molecules, that is the outer electron wave functions, varies about inversely as the ionization energy; thus

$$\frac{S_{ij}}{S_{oo}} \simeq \left(\frac{r_i + r_j'}{r_o + r_o'}\right)^2 \simeq \left[\frac{(I - E_i)^{-1} + (I' - E_j')^{-1}}{(I)^{-1} + (I')^{-1}}\right]^2 \qquad (4.12)$$

where I and I' are the ground-state ionization energies. Values of 2 to 5 are typical before cutoff is reached at kT below the ionization limit. The ratio $g_i g_j'/g_o g_o'$ is typically about 10, because excited states usually have somewhat larger degeneracies than ground states due to the fact that in most cases electron spins are not as completely paired in excited states. However, the factor which can exceed unity by the greatest margin is

$$\left(\frac{\beta E_{oo}^*}{m!}\right)^{m-1} < \frac{H_m(\beta E_{ij}^*)}{H_m(\beta E_{oo}^*)} < \left(\frac{E_{oo}^*}{E_{oo}^* - E_i - E_j'}\right)^{m-1} \qquad (4.13)$$

This ratio can be 10^2 or more. From Eq. (4.8) it follows that when $E_{ij}^* < 0$, the terms decrease as $\exp(\beta E_{ij}^*)$; thus the effects of exothermic collisions are essentially negligible.

The predicted cumulative effect of all these factors is illustrated in figure (4.3) for heavy particle-impact ionization involving a number of different collision partners. The Boltzmann distributions have been truncated 2kT below the ionization limit for atoms, and the molecular states are truncated kT below the dissociation limit in these calculations, the latter accounting for depopulation of high molecular levels by escape to dissociated fractions. Although the calculations are not expected to give exact quantitative results, in view of the various approximations used, the conclusion that α can be many orders of magnitude larger than α_{oo} is certainly valid. The result indicates that collisions involving excited species will dominate ionization reactions of this type, provided that the gas is dense enough so

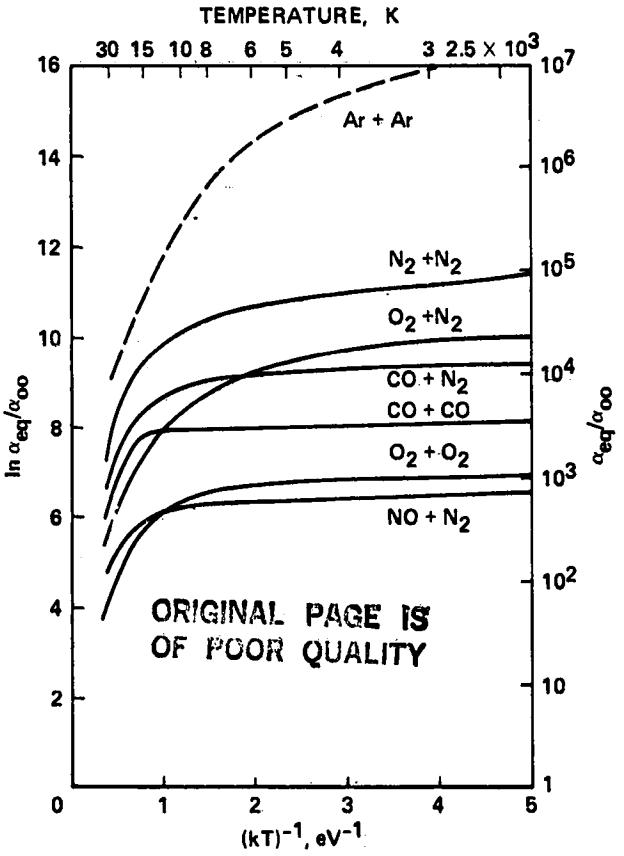

Figure 4.3- Effect of excited states on reaction rate coefficients for heavy particle impact ionization.

that populations of the excited species are established primarily by collisions, rather than radiative decay.

4.4 EFFECT OF EXCITED STATES ON APPARENT ACTIVATION ENERGY

The derivative ($-d \ln \alpha/d\beta$) has traditionally been equated with the true activation energy by reaction chemists (i.e., the negative slope of an Arrhenius plot, $\ln \alpha$ vs β). However, the apparent activation energy of the reaction is

$$-\frac{d \ln \alpha}{d\beta} = \left(-\frac{d \ln \alpha_{oo}}{d\beta}\right) - \left(\frac{d \ln \alpha/\alpha_{oo}}{d\beta}\right) \tag{4.14}$$

The first term is the true activation energy E* plus corrections for the shape of the cross-section function, if any, as discussed in chapter II. The second term is the decrease in apparent activation energy due to the increasing depopulation of upper levels at higher temperature. This is just the slope of the curves on figure 4.3. At 10^4 K these slopes are typically about 1 to 4 eV for the various reactions shown, which are rather large corrections. At lower temperatures the slopes vanish and the correction to the activation energy for the effect of excited states then becomes negligible, as does the correction for the shape of the cross-section function. Only at these low temperatures is it justified to equate the activation energy with the slope of an Arrhenius plot. In the literature it is common to identify this slope with the internal energy of some particular excited species which is presumed to be formed in the rate-controlling step of the total process. However, at high temperatures we see that this slope need not correspond with any particular energy level. A case in point is the excitation-ionization of argon.

4.5 HEAVY PARTICLE IMPACT IONIZATION OF ARGON

Heavy particle-impact ionization is not a reaction of importance in any practical problem; even the ionization of argon itself is rapidly dominated by electron-impact ionization as soon as a small fraction of electrons are formed, so at most, the heavy particle impact ionization of argon is significant only as a precursor event which triggers the principal ionization reactions as argon is suddenly heated in a shock tube, for example. Nevertheless, the reaction has been widely studied in shock tubes (refs. 3-5) because it is one of the few reactions which can be produced in gas phase in the shock tube without the ambiguity of competing reactions (at least during the initial stage while electron concentrations are low), since there are no other internal degrees of freedom for the argon atom. The ionization potential of argon (15.68 eV) is considerably lower than that of He (24.46 eV) and of Ne (21.47 eV), so the reaction is considerably easier to excite in argon with normal shock tube operating conditions, than in the latter two noble gas test specimens. Krypton (ionization potential 13.93 eV) and Xenon (ionization potential 12.08 eV) are even easier to ionize, and some ionization rate measurements have been made with shock tubes for these gases as well (ref. 5). Some recent measurements made by Schneider and Park (ref. 6) suggest that even these simple reactions may be masked by ionization of NaCl which is absorbed from the natural atmosphere on the shock tube walls and deadsorbed during the test interval, so at this point it is not clear whether the heavy particle-impact ionization of argon has even been measured correctly. However, the analysis of the experiment will nevertheless be instructive for our purposes here. Moreover,

heavy particle impact ionization of argon is the only reaction measured in the shock tube for which a corresponding cross section has been measured with molecular beam equipment (ref. 7). Thus, the reaction takes on major significance from a scientific viewpoint, even if not from an applications viewpoint, because it is the only reaction where some kind of comparison can be made between a measured rate coefficient and a measured cross section. Unfortunately, the cross sections have not been measured closely enough to threshold to provide a really convincing comparison, but again the comparisons which are possible provide some valuable insight into the reaction process.

The measurements of the bulk rates (refs. 3-5) differ from one another by a factor of about 10 as shown in figure 4.4, but all experimenters find an apparent activation energy ($-d \ln \alpha / d\beta$) of about 11.5 eV. The fact that 11.5 eV is the energy of the first excited multiplet of electronic states of Ar (including one metastable level $4s[3/2]^o$ with $J = 2$, which does not have a dipole transition to the ground level ^1S state of argon) naturally led all investigators to conclude that the production of excited Ar was rate controlling in the two-step process.

$$Ar + Ar \underset{\alpha_{rev}}{\overset{\alpha}{\rightleftharpoons}} Ar + Ar^* , \quad E^* = 11.5 \text{ eV} \qquad (4.14a)$$

$$Ar + Ar^* \xrightarrow{\alpha'} Ar + Ar^+ + e , \quad E^* = 4.2 \text{ eV} \qquad (4.14b)$$

If the concentration of Ar* is steady, the effective rate constant is

$$\alpha_{eff} = \frac{\alpha\alpha'}{\alpha_{rev} + \alpha'} \qquad (4.15)$$

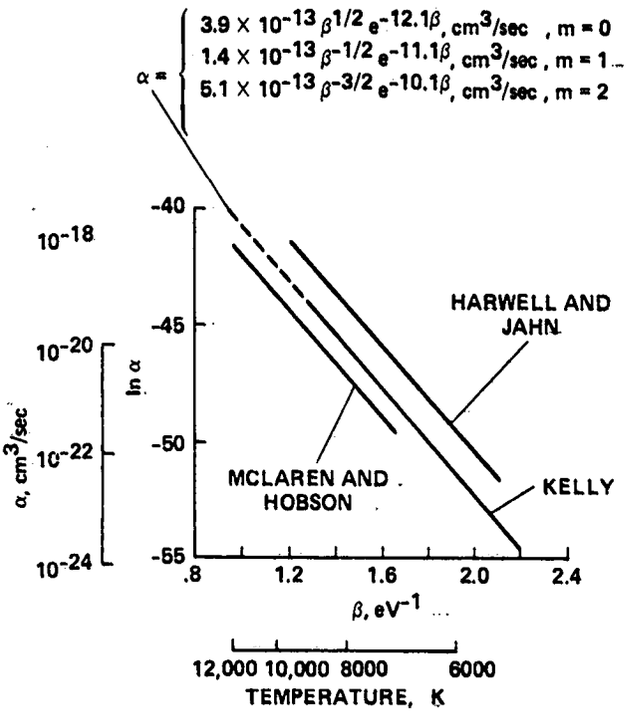

Figure 4.4- Argon ionization rate coefficient.

Thus, if $\alpha' >> \alpha_{rev}$, the first step of the reaction is rate controlling, $\alpha_{eff} \simeq \alpha$, and the activation energy is about 11.5 eV, neglecting the effects of the shape of the cross-section function. On the other hand, if $\alpha' << \alpha_{rev}$, then the effective rate coefficient is $\alpha_{eff} \simeq \alpha\alpha'/\alpha_{rev}$, and the activation energy is about the sum of the two activation energies, or the full ionization potential, 15.7 eV. At temperatures where the two rate coefficients are about equal, intermediate values of the apparent activation energy are expected.

Incidentally, the three equations shown for α in figure 4.4 all fit Kelley's data (ref. 4) equally well, and illustrate how the bulk rate data taken over a narrow range of temperature are not useful for determining the shape of the cross-section function. The three equations with pre-exponential factors $\beta^{1/2}$, $\beta^{-1/2}$, and $\beta^{-3/2}$ correspond to cross section functions with slopes $m = 0$, 1, and 2, respectively.

The data would need to be extended over a range of temperature difference of about a factor of 10, rather than a factor of 2, to differentiate between these functions.

As we see, the first step in the assumed reaction, Eq. (4.14a) is rate controlling only when $\alpha_{rev} << \alpha'$. Except at very high temperature, we do not expect this inequality to hold, since the second step requires 4.2 eV activation energy. The inequality would require an abnormally small cross section for the de-excitation process, Eq. (4.14a), which would then violate the principle of detailed balancing. For example, if we take the slope of the cross-section functions to be $m = 2$, for both the excitation and ionization processes of Eq. (4.14)

$$\alpha = \bar{u} S_1 \left(\frac{2kT}{E_1^*}\right) e^{-E_1^*/kT} \tag{4.16}$$

$$\alpha' = \bar{u} S_2 \left(\frac{2kT}{E_2^*}\right) e^{-E_2^*/kT} \tag{4.17}$$

From detailed balancing

$$\frac{\alpha}{\alpha_{rev}} = \left(\frac{n^*}{n_o}\right)_{eq} = \frac{g^*}{g_o} e^{-E_1^*/kT} \tag{4.18}$$

so for the two level model the ratio α_{rev}/α' is given by

$$\frac{\alpha_{rev}}{\alpha'} = \frac{g_o}{g^*} \frac{E_2^*}{E_1^*} \frac{S_1}{S_2} e^{E_2^*/kT} \tag{4.19}$$

The degeneracy ratio g^*/g_o is 12 for the case of argon if all states of the low lying multiplet are assumed to participate, 5 if only the metastable state participates and the remaining states are assumed to decay by radiative transition. The latter assumption would be appropriate at low densities where the radiative decay rate is rapid compared with the collision frequency, the former would be appropriate at high densities where the collision frequency is the larger. The cross sections will again be taken proportional to the size of the wave function overlap with the wave function assumed to vary in size as the inverse of the remaining ionization energy

$$\frac{S_2}{S_1} = \left(\frac{r_o + r_o^*}{2r_o}\right)^2 \simeq \left(\frac{(1/15.7) + (1/4.2)}{2/15.7}\right)^2 = 5.6 \tag{4.20}$$

Thus, the product of ratios

$$77 < \frac{g^*}{g_o} \frac{E_1^*}{E_2^*} \frac{S_2}{S_1} < 184 \tag{4.21}$$

is bracketed by the low- and high-density limits, both of which are the order of 100. On the other hand, the exponential factor, $\exp(E_2^*/kT)$, in Eq. (4.19) is the order of 4,000 at temperatures the order of 5,000 K, and decreases to the order of 100 only at temperatures the order of 10,000 K. Thus, we do not expect that the two-step

collision process assumed in Eq. (4.14) will become important in the heavy particle impact ionization of Ar except at temperatures the order of 10,000 K and higher, which are at the upper limits of the measurements made (see fig. 4.4). At lower temperatures and sufficiently high density so that the radiative decay processes do not deplete the upper states, we expect a collision induced, ladder climbing process to occur along the ladder of available electronic states, which will establish a Boltzmann-like distribution in the states of energy lower than about 2kT below the ionization limit. This leads to the large increase in observed rate coefficient indicated by the dashed line on figure 4.2, with its associated effects on the apparent activation energy. The slope of the argon curve on figure 4.3 is about 4 eV at 10,000 K, which gives an apparent activation energy of about 11.7 eV, well within the experimental uncertainty of the data in this case, 11.5 ≠ 0.5 eV. The ground-state cross section $S_{oo} = 4\times10^{-19}$ cm^2, with the slope m = 2, provides a reasonably good fit to the experimental data in this case, where the Boltzmann limit with a cutoff 2kT below the ionization limit is assumed in the calculations (ref. 8).

Once again, an adjustment of coefficients to provide a favorable comparison between theory and experiment is only a necessary condition, but not a sufficient condition to validate the theoretical model. The two step model can equally well be fit to experiment. All that has been demonstrated here is that more factors need to be considered than in the simple two step process. In fact, the ionizing argon gas is yet more complicated than our models have so far allowed. The fact that radiative decay should be included in the model has already been alluded to. Moreover, excited electronic states of argon, as well as the other noble gases, can form stable dimers Ar_2^*, due to the fact that the electron spin functions are not necessarily all paired and bonding electronic pairs can be formed between two atoms. The spectra from such noble gas dimers had long been observed by spectroscopists, and these dimers are now produced in electric discharge to provide inverted populations for violet gas lasers. Thus, Ar_2^* should be considered as one of the excited species available in the reaction process, and the observed activation energy could be as low as the lowest bound state energy. At present we do not know what this lowest bound state energy is, but it would at least be less than the lowest excited state atomic energy which is 11.5 eV for the case of Ar. The increased strength of observed spectral lines, and the experience with dimer lasers, suggest that the binding energy increases with molecular weight of the noble gas. That is, Xe_2^* is more stable than Kr_2^* which is more stable than Ar_2^*. Indeed, McLaren and Hobson (ref. 5) observe apparent activation energies for the ionization of these species which are well below the energy of the lowest electronically excited atomic states. Thus, in spite of all the experimental activity and analysis that have been done on noble gas ionization by heavy particle impact, the problem still contains several unresolved questions. Our analysis here serves primarily to indicate what some of the factors which need to be considered are, and what their qualitative effects may be.

One assumption used repeatedly in the above calculations on the effect of excited states at high densities, where the population of excited states is collision dominated rather than radiation decay dominated, is that a pseudo Boltzmann distribution is set up in the excited states which is truncated the order of kT below some dissociation or ionization limit. In Chapter V we will show that this is a reasonable approximation to the more exact distributions which are found as solutions to the master equations of reaction, involving reaction paths from a multiplicity of excited state levels.

4.6 CONCLUDING REMARKS

Because of the Boltzmann distribution of collision velocities that exists in gas phase, most reactions occur from excited levels that have an activation energy, with respect to the reaction products, that is the order of kT or less. In an equilibrium gas the excited species number densities are all related to the ground state species by the Boltzmann distribution, and in this case the reaction rate coefficients can be expressed in a form that is appropriate for reaction involving ground state species, having the full activation energy of these ground state species. However, this formulation fails to call attention to some important features of the reaction process; namely, that rates can be orders of magnitude higher than are reasonable for ground state species, when the known magnitudes of the cross sections are taken into account, and that the apparent activation energy can be considerably less than the full activation energy of the ground state species, except at relatively low temperatures. Even in nonequilibrium gases, the reaction probabilities are so greatly enhanced for the upper excited states, that reaction paths will usually proceed from these states; rigorous calculations of reaction rates and activation energies thus require solutions to a set of master equations for the nonequilibrium distribution of an excited state population.

REFERENCES

1. Utterback, N. G.; and Van Zyl, B.: Enhancement of Neutral-Neutral Ionization Processes by Internal Excitation Energy in the Colliding Particles. Phys. Rev. Letters, vol. 20, May 1968, pp. 1021-1024.

2. Keck, J. C.; and Carrier, G.: Diffusion Theory of Nonequilibrium Dissociation and Recombination. J. Chem. Phys., vol. 43, Oct. 1, 1965, pp. 2284-2298.

3. Harwell, K. E.; and Jahn, R. J.: Initial Ionization Rates in Shock-Heated Argon, Krypton, and Xenon. Phys. Fluids, vol. 7, Feb. 1964, pp. 214-222.

4. Kelley, A. J.: Atom-Atom Ionization Cross Sections of the Noble Gases — Argon, Krypton, and Xenon. J. Chem. Phys., vol. 45, Sept. 1966, pp. 1723-1732.

5. McLaren, T. I.; and Hobson, R. M.: Initial Ionization Rates and Collision Cross Sections in Shock Heated Argon. Phys. Fluids, vol. 11, Oct. 1968, pp. 2162-2172.

6. Schneider, K. P.; and Park, C.: Shock Tube Study of Ionization Rates of NaCℓ Contaminated Argon. Phys. Fluids, vol. 18, Aug. 1975, pp. 969-981.

7. Hayden, H. C.; and Amme, R. C.: Low-Energy Ionization of Argon Atoms by Argon Atoms. Phys. Rev., vol. 141, Jan. 1966, pp. 30-31.

8. Hansen, C. F.: Effect of Excited States on Ionization Rates. 6th International Symposium on Rarefied Gas Dynamics. 1968. Academic Press, New York, 1969, pp. 1403-1412.

CHAPTER V MASTER EQUATIONS FOR CHEMICALLY REACTING GASES

5.1 SUMMARY

The master equations are derived for simple dissociating diatomic gases and for ionizing atomic gases, for the case where inert particle collisions dominate the process. Solutions to these equations for the pseudosteady phase of the process are discussed, which is usually the phase of most concern to the experimenter. The truncation of the number of excited states involved in the ionization process by various perturbation interactions with other particles in the gas is considered, and sample solutions for the pseudosteady, nonequilibrium distribution of excited states in an ionizing atomic gas are given. The results for the ionization rates obtained are found to be duplicated quite well when the nonequilibrium distribution is replaced by a Boltzmann distribution truncated about 1.5 kT below the ionization limit. This simple approximation eliminates the need for obtaining the solutions to the set of master equations, and is as accurate as the current state of theory and experiment warrants.

5.2 INTRODUCTION

In the last chapter we found that chemical reactions have a strong tendency to occur from upper excited states. This means that up to the point where full equilibrium balancing is achieved, the reaction is a drain on the population of these upper states, and a nonequilibrium distribution of some sort establishes itself in these upper states of the gas molecules as the reaction proceeds to completion. The solution for this nonequilibrium distribution is obtained from a set of master equations, such as those derived by Keck and Carrier (ref. 1), which describe the rates of population of each molecular state due to reactions proceeding from other states of the same molecules, of both higher and lower energy. The reactions leading from one state to another can occur either by collision or by radiative transition. In order to simplify the analysis we shall assume gas densities that are high enough so that collision induced transitions are rapid compared with radiative transitions. However, the same general equations and procedures apply in either case. The assumption above is not a bad one in many practical situations. The fast radiative transition for atoms and molecules is the resonance transition between the ground state and the lowest excited state connected by optical dipole radiation, often the order of 10^8 transitions/sec. In this case, the radiative transitions may be much faster than the collision frequencies, which are typically the order of 10^6/sec, but the optical depth for absorption of the emitted photon is so short that except for a thin surface layer of the gas sample, where the radiation may escape, the resonance radiation is trapped and is in equilibrium with the Boltzmann population of excited states. Thus, the collisions involving these lowest states occur with the Boltzmann distribution frequency just as though collisions alone were responsible for maintaining the population distribution. The remaining strong radiative transitions in the gas generally occur between closer lying states. The spontaneous transition rate and the absorption coefficient both vary as the cube of the frequency (that is, inversely with the cube of the wavelength). Thus, the optical depth for the nonresonant transitions may be rather large and except for large gas samples, the photons may readily escape with the result that the radiation field at longer wavelengths can be far out of equilibrium with the Boltzmann population of excited states. However in this case, the radiative transition rates are so much smaller (several orders of magnitude or more) that at

usual densities the collision induced transitions dominate the population distribution. Only for very rarefied gas flow is it necessary to include radiative transitions in the master equations for chemical reaction.

5.3 DISSOCIATING DIATOMIC GAS

To illustrate the use of the master equations of chemical reaction, we will consider first the case where the reacting gas is a trace species, N_2, dissociating in a matrix of inert gas A, so that essentially all collisions are with an inert partner. This will simplify the analysis considerably, yet will serve to introduce the essential ideas of the method.

Two types of reaction occur; one an excitation of the molecule from state m to state n, and its reverse;

$$N_2(m) + A \leftrightharpoons N_2(n) + A \tag{5.1}$$

the other a dissociation from the level m

$$N_2(m) + A \leftrightharpoons N + N + A \tag{5.2}$$

The rates of these reactions may be expressed

$$\frac{dN_2(m)}{dt} = -(\alpha_{mn}N_A)N_2(m) = -P_{mn}N_2(m) \tag{5.3}$$

$$\frac{dN_2(m)}{dt} = -(\alpha_{mc}N_A)N_2(m) = -P_{mc}N_2(m) \tag{5.4}$$

The quantities P_{mn} are transition rates per unit time per molecule, which are the product of the rate coefficient α_{mn} and the number density N_A of the inert collision partner. The number densities of the molecules in state m and n are $N_2(m)$ and $N_2(n)$, respectively, and the term P_{mc} represents the rate of escape from level m to the continuum of levels c that exist for the dissociated state. The reason that the problem is easier to solve for an inert gas matrix is because the transition rates P_{mn} and P_{mc} are then independent of the population numbers $N_2(m)$. We thus arrive at linear equations in $N_2(m)$ to solve for the population distributions. The reader can, however, appreciate how the nonlinear equations which apply in the more general case could be solved by computer iteration, for example.

Define the equilibrium transition rates

$$R_{mn} = P_{mn}N_2^{eq}(m) = P_{nm}N_2^{eq}(n) = R_{nm} \tag{5.5}$$

$$R_{mc} = P_{mc}N_2^{eq}(m) = P_{cm}(N^{eq})^2 = R_{cm} \tag{5.6}$$

where $N_2^{eq}(m)$ and $N_2^{eq}(n)$ are the equilibrium number densities of molecular states m and n, and N^{eq} is the equilibrium number density of dissociated atoms. In addition, define

$$X_m = \frac{N_2(m)}{N_2^{eq}(m)} \qquad (5.7)$$

the ratio of the actual to the equilibrium number density. Then the sum over all possible transitions yields the set of master equations, which for steady state are equated to zero.

$$\frac{dX_n}{dt} = \sum_{m=1}^{L} R_{mn}(X_m - X_n) + R_{nc}\left[\left(\frac{N}{N^{eq}}\right)^2 - X_n\right] = 0 \qquad (5.8)$$

There are L vibrational-rotational levels available to the molecules, and L equations with n = 1 to L.

A trivial solution is apparent, $X_n = (N/N^{eq})^2$ for all n. However, this solution is of no interest. Normally, the adjacent transitions are the strongest, so if boundary conditions are fixed for X_1 and (N/N^{eq}), one can see that the solutions will be approximately

$$X_n \simeq X_1 \qquad \text{for small } n \qquad (5.9)$$

$$X_n \simeq \left(\frac{N}{N^{eq}}\right)^2 \qquad \text{for large } n \qquad (5.10)$$

as shown on the sketch of figure 5.1, which gives the form of the solution for X_n as a function of n. The boundary condition on X_1 is set by the total number of molecules in the gas.

$$N_2 = \sum_n N_2(n) = \sum_n X_n N_2^{eq}(n) \qquad (5.11)$$

The equilibrium distributions are, of course, the Boltzmann distributions

$$\frac{N_2^{eq}(n)}{N_2} = \frac{g_n \exp(-E_n/kT)}{Q} \qquad (5.12)$$

where Q is the partition function. Thus

$$\sum X_n g_n \exp(-E_n/kT) = Q \qquad (5.13)$$

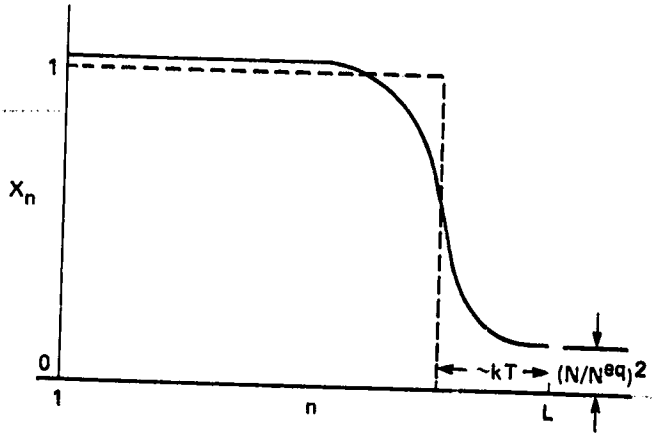

Figure 5.1- Form of the solutions to the master equations for diatomic molecule dissociation (—— exact, - - - - equivalent truncated equilibrium distribution).

In general, we shall choose a boundary condition $X_1 = 1$, solve the remaining L - 1 equations for the X_n involved, and then multiply all the ratios X_n, including X_1, by the factor $1 + \delta$, where δ is so chosen that the equality of Eq. (5.13) is satisfied. If the temperature is not too high, the partition function is approximately g_1, the ground state degeneracy, and in this case $X_1 \simeq 1$.

The total observed (that is, net) rate of production for a given experimental condition is

$$R = \sum_{n=1}^{L} R_{nc}\left[X_n - \left(\frac{N}{N^{eq}}\right)^2\right] \tag{5.14}$$

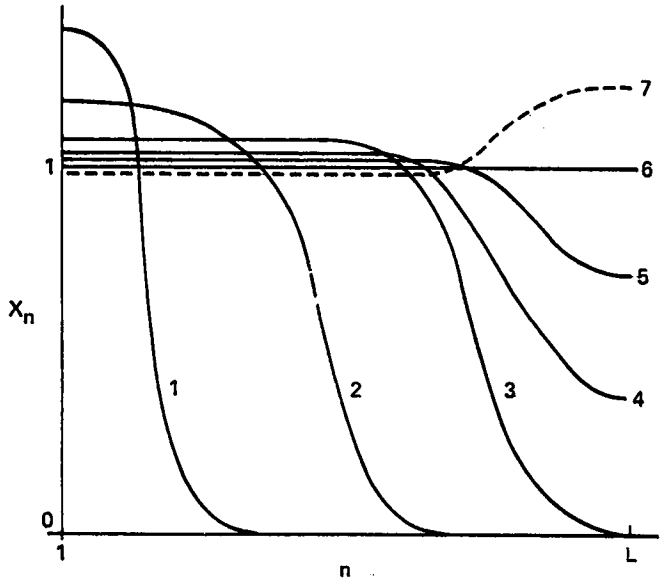

Figure 5.2- Growth of excited state distribution from initial condition 1 to final equilibrium 6 , and depletion of excited state distribution from initial condition 7 to equilibrium 6.

The back reaction term does not get very important until (N/N^{eq}) grows near unity, so the total net rate is pseudo-steady. The growth of the distribution from some initial distribution to final steady state is sketched in figure (5.2). Curves 1 and 2 represent a diffusion-like buildup of a pseudosteady population. This is an incubation period in which practically no dissociation occurs. Keck and Carrier (ref. 1) show that in this limit the master equations reduce to a diffusion equation in one dimension, and the solution can be approximated by known solutions to this diffusion equation. Curves 3, 4, and 5 are typical distributions during a pseudosteady net dissociation rate interval; during this period the back reactions are just about balanced by the increasing number of forward reactions. Finally, as the reaction nears full equilibrium, the numbers in the upper levels rapidly fill up to the full equilibrium value, where the forward rates and reverse rates exactly balance, and no net reaction is observed by the experimenter. Of course, equilibrium can also be approached from the other direction in which an excess of dissociated atoms exists initially. The dashed curve 7 on figure 5.2 is a typical distribution for the case $(N/N^{eq}) > 1$.

For present purposes we are interested in finding a value L* which is less than L, where a full equilibrium distribution can be truncated to give the same forward rate as Eq. (5.14)

$$R = \left[1 - \left(\frac{N}{N^{eq}}\right)^2\right] \sum_{n=1}^{L^*} R_{nc} = \sum_{n=1}^{L} R_{nc}\left[X_n - \left(\frac{N}{N^{eq}}\right)^2\right] \tag{5.15}$$

This effective truncation point will be found to lie between kT and 2kT below the dissociation limit for a wide variety of functional cross section forms, and moreover, the net rate is found to be insensitive to the total number of levels involved. This occurs because the rate equations all have an Arrhenius form

$$R_{mn} = A(T)e^{-(E_n - E_m)/kT}\, e^{-E_m/kT} \tag{5.16}$$

in which the temperature dependence of the pre-exponential factor A(T) is not very significant compared with the exponential term. Thus, the master equations take the form

$$\sum_m e^{-E_n/kT}(X_m - X_n) + e^{-D/kT}\left[\left(\frac{N}{N^{eq}}\right)^2 - X_n\right] = 0 \qquad (5.17a)$$

$$n = 1, \ldots L$$

$$\sum_m (X_m - X_n) + e^{-(D-E_n)/kT}\left[\left(\frac{N}{N^{eq}}\right)^2 - X_n\right] = 0 \qquad (5.17b)$$

$$n = 1, \ldots L$$

One can see that the influence of the boundary condition $(N/N^{eq})^2$ on the upper levels can only extend the order of kT away from the dissociation limit.

Since Eq. (5.8) is a set of L linear equations in L unknowns (the L values of X_n), the solutions may be found by standard matrix methods. The equations are first put in the linear form with constant coefficients

$$\sum_{n=1}^{L} a_{in}X_n = a_{ic} \; ; \quad i = 1 \text{ to } L \qquad (5.18a)$$

where

$$a_{in} = -\sum_{k\neq n} R_{nk} - R_{nc}\left(\frac{N}{N^{eq}}\right)^2 \qquad (5.18b)$$

and

$$a_{ic} = -R_{ic}\left(\frac{N}{N^{eq}}\right)^2 \qquad (5.18c)$$

Then the solutions are

$$X_n = \frac{\begin{vmatrix} a_{11} \cdots a_{c1} \cdots a_{\ell 1} \\ a_{12} \cdots a_{c2} \cdots a_{\ell 2} \\ \vdots \quad \vdots \quad \vdots \\ a_{1\ell} \cdots a_{c\ell} \cdots a_{\ell\ell} \end{vmatrix}}{\begin{vmatrix} a_{11} \cdots a_{n1} \cdots a_{\ell 1} \\ a_{12} \cdots a_{n2} \cdots a_{\ell 2} \\ \vdots \quad \vdots \quad \vdots \\ a_{1\ell} \cdots a_{n\ell} \cdots a_{\ell\ell} \end{vmatrix}} \qquad (5.19)$$

If we had not chosen an inert bath for the collision partners, the quantities P_{mn} of Eq. (5.3) would involve summations such as

$$P_{mn} = \sum_{jk} \alpha_{mnjk} N_A(j) \qquad (5.20)$$

in which different excited states of the collision partner - $N_A(j)$ take part in the process and can be excited or de-excited to other states k. The coefficients α_{mnjk} will then depend on the state of excitation j of the collision partner, generally increasing with the level of excitation because the cross section increases with size of the wave function. They will also depend on the final state $N_A(k)$, because the activation energy becomes smaller when the collision partner can be deactivated in the collision to a lower state of excitation k.

Where the dominant collision partners are the same species that are involved in the reaction of interest, the transition probabilities P_{mn} become dependent on the solutions for $N_2(k)$

$$P_{mn} = \sum_{k} \alpha_{mnkj} N_2(k) \qquad (5.21)$$

and the reader can see that the master equations then become quadratic in the unknowns $N_2(k)$. Such equations are solved by diagonalizing the matrices involved and finding the eigenvalues. This is a somewhat more laborious task than solving the linear equations above, but is within the range of modern computers for a reasonable number of levels, at least.

Normally, the dissociation rate problem is solved using the known number of vibrational levels as the limit L. For typical diatomic molecules in the ground state such as H_2, O_2, NO, N_2, and CO, L is the order of 15, 50, 50, 70, and 80, respectively. Halogens such as Cl_2 and Br_2 have about 20 and 100 levels, respectively. Matrices of these sizes are handled reasonably quickly by modern computers. Unfortunately, this simple approximation overlooks the effects of all the rotational states which are also members of the ladder of excited states leading to dissociation, as was discussed in the available energy theory of dissociation rates. The order of 100 or more rotational states would typically need to be included for each vibrational level, increasing the matrices involved to the order of 5,000 × 5,000, or larger. Even if such matrices could be handled economically, we do not have reliable expressions for the rotational transition probabilities at present. Thus, at best, we can perform only an approximate calculation of dissociation rates, even though a sophisticated set of master equations is used. The number of levels involved in a typical impact ionization problem is far more reasonable, so this reaction will be used to illustrate the type of results which are obtained from the master equations.

5.4 IONIZING ATOMIC GAS

Consider now the chemical equations for excitation of an atom from state m to state n by impact with an inert particle

$$A_m + Z \rightleftharpoons A_n + Z \qquad (5.22)$$

and the ionization of the atom from state m in a similar collision

$$A_m + Z \rightleftharpoons A^+ + e + Z \tag{5.23}$$

Of course, the ion A^+ may also possess a series of excited electronic states, but we will consider only the ground state of the ion for simplicity. The excited states can be reasonably ignored where they lie, as they often do, at very much higher energy levels. These equations can be put into the same form of master equations used for the dissociation process in the preceding section

$$\frac{dA_m}{dt} = -(\alpha_{mn}N_z)N_m = -P_{mn}N_m \tag{5.24}$$

$$\frac{dA_m}{dt} = -(\alpha_{mc}N_z)N_m = -P_{mc}N_m \tag{5.25}$$

where N_m and N_Z are the number densities of the excited atomic states A_m and of the collision partners Z, respectively. As before, only the inert collision partner situation is considered here so that the transition probabilities P are constants. This will lead to a linear set of equations, for which the principal characteristics of this ladder climbing type of rate process are easier to visualize. The subscript c again represents a continuum of kinetic energy states of the "dissociated" pair of particles, in this case the ion and the electron. These continuum states are, of course, actually quantized, but the quantized states lie so closely together in most practical situations that it is a very good approximation to treat them as a classical continuum.

As before, we define the equilibrium transition rates and use detailed balancing to obtain

$$R_{mn} = P_{mn}N_m^{eq} = P_{nm}N_n^{eq} = R_{nm} \tag{5.26}$$

$$R_{mc} = P_{mc}N_m^{eq} = P_{cm}N_eN_{A^+} = P_{cm}N_e^2 = R_{cm} \tag{5.27}$$

The electron density N_e has been assumed equal to the ion density N_{A^+} in Eq. (5.27), so this formulation is valid only for single ionization in a neutral plasma. The generalization of Eq. (5.27) to multiple ionization is left as an exercise for the reader. The ratios X_m are defined

$$X_m = \frac{N_m}{N_m^{eq}} \tag{5.28}$$

and then the steady-state master equations become

$$\frac{dX_m}{dt} = \sum_{n=1}^{L} R_{nm}(X_n - X_m) + R_{mc}\left[\left(\frac{N_e}{N_e^{eq}}\right)^2 - X_m\right] = 0 \tag{5.29}$$

At time zero after some instantaneous nonequilibrium state is established in the plasma, the derivatives (dX_m/dt) are finite and the master equations are a set of

diffusion-like equations as described by Keck and Carrier (ref. 1). Very quickly a pseudosteady population of X_m is established, however, which is relatively insensitive to the exact value of (N_e/N_e^{eq}), and it is the ionization from this pseudosteady distribution which is normally observed by the experimenter. The solutions for this pseudosteady distribution have the same characteristics shown in figures 5.1 and 5.2, X_n is approximately unity, that is the distribution is approximately the equilibrium one, up to about kT from the ionization limit, where the population is depleted by continual, essentially one-way, escape to the ionized continuum. The rates normally observed by the experimenter are essentially the rates of escape from those levels k' below the ionization limit.

The rates R_{mn} and R_{mc} will be expressed explicitly for cross sections having the following form for the excitation and ionization processes, respectively

$$S_{mn} = S_{mn}^{o}\left(1 - \frac{x_{mn}^*}{x}\right)^{p}, \quad x > x_{mn}^* \tag{5.30}$$

$$S_{mc} = S_{mc}^{o}\left(1 - \frac{x_{mc}^*}{x}\right)^{q}, \quad x > x_{mc}^* \tag{5.31}$$

where x is the dimensionless collision energy βE, and x_{ij}^* is the dimensionless threshold energy βE_{ij}^* for transition from state i to j. Normally, the limiting values of the cross sections, S_{mn}^o for the excitation process and S_{mc}^o for the ionization process are expected to be about equal. The slopes of log S vs log(E - E*) near threshold are expected to be the order of unity. In most of the examples that follow we assume $p = 1$, $q = 2$, and $(S_{mn}^o/S_{mc}^o) = 1$, but some calculations will be done varying these parameters to show that the results are not highly sensitive to their values.

Where $x_m < x_n$, the expression for R_{mn} is

$$R_{mn} = \alpha_{mn} N_m^{eq} N_z$$

$$= [\bar{u} S_{mn}^{o} \, e^{-(x_n - x_m)} \, H_p(x_n - x_m)] \frac{N_A g_m \, e^{-x_m}}{Q} N_z$$

$$\propto S_{mn}^{o} \, e^{-x_n} \, g_m H_p(x_n - x_m) \tag{5.32}$$

In the last expression of proportionality given in Eq. (5.32), the common factors, which are the mean collision velocity $\bar{u}$, the atom density N_A, the inert particle density N_z, and the atomic partition function Q, have all been factored out, as these common factors will not influence the solution to the set of simultaneous equations involved.

Where $x_m > x_n$, the rates are obtained by detailed balancing with the reverse process

$$\alpha_{mn} N_m^{eq} = \alpha_{nm} N_n^{eq} \tag{5.3}$$

from which we obtain

$$\alpha_{mn} = \alpha_{nm} \frac{g_n}{g_m} e^{-(x_n - x_m)}$$

$$= \bar{u} S^o_{nm} e^{-(x_m - x_n)} H_p(x_m - x_n) \frac{g_n}{g_m} e^{-(x_n - x_m)}$$

$$= \bar{u} S^o_{nm} \frac{g_n}{g_m} H_p(x_m - x_n) \tag{5.34}$$

Thus, in this case, the rate R_{mn} becomes

$$R_{mn} = \bar{u} S^o_{nm} \frac{g_n}{g_m} H_p(x_m - x_n) \frac{N_A g_m e^{-x_m}}{Q} N_z$$

$$\propto S^o_{nm} e^{-x_m} g_n H_p(x_m - x_n) \tag{5.35}$$

In a similar way the rates R_{mc} become

$$R_{mc} = \alpha_{mc} N_m^{eq} N_z$$

$$= [\bar{u} S^o_{mc} e^{-(x_o - x_m)} H_q(x_o - x_m)] \frac{N_A g_m e^{-x_m}}{Q} N_z$$

$$\propto S^o_{mc} e^{-x_o} g_m H_q(x_o - x_m) \tag{5.36}$$

where x_o is the dimensionless ionization energy, βI.

The variation in the size of the cross-section limits may be approximated, as before, with the variation in the size of the excited state wave functions

$$S^o_{mn} = \frac{S^o_{mn}}{S_o} S_o \simeq \left(\frac{r_m + r_o}{2 r_o} \right)^2 S_o \tag{5.37}$$

Since $r_m \propto (I - \epsilon_m)^{-1}$ and $r_o \propto I^{-1}$

$$S^o_{mn} \simeq \frac{1}{4} \left(\frac{I}{I - \epsilon_m} + 1 \right)^2 S_o \tag{5.38a}$$

$$S^o_{nm} \simeq \frac{1}{4} \left(\frac{I}{I - \epsilon_n} + 1 \right)^2 S_o \tag{5.38b}$$

$$S^o_{mc} \simeq \frac{1}{4} \left(\frac{I}{I - \epsilon_m} + 1 \right)^2 S^+_o \tag{5.38c}$$

where S_o represents a limiting size for collisions with the ground state, and I is the ionization energy. Equation (5.38c) has allowed for the possibility that this limit could be different for the ionization process than for the excitation process.

For simplification, the rates are all divided by e^{-x_o} and $S_o/4$, as well as the other common factors, to give matrix coefficients

$$R_{nc} = \frac{S_o^+}{S_o}\left(\frac{x_o}{x_o - x_n} + 1\right)^2 g_n H_q(x_o - x_n) \qquad (5.39a)$$

$$R_{mn} = \left(\frac{x_o}{x_o - x_m} + 1\right)^2 g_m\, e^{-(x_o - x_n)}\, H_p(x_n - x_m), \quad x_m < x_n$$

$$= \left(\frac{x_o}{x_o - x_n} + 1\right)^2 g_n\, e^{-(x_o - x_m)}\, H_p(x_m - x_n), \quad x_n < x_m \qquad (5.39b)$$

Recall that to a good approximation (see chapter IV)

$$H_p(x) = \frac{p!}{x^{p-1}}, \quad x < (p!)^{1/(p-1)}$$

$$= 1, \quad x > (p!)^{1/(p-1)} \qquad (5.40)$$

To summarize the calculation procedures:

a) The ratio (N_e/N_e^{eq}) is chosen for the conditions of interest, and the L simultaneous equations of Eq. (5.29) are solved using the matrix elements of Eq. (5.39) for R_{nc} and R_{mn} and with the boundary condition $X_1 = 1$.

b) The values of all X_n obtained, including X_1, are multiplied by the same factor, $1 + \delta$, to normalize the result to the given number density of atoms, by equating the nonequilibrium partition function to the equilibrium partition function

$$(1 + \delta) \sum_{n=1}^{L} X_n g_n\, e^{-x_n} = \sum_{n=1}^{L} g_n\, e^{-x_n} \qquad (5.41)$$

c) The total rate for the nonequilibrium gas is then calculated from

$$R = \sum_{m=1}^{L} \left[X_m - \left(\frac{N_e}{N_e^{eq}}\right)^2\right] R_{mc} \qquad (5.42)$$

d) Finally, an equivalent truncation of the equilibrium distribution, L*, which gives the same rate, is found

$$\left[1 - \left(\frac{N_e}{N_e^{eq}}\right)^2\right] \sum_{n=1}^{L^*} R_{nc} = R \qquad (5.43)$$

The one remaining factor which has not yet been dealt with is the choice of the number of levels, L, which should be considered. The ionization problem is different from the dissociation problem in this respect; in the latter, a finite number of vibrational and rotational levels up to the dissociation limit is found to exist naturally, but in the ionization problem, an infinite number of excited electronic states exist up to the ionization energy limit.

5.5 PERTURBATION LOWERING OF THE IONIZATION POTENTIAL

Normally, just one electron is promoted to higher energy in excited states, and these electronic states become hydrogen-like in the upper levels for all atoms and molecules as the excited electron orbits farther away from the singly charged nuclear cluster which remains at the center of mass. Thus, a highly excited state with quantum number $n >> 1$ has a degeneracy of $2n^2$ and an energy, $-E_1/n^2$ below the ionization limit, where $-E_1$ is the ground state energy of the hydrogen atom. Obviously, an infinite number of such states exist, $1 \leq n < \infty$, below the ionization limit.

Fortunately, for purposes of computation, the perturbations of neighboring gas molecules, ions, and electrons perturb the highest electronic states such that they become merged with the continuum. Once the electron reaches this continuum, it becomes free to wander around from particle to particle as an independent species in the gas, with a Boltzmann distribution of kinetic energies established by the collision encounters with the other particles. This effect is known as the lowering of the effective ionization potential. The magnitude of the effect depends upon the strength of the perturbations involved. The effective ionization potential is increasingly lowered as the gas becomes more dense, or as the number of strong perturbers like electrons and ions increase in the gas at the expense of neutral species which are weaker perturbing influences. The lowered ionization potential cuts off the number of levels of excited electronic states that need to be considered in the gas to a rather reasonable number, the order of 10 to 100 in most situations of practical interest, numbers which can be managed with reasonable efficiency and speed in the matrix calculations that are performed by the computer. The reason that the perturbations truncate the number of levels that need be considered at these values is that electronic states increase in energy very rapidly as the quantum number increases from small numbers; the bulk of the states occur at energies very close to the ionization limit.

For present purposes we need only know that the electronic levels are truncated at certain energies by the perturbation effects in order to proceed with sample calculations illustrating typical solutions to the master equations. However, it may be interesting to briefly review the several types of perturbation that need to be considered in numerical evaluation of the lowered ionization potential. A more complete review of the ionization lowering effect is given by Drawin and Felenbok (ref. 2), by Margenau and Lewis (ref. 3), and by Hansen (ref. 4). Other references to original work on the subject may be found in these reviews.

First of all, neutral particles perturb the higher excited states whose orbits reach out to the positions occupied by the nearest neighboring particles. The average size of an excited orbit with large quantum number n is

$$\bar{r}_n = \frac{n^2 a_o}{Z} \tag{5.44}$$

where a_o is the Bohr radius and Z is the charge on the residual nucleus when the excited electron is stripped away. For neutral particles Z is unity. The maximum quantum number can be taken approximately equal to the quantum level where $\bar{r}_n$ equals the average spacing between neutral particles in the gas

$$n_{max} = \frac{Z^{1/2}}{[a_o^3 N(4\pi/3)]^{1/6}}$$

$$= \left(\frac{N_o}{N}\right)^{1/6} \frac{Z^{1/2}}{[a_o^3 N_o(4\pi/3)]^{1/6}} \qquad (5.45)$$

where N is the gas number density and N_o is the density at standard conditions (1 amagat). One can see that the cutoff level is very weakly dependent on density, varying inversely as the one-sixth power of density. At one amagat the cutoff is $n_{max} = 6$. This is a rather high density at the high temperatures where ionization rates become appreciable, the order of 10^4 K, and a more typical density would be 10^{-6} amagats, with a cutoff at $n_{max} = 62$.

Although the cutoff found above illustrates some of the general concepts involved, the static particle perturbations are not usually the ones which limit the number of excited levels. At the usual temperatures and densities of interest, the collisions cause a broadening of energy levels, and where these levels merge together the electron may be considered free, able to enter the Boltzmann continuum through a sequence of small energy transfer collisions. Recall that heavy particles transfer kinetic energy very inefficiently to the light weight electrons; only when collisions with other electrons become frequent is a fast relaxation to a Boltzmann population at the equilibrium electron temperature observed, and this temperature may remain out of equilibrium with the heavy particle temperature for relatively long intervals. The half width of a collision broadened level is given in energy units by an expression of the following form (ref. 5)

$$\Delta_c = \hbar\theta = \hbar N S \bar{u} \qquad (5.46)$$

where θ is the collision rate, or $NS\bar{u}$, the product of the number density and cross section and mean collision velocity. When this broadening equals half the space between levels, the lines merge

$$\frac{1}{2}\frac{dE_n}{dn} = \frac{Z^2 e^2}{2a_o n^3} = \hbar N S \bar{u} \qquad (5.47)$$

thus

$$n_m^3 = \frac{Z^2(e^2/2a_o)}{\hbar N S \bar{u}} \qquad (5.48)$$

For the hydrogen-like excited states the collision cross sections will be approximately

$$S = \pi(r_o + r_n)^2 \simeq \pi r_n^2 = \pi Z^2 n^4 a_o^2 \qquad (5.49)$$

and a final expression for the excited state level at cutoff is

$$n_m^7 = \frac{N_o}{N} \frac{e^2/2a_o}{N_o a_o^2 \bar{u}h} \qquad (5.50)$$

This expression varies more weakly with density than even Eq. (5.45), inversely as the one-seventh power of N. The dependence on temperature is even weaker; n_m varies as the one-fourteenth power of temperature. For typical gases and temperatures of interest μ/kT is the order of 1 to 10 atomic mass units per eV, and the value of n_{max} is the order of 9 at 1 amagat density. In other words, at high densities the collision broadening effect is not as important as the static perturbation effect discussed previously. However, because of the weaker dependence on density, the collision broadening becomes more important as density decreases until it typically equals the static perturbation effect at 10^{-6} amagats, and becomes dominant at lower densities.

However, the perturbations produced by ions and electrons are so much stronger than those produced by neutral gas particles, that these charged particles dominate the ionization lowering effect whenever they are present in appreciable numbers, which is usual in most experimental situations where ionization rates are observed. The nearby positive ions may be treated as static perturbers with long range coulomb attractive potentials $-Ze^2/r$. When the electron is excited to a level which equals the energy of this long-range potential well, it is swept away from its bound state into the well where it can then slide from one ion field into another, into another, etc., and becomes essentially a free electron, able to enter the continuum Boltzmann distribution of free electrons. The nearby ions cause a lowering of the ionization potential

$$\Delta E = 3e^2 Z \left(\frac{4\pi n_e}{3Z}\right)^{1/3} \qquad (5.51)$$

where n_e is the number density of positive ions in the gas. In the case of single ionization in neutral plasmas, this equals the number density of electrons, of course. When this change in ionization potential is equated to the spacing between levels, the maximum bound state quantum number n_m is obtained

$$n_m = \frac{Z^{2/3}}{6^{1/2}} \left(\frac{3}{4\pi n_e a_o^3}\right)^{1/6}$$

$$= \left(\frac{N_o}{N}\right)^{1/6} \left(\frac{1}{f}\right)^{1/6} \frac{Z^{2/3}}{6^{1/2}} \left(\frac{3}{4\pi N_o a_o^3}\right)^{1/6} \qquad (5.52)$$

where f is the fraction ionized, and n_e equals Nf or $N_o(N/N_o)f$. Once again n_m varies weakly with density, inversely, as density to the one-sixth power. For a typical case near full ionization, and Z = 1, the cutoffs are $n_m = 3$ at 1 amagat, and 26 at 10^{-6}, which would be more important than either of the previous two cases considered. At 1% ionization the static positive ion perturbations are typically about equal in importance to the neutral particle perturbations, and become less important at lesser degrees of ionization.

Still other effects occur in plasmas that can dominate ionization potential lowering, however. The ions, either positive or negative, exert long-range coulomb fields, $Z_i e^2/r$, which cause Stark broadening of the energy levels. An expression for the Stark broadening of a hydrogen-like level is

$$\Delta E = \frac{3n}{2}(n - 1)a_o \frac{Z_i e^2}{r^2} \tag{5.53}$$

When the distance to the ion, r, is replaced by the average distance to the closest ion neighbors, and ΔE is equated to the spacing between levels at the quantum state n_m, one obtains the expression

$$n_m = \frac{Z^{1/5} Z_i^{2/15}}{6^{1/5}} \left(\frac{N_o}{Nf}\right)^{2/15} \left(\frac{3}{4\pi N_o a_o^3}\right)^{2/15} \tag{5.54}$$

where Z is the charge on the nucleus of the excited particle and Z_i is the charge on the perturbing ion, and again f is the fraction of particles singly ionized. At 1% ionization and 1 amagat the cutoff occurs at n_m about 6, at 10^{-6} amagat the cutoff occurs at n_m about 41.

Next we have a Debye shielding effect to consider. The range of a nuclear coulomb field is essentially limited in plasmas of reasonable density by the shielding of surrounding charged particles. The effective range of a charged particle's potential is given by the well-known Debye formula

$$D^2 = \frac{kT}{4\pi e^2 \left(n_e + \sum_i Z_i^2 n_i\right)} \tag{5.55}$$

where n_e is the electron number density and n_i is the density of ions with charge Z_i. The maximum radius of a bound state is equated to the Debye length, where the nuclear potential is nullified, and therefore, where the electron becomes free.

$$n_m = Z^{1/2}\left[\frac{kT}{8\pi(e^2/2a_o)n_e a_o^3(1 + Z_i)}\right]^{1/4}$$

$$= \left(\frac{N_o}{Nf}\right)^{1/4} Z^{1/2}\left[\frac{kT}{8\pi(e^2/2a_o)N_o a_o^3(1 + Z_i)}\right]^{1/4} \tag{5.56}$$

In Eq. (5.56) it has been assumed that only one ion perturber with charge Z_i exists. For single ionization of neutral particles, both Z and Z_i would be unity. The Debye shielding effect gives the strongest density dependence, so at very low densities the values of n_m obtained are always much higher than the previous effects discussed. However, at high densities and relatively low temperatures, where the Debye length becomes small, the Debye shielding effect on lowering of ionization potential can become dominant.

Finally, one more effect needs to be considered, namely, the electron impact broadening of energy levels. Because electrons are very lightweight and move with high velocities in plasmas, they can dominate the broadening of energy levels. A suitably simple analytic approximation for electron impact broadening (ref. 6), equated to the spacing between levels at quantum level n is

$$\Delta E = \frac{72\pi^2 a_o^2 e^4}{h}\left(\frac{\pi m_e}{8kT_e}\right)^{1/2} N_e n^4 = \frac{Z^2 e^2}{2a_o n^3} \tag{5.57}$$

This results in the expression for the cutoff bound state quantum number n_m

$$n_m = Z^{2/7}\left(\frac{h}{144\pi^2 a_o^3 e^2 N_o}\right)^{1/2}\left(\frac{8kT_e}{\pi m_e}\right)^{1/14}\left(\frac{N_o}{Nf}\right)^{1/7} \tag{5.58}$$

This effect is generally slightly more dominant than ion broadening except at high temperature, kT > 1 eV, in which case Stark broadening by the positive ions dominates.

In a numerical calculation procedure, one would need to investigate each of the above limits separately and choose the lowest value obtained for n_m as the cutoff level for the solution of the set of master equations for that particular plasma condition. Each time one considers a different plasma condition, the process is repeated to determine a new cutoff appropriate to that condition. The theoretical models of ionization potential lowering need not be highly accurate because the results are so weakly dependent on density and temperature that a rather approximate model will do for the present purposes. The point to note is that all the theories predict cutoffs which range from excited level quantum numbers n_m the order of 5 to 100 at the usual conditions where ionization rates are important. We can, therefore, illustrate solutions to the master equations which are realistic for ionization problems, choosing values of n_m within this range. In figures 5.3, 5.4, and 5.5 solutions are shown where L, the total number of levels used, is 6, 18, and 54. For these values the ionization potential has been lowered 0.277 eV, 0.0377 eV, and 0.0045 eV, respectively; the lowering may have been produced by any combination of the effects discussed previously: static neutral particle perturbation, neutral particle collision broadening, static ion potential perturbation, ion-electric field Stark broadening, Debye plasma shielding, or electron impact broadening. In any case, the solutions to the set of master equations are the same for a given cutoff level L.

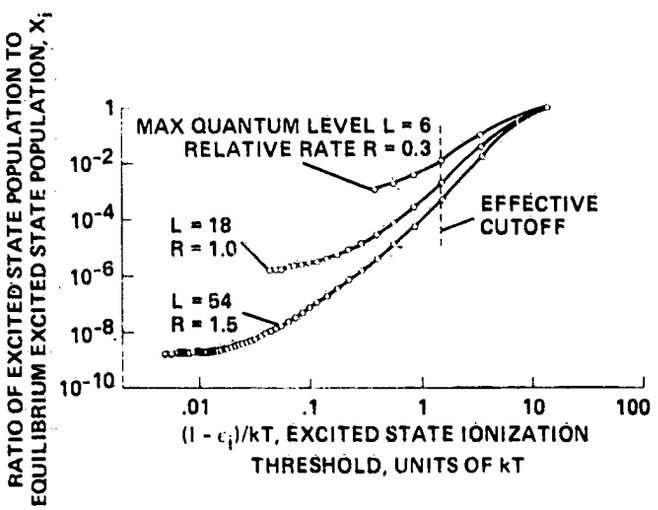

Figure 5.3- Effect of maximum quantum level L on relative net rate R; kT = 1 eV, ion density $(N_e/N_e^{eq}) = 0.0$.

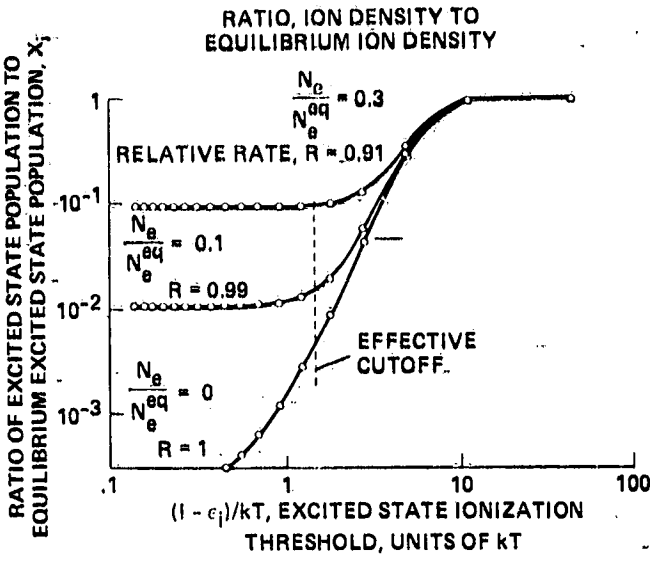

Figure 5.4- Effect of approach to equilibrium on the relative net rate R; kT = 0.3 eV, maximum quantum level L = 18.

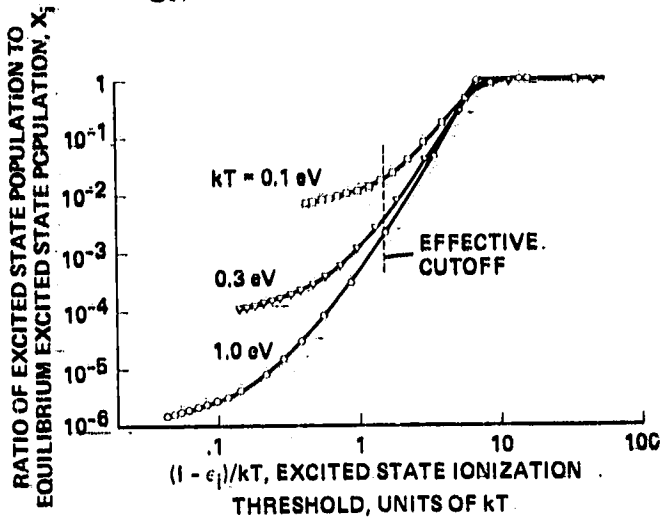

Figure 5.5- Effect of temperature on population distribution; $(N_e/N_e^{eq}) = 0.0$, L = 18.

5.6 CALCULATIONS OF NONEQUILIBRIUM DISTRIBUTIONS FOR IONIZING GAS

Some sample calculations for the case where $(S_o^+/S) = 1$, p = 1, and q = 2 are shown in figures 5.3, 5.4, and 5.5. Figure 5.3 shows the effect of lowering the effective ionization potential, for the case where the ionization level, N_e/N_e^{eq}, is zero, and the temperature kT is 1 eV. The solution for truncation at quantum level 18, corresponding to an effective ionization potential 0.0377 eV below the full ionization potential, is shown as a relative rate of unity. The relative rate is decreased by a factor of about 3 at higher densities where the perturbations limit the number of bound states to quantum level 6 and lower the effective ionization potential 0.277 eV below the full ionization potential; the relative rate is increased by 1.5 at lower densities where the cutoff occurs at quantum level 54 and lowers the ionization potential by only 0.0045 eV. Thus, the total rate has changed only by a factor of 5, whereas the total number of bound quantum states involved

$$\sum_{n=1}^{L} 2n^2 = L(L + 1)(2L + 1)/3 \qquad (5.59)$$

has changed by a factor of 590. One can see that the character of the solutions requires X_n to approach unity near the ground state and drop off rapidly at levels in the region kT below the ionization limit. The effective cutoff for a truncated Boltzmann distribution giving the same total rate, according to Eq. (5.43), is shown at about 1.5 kT below the ionization limit.

Figure 5.4 shows the effect of changing ion density, in other words increasing the level of the reverse reaction rate, for conditions where the distribution is truncated at level 18 and kT is 0.3 eV. Increasing the ion density has the effect of leveling out the values of X_n in the higher excited states at $(N_e/N_e^{eq})^2$, but the

total forward rate is not affected very much until (N_e/N_e^{eq}) grows larger than 0.3. Thus, the experimenter can expect to observe a relatively constant rate as long as the ionization has not proceeded beyond this point. Again, the effective cutoff for a Boltzmann distribution is essentially constant, 1.5 kT.

Figure 5.5 shows the effect of changing temperature on the population distribution, in the case where the distribution is truncated at level 18 and the ionization is vanishingly small. As temperature is increased, the ratios X_i are decreased in the upper levels. Of course, the equilibrium number densities are increased in this case, so the actual densities in the upper levels are not affected much. Again the effective truncation point for a Boltzmann distribution is about 1.5 kT below the ionization limit for all cases.

Finally, figure 5.6 shows the effect of changing some of the parameters in the cross section functions, for the case of zero ionization and kT = 1 eV. The distribution functions are not changed very much by changes in S_o^+/S_o or in the exponent q. The total rates are essentially the same for all these cases. Only when the exponent p on the excitation cross section is changed are the distribution and the rate affected appreciably. As p is increased to 2, the cross section increases less rapidly near threshold than for p = 1 and the population of all the excited states is depressed somewhat, with a corresponding decrease in net ionization rate. The escape from the upper levels involves such a small activation energy that the shape of the cross section near threshold doesn't make very much difference, and thus the results are less sensitive to the value of q, the logarithmic slope for the ionization cross section. However, if the ionization cross section limit is depressed, $S_o^+/S_o = 0.3$, the distribution is dammed up in the upper levels. Conversely, if the ionization cross-section limit is enhanced, $S_o^+/S_o = 3.0$, the distribution is depleted in the upper levels. Actually, the results are not highly sensitive to any of these parameters, in view of the usual uncertainties that exist in both theoretical and experimental values for rate coefficients.

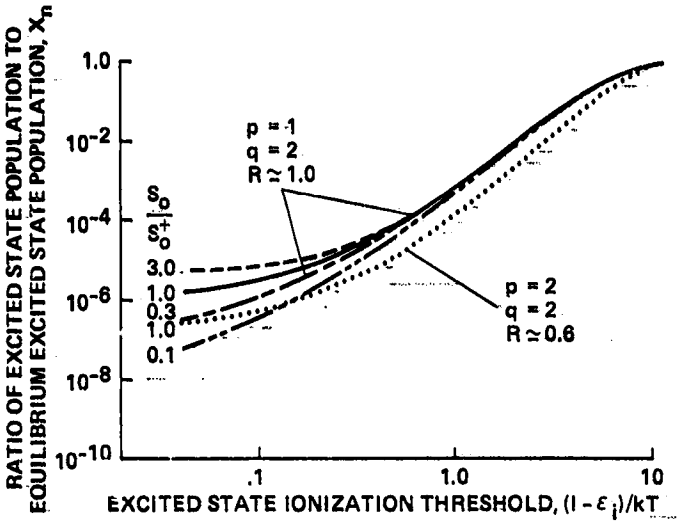

Figure 5.6- Effect of changing cross section function on population distributions, X_n, and relative rate R.

Exercise 5.1: In calculations involving upper electronic excited states it sometimes becomes convenient to group together close lying states that fall within an energy band ΔE. Derive the expression for the sum of degeneracies within this band

$$\frac{\Delta g}{\Delta E} = \frac{n^5}{E_H}$$

assuming that the levels are hydrogen-like with $g_n = 2n^2$ and $E_n = -E_H/n^2$, where $-E_H$ is the energy of the ground-state hydrogen atom and n is an average quantum number representing all the states within the band ΔE. Note that in grouping levels together in this way ΔE must be much less than kT, otherwise the effective spacing between these collected states becomes artificially large and the grouped levels then represent a barrier to the flow of systems through these states. The numerically calculated distributions, such as shown in figure 5.3, then flatten off at a larger value of X_n for the lower quantum state, and then suffer a discontinuity in the slope at the point where the collected states are assumed, leading to artificially low values of X_n for the higher quantum states.

Exercise 5.2:

a) Calculate the effective quantum cutoff of excited states for hydrogen-like systems due to static neutral particle perturbations for particle radius $a_o = 0.53\times10^{-8}$ cm, Z = 1, and particle densities $N = 1, 10^{-3}$ and 10^{-6} amagat.

b) Calculate the effective quantum cutoff of excited states due to neutral particle collision broadening for the same conditions as above and for temperatures of 0.1 and 1.0 eV.

c) Calculate the effective quantum cutoff of excited states due to static ion perturbations for the above densities and for 1% and 10% ionized fractions.

d) Calculate the effective quantum cutoff of excited states due to Debye shielding, again for the above densities and for 1% and 10% ionized fractions. What are the characteristic Debye lengths at these conditions?

e) Calculate the effective quantum cutoff of excited states due to electron impact for the above densities, for 1% ionization fraction, and for electron temperatures of 0.3, 1.0, and 3.0 eV.

f) Calculate the effective quantum cutoff of excited states due to ion Stark broadening for the above densities and for 1% and 10% ionized fractions, assuming singly charged perturbing ions.

What is the lowest quantum cutoff at each of the above densities and temperatures? What is the total sum of excited states considered at each of these cutoffs?

5.7 CONCLUDING REMARKS

In conclusion, the ionization process starting from some nonequilibrium transient increase in temperature, such as produced in the shock tube, is visualized as occurring in three stages. First, a diffusion-like solution to the master equations describes a rapid buildup to a pseudosteady population distribution in the excited states, which is Boltzmann-like in the lower levels and is almost depleted in the upper levels near the dissociation limit. Observed rates may be very small in this initial excitation stage interval. In the second stage, the rate of ion production is relatively constant, and is determined largely by escape from the levels around - kT below the dissociation limit and repopulation of these same levels by recombination. Finally, as the ion level builds to about 30% of the equilibrium value, the rates are slowed in the final exponential approach to equilibrium.

The form of the solutions for the pseudosteady, second-stage nonequilibrium population distributions in an ionizing gas can be obtained quite well from the master equations because, in this case, the excited-state energy values, the sizes of the wave functions for these excited states, the effective lowering of the ionization potential by perturbations which truncate the number of bound states, and the shape of the cross-section functions, can all be estimated within reasonable limits. From a practical engineering point of view, the important result is that the net rate of ionization can be estimated by truncating an equilibrium Boltzmann distribution 1.5 kT below the ionization limit. The results are relatively insensitive to the exact form and size of the cross sections used, at least in terms of the uncertainties that presently exist in both theory and experimental results for reactions of this type. The most sensitive parameter appears to be the shape of the excitation cross section near threshold.

The nonequilibrium populations have been deduced for the case of an ionizing atomic gas, but the results should be qualitatively valid for an ionizing gas of small (diatomic) molecules as well, since the excited electronic states at high quantum levels tend to be hydrogen-like in either case. Where electron collision partners are the important ones in the excitation and ionization process, the theorist must take care to differentiate between the electron temperature and the heavy particle

temperature, if these differ from one another as they often do in realistic plasma situations. The electron temperature must be used in the expressions for collision velocity and cross-section function; the heavy particle temperatures are to be used wherever the equilibrium heavy particle number densities are involved.

Exercise 5.3: Tabulate the degeneracies and the ionization potentials for the 10 lowest lying levels of neutral argon given by C. E. Moore (ref. 7). Use the approximation that the cross section of each level is inversely proportional to the ionization potential from that state and compare the product of degeneracy and cross section for each level with the ground state value as an indication of the relative collision frequency for electron detachment. For collisions with the ground state atoms, what are the factors $(S_{io}/S_{oo})(g_i/g_o)$ required in the formula of Eq. (4.11)?

REFERENCES

1. Keck, J.; and Carrier, G.: Diffusion Theory of Nonequilibrium Dissociation and Recombination. J. Chem. Phys., vol. 43, Oct. 1965, pp. 2284-2298.

2. Drawin, Hans Werner; and Felenbok, Paul: Data for Plasmas in Local Thermodynamic Equilibrium. Gauthier-Villars, Paris, 1965.

3. Margenau, H.; and Lewis, M.: Structure of Spectral Lines from Plasmas. Rev. Mod. Phys., vol. 31, July 1959, pp. 569-615.

4. Hansen, C. F.: Molecular Physics of Equilibrium Gases. NASA SP-3096, Chap. VII, 1976.

5. Aller, L. H.: Astrophysics, The Atmospheres of the Sun and Stars. Ronald Press, N.Y., 1953.

6. Hansen, C. F.: Combined Stark and Doppler Line Broadening. JOSA, vol. 54, Oct. 1964, pp. 1198-1203.

7. Moore, C. E.: Atomic Energy Levels. NBS Circular 467, vol. 1, U.S. Government Printing Office, Washington, D.C., June 1949.

CHAPTER VI COLLISION INDUCED VIBRATIONAL EXCITATION

6.1 SUMMARY

Collision-induced vibrational transition theory is reviewed, first in the classical approximation, and then in the semiclassical approximation where the collision trajectory is assumed to be classical and establishes a time-dependent perturbation which transforms the quantum wave functions to new steady state eigenfunctions. Analytic approximations can be carried through with this model all the way to a three-dimensional transition probability, collision cross section, and reaction rate. These approximations thus afford valuable insight to the total problem and serve as a guide for more rigorous numerical calculations performed with digital computer. Although this renders the vibrational transition reaction the only completely developed rate problem, so that it serves as a good model for the problem of rate processes in general, vibrational transitions are not yet completely solved. In particular, coupled rotational transitions are found to occur with the three-dimensional collision perturbations, and the number of closely coupled equations required for a complete solution is too large even for modern computers to handle.

6.2 INTRODUCTION

The rates of vibrational transition produced by molecular collisions are important in a number of practical problems. For example, vibrational excitation influences the structure of shock waves and produces variations in the equation of state which are important in gas dynamic flow. Vibrational excitation causes absorption and dispersion of sound. Recently, nonequilibrium vibrational excitation processes have become important means of effecting population inversions in upper vibrational states for the purpose of producing high power gasdynamic lasers. The principal reason we are interested in the problem here is because it is the only reaction which has, to date, been analyzed by analytic approximation through the entire sequence giving transition probability, three-dimensional collision cross section, and rate coefficient as outlined in chapter II. Thus, it serves as a good illustration of the kind of analysis we wish it were possible to perform for reaction rates in general. However, as we shall see, some of the approximations involved leave more work to be done, even for the vibrational excitation process, before we can say that this problem has been adequately treated.

So many studies of vibrational excitation have been published that it is practical to recall only a few of the principal landmark papers here. A classic paper by Landau and Teller (ref. 1) in 1936 analyzes the one-dimensional collision excitation of harmonic oscillators in connection with dispersion of sound. Landau and Teller deduce the result that the vibrational relaxation rate varies as $\exp -(\theta/T)^{1/3}$, where θ is a characteristic temperature; this result is derived using purely classical arguments about the form of the impulse produced in collision. Almost every set of vibrational relaxation data ever obtained has been compared with this result, generally with reasonably good agreement (refs. 2-5). The Laundau-Teller model was refined by Bethe and Teller (ref. 6) in 1945, but little else was accomplished until 1952 when Schwartz, Slawsky, and Herzfeld (ref. 7) published a quantum treatment of energy exchange in one-dimensional collisions with harmonic oscillators. This work was based on methods derived by Zener (ref. 8) and by Jackson and Mott (ref. 9), and has been widely accepted as the most rigorous analysis of the problem which seems

practical. Schwartz and Herzfeld (ref. 10) followed with a three-dimensional treatment using the method of partial waves (ref. 11). They were unable to deduce the cross sections, but did conclude that thermally averaged transition probabilities in three-dimensions have the same form given by the one-dimensional models. Essentially, the same results for both one- and three-dimensional collisions were published independently by Takayanagi (ref. 12).

Most of the work subsequent to the above has employed the semiclassical approach. In this method the classical trajectory for motion between the collision partners is used to obtain a time-dependent perturbation potential; then transitions produced by this perturbation are calculated by quantum principles. The deBroglie wavelengths of heavy gas particles are normally much smaller than the scale distance for potential changes involved, so the classical trajectory is a good approximation, as accurate as needed for many practical purposes. In fact, Rapp (ref. 13) shows that a complete classical treatment of one-dimensional collision excitation of harmonic oscillators from the ground state to the first excited level leads to the same result as the quantum treatment by Herzfeld (ref. 14). The semiclassical method was used by Rapp and Sharp (refs. 15, 16) to investigate vibration excitation produced in very high energy collisions, and by Rapp and Golden (ref. 17) to analyze resonant vibration exchange. Kerner (ref. 18) developed relations between quantum and classical transition probabilities of harmonic oscillators subject to large perturbations where multiple quantum jumps occur, and Treanor (ref. 19) showed that Kerner's results are consistent with the numerical results obtained by Sharp and Rapp (ref. 16). An excellent survey of the results to 1968 is given by Rapp and Kassal (ref. 20).

6.3 CLASSICAL HARMONIC OSCILLATOR EXCITATION

A harmonic oscillator subject to some arbitrary impulse function of time, $f(t)$, such as caused by collision, obeys the inhomogeneous differential equation

$$\ddot{y} + \omega^2 y = \frac{f(t)}{\mu} \tag{6.1}$$

where y is the displacement of the oscillator from the equilibrium position, ω is the oscillator's resonant frequency in the absence of the perturbing impulse, and μ is the reduced mass. There are two linearly independent solutions to the homogeneous part, and the general solution when $f(t) = 0$ is a linear combination of these

$$y(t) = Ay_1(t) + By_2(t) \tag{6.2}$$

where the constants A and B are chosen such that the value of $y(a)$ and its time derivative $\dot{y}(a)$ are specified at some reference time $t = a$. If y_1 and y_2 are chosen such that

$$\begin{aligned} y_1(a) &= 1 \qquad \dot{y}_1(a) = 0 \\ y_2(a) &= 0 \qquad \dot{y}_2(a) = 1 \end{aligned} \tag{6.3}$$

then

$$y(t) = y(a)y_1(t) + \dot{y}(a)y_2(t) \tag{6.4}$$

The normalized equalities specified in Eq. (6.3) can, of course, be fitted to other numerical values by merely stretching the y and t coordinates appropriately.

Now let $f(t)$ be finite in the interval $\xi - \delta < t < \xi + \delta$. Integrate Eq. (6.1) with respect to time to obtain

$$\dot{y}(\xi + \delta) - \dot{y}(\xi - \delta) + \omega^2 \int_{\xi-\delta}^{\xi+\delta} y(t)dt = \int_{\xi-\delta}^{\xi+\delta} \frac{f(t)}{\mu} dt \tag{6.5}$$

Let $f(t)$ increase as $\delta \to 0$ in such a way that the integral on the right remains unity

$$\int_{\xi-\delta}^{\xi+\delta} \frac{f(t)dt}{\mu} = 1 \tag{6.6}$$

If $y(t)$ is finite and continuous at $t = \xi$, then

$$\dot{y}(\xi + \delta) - \dot{y}(\xi - \delta) \to 1 \tag{6.7}$$

This means that $\dot{y}$ is discontinuous at $t = \xi$ and that the increment is unity.

Now a general solution to the <u>inhomogeneous</u> equation, Eq. (6.1), is the general solution to the homogeneous part $y_o(t)$, which satisfies the boundary conditions, plus the Green's function $G(t,\xi)$

$$\begin{aligned} y(t) &= y_o(t) , \qquad t < \xi \\ &= y_o(t) + G(t,\xi) , \qquad \xi < t \end{aligned} \tag{6.8}$$

where Green's function is that <u>solution to the homogeneous equation which vanishes at $t = \xi$ and whose derivative there is unity</u>

$$\begin{aligned} G(\xi,\xi) &= 0 \\ \dot{G}(\xi,\xi) &= 1 \end{aligned} \tag{6.9}$$

To construct a solution of Eq. (6.1) for any arbitrary function $f(t)$, superpose all the impulse solutions

$$y(t) = y_o(t) + \int_a^t G(t,\xi) \frac{f(\xi)}{\mu} d\xi \tag{6.10}$$

Exercise 6.1: Verify that Eq. (6.10) is a solution to the inhomogeneous equation, Eq. (6.1).

By inspection, one can see that Green's function is

$$G(t,\xi) = \mathrm{Re}\,\frac{e^{i\omega(t-\xi)}}{i\omega} = \frac{\sin\,\omega(t-\xi)}{\omega} \tag{6.11}$$

Thus, the general solution of the impulse excited harmonic oscillator is

$$y(t) = y_o(t) + \frac{1}{\omega}\int_a^t \sin\,\omega(t-\xi)\,\frac{f(\xi)}{\mu}\,d\xi$$

$$= y_o(t) + \frac{\sin\,\omega t}{\omega}\int_a^t \frac{f(\xi)}{\mu}\cos\,\omega\xi\,d\xi - \frac{\cos\,\omega t}{\omega}\int_a^t \frac{f(\xi)}{\mu}\sin\,\omega\xi\,d\xi$$

$$= y_o(t) + \mathrm{Re}\int_a^t \frac{f(\xi)}{\mu}\,\frac{e^{i\omega(t-\xi)}}{i\omega}\,d\xi \tag{6.12}$$

Generally, we are interested in the state of excitation after the collision event has been completed.

$$y(\infty) = y_o(\infty) + \mathrm{Re}\;e^{i\omega t}\int_{-\infty}^{\infty} \frac{f(\xi)e^{-i\omega\xi}}{i\omega\mu}\,d\xi \tag{6.13}$$

Consider now a diatomic molecule subject to the linearized perturbation potential

$$U(t,y) = U_e + \left(\frac{\partial U}{\partial y}\right)_e y + \ldots \tag{6.14}$$

where U_e and $(\partial U/\partial y)_e$ are the potential and its gradient at the equilibrium value, $y = 0$, both functions of time. The force on the oscillator is just

$$f(t) = \frac{\partial U(t,y)}{\partial y} = \left(\frac{\partial U}{\partial y}\right)_e + \ldots \tag{6.15}$$

Starting from rest at time $t = -\infty$, the amplitude y at time t is

$$y = \int_{-\infty}^{t} \frac{(\partial U/\partial y)_e}{\mu\omega}\sin\,\omega(t-\xi)d\xi \tag{6.16}$$

and the maximum amplitude Y, excited by the collision at time t, may be expressed

$$Y = \left| \int_{-\infty}^{t} \frac{(\partial U/\partial y)_e}{\mu\omega} e^{i\omega\xi} \, d\xi \right| \tag{6.17}$$

The net amount of vibrational energy excited is, in units of $\hbar\omega$, just the square of the Fourier transform of $f(t)$ or $(\partial U/\partial y)_e$ divided by $2\mu\hbar\omega$.

$$\frac{\Delta E}{\hbar\omega} = \frac{\mu\omega^2 Y^2}{2\hbar\omega} = \frac{1}{2\mu\hbar\omega} \left| \int_{-\infty}^{t} \left(\frac{\partial U}{\partial y}\right)_e e^{i\omega t} \, dt \right|^2 \tag{6.18}$$

As we shall see later, this quantity is exactly the same as the transition probability P_{01}, for transition from the ground state to the first excited state given by small perturbation quantum theory. However, the strictly classical model is not so simply related to transition probability when transitions from excited quantum states are involved.

Interaction potentials are typically taken to be exponential in character during collision

$$U(y,t) = U_o \exp\left(\frac{y - r}{L}\right) \tag{6.19}$$

where r is the distance between centers of mass of the collision partners, a function of t, U_o establishes the magnitude of the interaction potential, and L is a potential scale parameter. In this case

$$\frac{\partial U}{\partial y} = \frac{U(y,t)}{L}, \qquad \left(\frac{\partial U}{\partial y}\right)_e = \frac{U_o}{L} e^{-r/L}. \tag{6.20}$$

If the collisions are not too energetic, that is, if gas temperatures are not too high, the vibrational amplitudes y induced by collision are small compared with the potential scale parameter L, which is typically the order of 0.2 Å, and the exponential potential may in this case be linearized and the expression for $(\partial U/\partial y)_e$ from Eq. (6.20) substituted in Eq. (6.18).

Exercise 6.2: Use ω^{-1} for the units of t and $(\hbar/\mu\omega)^{1/2}$ for the units of y, and show that the oscillator differential equation reduces to the dimensionless form

$$\ddot{y} + y = a(t) = \left(\frac{\mu\omega}{\hbar}\right)^{1/2} \frac{f(t)}{\mu\omega^2}$$

Show that the solution for $y(t)$ for the forcing function

$$a(t) = 0 \quad , \quad t < 0$$

$$= -a_o \quad , \quad t > 0$$

is, for the case $y_o(t) = 0$,

$$y = 0 \quad , \quad t < 0$$

$$= -a_o(1 - \cos t) \quad , \quad 0 < t$$

The negative impulse force represents a force which compresses the oscillator to a new equilibrium position $-a_o$. The oscillator is seen to oscillate with the amplitude a_o about this new equilibrium point as long as the impulse exists.

Show that if the constant forcing function is terminated at $t = 2n\pi$

$$y(t) = 0 , \quad 2n\pi < t$$

whereas, if the forcing function is terminated at $t = (2n + 1)\pi$

$$y(t) = 2a_0 \cos t , \quad (2n + 1)\pi < t$$

which has the amplitude $2a_0$, and is in phase with the forced oscillations. Finally, show that if the impulse lasts for the interval $(2n + 1)\pi/2$

$$y(t) = a_0(\cos t \pm \sin t) , \quad (2n + 1)\pi/2 < t$$

where the $\pm$ sign obtains if n is even and odd, respectively. This oscillation has an amplitude $\sqrt{2}a_0$ and is shifted in phase by $\pi/4$ or $3\pi/4$ for n even and odd, respectively. Thus, we see that impulse functions of varying length can produce quite different amplitudes and phases for the oscillations induced.

Exercise 6.3: Find solutions for $y(\infty)$ and $y(t)$ for the impulse function

$$a(t) = -a\, e^{-b|t|} .$$

What is the character of the solution up to $t = 0$? How does this differ from the solution for $t > 0$?

Exercise 6.4: Show that if the impulse is very short compared with the oscillator's period, ω^{-1}, the solutions for $y(\infty)$ depend only on the total impulse, I,

$$y = y_0(t) + \frac{I}{\mu\omega} \sin \omega t$$

where

$$I = \int_{-\infty}^{\infty} f(t)dt$$

Note that this solution is independent of the shape of the impulse function, $f(t)$.

6.4 QUANTUM OSCILLATOR EXCITATION

The time-dependent Schroedinger equation expresses the manner in which the complete wave function ψ of a system of particles changes with time

$$\tilde{H}\psi = i\hbar \frac{\partial \psi}{\partial t} \tag{6.21}$$

Where $\tilde{H}$ is the Hamiltonian operator for the system. In the perturbation method of solving this equation, the Hamiltonian is written as the sum of a steady state part H^o and a time-dependent perturbation H'

$$H = H^o + H' \tag{6.22}$$

The unperturbed wave functions ψ^o satisfy the equation

$$\tilde{H}^o\psi^o = i\hbar \frac{\partial \psi^o}{\partial t} \tag{6.23}$$

and since $\tilde{H}_o$ is independent of time, the wave functions which are eigenfunctions of this equation have the form

$$\psi_n^o(q,t) = \phi_n(q)e^{-iE_nt/\hbar} \tag{6.24}$$

This set of eigenfunctions forms a complete orthogonal set; thus, any arbitrary function, for example the solution to Eq. (6.21) which we seek, can be expanded into a sum of these functions

$$\psi(q,t) = \sum_n a_n(t)\psi_n^0(q,t) \tag{6.25}$$

Substituting Eq. (6.25) into Eq. (6.21), we obtain

$$\sum_n a_n\tilde{H}^0\psi_n^0 + \sum_n a_n\tilde{H}'\psi_n^0 = i\hbar\sum_n \dot{a}_n\psi_n^0 + i\hbar\sum_n a_n\frac{\partial\psi_n^0}{\partial t} \tag{6.26}$$

The first term on the left side equals the last term on the right, in accordance with Eq. (6.23), so

$$\sum_n a_n\tilde{H}'\psi_n^0 = i\hbar\sum_n \dot{a}_n\psi_n^0 \tag{6.27}$$

If the number of energy levels is finite, as is the case for diatomic molecule oscillators, this leaves a finite set of coupled equations to solve for the unknown coefficients a_n. Explicit expressions for the time derivatives $\dot{a}_n$ may be obtained by using the orthogonality properties of the eigenfunctions ψ_n^0; multiply both sides of Eq. (6.27) by ψ_m^{0*} and integrate over all coordinate space to obtain

$$\begin{aligned}\dot{a}_m &= -\frac{i}{\hbar}\sum_n a_n(t)\int \psi_m^{0*}\tilde{H}'\psi_n^0\,dq \\ &= -\frac{i}{\hbar}\sum_n a_n(t)e^{-i\omega_{mn}t}H_{mn}(t)\end{aligned} \tag{6.28}$$

where the circular frequencies ω_{mn} are

$$\omega_{mn} = \frac{E_n - E_m}{\hbar} \tag{6.29}$$

and the matrix elements $H_{mn}(t)$ are

$$H_{mn}(t) = \int \phi_m^*(q)H'(q,t)\phi_n(q)dq \tag{6.30}$$

At time zero, the system is specified to be in one particular eigenstate so that $a_m(-\infty) = 1$ and $a_n(-\infty) = 0$ for all $n \neq m$. The set of coupled Eqs. (6.28) does not involve any approximation, and in a general case, it can be integrated numerically with modern computers, if the total number of levels is not too large. This is known as the close-coupling method of solution. The solutions can be performed for anharmonic oscillators as well as for harmonic oscillators if the eigenfunctions, ϕ_n^0, for the unperturbed state of these oscillators are known. In this case, the matrix elements H_{mn} may need to be determined by numerical integration, but where the perturbation Hamiltonian $H'(t)$ has a known form separable in q and t, this can be done independently and the results tabulated in computer memory before the numerical integrations of the coupled set of equations is performed. Also, the perturbations can be of any arbitrary size in this method; they are not limited to small energy

compared with the steady state, unperturbed energy levels of the oscillator as in the small perturbation method which follows.

The small perturbation method is limited to cases where H' is much smaller than H^0, but this is a condition which is satisfied in many practical cases of excitation of molecular oscillators in gases, as long as the temperature is not too high. In this case the solutions can be carried out in analytic form, which gives us a great advantage in understanding the process and in efficiently programming the more exact numerical solutions of the coupled set of equations. In the small perturbation method we let the system be in state m initially, $a_m(-\infty) = 1$ and $a_{n\neq m}(-\infty) = 0$, and neglect all terms on the right side of Eq. (6.28) except the term $n = m$. For a short impulse then the equations become

$$\dot{a}_m(t) \simeq -\frac{i}{\hbar} H_{mm}(t) \qquad (6.31)$$

$$\dot{a}_n(t) \simeq -\frac{i}{\hbar} H_{mn}(t) e^{i\omega_{mn}t} \qquad (6.32)$$

for which solutions are

$$a_m(t) \simeq 1 - \frac{i}{\hbar}\int_{-\infty}^{t} H_{mm}(t)dt \qquad (6.33)$$

$$a_n(t) \simeq -\frac{i}{\hbar}\int_{-\infty}^{t} H_{mn}(t) e^{i\omega_{mn}t}\, dt \qquad (6.34)$$

Exercise 6.5: Show that if H' is a constant in time, the perturbed wave function is a steady-state wave function

$$a_m(t)\psi_m^0 = \phi_m(q) e^{-(i/\hbar)(E_m^0 + H_{mm})t}$$

and the time dependent factor contains the first-order energy eigenvalue, $E_m^0 + H_{mm}$, as required by the time independent perturbation theory. Also show that the coefficient for a short constant impulse of duration Δt is

$$a_n = \frac{H_{mn}}{E_n - E_m}\left[1 - e^{-(i/\hbar)(E_n - E_m)\Delta t}\right] \simeq \frac{i}{\hbar} H_{mn}\Delta t$$

and the probability that the system will be found in state n after such an impulsive collision is

$$a_n^2 \simeq \frac{H_{mn}^2 (\Delta t)^2}{\hbar^2}$$

Exercise 6.6: Show that if H_{mn} varies slowly in a time interval $2\pi/\omega_{mn}$ the matrix element and the transition probability nearly vanish. This type of collision is thus adiabatic. If on the other hand H_{mn} varies rapidly and remains constant at time $t > t_0$, as a step function, the integral diverges. This can be handled by integration by parts

$$a_n = -\frac{i}{\hbar}\int_{-\infty}^{t} H_{mn}\, e^{i\omega_{mn}t}\, dt = -\frac{H_{mn}\, e^{i\omega_{mn}t}}{\hbar\omega_{mn}}\bigg|_{-\infty}^{t} + \int_{-\infty}^{t} \frac{dH_{mn}}{dt}\frac{e^{i\omega_{mn}t}}{\hbar\omega_{mn}}\, dt$$

The first term vanishes at the lower limit because $H_{mn}(-\infty) = 0$. At the upper limit it is just the steady-state perturbation solution to level m; the time dependent part of the transition probability is the square of the second term. Show that if the derivative is large, that is, the step function perturbation is applied very quickly on the time scale $2\pi/\omega_{mn}$,

$$P_{mn} \simeq \frac{H_{mn}^2}{\hbar^2\omega_{mn}^2}$$

The probability that transition to another state n has occurred at any time t is a_n^2, or $a_n^* a_n$ if a_n should be complex,

$$P_{m \to n} = a_n^2 = \frac{1}{\hbar^2} \left| \int_{-\infty}^{t} H_{mn} \, e^{i\omega_{mn} t} \, dt \right|^2 \qquad (6.35)$$

The probability of transition induced by the entire collision event is given when the upper limit of the integral is $+\infty$; that is, the probability is the square of the Fourier transform of the matrix element H_{mn}.

Consider now a harmonic oscillator subject to the linearized perturbation of Eq. (6.14)

$$U' = \left(\frac{\partial U}{\partial y}\right)_e y + \ldots \qquad (6.36)$$

where y is the dimensionless oscillator displacement of Ex. 6.2

$$y = \left(\frac{\mu\omega}{\hbar}\right)^{1/2} (\rho - \rho_e) \qquad (6.37)$$

and ρ and ρ_e are the dimensioned values of the oscillator coordinate. In this case the wave functions are the well known solutions to Schroedinger's equation with the potential $V = \mu\omega^2(\rho - \rho_e)^2/2$

$$\phi_n(y) = N_n \, e^{-y^2/2} \, H_n(y) \qquad (6.38)$$

where $H_n(y)$ is the nth order Hermite polynomial and N_n is the normalization constant required

$$N_n = \left(\frac{\mu\omega}{\pi\hbar}\right)^{1/4} \left(\frac{1}{2^n n!}\right)^{1/2} \qquad (6.39)$$

such that the integral of ϕ_n^2 over all displacement ρ is unity. The transition matrix elements $H_{n,n+1}$ are in this case

$$H_{n,n+1} = \int_0^{\infty} \phi_n \left(\frac{\partial U}{\partial y}\right)_e y \phi_{n+1} \, d\rho$$

$$= \left(\frac{\hbar}{\mu\omega}\right)^{1/2} \left(\frac{\partial U}{\partial y}\right)_e N_n N_{n+1} \int_{-\infty}^{\infty} e^{-y^2} \, H_n y H_{n+1} \, dy$$

$$= \left(\frac{\hbar}{\mu\omega}\right)^{1/2} \left(\frac{\partial U}{\partial \rho}\right)_e \left(\frac{n+1}{2}\right)^{1/2} \qquad (6.40)$$

The circular frequency for this transition in the harmonic oscillator is just the fundamental frequency ω, of course

$$\omega_{n,n+1} = \frac{(n+1)\hbar\omega - n\hbar\omega}{\hbar} = \omega \qquad (6.41)$$

and the transition probability thus becomes

$$P_{n,n+1} = (n+1)\frac{1}{2\mu\hbar\omega}\left|\int_{-\infty}^{t}\left(\frac{\partial U}{\partial \rho}\right)_e e^{i\omega t}\,dt\right|^2 \qquad (6.42)$$

All other transitions except a change in vibrational quantum number by ±1 vanish for the linearized perturbation of Eq. (6.36). Of course, in real collisions higher order terms in the interaction potential are present and multiple quantum jumps will occur with finite probability, even though with much smaller probability than the jumps to adjacent levels given above. For transition from the ground state to the first excited state, the collision-induced transition probability for the linearized potential is

$$P_{01} = \frac{1}{2\mu\hbar\omega}\left|\int_{-\infty}^{\infty}\left(\frac{\partial U}{\partial \rho}\right)_e e^{i\omega t}\,dt\right|^2 \qquad (6.43)$$

which is exactly the same expression obtained for $\Delta E/\hbar\omega$ with the classical harmonic oscillator model, Eq. (6.18).

Exercise 6.7: Use the recursion relation between Hermite polynomials

$$yH_n = \tfrac{1}{2}H_{n+1} + nH_{n-1}$$

and the orthogonality relation

$$\left(\frac{h}{\mu\omega}\right)^{1/2} N_n^2 \int_{-\infty}^{\infty} e^{-y^2} H_n H_m\,dy = \delta_{nm}$$

to derive the result of Eq. (6.40). Also show that H_{nm} vanishes for the linearized perturbation, except for $m = n \pm 1$.

6.5 SEMICLASSICAL APPROXIMATION, COLLINEAR COLLISIONS

In a strictly quantum solution, the incoming particle colliding with the oscillator is treated as a wave function with wavelength $(E - U)/hc$, where E is the total energy and U is the interaction potential. The perturbation method outlined in the last section then proceeds using the total wave function for the entire collision system rather than just the oscillator wave function alone. Although such wave functions can be obtained numerically, once the interaction potential is specified, the semiclassical approximation is a somewhat simpler procedure, which for an exponential interaction potential leads to analytic solutions which conveniently express the important parameters of the process. In the semiclassical method the classical trajectory for motion between the colliding particles is used to obtain a time-dependent potential perturbation; then the transitions produced by this perturbation are calculated by the quantum methods used in the previous section. The deBroglie wavelengths

of heavy gas particles are normally much smaller than the scale dimensions of the potentials involved, that is, the distance over which the potential changes by an appreciable amount, so the classical trajectory is a good approximation and the semi-classical results are, in principle, as accurate as needed for many purposes.

For the present, we will restrict the collision to a one-dimensional, collinear event, which is a collision that is so atypical as to occur with zero probability but nevertheless illustrates all the principles involved. Later we will consider the full three-dimensional case. The collinear collision is diagrammed in figure 6.1.

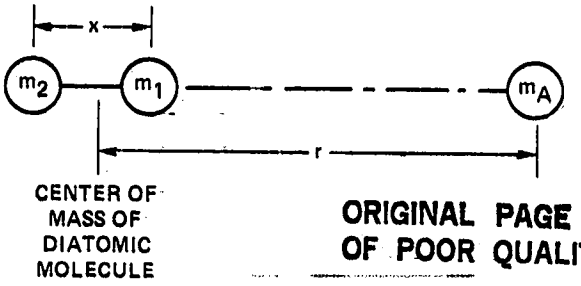

Fig. 6.1--Collinear collision between diatomic oscillator and inert collision partner.

The diatomic oscillator consists of atoms of mass m_1 and m_2, x is the interatomic distance of the oscillator, and r is the distance from the center of mass to the center of an inert collision partner which approaches the oscillator along the molecular axis and strikes the atom with mass m_1. The interaction potential is commonly expressed as the sum of two exponential, repulsive terms

$$U = A\left\{\exp\left[-\left(r - \frac{m_2 x}{m_1 + m_2}\right)\Big/L\right] + \exp\left[-\left(r + \frac{m_1 x}{m_1 + m_2}\right)\Big/L\right]\right\} \tag{6.44}$$

Expand this about the equilibrium oscillator separation, x_e

$$U = A\exp\left(-\frac{r}{L}\right)\exp\left(\frac{\mu x_e}{m_1 L}\right)\exp\left[\frac{\mu}{m_1}\left(\frac{x - x_e}{L}\right)\right]\left\{1 + \exp\left(-\frac{x_e}{L}\right)\exp\left[-\frac{x - x_e}{L}\right]\right\} \tag{6.45}$$

where μ is the reduced mass of the oscillator, $m_1 m_2/(m_1 + m_2)$. Let the constant U_o represent the value at $r = \sigma$ and $x = x_e$

$$U_o = A\exp\left(-\frac{\sigma}{L}\right)\exp\left(\frac{\mu}{m_1}\frac{x_e}{L}\right)\left[1 + \exp\left(-\frac{x_e}{L}\right)\right] \tag{6.46}$$

Then to terms of first order in $x - x_e$, the interaction potential becomes

$$U = U_o\exp\left(-\frac{r - \sigma}{L}\right)\left[1 + \frac{\mu}{m_1}\left(\frac{x - x_e}{L}\right) + \ldots\right] \tag{6.47}$$

To first order, σ represents the distance of closest approach in the classical trajectory and U_o is the potential at that point, which for the collinear collision is the total kinetic energy of the collision pair. In a three-dimensional collision

C-2

there would, of course, be some residual kinetic energy at the point of closest approach, but in the present case the kinetic energy is completely absorbed in the interaction potential at this point.

To obtain the classical trajectory, the potential is averaged over all values of x and the trajectory is assumed to be that which obtains for this average potential. Because of the orthogonality relations of the normalized harmonic oscillator wave functions, the first term in Eq. (6.47) is multiplied by unity, the second term vanishes, and the average potential is simply

$$\bar{U} = \left\langle \phi_n^* | U | \phi_n \right\rangle = U_o \exp\left(-\frac{r - \sigma}{L}\right) \tag{6.48}$$

The value of the collision velocity $\dot{r}$ as a function of time is given by

$$\dot{r} = \sqrt{\frac{2}{m}(U_o - U)} = \sqrt{\frac{2U_o}{m}}\left[1 - \exp\left(-\frac{r - \sigma}{L}\right)\right]^{1/2} \tag{6.49}$$

where the mass m is the reduced mass of the collision pair

$$m = \frac{m_A(m_1 + m_2)}{m_A + m_1 + m_2} \tag{6.50}$$

Let time zero occur at the point of closest approach and integrate Eq. (6.49) to obtain

$$\sqrt{\frac{2U_o}{m}}\, t = ut = \int_\sigma^r \frac{dr}{[1 - \exp -(r - \sigma/L)]^{1/2}}$$

$$= 2L \tanh^{-1}\left[1 - \exp\left(-\frac{r - \sigma}{L}\right)\right]^{1/2}$$

Thus the exponential term in Eq. (6.48) becomes

$$\exp\left(-\frac{r - \sigma}{L}\right) = 1 - \tanh^2 \frac{ut}{2L} = \operatorname{sech}^2 \frac{ut}{2L} \tag{6.51}$$

and the interaction potential of Eq. (6.47) can be expressed as the time dependent function

$$U = U_o \operatorname{sech}^2 \frac{ut}{2L}\left[1 + \frac{\mu}{m_1}\left(\frac{x - x_e}{L}\right) + \ldots\right] \tag{6.52}$$

The transition matrix elements H_{mn} of Eq. (6.30) vanish for the first term of Eq. (6.52) because of the orthogonality relation between the oscillator wave functions, and only the second term in $(x - x_e)$ contributes a finite result.

The transition probability of Eq. (6.35) may be expressed

$$P_{n,n\pm1} = \gamma^2_{n,n\pm1}\left(\frac{E}{\hbar\omega}\right)^2 F^2 \tag{6.53}$$

where $\gamma_{n,n\pm1}$ is the matrix element average

$$\gamma_{n,n\pm1} = \left\langle \phi^*_{n\pm1} \left| \frac{\mu}{m_1} \frac{x - x_e}{L} \right| \phi_n \right\rangle$$

$$= \left(\frac{n + 1/2 \pm 1/2}{4m_1 \omega L^2/\hbar} \right)^{1/2} \tag{6.54}$$

and F is the dimensionless Fourier transform of the time-dependent part of the perturbation

$$F = \omega \int_{-\infty}^{\infty} \operatorname{sech}^2(at) e^{i\omega t}\, dt$$

$$= \pi \left(\frac{\omega}{a}\right)^2 \operatorname{csch}\left(\frac{\pi\omega}{2a}\right) \tag{6.55}$$

where $a = u/2L$. The first term of the potential of Eq. (6.52) contributes nothing to the transition probability because all the matrix elements for this term vanish due to the orthogonality of the oscillator wave functions, whether harmonic or not. The matrix elements $\gamma_{n,n\pm1}$ are the only finite elements for harmonic oscillators with a perturbation term proportional to $(x - x_e)$; all other elements vanish unless higher order terms in the expansion of the potential are retained or anharmonic oscillator wave functions are used.

Except at very high temperature the ratio $\pi\omega/2a$ is normally much larger than unity, and to a good approximation

$$|F|^2 \simeq 4\pi^2 \left(\frac{\omega}{a}\right)^4 e^{-\pi\omega/a} \tag{6.56}$$

Then the total transition probability is

$$P_{n,n\pm1} = 4\pi^2 \left(\frac{n + 1/2 \pm 1/2}{4m_1 \omega L^2/\hbar} \right) \left(\frac{E}{\hbar\omega}\right)^2 \left(\frac{\omega}{a}\right)^4 e^{-\pi\omega/a} \tag{6.57}$$

If a characteristic energy E_c is defined

$$E_c = 4\pi^2 m\omega^2 L^2 \tag{6.58a}$$

and a dimensionless characteristic energy x_c is defined

$$x_c = \frac{E_c}{2kT} = \frac{2\pi^2 m\omega^2 L^2}{kT} \tag{6.58b}$$

where m is the reduced mass of the collision pair, the transition probability becomes the simple expression

$$P_{n,n\pm1} = \left(n + \frac{1}{2} \pm \frac{1}{2}\right) \left(\frac{m}{m_1}\right) \left(\frac{E_c}{\hbar\omega}\right) e^{-(x_c/x)^{1/2}} \tag{6.59}$$

where x is the dimensionless collision energy $mu^2/2kT$.

Note that if the gas is a pure gas of homonuclear diatomic molecules $m_1 = m_2 = m$. If the oscillator is heteronuclear, the transition probabilities are greatest when the collision occurs with the light atom end of the oscillator. With HCl, for example, the transition probabilities are about 35 times greater when the H atom of the molecule is struck than when the heavy Cl atom is impacted by the collision partner.

Exercise 6.8: Evaluate the Fourier transform

$$F = \omega \int_{-\infty}^{\infty} \mathrm{sech}^2(at) e^{i\omega t}\, dt = \pi \left(\frac{\omega}{a}\right)^2 \mathrm{csch}\left(\frac{\pi\omega}{2a}\right)$$

Note that poles exist for the integrand at $\pm(i\pi/2)$, $\pm(3i\pi/2$, $\pm(5i\pi/2)$, etc. Choose a path of integration around the singularity $i\pi/2$ and integrate in the complex plane along the real axis x and back along the axis $x + i\pi$. Show that the integral vanishes at the limits, then equate the integral to the residue at the pole enclosed.

At this point the one-dimensional theory is made three-dimensional by taking the transition cross section equal to the product $S_o P$, where S_o is a constant suitably chosen to fit the magnitude of vibrational relaxation rate data. The rate coefficient is the cross section averaged over a Boltzmann distribution of collision energies

$$\alpha = \frac{\bar{u} S_o}{s} \int_0^{\infty} P(x) e^{-x}\, x\, dx \qquad (6.60)$$

where P is expressed in terms of the dimensionless collision energy x or E/kT.

The rate coefficient α thus becomes

$$\alpha_{n,n\pm1} = \frac{\bar{u} S_o}{s} \left(n + \frac{1}{2} \pm \frac{1}{2}\right)\left(\frac{m}{m_1}\right)\left(\frac{E_c}{\hbar\omega}\right) \int_0^{\infty} x\, e^{-(x_c/x)^{1/2} - x}\, dx \qquad (6.61a)$$

The integrand of Eq. (6.61a) has a sharp peak near the minimum of the exponent $x + (x_c/x)^{1/2}$, which occurs where its derivative vanishes.

$$1 - \frac{x_c^{1/2}}{2x_m^{3/2}} = 0 \; ; \quad x_m = \left(\frac{x_c}{4}\right)^{1/3} = \left(\frac{E_c}{8kT}\right)^{1/3} \; ; \quad E_m = \frac{E_c^{1/3}(kT)^{2/3}}{2} \qquad (6.62)$$

The exponent is now expanded about the point x_m

$$x + \left(\frac{x_c}{x}\right)^{1/2} = x_m + \left(\frac{x_c}{x_m}\right)^{1/2} + \frac{3x_c^{1/2}}{4x_m^{5/2}} (x - x_m)^2 + \cdots$$

$$= 3x_m + \frac{3}{2x_m} (x - x_m)^2 + \cdots$$

while the pre-exponential terms in the integral are pulled outside the integral and evaluated at x_m.

$$\alpha = \frac{\bar{u}S_o}{s}\left(n + \frac{1}{2} \pm \frac{1}{2}\right)\left(\frac{m}{m_1}\right)\left(\frac{E_c}{\hbar\omega}\right) x_m\, e^{-3x_m} \int_0^\infty e^{-(3/2x_m)(x-x_m)^2}\, dx \qquad (6.61b)$$

Since x_m is normally very large compared to unity, the integral can be performed over the entire range from $-\infty$ to ∞ without introducing appreciable error, which yields $(2\pi x_m/3)^{1/2}$ for the definite integral and a final result for the rate coefficient.

$$\alpha = \frac{\bar{u}S_o}{s}\left(n + \frac{1}{2} \pm \frac{1}{2}\right)\left(\frac{m}{m_1}\right)\left(\frac{E_c}{\hbar\omega}\right)\left(\frac{2\pi}{3}\right)^{1/2} x_m^{3/2}\, e^{-3x_m} \qquad (6.61c)$$

This is the final result for the rate coefficient for harmonic oscillator excitation in the usual one-dimensional collision approximation. The dominant factor in the above relation is the exponential term $\exp(-3x_m)$, and so the logarithm of α is seen to vary primarily as $(kT)^{-1/3}$

$$\ln \alpha \sim -3x_m = -3\left(\frac{E_c}{8kT}\right)^{1/3} = -\left(\frac{\theta}{T}\right)^{1/3} \qquad (6.63a)$$

where

$$\theta = 27\,\frac{E_c}{8k} \qquad (6.63b)$$

This is the famous result originally obtained by Landau and Teller (ref. 1). However, for our purposes here we shall want to include corrections for: (a) conservation of energy in the collision process, (b) attractive long-range potential interaction, and (c) the 3-dimensional collision effects, all of which are missing in the above derivation.

6.6 ENERGY CONSERVATION IN VIBRATIONAL TRANSITION

It is easy to see that an allowance must be made to account for conservation of energy, otherwise the rate coefficients $\alpha_{n,n+1}$ and $\alpha_{n+1,n}$ will be the same, in violation of the principle of detailed balancing at equilibrium. Rapp (ref. 13) lets the effective collision velocity u be the average of initial and final velocities, $(u_i + u_f)/2$, and Herzfeld (ref. 14) points out that this substitution is necessary to reconcile the classical and quantum results. To terms of second order, this is the same as letting the effective collision energy be the average of initial and final energies

$$x = x_i \pm \frac{\hbar\omega}{2kT} \qquad (6.63c)$$

The $\pm$ sign is used depending upon whether the transition is to the adjacent lower or upper vibrational state, respectively. The cross section is assumed to be a function of the energy at the turning point, and thus it will be convenient to change the variable of integration to x rather than x_i, in which case

$$\alpha_{\pm} = \frac{\bar{u}}{s} \exp\left(\mp \frac{\hbar\omega}{2kT}\right) \int_{\hbar\omega/2kT}^{\infty} S(x)\left(x \pm \frac{\hbar\omega}{2kT}\right) e^{-x}\, dx \qquad (6.61d)$$

The factor $\exp(\mp\hbar\omega/2kT)$ is just that required so the ratio of the forward rate to the reverse rate is the Arrhenius factor $\exp(-\hbar\omega/kT)$ which preserves detailed balancing at equilibrium. The lower limit of the integral, Eq. (6.61d), is the same for either excitation or de-excitation, since the excitation cross section vanishes for collision energy less than $\hbar\omega$.

6.7 EFFECT OF LONG-RANGE INTERACTION POTENTIALS ON VIBRATIONAL TRANSITION

Still one more correction can be added very simply for the usual case where a long range attractive potential exists as well as the short-range, steep, repulsive potential. A typical form of the potential is shown in figure 6.2, where the short-range potential decreases exponentially with the intermolecular distance r, while the long range potential increases inversely as the nth power of r, leading to a potential minimum ϵ below the free particle potential at infinite separation. The Fourier transform of the collision perturbation, Eq. (6.35), is still almost totally determined by the exponential character of the perturbation near the turning point; only the initial and final velocities which the system senses at the turning point are all increased by an additional kinetic energy amount ϵ. Thus, the effective collision energy is now related to the initial interaction energy, which appears in the Boltzmann distribution, by

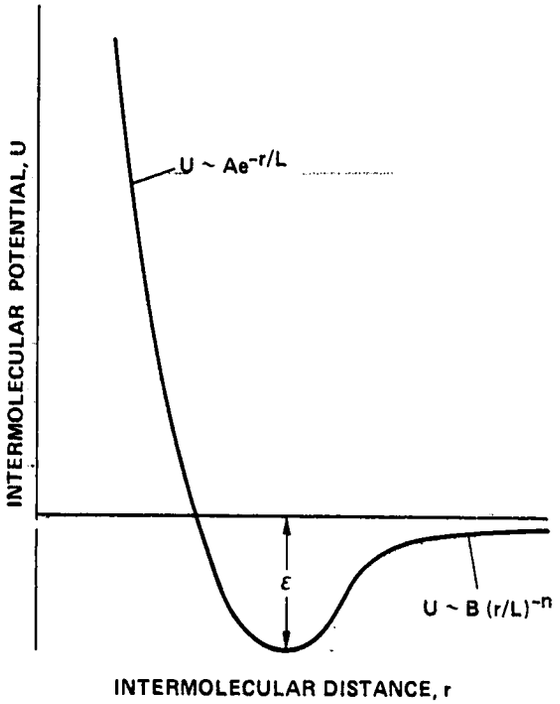

Figure 6.2- Typical intermolecular collision potential.

$$x = x_i \pm \frac{\hbar\omega}{2kT} + \frac{\epsilon}{kT} \qquad (6.63d)$$

In other words, the Maxwell-Boltzmann distribution of kinetic energies is shifted by the amount ϵ, at the point where the collision systems climb the repulsive interaction. To account for this, Eq. (6.61d) is modified as follows, again changing the variable of integration from x_i, the dimensionless initial kinetic energy, to x, the dimensionless effective kinetic energy at the turning point.

$$\alpha_{\pm} = \frac{\bar{u}}{s} \exp\left(\mp \frac{\hbar\omega}{2kT} + \frac{\epsilon}{kT}\right) \int_{(\hbar\omega/2kT)+(\epsilon/kT)}^{\infty} S(x)\left(x \pm \frac{\hbar\omega}{2kT} - \frac{\epsilon}{kT}\right) e^{-x}\, dx \qquad (6.61e)$$

Except at extremely high temperatures beyond the range of usual interest, the value of x_c is so large that the approximation of Eq. (6.56) for the Fourier transform is fully justified. Also, the value of $x \pm \hbar\omega/2kT - \epsilon/kT$ may be adequately

replaced by simply x_m, when this quantity is pulled outside of the integral, and finally the lower limit of the integral can be adjusted to give the entire Gaussian definite integral without serious error. Then the final expression for the rate coefficient given by the one-dimensional collision model, including the effect of an attractive potential and of energy conservation, is

$$\alpha_{\pm} = \frac{\bar{u}S_o}{s}\left(n + \frac{1}{2} \pm \frac{1}{2}\right)\left(\frac{m}{m_1}\right)\left(\frac{E_c}{\hbar\omega}\right)\left(\frac{2\pi}{3}\right)^{1/2} x_m^{3/2}\, e^{-3x_m \mp(\hbar\omega/2kT)+(\varepsilon/kT)} \qquad (6.61f)$$

6.8 RELAXATION RATE OF DIATOMIC, HARMONIC OSCILLATOR GASES

Usually the experimenter does not measure transition rates to and from a single vibrational level, though this is now possible in some cases with the extreme selectivity afforded by laser absorption measurements, but rather he typically measures a total relaxation rate for the flow of energy into or out of the vibrational mode after a sudden disruption of the equilibrium state, such as provided in a shock tube or a supersonic expansion nozzle. To compare theory with the experimental results in this case we are interested in the relation between the different rate coefficients

$$\alpha_{n+1,n} = (n + 1)\alpha_{10} \qquad (6.64a)$$

$$\alpha_{n,n+1} = (n + 1)\alpha_{01} = (n + 1)\alpha_{10}\, e^{-\hbar\omega/kT} \qquad (6.64b)$$

The relations given by Eqs. (6.64) merely reflect the dependence of the matrix elements γ^2 on the quantum number, of course.

The total relaxation process in the gas is described by a set of master equations, which for inert collision partners with number density N_a, is

$$\begin{aligned}
\frac{-dN_o}{dt} &= (\alpha_{01}N_o - \alpha_{10}N_1)N_a \\
\frac{-dN_1}{dt} &= (\alpha_{12}N_1 + \alpha_{10}N_1 - \alpha_{21}N_2 - \alpha_{01}N_o)N_a \\
&\vdots \\
\frac{-dN_n}{dt} &= (\alpha_{n,n+1}N_n + \alpha_{n,n-1}N_n - \alpha_{n+1,n}N_{n+1} - \alpha_{n-1,n}N_{n-1})N_a
\end{aligned} \qquad (6.65a)$$

where N_n is the number of oscillators in the nth quantum level. Each of these equations for $-dN_n/dt$ is multiplied by the appropriate quantum number n, and all are added together to give

$$-\frac{d}{dt}\sum_0^\infty nN_n = \left(\sum_0^\infty n\alpha_{n,n+1}N_n + \sum_1^\infty n\alpha_{n,n-1}N_n - \sum_0^\infty n\alpha_{n+1,n}N_{n+1} - \sum_1^\infty n\alpha_{n-1,n}N_{n-1}\right)N_a \qquad (6.65b)$$

The summations can all be started at $n = 1$, of course, without changing the equality. Collecting like terms in the first and fourth sums and in the second and third sums of the right side of Eq. (6.65b), by appropriate changes of the summation indices, we obtain

$$-\frac{d}{dt}\sum_{0}^{\infty} nN_n = \left(\sum_{1}^{\infty} \alpha_{n,n-1}N_n - \sum_{0}^{\infty} \alpha_{n,n+1}N_n\right)N_a \tag{6.65c}$$

Now introducing the relations of Eq. (6.64)

$$-\frac{d}{dt}\sum_{0}^{\infty} nN_n = \left[\sum_{1}^{\infty} n\alpha_{10}N_n - \sum_{0}^{\infty} (n+1)\alpha_{01}N_n\right]N_a$$

$$= \left[\alpha_{10}\sum nN_n - \alpha_{01}\sum (n+1)N_n\right]N_a \tag{6.65d}$$

The sum $\hbar\omega\sum nN_n$ is just the total vibration energy, E_v, and $\sum N_n$ is just the total number of oscillators N. Multiplying Eq. (6.65d) by $\hbar\omega$, we obtain

$$-\frac{dE_v}{dt} = [(\alpha_{10} - \alpha_{01})E_v - \hbar\omega\alpha_{01}N]N_a$$

$$= (\alpha_{10} - \alpha_{01})N_a\left(E_v - \hbar\omega N\frac{\alpha_{01}}{\alpha_{10} - \alpha_{01}}\right) \tag{6.66}$$

The relaxation time τ is defined as the constant

$$\tau = \frac{1}{(\alpha_{10} - \alpha_{01})N_a} \tag{6.67}$$

and the constant term $\hbar\omega N\alpha_{01}/(\alpha_{10} - \alpha_{01})$ is just the equilibrium vibrational energy in N harmonic oscillators given by the Einstein formula

$$\frac{N\hbar\omega\alpha_{01}}{\alpha_{10} - \alpha_{01}} = \frac{N\hbar\omega\, e^{-\hbar\omega/kT}}{1 - e^{-\hbar\omega/kT}} = E_v^{eq} \tag{6.68}$$

thus, Eq. (6.66) may be written

$$-\frac{d(E_v - E_v^{eq})}{dt} = \frac{E_v - E_v^{eq}}{\tau} \tag{6.69}$$

which can be integrated to give

$$E_v(t) - E_v^{eq} = [E_v(0) - E_v^{eq}]e^{-t/\tau} \tag{6.70}$$

The pressure and the relaxation times are measured by the experimenter, and the product of these two is related to the rate coefficients for $0 \leftrightarrow 1$ transitions by Eq. (6.67), with $N_a = p/kT$.

$$p\tau = \frac{kT}{\alpha_{10} - \alpha_{01}} = \frac{kT}{\alpha_{10}[1 - \exp(-\hbar\omega/kT)]} \tag{6.71}$$

The dominant factor in this relation is the exponential variation of α_{10} with $\exp[-(\theta/T)^{1/3}]$ as given by Eq. (6.63a). Thus, a Landau-Teller plot of $\ell n(p\tau)$ vs $T^{-1/3}$ yields essentially a straight line over a wide range of T. However, the temperature dependence of the pre-exponential terms and of the additional $\exp(-\hbar\omega/2kT)$ result in a nonlinear Landau-Teller plot at very high and very low temperatures. This additional temperature dependence must be accounted for if one seeks to deduce an accurate value for Ec, and therefore of the potential scale factor L, from the slope of the Landau-Teller plot. For example, the total temperature dependence of α_{10} given by the one-dimensional analysis leading to Eq. (6.61f) is

$$\alpha_{10} \sim e^{-(\theta/T)^{1/3}+(h\omega/2kT)+(\varepsilon/kT)} \tag{6.72}$$

where θ is $27E_c/8k$. Note that in the pre-exponential factors of Eq. (6.61f), the temperature dependence of $\bar{u}$ just cancels the dependence of $x_m^{3/2}$ or $(E_c/kT)^{1/2}$. However, in a subsequent section on 3-dimensional collisions it will be found that the quantity S_o is not really constant, but varies as velocity u or $(kTx)^{1/2}$. Then, evaluating S_o at x_m, for purposes of integration, leads to the corrected expression

$$\alpha_{10} \sim \left(\frac{T}{\theta}\right)^{1/3} e^{-(\theta/T)^{1/3}+(\hbar\omega/2kT)+(\varepsilon/kT)} \tag{6.73}$$

Thus the product $p\tau$ given by Eq. (6.71) varies as

$$p\tau = \frac{C(T/\theta)^{2/3}\, e^{(\theta/T)^{1/3}-(\varepsilon/kT)}}{\sinh \hbar\omega/2kT} \tag{6.74}$$

This is the expression that should be compared with the slope of a Landau-Teller plot to obtain a quantitative value of θ and L. If we let $\xi = (kT)^{-1/3}$

$$p\tau \sim \sinh \frac{\hbar\omega\xi^3}{2} \exp[(k\theta)^{1/3}\xi - \varepsilon\xi^3] \tag{6.74a}$$

$$\frac{d\ \ell n(p\tau)}{d\xi} = (k\theta)^{1/3} - 2(kT)^{1/3} - \frac{3}{(kT)^{2/3}}\left(\varepsilon + \frac{\hbar\omega}{2}\coth\frac{\hbar\omega}{2kT}\right) \tag{6.74b}$$

Thus, we see that if kT is neither too large nor too small, the slope of the Landau plot is just $(k\theta)^{1/3}$. However, if kT is large enough to compare with $k\theta$, the slope is reduced by the second term in Eq. (6.74b). On the other hand, if kT is small compared with $\hbar\omega$ or ε, the last term in Eq. (6.74b) can reduce the slope considerably. Thus, $\ell n(p\tau)$ will follow an S-shaped curve when plotted as a function of $(kT)^{-1/3}$ over a wide enough range of temperature.

Figures 6.3(a), 6.3(b), and 6.3(c) show some examples of Landau-Teller plots fo N_2, O_2, and CO for various collision partners. The theoretical relation is fit to tl range of experimental data on each plot. Within this range, the plot is generally linear, though at low temperatures some curvature has been observed. The values of the constant coefficients θ and C, defined by Eq. 6.74, which fit these experimental data are summarized in table 6.1. The potential well-depths, ε/k, are those determined for Lennard-Jones potentials that fit viscosity data for the pure gases; for unlike collision partners i and j the well-depth has been taken as the geometric mean, that is $\varepsilon = (\varepsilon_i \varepsilon_j)^{1/2}$. The characteristic length L of the potential interaction is calculated from (see Eq. 6.58a)

$$L^2 = \frac{E_c}{4\pi^2 m\omega^2} = \frac{2k\theta}{27\pi^2 m\omega^2} \tag{6.75}$$

The values of L are seen to lie in the range from 0.2 to 0.3 Å; this is about 30% larger than the values obtained by fitting simple linear expressions to a Landau-Teller plot, that is, neglecting the corrections for the impact velocity increase due to the potential well and also for the energy conservation leading to detailed balancing between α_{01} and α_{10}. Such linear fits are shown by the dotted curves in figure 6.3.

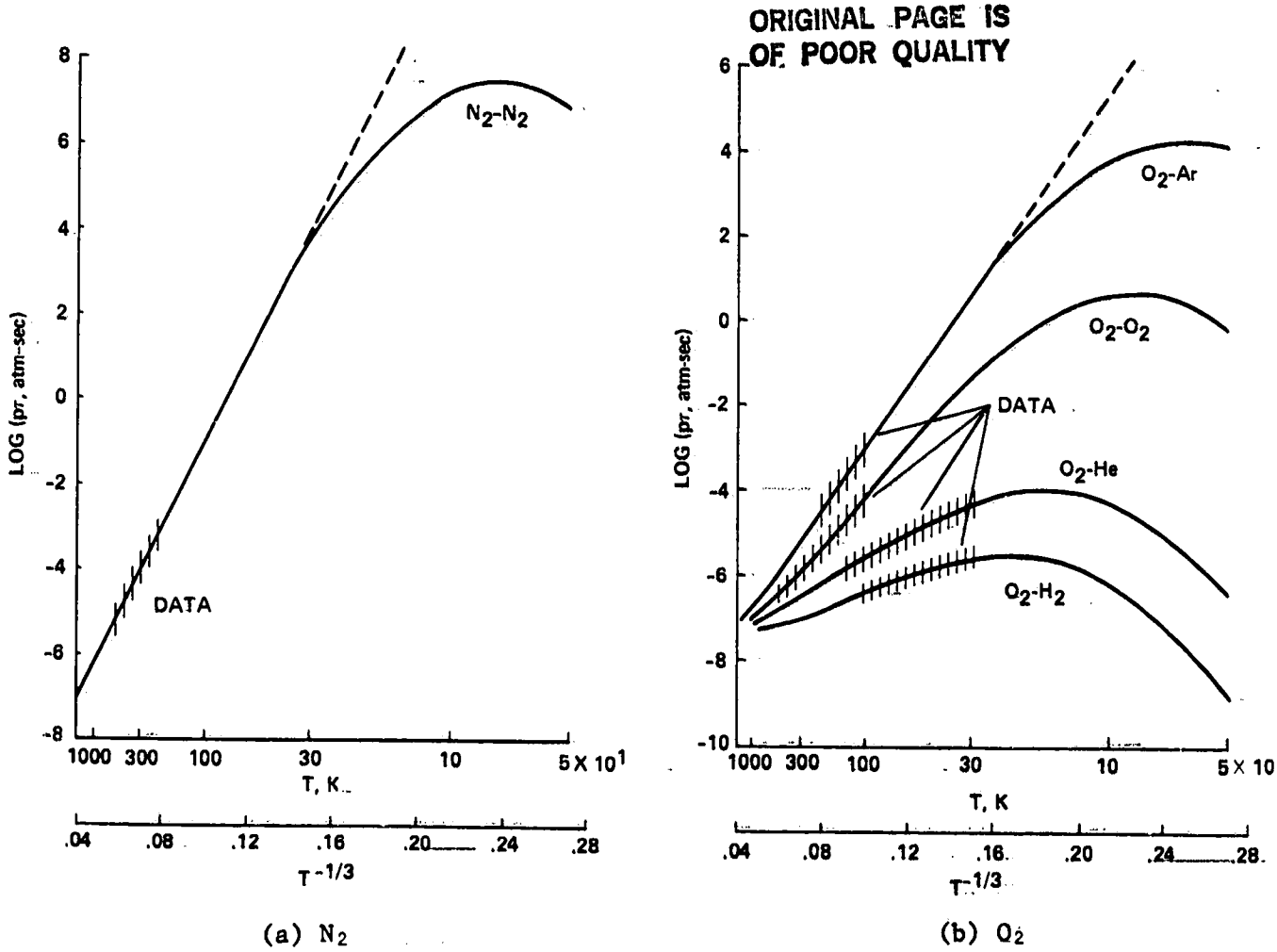

Figure 6.3- Landau-Teller plots.

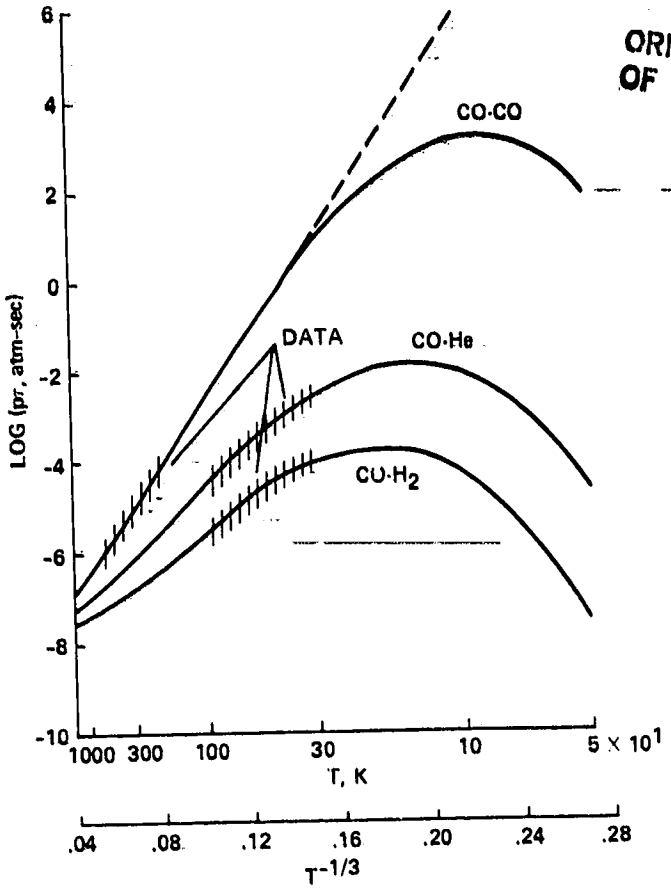

(c) CO

Figure 6.3- Concluded.

TABLE 6.1.- CHARACTERISTIC CONSTANTS WHICH FIT 3-DIMENSIONAL THEORY TO MEASURED VIBRATIONAL RELAXATION TIMES

Relaxing oscillator	$h\omega/k$, K	Collision partner	ϵ/k, K	C, atm-sec	θ, K	L, Å
N_2	3395	N_2	95.9	7.01×10^{-12}	3.12×10^{7}	0.27
O_2	2297	Ar	118.7	2.75×10^{-11}	1.47×10^{7}	.24
		O_2	118.0	7.58×10^{-11}	8.60×10^{6}	.19
		He	29.5	1.49×10^{-9}	2.26×10^{6}	.21
		H_2	60.2	9.63×10^{-10}	1.43×10^{6}	.23
CO	3122.5	CO	101.6	3.83×10^{-11}	1.66×10^{7}	.21
		He	27.4	1.78×10^{-10}	6.38×10^{6}	.26
		H_2	55.8	1.28×10^{-10}	4.37×10^{6}	.30

The values of A giving the magnitude of the repulsive potential in Eq. (6.44) can be derived from the constant C; typical values are the order of 1000 eV. However, the value of A is extremely sensitive to the exact fit to the data which is chosen, and considering the scatter in the data and the narrow range of temperature over which data is available, these values are uncertain by at least factors of 3 or more.

6.9 SEMICLASSICAL APPROXIMATION, THREE-DIMENSIONAL COLLISIONS

The perturbation potential is commonly assumed to be a linear superposition of exponential repulsions (refs. 21, 22), as previously done for the one-dimensional model. Mies (ref. 23) suggests that this may be an acceptable approximation for heavy atom harmonic diatomic oscillators, but shows that such a potential does not closely reproduce the time interactions for the $He-H_2$ collisions. Thus, although the linear superposition model will usefully illustrate the procedures involved, the quantitative results must be viewed with some skepticism. To proceed, we consider a homonuclear diatomic oscillator impacted by an inert collision partner and let the interaction potential be

$$U = A(e^{-r_1/L} + e^{-r_2/L}) \tag{6.76}$$

where again A determines the scale size of the potential and L is a characteristic length. The distances r_1 and r_2 are measured between the atoms of the diatomic oscillator and the inert collision partner. Figure 6.4 illustrates the geometry of a three-dimensional collision with miss distance b and with the center of mass of the diatomic molecule at the origin. Only one atomic nucleus is shown; the other is diametrically placed. The relative motion between the oscillator and its collision partner is assumed to be determined by the spherical part of the interaction potential. With this assumption, the collision trajectory lies in a single plane (the XY plane of fig. 6.4) and the distances r_1 and r_2 are

$$r_{1,2} = r\left[1 \mp \left(\frac{\rho}{r}\right)\sin\theta\cos(\phi - \chi) + \left(\frac{\rho}{2r}\right)^2\right]^{1/2} \tag{6.77}$$

where r and χ contain the functional dependence on time involved, and ρ is the distance between the atoms of the harmonic oscillator. We assume the collisions are weak enough that $(\rho/r) < 1$ for all r. Then reasonable approximations are

$$r_{1,2} \simeq r \mp \frac{\rho}{2}\sin\theta\cos(\phi - \chi) \tag{6.78}$$

$$U \simeq 2A\, e^{-r/L}\cosh\left[\frac{\rho}{2L}\sin\theta\cos(\phi - \chi)\right] \tag{6.79}$$

The bond length ρ is very nearly equal to its equilibrium value ρ_e, and the angle χ is small in the region near the turning point where the perturbation contributes most to the Fourier transform of Eq. (6.35). Accordingly, the perturbation is expanded to terms of first order in $(\rho - \rho_e)$ and χ

$$\rho\sin\theta\cos(\phi - \chi) \simeq \rho_e\sin\theta\cos\phi + \chi\rho_e\sin\theta\sin\phi + (\rho - \rho_e)\sin\theta\cos\phi \tag{6.80}$$

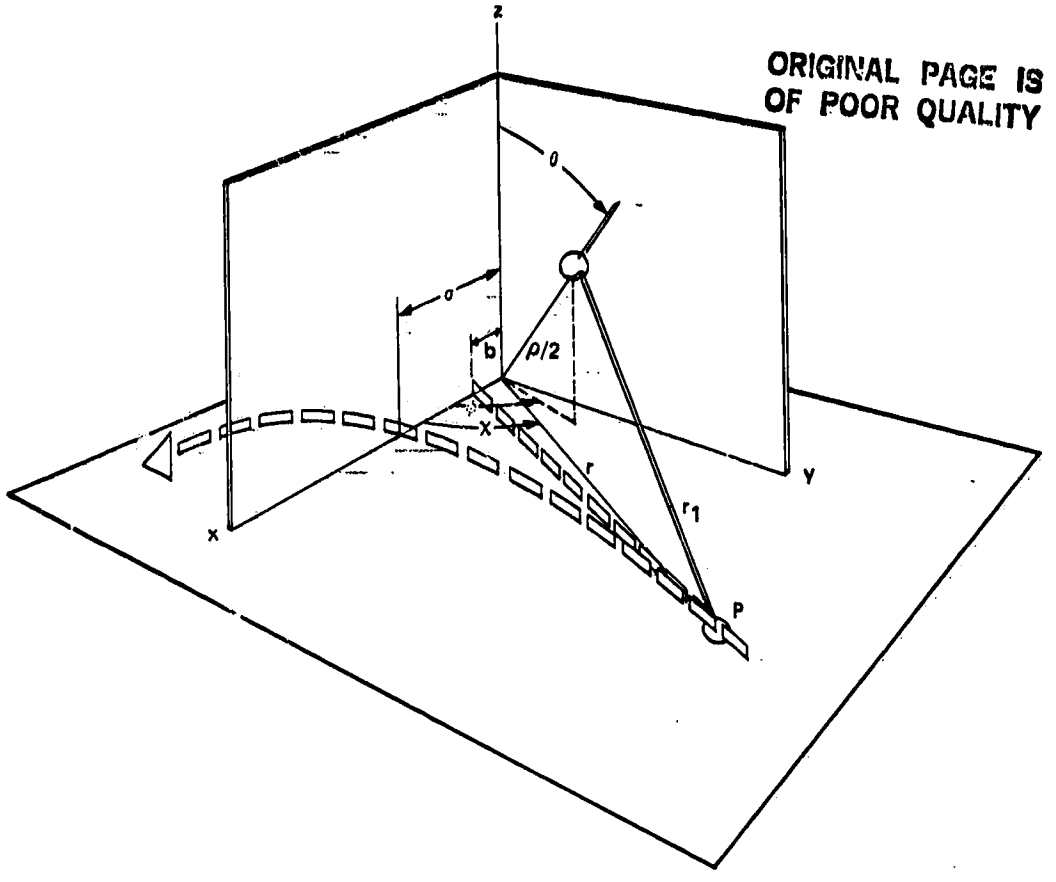

Figure 6.4- Diagram showing collision coordinates.

Then if we let $\delta = \rho_e/2L$

$$U \simeq 2A\, e^{-r/L}\left[\cosh(\delta \sin\theta\cos\phi) + \chi\delta \sin\theta \sin\phi \sinh(\delta \sin\theta\cos\phi) + \frac{\rho - \rho_e}{2L}\sin\theta\cos\phi \sinh(\delta \sin\theta\cos\phi) + \ldots\right] \tag{6.81}$$

The spherically symmetric part of the potential used to determine the collision trajectory is obtained by averaging U over all configurations of θ and ϕ

$$\bar{U} = 2A\, e^{-r/L}\langle\cosh(\delta \sin\theta\cos\phi)\rangle \tag{6.82a}$$

Strictly speaking, this average should be performed weighted by appropriate wave functions. For example, in small perturbation type collisions where the perturbed wave function remains essentially in the initial state, the average would be performed weighted by its initial state wave function. Unfortunately, the rotational states of molecules are strongly perturbed during the collisions of interest, that is, those collisions with sufficient energy to promote vibrational transitions. The assumption most often used in the literature to get around this complex and mathematically awkward situation, is that the rotational wave functions are so strongly mixed during the perturbation over a variety of angular momentum quantum numbers ℓ and their projections m, that the rigorous average is approximately the simple spherical

average as though the molecule were in its ground rotational state during the collision

$$\bar{U} \simeq 2A\, e^{-r/L}\, \frac{\sinh \delta}{\delta} \qquad (6.82b)$$

Stallcop (ref. 24) has further analyzed this type of approximation, weighting the interaction potential with the initial wave functions for transitions from ℓ to $\ell, \ell \pm 2$, and $\ell \pm 4$ for all possible values of the projection quantum number m and averaging the resulting probabilities over all values of m. He finds that the transition probabilities are decreased by factors the order of 2 for typical molecules and collision velocities of interest. For simplicity we will use the spherical average of Eq. (6.82b) to determine the classical trajectory; this will suffice to illustrate all the methods involved, at least.

Let the distance of closest approach be $r = \sigma$; then the potential can be expressed

$$U = \bar{U}_o\, e^{-(r-\sigma/L)} \Big[\cosh(\delta \sin\theta \cos\phi) + \chi\delta \sin\theta \sin\phi \sinh(\delta \sin\theta \cos\phi) + \frac{\rho - \rho_e}{2L} \sin\theta \cos\phi \sinh(\delta \sin\theta \cos\phi) + \ldots \Big] \frac{\delta}{\sinh \delta} \qquad (6.83)$$

where $\bar{U}_o$ is the spherically averaged potential at the point of closest approach

$$\bar{U}_o = 2A \big\langle \cosh(\delta \sin\theta \cos\phi) \big\rangle e^{-\sigma/L} = \frac{2A \sinh \delta}{\delta}\, e^{-\sigma/L} \qquad (6.84)$$

Exercise 6.9: Derive Eq. (6.84).

The first two terms of Eq. (6.83) are functions only of the rotational angular coordinates and are responsible for elastic scattering and pure rotational transitio only. The third term, linear in $(\rho - \rho_e)$, leads to single quantum jump vibrational transitions in the case of harmonic oscillators. The higher order terms or anharmon terms in the wave functions would, of course, introduce multiple quantum jump transitions.

Since the third term of the perturbation, Eq. 6.83, is the only one which contributes strongly to the vibrational transitions of interest, this is the only term which needs to be considered in the perturbation for present purposes. We will expand this potential to terms of order δ^3

$$U = \bar{U}_o\, e^{-(r-\sigma/L)}\, \frac{\rho - \rho_e}{2L} \left(\delta \sin^2\theta \cos^2\phi \pm \frac{\delta^3}{6} \sin^4\theta \cos^4\phi \pm \ldots \right) \frac{\delta}{\sinh \delta} \qquad (6.85)$$

and use these terms as the total perturbation. The full series is convergent, but converges slowly, so the truncated series above no longer exactly represents the sum of exponential terms postulated in setting up the problem, Eq. (6.76). However, the true interaction potentials are not exactly of exponential form anyway, so the approximation involved is not conceptually important; its use will greatly simplify the mathematics required and will suffice to illustrate all the methods used.

When rigid-rotator, harmonic-oscillator wave functions are used with the perturbation of Eq. (6.85), the transitions are limited to single vibrational quantum jumps ($\Delta v = \pm 1$) and even numbered rotational and magnetic quantum jumps ($\Delta \ell = 0, \pm 2, \pm 4$ and $\Delta m = 0, \pm 2, \pm 4$). Note that the symmetry of the rotational wave function is preserved in these transitions, consistent with the expectation that collisions are unlikely to change nuclear spin. In this case, rotational symmetry must be preserved to maintain antisymmetry of the total wave function.

The time dependence of the perturbation is contained in the factor $\exp[-(r - \sigma)/L]$. If energy and angular momentum changes in the internal state of the molecule are negligible compared with the kinetic energy and angular momentum of the collision partners, the latter two may be treated as conserved quantities. The classical trajectory in this case is defined by Eqs. (2.29) and (2.30). When the collision is head on ($b = 0$) the trajectory is that given by Eq. (6.51). Expand a solution of this form about the point $b = 0$ and stipulate that it must have the correct first- and second-order time derivatives at the point of closest approach ($r = \sigma$, $t = 0$). Such a solution is

$$e^{-(r-\sigma/L)} = \operatorname{sech}^2 at \tag{6.86}$$

where

$$a^2 = \frac{\ddot{r}_o}{2L} = \frac{1}{2L}\left(\frac{\bar{U}_o}{mL} + \frac{u^2 b^2}{\sigma^3}\right) = \left(\frac{u}{2L}\right)^2\left[1 - (1 - \varepsilon)\left(1 - \frac{2L}{\sigma}\right)\right] \tag{6.87}$$

$$\varepsilon = \frac{2\bar{U}_o}{mu^2} \tag{6.88}$$

This value of a gives the potential the correct form near the turning point at the expense of some mismatch in the asymptotic behavior. However, the Fourier transform, Eq. 6.55, is but slightly affected by the slowly varying part of the potential far from the turning point; it is primarily determined by the region where U changes rapidly, that is, near the turning point.

The transition probability may now be expressed in the same form as for the one-dimensional collinear collisions

$$P = 4\pi^2\gamma^2 \left(\frac{\varepsilon E}{\hbar\omega}\right)^2\left(\frac{\omega}{a}\right)^4 e^{-\pi\omega/a} \tag{6.89}$$

except that ε the fraction of total kinetic energy E which is converted into perturbation potential at the turning point, Eq. (6.88), is now included in the pre-exponential term. Also the matrix element is for a specific transition including not only a transition in vibrational quantum number n, but also in rotational and magnetic quantum numbers ℓ and m

$$\gamma_{n\ell m \to n'\ell'm'} = \left\langle \phi_{n'\ell'm'} \left| \frac{\rho - \rho_e}{2L}\left(\delta \sin^2\theta \cos^2\phi + \frac{\delta^3}{6}\sin^4\theta\cos^4\phi\right)\right| \phi_{n\ell m}\right\rangle \frac{\delta}{\sinh\delta} \tag{6.90}$$

Indices on P, γ, and ω indicating the specific transition have been dropped for economy of notation, but these will be introduced later. At the moment, we wish to obtain an analytic expression for the cross section. Let P_o, a_o, and σ_o denote the particular values of P, a, and σ for head on collision ($b = 0$). The cross section for transition may then be expressed

$$S = P_o \int_o^\infty \frac{P}{P_o} 2\pi b \, db \qquad (6.91)$$

According to Eq. (6.89)

$$\frac{P}{P_o} = \epsilon^2 \left(\frac{a_o}{a}\right)^4 \exp\left[-\frac{\pi\omega}{a_o}\left(\frac{a_o}{a} - 1\right)\right] \qquad (6.92)$$

and from Eq. (6.87)

$$\frac{a_o}{a} = \left[1 - (1 - \epsilon)\left(1 - \frac{2L}{\sigma}\right)\right]^{-1/2} \qquad (6.93)$$

For the exponential form of the interaction potential assumed here

$$\sigma = \sigma_o\left(1 - \frac{L}{\sigma_o} \ln \epsilon\right) , \quad \frac{d\sigma}{d\epsilon} = -\frac{L}{\epsilon} \qquad (6.94)$$

in which case (see Eq. 2.30)

$$b^2 = \sigma^2(1 - \epsilon) , \quad 2\pi b \, db = -\pi\sigma^2\left[1 + \frac{2L}{\sigma}\left(\frac{1 - \epsilon}{\epsilon}\right)\right]d\epsilon \qquad (6.95)$$

With change in the variable from b to ϵ, the cross section of Eq. (6.91) becomes

$$S = P_o \int_o^1 \frac{\pi\sigma^2}{1 + (2L/\sigma)[(1 - \epsilon)/\epsilon]} e^{-(\pi\omega/a_o)(a_o/a - 1)} d\epsilon \qquad (6.96)$$

Since $(\pi\omega/a_o) >> 1$, the major contribution to the integral of Eq. (6.96) comes from the region $a \simeq a_o$ and $\epsilon \simeq 1$. The integrand is therefore expanded about this point to terms of first order in $(1 - \epsilon)$:

$$\frac{\pi\sigma^2}{1 + (2L/\sigma)[(1 - \epsilon)/\epsilon]} \simeq \pi\sigma_o^2 \frac{1 + (2L/\sigma_o)(1 - \epsilon) + \ldots}{1 + (2L/\sigma_o)(1 - \epsilon) + \ldots} \simeq \pi\sigma_o^2 \qquad (6.97)$$

while from Eq. (6.93)

$$\frac{a_o}{a} - 1 \simeq \frac{1}{2}\left(1 - \frac{2L}{\sigma_o}\right)(1 - \epsilon) \qquad (6.98)$$

To this approximation the cross section becomes

$$S = \pi\sigma_o^2 P_o \int_0^1 \exp\left[-\frac{\pi\omega}{2a_o}\left(1 - \frac{2L}{\sigma_o}\right)(1 - \varepsilon)\right] d\varepsilon$$

$$= \pi\sigma_o^2 P_o \frac{1 - \exp[-(\pi\omega/2a_o)(1 - 2L/\sigma_o)]}{(\pi\omega/2a_o)[1 - (2L/\sigma_o)]} \xrightarrow{\frac{\pi\omega}{a_o} >> 1} \frac{\pi\sigma_o^2 P_o}{(\pi\omega/2a_o)[1 - (2L/\sigma_o)]} \quad (6.99)$$

The factor $(2a_o\sigma_o^2/\omega)(1 - 2L/\sigma_o)^{-1}$ is the effective total cross section for vibrational transition to be used with the one-dimensional collision transition probability P_o. This factor is not constant, as was assumed in the one-dimensional model, but is approximately proportional to a_o or the collision velocity u.

Next, the cross section is averaged over the Boltzmann distribution of collision energies to obtain the rate coefficient α. As in the one-dimensional case, we approximately account for conservation of energy during collision by letting the effective collision energy be the average of initial and final energies, as in Eq. (6.63c), and express the rate coefficient as Eq. (6.61e). The cross section has the form

$$S = S^*\left(\frac{\pi\sigma_o^2}{1 - 2L/\sigma_o}\right)\left(\frac{4x}{x_c}\right)^{1/2} e^{-(x_c/x)^{1/2}} \quad (6.100)$$

where the constant S^* is

$$S^* = \left(n + \frac{1}{2} \pm \frac{1}{2}\right)\left(\frac{m}{2\mu}\right)\left(\frac{E_c}{\hbar\omega}\right) \quad (6.101)$$

Substituting these relations in Eq. (6.61e) one obtains

$$\alpha_\pm = \frac{\bar{u}S^*}{s} e^{\mp(\hbar\omega/2kT)+(\varepsilon/kT)} \int_{(\hbar\omega+2\varepsilon)/2kT}^{\infty} \frac{\pi\sigma_o^2}{1 - (2L/\sigma_o)} \left(\frac{4x}{x_c}\right)^{1/2} \left(x \pm \frac{\hbar\omega}{2kT} - \frac{\varepsilon}{kT}\right) e^{-x-(x_c/x)^{1/2}} dx \quad (6.102)$$

where α_+ gives the rate coefficient going to the adjacent higher vibrational level while α_- gives the rate coefficient going to the adjacent lower vibrational level. The integrand is evaluated at the maximum just as before, including the distance of closest approach σ_o

$$\alpha_\pm = \frac{\bar{u}S^*}{s}\left(\frac{4x_m^3}{x_c}\right)^{1/2}\left(\frac{\pi\sigma_o^2}{1 - (2L/\sigma_o)}\right)_{x_m} e^{-3x_m \mp(\hbar\omega/2kT)+(\varepsilon/kT)} \int_{(\hbar\omega+2\varepsilon)/2kT}^{\infty} e^{-(3/2x_m)(x-x_m)^2} dx \quad (6.103)$$

Performing the integral and noting that $4x_m^3 = x_c$ this becomes

$$\alpha_\pm = \frac{\bar{u}}{s}\left(n + \frac{1}{2} \pm \frac{1}{2}\right)\left(\frac{m}{2\mu}\right)\left(\frac{E_c}{\hbar\omega}\right)\left(\frac{\pi\sigma_o^2}{1 - 2L/\sigma_o}\right)_{x_m}\left(\frac{\pi x_m}{6}\right)^{1/2} e^{-3x_m \mp(\hbar\omega/2kT)+(\varepsilon/kT)} \quad (6.104)$$

To express σ_o in terms of the temperature T, use the relation expressed by Eq. (6.84).

$$\sigma_o = L \ln \frac{\bar{A}}{E} ; \quad \bar{A} = 2A \frac{\sinh \delta}{\delta} \tag{6.105a}$$

$$(\sigma_o)_{x_m} = L \ln \frac{\bar{A}}{x_m kT} = L \ln \frac{2\bar{A}}{E_c^{1/3}(kT)^{2/3}} \tag{6.105b}$$

Then the cross-section factor becomes

$$\left(\frac{\pi\sigma_o^2}{1 - 2L/\sigma_o}\right)_{x_m} = \frac{\pi L^2 \ln^2[2\bar{A}/E_c^{1/3}(kT)^{2/3}]}{1 - 2/\ln[2\bar{A}/E_c^{1/3}(kT)^{2/3}]} \tag{6.106}$$

This logarithmic dependence on temperature is very weak, so the pre-exponential factor in α varies essentially as the product of $\bar{u}$ and $x_m^{1/2}$ (see Eq. 6.104), or in other words as the product of $T^{1/2}$ and $T^{-1/6}$. Thus, the overall variation of α with temperature is taken to be

$$\alpha \sim T^{1/3} \exp[-(\theta/T)^{1/3} + (\varepsilon/kT) \mp (\hbar\omega/2kT)]$$

as in Eqs. (6.73) and (6.74), and in calculating the values of θ and C in Table 6.1 and the curves of $p\tau$ in figures 6.3(a-c).

6.10 VIBRATION-ROTATION EXCITATION

Now recall that the matrix element γ is a function of the initial and final quantum numbers. Consequently, the rate coefficient α describes the rate of transition only between those two states. In order to compare with vibrational relaxation data, a total rate coefficient for the vibrational transition $n \to n \pm 1$ is needed; in particular for the $1 \to 0$ transition. The matrix element is viewed as a function of the differences

$$\Delta n = n' - n , \quad \Delta \ell = \ell' - \ell \quad \text{and} \quad \Delta m = m' - m.$$

$$\gamma^2(\Delta n, \Delta \ell, \Delta m) = \gamma^2(n, \ell, m; n + \Delta n, \ell + \Delta \ell, m + \Delta m) \tag{6.107}$$

where $\Delta n = \pm 1$, $\Delta \ell = 0, \pm 2, \pm 4$, and $\Delta m = 0, \pm 2, \pm 4$ for the perturbation used here and rigid rotator, harmonic oscillator wave functions. The total rate coefficient for a given vibrational rotational transition is found by summing γ^2 over all possible magnetic quantum number changes Δm and averaging over all initial values of m.

$$\gamma^2(\Delta n, \Delta \ell) = \frac{1}{2\ell + 1} \sum_{m=-\ell}^{\ell} \sum_{\Delta m = 0, \pm 2, \pm 4} \gamma^2(\Delta n, \Delta \ell, \Delta m) \tag{6.108}$$

Hansen and Pearson (ref. 25) evaluate these matrix elements for the perturbation of Eq. (6.85), as given in appendix 6A.

$$\gamma^2(\pm1,0) = \left(\frac{2}{15} + \frac{\delta^2}{35} + \frac{\delta^4}{630}\right)\left\langle\cosh(\delta \sin\theta \cos\phi)\right\rangle^2\left(\frac{n + (1/2) \pm (1/2)}{8mL^2\omega/\hbar}\right) \quad (6.109)$$

$$\gamma^2(\pm1,\pm2) = \left(\frac{1}{30} + \frac{\delta^2}{105} + \frac{2\delta^4}{2835}\right)\left\langle\cosh(\delta \sin\theta \cos\phi)\right\rangle^2\left(\frac{n + (1/2) \pm (1/2)}{8mL^2\omega/\hbar}\right) \quad (6.110)$$

$$\gamma^2(\pm1,\pm4) = \left(\frac{\delta^4}{22680}\right)\left\langle\cosh(\delta \sin\theta \cos\phi)\right\rangle^2\left(\frac{n + (1/2) \pm (1/2)}{8mL^2\omega/\hbar}\right) \quad (6.111)$$

The sperhically averaged angular part of the potential may in a first approximation be equated to $(\sinh\delta)/\delta$, as in Eq. (6.82b), but in more rigorous fashion would be a sum over all ℓ and m, which would depend somewhat on vibrational quantum level n.

Stallcop (ref. 26) derives similar expressions for a complete expansion of the interaction potential and finds corrections for the higher order terms in δ

$$\gamma^2(\pm1,0) = \left(\frac{2}{15} + \frac{\delta^2}{35} + \frac{\delta^4}{378} + \frac{\delta^6}{7128} + \ldots\right)\ldots$$

$$\gamma^2(\pm1,\pm2) = \left(\frac{1}{30} + \frac{\delta^2}{105} + \frac{5\delta^4}{4536} + \frac{17\delta^6}{249480} + \ldots\right)\ldots \quad (6.112)$$

$$\gamma^2(\pm1,\pm4) = \left(\frac{\delta^4}{22680} + \frac{\delta^6}{166320} + \ldots\right)\ldots$$

It can be seen by comparison with the relations above that the results are the same as for the truncated potential up to terms of order δ^2 but are larger in the higher order terms. Stallcop (ref. 26) also develops corrections for some of the other terms dropped in the expansions leading to the rate coefficients and finds that for realistic values of δ and L these can change some of the values by factors the order of 2. The general results are, however, similar to the above.

Perhaps the most important correction to include is the change in circular frequency ω that occurs at different rotational levels. To terms of second order the energy eigenvalue of a given state is

$$E_{n,\ell} = \hbar\omega_o\left(n + \frac{1}{2}\right) + B\ell(\ell + 1) + \ldots \quad (6.113)$$

where ω_o is the harmonic oscillator frequency and B is the rotational energy constant. To terms of first order in ℓ

$$\frac{\omega}{\omega_o} = \Delta n + \left(\frac{2B\,\Delta\ell}{\hbar\omega_o}\right)\ell + \ldots \quad (6.114)$$

The rate coefficients (Eq. (6.104)) are proportional to $\omega^{4/3}\exp(-3x_m)$. (The exponent on ω is incorrectly given as 7/3 in ref. 25). Note that the circular frequency that appears in γ^2 in Eqs. (6.109)-(6.111) is the uncorrected value, or ω_o — and corrections to the first-order rate coefficient can be expressed

$$R(\Delta\ell) = \frac{\alpha}{\alpha_o} = \left(\frac{\omega}{\omega_o}\right)^{4/3} e^{-3x_m[(\omega/\omega_o)^{2/3}-1]} \quad (6.115)$$

where α_o is the rate coefficient obtained when ω is equated to ω_o. Expand to terms of first order in λ

$$\lambda = \frac{2B|\Delta\ell|}{\hbar\omega_o} \tag{6.116}$$

which is typically less than 0.01 for realistic molecules and $|\Delta\ell| = 4$, to obtain

$$R(\Delta\ell) \simeq (1 - \lambda\ell)^{4/3} e^{2x_m\lambda\ell} + (1 + \lambda\ell)^{4/3} e^{-2x_m\lambda\ell} \tag{6.117}$$

The correction factors are now averaged over all initial rotational quantum numbers

$$\langle R(\Delta\ell)\rangle = \frac{B}{kT} \sum_{\ell=0} R(\Delta\ell)(2\ell + 1) e^{-B\ell(\ell+1)/kT} \tag{6.118}$$

Hansen and Pearson (ref. 25) use an approximate integral expression and Stallcop (ref. 26) uses a Laplace method that gives a better approximation at high temperature; both find that the correction for this dependence of ω on the rotational quantum number ℓ can increase the total rate coefficient by about 50%.

The potentials responsible for vibrational excitation are not necessarily the same as those responsible for scattering. For example, if the total electron spin and orbital momentum are not zero for the colliding particles, these can couple in different ways to yield a multiplicity of interaction potentials such as shown in figure 2.8 for collision between two atoms. Then scattering could largely be due to long range potentials with larger values of total electron spin, and therefore larger multiplicities; presumably these would have larger effective values of L. On the other hand, vibrational excitation would be dominated by steeper inner potentials resulting from lower total spin coupling. In such cases the potentials deduced from vibrational relaxation and from scattering represent different weighted averages of more than one interaction potential. However, in the case of N_2 the ground state is $^1\Sigma_g$, that is, a state with zero total spin and zero total orbital momentum; one thus expects a single potential surface to apply to N_2-N_2 or N_2-Ar collisions (unless the simple LS coupling scheme is broken in very strong collision perturbation). However, even this single potential is not necessarily fit by a single exponential function over the entire range of interaction. L = 0.27 Å was deduced to fit vibrational relaxation data to the steep part of the N_2-N_2 potential, whereas Meador (ref. 27) calculates that L = 0.4 Å for the longer range part of the potential that contributes most to scattering. Viscosity measurements on the other hand suggest that the N_2-N_2 potential also has a Van derWaals attractive well with a depth about 0.1 eV, and it is not clear how all these trends fit into a single potential surface.

6.11 HIGH ENERGY IMPACT VIBRATIONAL TRANSITIONS

Up to this point the vibrational transitions have been treated as a small perturbation problem. At low collision energies this is justified because the transition probabilities are all very small. However, at high collision energies the transition probabilities become large and may exceed unity, at which point the theoretical model obviously breaks down. In fact, Rapp and Sharp (refs. 15-17) performed some numerical calculations using a close-coupled set of equations such as Eq. (6.28) and show that the small perturbation fails considerably before transition probabilities reach unity and that multiple quantum jumps occur. Moreover, they found that it was necessary to include a much larger number of vibrational levels than were excited at the finish of the collision event, because some of the higher levels were transiently excited during the peak of the collision and then transferred their energy

back to the translational mode and to lower-lying levels as the collision event was completed. Such numerical solutions can be accomplished on any reasonably fast large digital computer, but an analytic solution for multiple quantum vibrational transitions, which is due to Kerner (ref. 18), is more helpful in understanding the process. Therefore, Kerner's method will be outlined here.

Kerner sets up the Schroedinger equation starting from the classical equation of motion of a one-dimensional harmonic oscillator subject to an external force $f(t)$

$$\mu\ddot{y} + ky = f(t) \tag{6.119}$$

where y is now the displacement from the oscillator's equilibrium position. As the oscillator moves, it does work against the external force

$$W = \int f(t) \cdot dy \tag{6.120}$$

Note that if $f(t)$ is in the negative y direction, W is positive as y increases and this amount of energy is lost by the system. If $f(t)$ varies slowly compared with the period of oscillation in y, this work may be approximated by

$$W \simeq f(t)y \simeq \frac{\partial W}{\partial y}\, y \tag{6.121}$$

The Hamiltonian of the oscillator system is thus

$$H = \frac{p^2}{2\mu} + \frac{ky^2}{2} - \int f(t)dy$$

$$\simeq \frac{p^2}{2\mu} + \frac{ky^2}{2} - f(t)y \tag{6.122}$$

Replacing the momentum p with the derivative operator $i\hbar\partial/\partial y$, Kerner obtains the Schroedinger equation

$$-\frac{\hbar^2}{2\mu}\frac{\partial^2\psi}{\partial y^2} + \left[\frac{ky^2}{2} - yf(t)\right]\psi = i\hbar\frac{\partial\psi}{\partial t} \tag{6.123}$$

He then proceeds to construct a solution from the unforced solutions which are known. Make the transformation

$$\psi = \phi(y - u,t)e^{gy} \tag{6.124}$$

where u and g are functions of time to be determined. Let $z = y - u$. The elements in the Schroedinger equation then become

$$\left.\begin{aligned}
\frac{\partial^2\psi}{\partial y^2} &= \frac{\partial^2\phi}{\partial z^2}\, e^{gy} + 2g\, e^{gy}\frac{\partial\phi}{\partial z} + g^2\phi\, e^{gy} \\
\frac{\partial\psi}{\partial t} &= \frac{\partial\phi}{\partial t}\, e^{gy} + (z + u)\dot{g}\phi\, e^{gy} + \frac{\partial\phi}{\partial z}\frac{dz}{dt}\, e^{gy} \\
\frac{ky^2}{2} &= \frac{kz^2}{2} + kuz + \frac{ku^2}{2} \\
yf &= (z + u)f
\end{aligned}\right\} \tag{6.125}$$

and the transformed Schroedinger equation is

$$-\frac{\hbar^2}{2\mu}\frac{\partial^2\phi}{\partial z^2}+\left(i\hbar\dot{u}-\frac{\hbar^2 g}{\mu}\right)\frac{\partial\phi}{\partial z}+\left[\frac{kz^2}{2}+(ku-f-i\hbar\dot{g})z+\frac{ku^2}{2}-fu-i\hbar u\dot{g}-\frac{\hbar^2 g^2}{2\mu}\right]\phi=i\hbar\frac{\partial\phi}{\partial t} \tag{6.126}$$

Now choose g and u such that the coefficients in $\partial\phi/\partial z$ and z all vanish

$$-\mu\dot{u}=i\hbar g \tag{6.127a}$$

$$ku-f-i\hbar\dot{g}=0 \tag{6.127b}$$

From Eqs. (6.127a and b) we observe

$$\mu\ddot{u}+ku=f(t) \tag{6.128}$$

In other words u is just the solution for the classical oscillator subject to a forcing function, which we considered in section 6.2. The initial conditions are $u(-\infty)=0$, $\dot{u}(-\infty)=0$. The Schroedinger equation now reduces to

$$-\frac{\hbar^2}{2\mu}\frac{\partial^2\phi}{\partial z^2}+\left(\frac{kz^2}{2}+\frac{ku^2}{2}-fu-i\hbar u\dot{g}-\frac{\hbar^2 g^2}{2\mu}\right)\phi=i\hbar\frac{\partial\phi}{\partial t} \tag{6.129}$$

Now let

$$\begin{aligned}\delta(t)&=\frac{ku^2}{2}-fu-i\hbar u\dot{g}-\frac{\hbar^2 g^2}{2\mu}\\&=\frac{ku^2}{2}-fu+(fu-ku^2)+\frac{\mu^2\dot{u}^2}{2\mu}\\&=\frac{\mu\dot{u}^2}{2}-\frac{ku^2}{2}=T-V\end{aligned} \tag{6.130}$$

thus $\delta(t)$ is just the classical Lagrangian.

$$-\frac{\hbar^2}{2\mu}\frac{\partial^2\phi}{\partial z^2}+\left[\frac{kz^2}{2}+\delta(t)\right]\phi=i\hbar\frac{\partial\phi}{\partial t} \tag{6.131}$$

Next separate the variables z and t

$$\phi=\phi(z)\theta(t) \tag{6.132}$$

Then

$$\begin{aligned}&-\frac{\hbar^2}{2\mu}\frac{d^2\phi}{dz^2}\theta+\left(\frac{kz^2}{2}+\delta\right)\phi\theta=i\hbar\phi\frac{\partial\theta}{\partial t}\\&-\frac{\hbar^2}{2\mu}\frac{d^2\phi}{dz^2}\frac{1}{\phi}+\frac{kz^2}{2}=-\delta+\frac{i\hbar}{\theta}\frac{d\theta}{dt}=\text{constant}\end{aligned} \tag{6.133}$$

Initially at $t=-\infty$, $u=0$, $z=y$, and $\phi=\psi_n$

$$-\frac{\hbar^2}{2\mu}\frac{d^2\psi_n}{dy^2}+\frac{ky^2}{2}\psi_n=E_n\psi_n \tag{6.134}$$

hus, the constant in question is just the initial vibrational energy $E_n = (n+1/2)\hbar\omega$ nd the functions $\phi(z)$ are the harmonic oscillator wave functions

$$\phi_n(z) = N_n\, e^{-\alpha^2 z^2/2}\, H_n(\alpha z) \tag{6.135}$$

ere

$$N_n^2 = \frac{\alpha}{\sqrt{\pi}2^n n!}, \qquad \alpha^2 = \left(\frac{\mu k}{\hbar^2}\right)^{1/2} = \frac{\mu\omega}{\hbar} \tag{6.136}$$

e function $\theta(t)$ is the solution to

$$\frac{d\theta}{dt} = \frac{[E_n + \delta(t)]\theta}{i\hbar} \tag{6.137}$$

ich is

$$\theta = \exp\left[-\frac{i}{\hbar}\int_{-\infty}^{t}[E_n + \delta(t)]dt\right] \tag{6.138}$$

Thus, we have a class of solutions formed from the stationary states of the unforced problem and with a phase $\hbar^{-1}\int(E_n + \delta)dt$

$$\psi_n(x,t) = \phi_n\, e^{gy} = \phi_n\, e^{i\mu\dot{u}y/\hbar} = \phi_n\, e^{ipy/\hbar}$$

$$= N_n \exp\frac{i}{\hbar}\left[py - \int_{-\infty}^{t}(E_n + \delta)dt\right] e^{-\alpha^2(y-u)^2/2}\, H_n[\alpha(y-u)] \tag{6.139}$$

where $p(t)$ is the classical momentum $\mu\dot{u}(t)$ and $u(t)$ is the classical displacement of the oscillator starting from rest and subjected to the forcing function $f(t)$. Next we expand this wave function in the orthonormal set of harmonic oscillator wave functions

$$V_n(y,t) = N_n\, e^{-\alpha^2 y^2/2}\, H_n(\alpha y) e^{-iE_n t/\hbar} \tag{6.140}$$

Let m be the initial state designation

$$\psi_m(y,t) = \sum_{n=0}^{\infty} b_{mn}(t)V_n(y,t) \tag{6.141}$$

Multiply both sides of Eq. (6.141) by $V_n^*(y,t)$ and integrate over all y

$$b_{mn}(t) = \int_{-\infty}^{\infty}\psi_m(y,t)V_n^*(y,t)dy \tag{6.142}$$

then the transition probability, at time t, that the oscillator finds itself in the unperturbed state n, after starting from initial state m, is b_{mn}^2

$$b_{mn} = N_m N_n \exp\left\{\frac{i}{\hbar}\left[E_n t - \int_{-\infty}^{t}(E_m + \delta)dt\right]\right\}$$

$$\times \int_{-\infty}^{\infty} \exp\left(\frac{i}{\hbar}\mu\dot{u}y\right)\exp\left[-\frac{\alpha^2}{2}(y-u)^2 - \frac{\alpha^2 y^2}{2}\right]H_m[\alpha(y-u)]H_n(\alpha y)dy \qquad (6.143)$$

$$P_{mn} = N_m^2 N_n^2 \left| \int_{-\infty}^{\infty} \exp\left[\frac{i}{\hbar}\mu\dot{u}y - \frac{\alpha^2}{2}(y-u)^2 - \frac{\alpha^2 y^2}{2}\right] H_m[\alpha(y-u)]H_n(\alpha y)dy \right|^2 \qquad (6.144)$$

Transform variables to $x = \alpha y$, $v = \alpha u$, $\alpha^2 = \mu\omega/\hbar$ and define

$$I_{mn} = \int_{-\infty}^{\infty} \exp\left[\frac{i\dot{v}x}{\omega} - \frac{(x-v)^2}{2} - \frac{x^2}{2}\right]H_m(x-v)H_n(x)dx \qquad (6.145)$$

then the transition probability may be expressed

$$P_{mn} = \frac{|I_{mn}|^2}{\pi 2^{m+n} m!n!} \qquad (6.146)$$

The integral I_{mn} is evaluated using the Hermite polynomial moment generating functions

$$S = \exp[x^2 - (s-x)^2] = \sum_n \frac{H_n(x)s^n}{n!} \qquad (6.147a)$$

$$T = \exp\{(x-v)^2 - [t-(x-v)]^2\} = \sum_m \frac{H_m(x-v)t^m}{m!} \qquad (6.147b)$$

$$\int ST \exp\left(\frac{i\dot{v}x}{\omega} - x^2 + xv - \frac{v^2}{2}\right)dx = \sum_n\sum_m \frac{s^n t^m}{n!m!}\int_{-\infty}^{\infty} \exp\left(\frac{i\dot{v}x}{\omega} - x^2 + xv - \frac{v^2}{2}\right)H_m(x-v)H_n(x)dx$$

$$= \sum_n\sum_m s^n t^m \frac{I_{mn}}{n!m!} \qquad (6.147c)$$

Complete the square of the exponential term in the integral on the left side of Eq. (6.147c) and integrate to obtain

$$\int_{-\infty}^{\infty} \exp\left\{-\left[x - \left(s + t + \frac{v}{2}\right)\right]^2 + 2st + sv - tv - \frac{v^2}{4} + \frac{i\dot{v}x}{\omega}\right\} dx$$

$$= \exp\left(2st + sv - tv - \frac{v^2}{4}\right) \exp\left[\frac{i\dot{v}}{\omega}\left(s + t + \frac{v}{2}\right)\right] \int_{-\infty}^{\infty} \exp\left\{-\left[x - \left(s + t + \frac{v}{2}\right)\right]^2 + \frac{i\dot{v}}{\omega}\left[x - \left(s + t + \frac{v}{2}\right)\right]\right\} d\left[x - \left(s + t + \frac{v}{2}\right)\right] \tag{6.148}$$

The integral on the right side of Eq. (6.148) is just $\sqrt{\pi}\exp[-(\dot{v}/\omega)^2/4]$. Thus we have

$$\sqrt{\pi}\exp\left[-\frac{1}{4}\left(v^2 + \frac{\dot{v}^2}{\omega^2}\right) + \frac{i\dot{v}v}{2\omega} + 2st + \left(v + \frac{i\dot{v}}{\omega}\right)s - \left(v - \frac{i\dot{v}}{\omega}\right)t\right] = \sum_n \sum_m \frac{s^n t^m I_{mn}}{m!n!} \tag{6.149}$$

Now $v = \alpha u$, $\alpha^2 = \mu\omega/\hbar$, and $k = \mu\omega^2$, so

$$\frac{\dot{v}^2}{\omega^2} + v^2 = \frac{\mu\dot{u}^2 + \mu\omega^2 u^2}{\hbar\omega} = 2\varepsilon \tag{6.150}$$

where ε is the ratio of the classical energy excited to the vibrational quantum $\hbar\omega$. Expanding the last three exponential factors on the left side of Eq. (6.149), we obtain

$$\sqrt{\pi}\exp\left(-\frac{\varepsilon}{2} + \frac{i\dot{v}v}{2\omega}\right) \sum_j \frac{2^j s^j t^j}{j!} \sum_k \frac{2^{k/2}\left(\frac{v}{\sqrt{2}} + \frac{i\dot{v}}{\sqrt{2}\omega}\right)^k s^k}{k!} \cdot \sum_\ell \frac{2^{\ell/2}(-1)^\ell\left(\frac{v}{\sqrt{2}} - \frac{i\dot{v}}{\sqrt{2}\omega}\right)^\ell t^\ell}{\ell!}$$

$$= \sum_n \sum_m s^n t^m \frac{I_{mn}}{m!n!} \tag{6.151}$$

For purposes of evaluating the integrals I_{mn}, we are interested only in those terms of the product where $j + k = n$, $j + \ell = m$ or $k = n - j$, $\ell = m - j$. Let $m < n$

$$\sqrt{\pi}\, e^{-\varepsilon/2}\, e^{i\dot{v}v/2\omega} \sum_{j=0}^{m} \frac{(-1)^{m-j} 2^{(m+n)/2}\left(\frac{v}{\sqrt{2}} + \frac{i\dot{v}}{\sqrt{2}\omega}\right)^{n-j}\left(\frac{v}{\sqrt{2}} - \frac{i\dot{v}}{\sqrt{2}\omega}\right)^{m-j}}{j!(m-j)!(n-j)!} = \frac{I_{mn}}{m!n!} \tag{6.152}$$

thus

$$I_{mn}^2 = (m!)^2(n!)^2\pi\, e^{-\varepsilon}\left(\frac{v^2}{2} + \frac{\dot{v}^2}{2\omega^2}\right)^{m+n} 2^{m+n}\left|\sum_{j=0}^{m}\frac{(-1)^j\left(\frac{v^2}{2} + \frac{\dot{v}^2}{2\omega^2}\right)^{-j}}{j!(m-j)!(n-j)!}\right|^2$$

$$= (m!)^2(n!)^2\pi\, e^{-\varepsilon}\,\varepsilon^{m+n}2^{m+n}\left|\sum_{j=0}^{m}\frac{(-1)^j\varepsilon^{-j}}{j!(m-j)!(n-j)!}\right|^2 \qquad (6.153)$$

The final result for the transition probability is

$$P_{mn} = \frac{I_{mn}^2}{\pi 2^{m+n} m!n!} = m!n!\, e^{-\varepsilon}\,\varepsilon^{m+n}\left|\sum_{j=0}^{m}\frac{(-1)^j\varepsilon^{-j}}{j!(m-j)!(n-j)!}\right|^2 \qquad (6.154)$$

Equation (6.154) relates the quantum mechanical transition probability to the classical energy change ε in the oscillator, subject to the forcing function $f(t)$, in units of $\hbar\omega$. Recall that ε is the energy gained by a classical oscillator starting from rest (see Eq. (6.150)), that is, it is identical with $\Delta E/\hbar\omega$ given by Eq. (6.18) When ε is very small, the transition P_{01} reduces to the usual small perturbation value

$$P_{01} = \varepsilon\, e^{-\varepsilon} \xrightarrow[\varepsilon << 1]{} \varepsilon \qquad (6.155)$$

but at large ε, P_{01} becomes vanishingly small due to the exponential term in Eq. (6.155). The probability of adiabatic collision P_{00} also falls off as the exponential

$$P_{00} = e^{-\varepsilon} \xrightarrow[\varepsilon << 1]{} 1 - \varepsilon \qquad (6.156)$$

rather than remaining unity as given by the small perturbation theory. As ε becomes large compared with unity, the transitions P_{02}, P_{03}, etc. grow larger and each goes through a maximum at a characteristic value of ε. These harmonic oscillator transition probabilities are graphed in figure 6.5. Values of P_{0k} are shown in figure 6.5(a). The small perturbation value of P_{01} is shown as a dashed line for reference. The sum of all probabilities is unity as it should be

$$\sum_{k=0}^{\infty} P_{0k} = \sum_{k=0}^{\infty} e^{-\varepsilon}\frac{\varepsilon^k}{k!} = 1 \qquad (6.157)$$

The classical oscillator energy gain ε is, of course, related to collision velocity, increasing as the velocity increases.

Figure 6.5(b) shows the transition probabilities P_{1k}. The probability P_{10} is the same as P_{01}. The small perturbation value of P_{12} is just $2P_{01}$ as given by Eqs. (6.53) and (6.54) and is also the limit of Kerner's value for small ε

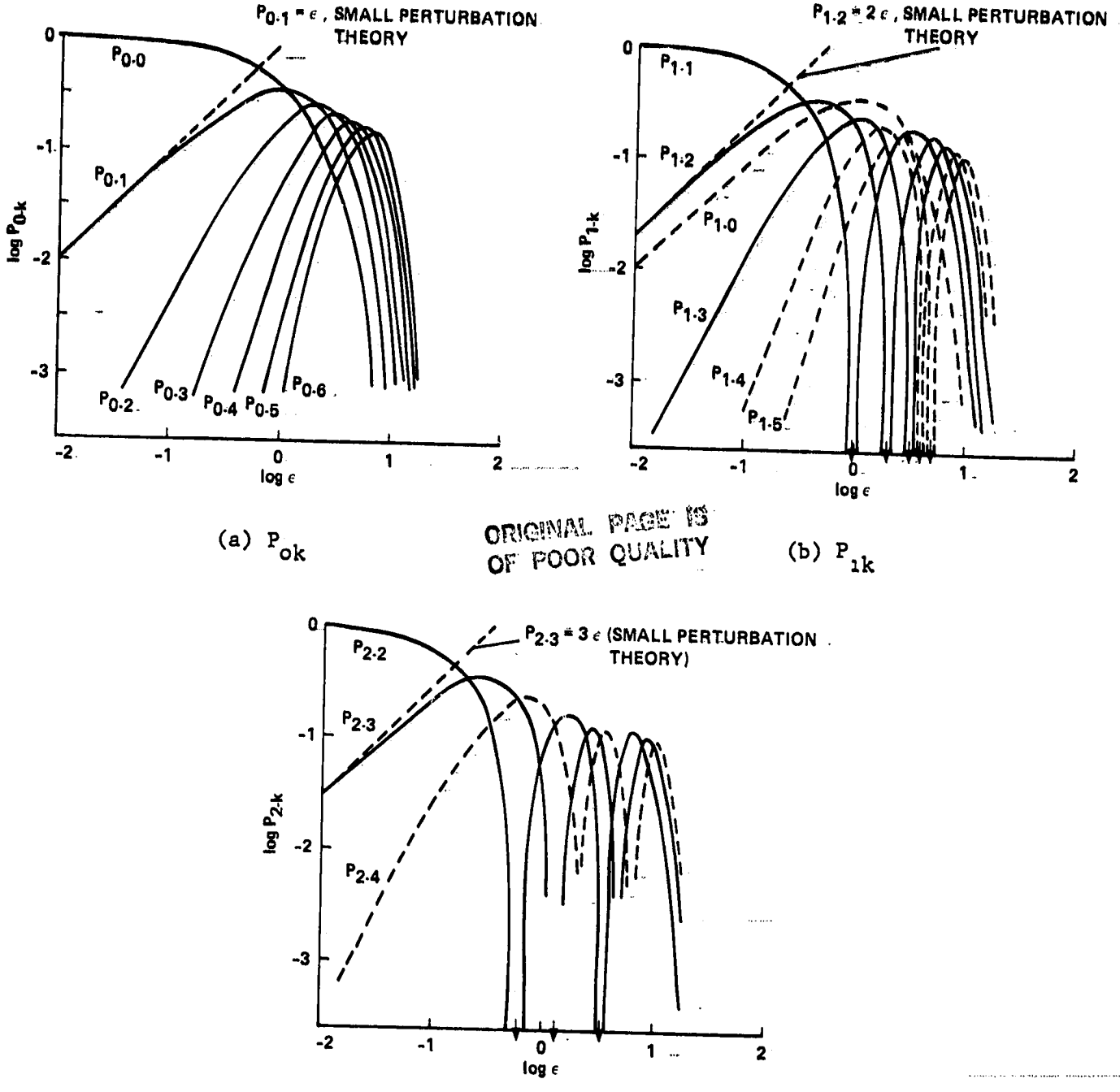

(a) P_{ok}

(b) P_{1k}

(c) P_{2k}

Figure 6.5- Harmonic oscillator vibrational transition probabilities.

$$P_{12} = 2\varepsilon\, e^{-\varepsilon}\left(1 - \frac{\varepsilon}{2}\right)^2 \xrightarrow[\varepsilon << 1]{} 2\varepsilon \qquad (6.158)$$

The adiabatic transition probability P_{11} is

$$P_{11} = e^{-\varepsilon}(1 - \varepsilon)^2 \xrightarrow[\varepsilon << 1]{} 1 - 3\varepsilon \qquad (6.159)$$

The transitions involving excited states are seen to have nodes at characteristic values of ε and several maxima. The number of nodes equals the lowest value of m or n. This is characteristic of the solutions to the coupled set of equations, Eq. (6.28), and shows up in the numerical integrations of Rapp and Sharp (refs. 15,16) For these numerical solutions one wants to truncate the number of equations involved at as small a level as possible to conserve computing time. The number of levels required can be determined by observing the minimum number which leads to a pronounced dip in the solution approximating the nodal point with sufficient accuracy. Additional levels will need to be retained if solutions are desired at higher collision energies where the second- and higher-order nodes occur. Treanor (ref. 19) has compared Kerner's solutions with the numerical solutions of Rapp and Sharp, and finds satisfactory agreement. Figure 6.5(c) shows some of the transition probabilities P_{2k}, showing the two nodes in the solution involved in this case. The sum of all possible transition probabilities, starting from a given quantum number, is always unity, of course.

6.12 INELASTIC COLLISION EFFECTS ON VIBRATIONAL TRANSITION

Up to this point the classical trajectory has been treated as though it were obtained in an adiabatic collision, and as a consequence the impulse function is taken to be perfectly symmetric as it would be in adiabatic collision. The conservation of kinetic energy before and after collision was treated in a rather approximate manner by assuming that the effective collision energy was the average of the initial and final kinetic energies. However, one additional sink of energy is the upper vibrational modes that become excited during the collision process. This excitation may only be a transient one; that is, the energy is transferred back to the kinetic energy mode as the collision partners recede from one another; but no attempt has been made to account for the conservation of energy during the peak of the impulse. Rapp and Sharp did account for this in their numerical solutions, but the simplicity of Kerner's formulas cannot be utilized unless one uses a corrected expression for ε. Hansen and Pearson (ref. 28) developed an analytic approximation for ε that is useful for this purpose. This will be carried through for the one-dimensional collinear collisions, and the corrections for three-dimensional effects can be added by the methods of section 6.6.

When a transition to another vibrational state occurs, the classical trajectory is distorted. The symmetrical part of this distortion has been accounted for to first order by letting the collision velocity be the average of the final and initial velocities. However, an asymmetrical distortion is also involved. A skewed perturbation which conveniently fits the boundary conditions is

$$U = U_o\, e^{-(r-\sigma)/L} = U_o\, e^{bt}\, \mathrm{sech}^2(at) \qquad (6.160)$$

The relative velocity between collision partners is in this case

$$\frac{\dot{r}}{L} = 2a \tanh(at) - b \tag{6.161}$$

and the constants a and b which fit the limiting conditions at $|t| = \infty$ are

$$a = \frac{u_i + u_f}{4L} = \frac{u}{2L} \tag{6.162}$$

$$b = \frac{u_i - u_f}{2L} \tag{6.163}$$

The transitions of harmonic oscillators involve just one quantum of vibrational energy, so

$$\frac{1}{2} m(u_i^2 - u_f^2) = \pm\hbar\omega$$

$$\frac{b}{a} = 2 \frac{u_i^2 - u_f^2}{(u_i + u_f)^2} = \pm \frac{\hbar\omega}{mu^2} = \pm \frac{\hbar\omega}{2E} \tag{6.164}$$

Vibrational transitions occur with sizable probability only when collision energy is large compared with $\hbar\omega$; thus $(b/a) << 1$ in most cases of interest, and the perturbation has nearly the same shape as for the adiabatic type collision trajectory assumed previously. The dimensionless Fourier transform to be used in Eq. (6.53) is now, however,

$$F = \omega \int_{-\infty}^{\infty} e^{bt} \operatorname{sech}^2(at) e^{i\omega t}\, dt \tag{6.165}$$

In appendix 6B the square of this transform is shown to become, for small ω/a,

$$|F|^2 \xrightarrow[\omega/a << 1]{} 4\pi^2 \left(\frac{\omega}{a}\right)^4 e^{-\pi\omega/a} \left(1 + \frac{b^2}{\omega^2}\right) \tag{6.166}$$

This result is the same as obtained before (see Eq. (6.56)), except for the factor $(1 + b^2/\omega^2)$, which represents the corrections for skewness in the impulse shape. In terms of the constant E_c

$$\left(\frac{b}{\omega}\right)^2 = \left(\frac{b}{a}\right)^2 \left(\frac{a}{\omega}\right)^2 = \frac{\pi^2 (\hbar\omega)^2}{2E_c E} \tag{6.167}$$

Normally, the ratio $\hbar\omega/E_c \approx 10^{-2}$ and $\hbar\omega/E < 1$ for the collisions of interest, thus $(b/\omega)^2$ is the order of 10^{-2}. We conclude that the effect of skewness of the perturbation potential on the transition probability is small. This small correction can be accounted for by evaluating b/ω at the value of collision energy E_m which maximizes the integral of the rate coefficient

$$1 + \left(\frac{b}{\omega}\right)_m^2 = 1 + \frac{\pi^2(\hbar\omega)^2}{E_c^{4/3}(kT)^{2/3}} \tag{6.168}$$

Since this correction is small it will be ignored in the following, in which effects of transient storage of energy in upper vibrational levels during the collision process are analyzed. It could, however, be carried along without undue mathematical complexity.

For transitions from the ground state, which are of interest here for purposes of comparing theory with experimentally observed relaxation-rate data, the classical energy excited in a harmonic oscillator at any time t by the perturbation potential $U(t)$ may be expressed

$$V(t) = \hbar\omega\left(\frac{\gamma_{o1}}{\hbar}\right)^2\left|\int_{-\infty}^{t} U_e(t)e^{i\omega t}\,dt\right|^2 \tag{6.169}$$

where γ_{o1} is the harmonic oscillator matrix element of Eq. (6.54) when $n = 0$, and $U_e(t)$ is the perturbation when the oscillator is in its equilibrium position. The subscripts on these terms will be dropped from this point on for convenience.

The value of V and all its derivatives at $t = 0$ can be deduced from Eq. (6.169), and to terms of first order in ω^{-1} (see appendix 6C)

$$V_o = \frac{\gamma^2 U_o^2}{\hbar\omega} \tag{6.170a}$$

$$\left(\frac{dV}{dt}\right)_o = \left(\frac{d^2V}{dt^2}\right)_o = \left(\frac{d^3V}{dt^3}\right)_o = 0 \tag{6.170b}$$

$$\left(\frac{d^4V}{dt^4}\right)_o = \frac{2\gamma^2\omega}{\hbar}U_o\ddot{U}_o = 2V_o\left(\frac{\omega^2\ddot{U}_o}{U_o}\right) \tag{6.170c}$$

The subscript o refers to $t = 0$. These results are independent of the exact form of U, provided the duration of the impulse is long compared with ω^{-1}.

Now assume that the collision perturbation has the form given for adiabatic elastic collision but with a correction factor $\phi(t)$ which will be adjusted to satisfy conservation of energy near the turning point

$$U = U_o\, e^{-(r-\sigma)/L} = U_o\phi(t)\,\mathrm{sech}^2(at) \tag{6.171}$$

Note that $\phi(t)$ would include the asymmetry factor e^{bt} discussed above, if we wished to carry this term along. For the present, however, we will be concerned with only the symmetrical expansion of ϕ about $t = 0$. If U is considered symmetrical about the turning point ($\dot{U}_o = 0$), ϕ and its derivatives at $t = 0$ deduced from Eq. (6.171) are

$$\phi_o = 1 \tag{6.172a}$$

$$\dot{\phi}_o = \left(\frac{d^3\phi}{dt^3}\right)_o = \left(\frac{d^{2n+1}\phi}{dt^{2n+1}}\right)_o = 0 \tag{6.172b}$$

$$\ddot{\phi}_o = \frac{\ddot{U}_o}{U_o} + 2a^2 \tag{6.172c}$$

$$\left(\frac{d^4\phi}{dt^4}\right)_o = \frac{(d^4U/dt^4)_o}{U_o} + 12a^2\,\frac{\ddot{U}_o}{U_o} + 8a^4 \tag{6.172d}$$

The function ϕ is required to be the order of unity in the interval $|t| < 2/a$, where the significant contributions to the Fourier transform appear, but we need not be concerned with the behavior of ϕ outside this interval. For example, we can let $\dot{\phi}$ vanish at $|t| >> 2/a$ without loss of generality, so that a can take its usual definition, $u/2L$, to satisfy the boundary conditions on collision velocity

$$\frac{\dot{r}}{L} = 2a\,\tanh(at) - \frac{\dot{\phi}}{\phi} \tag{6.173}$$

The asymmetrical factor e^{bt} would be required to match the exact boundary conditions, of course.

With the perturbation potential having the form given by Eq. (6.171), the kinetic energy is

$$T = \frac{m\dot{r}^2}{2} = \frac{mL^2}{2}\left(\frac{\dot{U}}{U}\right)^2 \tag{6.174}$$

To conserve energy, the vibrational energy must be

$$V = E - T - U = E - \left[\frac{mL^2}{2}\left(\frac{\dot{U}}{U}\right)^2 + U\right] \tag{6.175}$$

The value of V and its derivatives at the turning point, in terms of U and its derivatives, are thus

$$V_o = E - U_o \tag{6.176a}$$

$$\dot{V}_o = \left(\frac{d^3V}{dt^3}\right)_o = 0 \tag{6.176b}$$

$$\left(\frac{d^2V}{dt^2}\right)_o = -mL^2\left(\frac{\ddot{U}_o}{U_o}\right)^2 - \ddot{U}_o \tag{6.176c}$$

$$\left(\frac{d^4V}{dt^4}\right)_o = -4mL^2\,\frac{\ddot{U}_o(d^4U/dt^4)_o}{U_o^2} + 12mL^2\,\frac{\ddot{U}_o^3}{U_o^3} - \left(\frac{d^4U}{dt^4}\right)_o \tag{6.176d}$$

When these values are matched with the values given by Eqs. (6.170), we obtain expressions for U_o and its derivatives at the turning point which, in turn, determine the expansion $\phi(t)$ about this point, Eq. (6.172).

First match Eq. (6.170a) with Eq. (6.176a) to obtain a quadratic relation for E/U_o

$$\left(\frac{E}{U_o}\right)^2 - \left(\frac{E}{U_o}\right) - \frac{\gamma^2 E}{\hbar\omega} = 0 \qquad (6.177)$$

for which the solution is

$$\frac{E}{U_o} = \frac{1}{2}\left[1 \pm \left(1 + \frac{4\gamma^2 E}{\hbar\omega}\right)^{1/2}\right] \qquad (6.178)$$

The positive root is the one of interest here. The quantity $4\gamma^2 E/\hbar\omega$ is normally small compared with unity. For the homogenous diatomic molecule harmonic oscillator matrix element γ_{o1}, Eq. (6.54),

$$\frac{4\gamma_{o1}^2 E}{\hbar\omega} = \frac{E}{m_1\omega^2 L^2} = 4\pi^2\left(\frac{m}{m_1}\right)\frac{E}{E_c} \qquad (6.179)$$

typically $(m/m_1) \cong 1$ and E/E_c is the order of 0.001. Thus $4\gamma^2 E/\hbar\omega$ is the order of 0.04, and approximate expressions for U_o and V_o are

$$U_o \simeq E\left(1 - \frac{\gamma^2 E}{\hbar\omega}\right) \qquad (6.180a)$$

$$V_o \simeq \frac{\gamma^2 E^2}{\hbar\omega} \qquad (6.180b)$$

With U_o and V_o determined, the remaining derivatives of U at $t = 0$ are easily found by matching the remainder of Eqs. (6.170) with Eqs. (6.176)

$$\dot{U}_o = \left(\frac{d^3U}{dt^3}\right)_o = 0 \qquad (6.180c)$$

$$\ddot{U}_o = -\frac{U_o^2}{mL^2} \qquad (6.180d)$$

$$\left(\frac{d^4U}{dt^4}\right)_o = \frac{2\omega^2}{3}\frac{V_o\ddot{U}_o}{U_o} - 4mL^2\left(\frac{\ddot{U}_o}{U_o}\right)^3 \qquad (6.180e)$$

These derivatives may alternatively be expressed in terms of the collision energy E, and the characteristic energy E_c or $4\pi^2 m\omega^2 L^2$

$$\ddot{U}_o = -\frac{4\pi^2\omega^2 U_o^2}{E_c} \simeq -\frac{4\pi^2\omega^2 E^2}{E_c} \qquad (6.181a)$$

$$\left(\frac{d^4U}{dt^4}\right)_o \simeq \left(\frac{8\pi^2\omega^4E^2}{E_c}\right)\left(\frac{8\pi^2E}{E_c} - \frac{\gamma^2E}{3\hbar\omega}\right) \qquad (6.181b)$$

Now a Taylor series expansion can be constructed for ϕ to terms of fourth order in time

$$\phi(t) = 1 + \alpha(at)^2 + \beta(at)^4 \qquad (6.182a)$$

Where the coefficients α and β are

$$\alpha = \frac{\ddot{\phi}_o}{2a^2} = 1 - \frac{U_o}{E} = \frac{V_o}{E} \simeq \frac{\gamma^2E}{\hbar\omega} \qquad (6.182b)$$

$$\beta = \frac{(d^4\phi/dt^4)_o}{24a^4} = \frac{2}{3}\left[\left(\frac{U_o}{E}\right)^2 - 1\right] + \left(1 - \frac{U_o}{E}\right) - \frac{1}{18}\left(\frac{\omega}{a}\right)^2\frac{V_o}{E}$$

$$\simeq -\frac{1}{18}\left(\frac{\omega}{a}\right)^2\frac{\gamma^2E}{\hbar\omega} = -\frac{\gamma^2E_c}{36\pi^2\hbar\omega} \qquad (6.182c)$$

The order of magnitude of these coefficients is easily estimated from the one-dimensional collinear collision case where γ is given by Eq. (6.54)

$$\alpha \simeq \left(\frac{\pi^2m}{2\mu}\right)\frac{E}{E_c} \simeq \mathcal{O}(10^{-2}) \qquad (6.183a)$$

$$\beta \simeq -\frac{m}{72\mu} \simeq \mathcal{O}(-3\times10^{-2}) \qquad (6.183b)$$

These magnitudes indicate that ϕ is indeed well behaved in the interval $|at| < 2$, as required. The correction ϕ flattens the usual adiabatic-like impulse near the turning point but makes the impulse steeper in the region $|at| \cong 1$, where the contribution to the Fourier transform is largest. This transform is now

$$F = \omega\int_{-\infty}^{\infty}[1 + \alpha(at)^2 + \beta(at)^4]\mathrm{sech}^2(at)e^{i\omega t}\,dt \qquad (6.184)$$

which in the limit $(\omega/a) >> 1$ is found in appendix 6.B to yield

$$|F|^2 = 4\pi^2\left(\frac{\omega}{a}\right)^4 e^{-\pi\omega/a}\left(1 - \frac{\pi^2\alpha}{4} + \frac{\pi^4\beta}{16} + \ldots\right)^2 \qquad (6.185)$$

Again this is the same result as for adiabatic elastic collision trajectory at the velocity u except for the last factor, which is the correction for distortion of the impulse shape required by conservation of energy.

For one-dimensional collinear collision matrix elements γ, the correction factor to be applied for the effect of energy conservation during the collision impulse is approximately given when the relations of Eqs. (6.183) are used for α and β

$$R \simeq \left[1 - \frac{\pi^4 m}{8\mu}\left(\frac{1}{144} + \frac{E}{E_c}\right)\right]^2 \tag{6.186}$$

Normally, E/E_c is somewhat less than 1/144, so the result is but weakly dependent on collision energy and primarily depends on the ratio of collision-reduced mass to oscillator-reduced mass, m/μ.

For calculation of the rate coefficients α or relaxation times τ, the correction should be evaluated at the collision energy E_m given by Eq. (6.62)

$$\frac{\tau}{\tau_a} \simeq \frac{\alpha_a}{\alpha} = \left[1 - \frac{\pi^2 m}{32\mu}\left(\frac{kT}{E_c}\right)^{2/3} - \frac{\pi^2 m}{1152\mu}\right]^{-2} = \left\{1 - \frac{\pi^2}{16}\left(\frac{m}{\mu}\right)\left[\frac{1}{72} + \left(\frac{kT}{E_c}\right)^{2/3}\right]\right\}^{-2} \tag{6.187}$$

where τ_a is the relaxation time and α_a is the rate coefficient obtained theoretically for the adiabatic-like collisions. Similar results obtain in the case of three-dimensional theory, only the expression for γ^2 is then somewhat more complex.

The total correction for both symmetric and asymmetric distortions of the collision impulse is just the product of two separate corrections. This result is obtained when the Fourier transform is performed on the perturbation potential

$$U(t) = U_o e^{bt}[1 + \alpha(at)^2 + \beta(at)^4]\mathrm{sech}^2(at) \tag{6.188}$$

The fraction of the collision energy transiently transferred to the vibrational mode at the turning point is just the coefficient α, which is typically the order of 1%; the permanent energy transfer is typically the order of 10%. Although the amount of transient energy transfer is small, it causes transition probabilities to decrease by factors of about 1.5 to 2 because of the high sensitivity of the Fourier transform to the shape of the impulse function. Figure 6.6 shows the ratio $\tau/\tau a$ given by Eq. (6.187) for O_2-Ar and N_2-N_2 collisions where the logarithmic potential gradients are 0.24 and 0.27 Å, respectively. The correction is plotted as a function of $T^{-1/3}$ to show the departures from Landau-Teller theory, as illustrated by the small curvature that appears at the

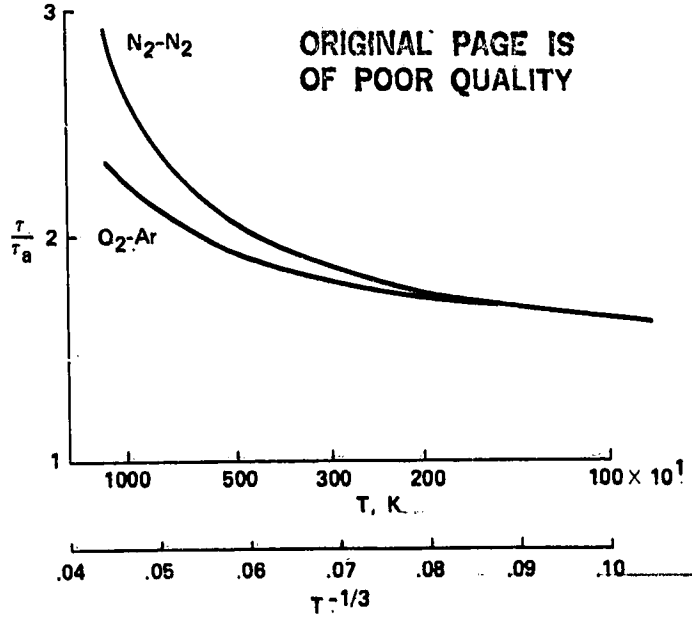

Figure 6.6- Correction to vibrational relaxation times for N_2-N_2 and O_2-Ar collision.

high temperature end of the plot. The effect is also shown in the dashed theoretical curve of figure 6.7. The data on this figure are those of Appleton (ref. 29), and curvature of about the predicted magnitude appears at high temperatures, near 10,000 K. This is the only data presently known at these high temperatures where the effect is observed.

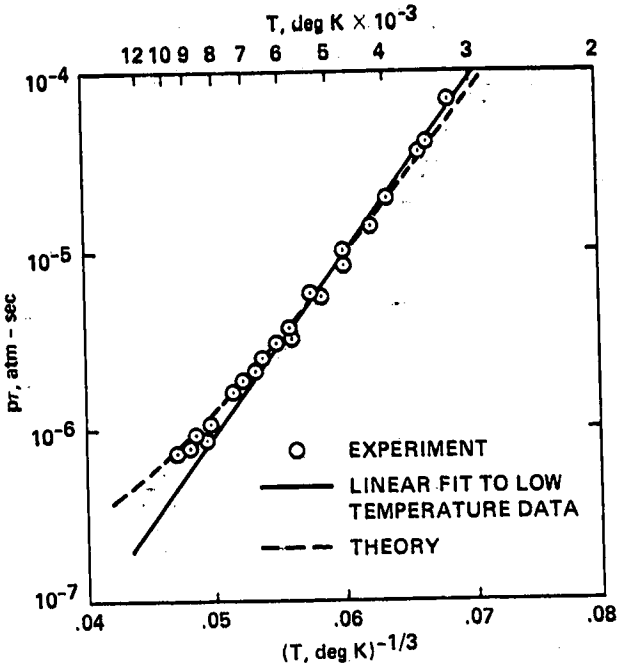

Figure 6.7- Landau-Teller plot, N_2-N_2 vibrational relaxation.

6.13 CONCLUDING REMARKS

A large amount of theoretical and experimental research has been invested in the vibrational relaxation problem, so much that one would think the problem would have been completely solved by this time. However, a large amount of additional work is still possible on the problem because of the various approximations and limitations involved in previous work. We have devoted ourselves mainly to the semiclassical treatment because this method is conducive to the derivation of analytic approximations that lead to better insight about the meaning of parameters important to the problem. In principle, numerical solutions of the coupled set of differential equations involved can be performed as accurately as desired. In practice, most of these solutions have been devoted to one-dimensional collinear collisions because of the exorbitant amount of computing time required for the three-dimensional case. However, the semiclassical results furnish a convenient, though approximate, relation between the one-dimensional and the three-dimensional case which can be applied to the more rigorous one-dimensional calculations. Many of the one-dimensional calculations are still based on the sech(at) type of interaction potential, which is rather approximate; others are based on the exponential interaction and the classical equations of motion are numerically integrated for this interaction, including the effects of step-by-step energy conservation. However, the real potentials are unknown, and until these are available from fundamental quantum calculations there is not really much point in being carried away with long computations of rigorous solutions. The

present semiclassical results are perhaps as accurate as needed considering our state of knowledge of the interaction potentials.

Two problems which are of current interest merit comment. One is that transition between upper vibrational levels is of great concern to scientists analyzing gas-dynamic lasers. These transitions are responsible for establishing the nonequilibrium population of excited states that occur in these lasers, particularly the V-V transitions where both the oscillator and its collision partner change vibrational state. This problem requires that the vibrational wave functions and transition matrix elements for the collision partner be included. In the upper levels, the anharmonic effects become stronger and can produce sizable phase shifts in the probability amplitudes because of the extreme sensitivity of the Fourier transforms to phase. Finally, after all these considerations, we must admit that the problem has not even been solved correctly yet, because the effects of coupled rotational transitions have not been properly included. We observed how the dependence of the perturbation potential on angular coordinates led to coupled vibration-rotation transitions, predominantly with $\Delta\ell = 0, \pm 2$, and ± 4, when the three-dimensional aspects of the problem were considered. However, this analysis was only performed in the small perturbation limit, whereas multiquantum rotational transitions occur in normal collisions with high probability and these cannot be treated by small perturbation methods. To be done correctly, the problem should be performed with every rotation-vibration eigenfunction available to the molecule represented by one equation in the close-coupled set of equations discussed in this chapter. This method becomes too large a computation problem even for modern computers, because of the large number of equations involved and the three-dimensional characteristics of the problem. What is needed is a set of approximate expressions for the rotational transitions produced in collision as a function of time, which can be coupled into the equations for vibrational transition as a reasonably fast subroutine.

The physical picture we have of the collision process and the elements necessary for the solution of transition probabilities are quite clear at this point, however. The diatomic molecule starts in a known vibration-rotation state. Given the interaction potential with an incoming collision partner, the eigenfunction is first distorted to include a number of unperturbed rotational eigenfunctions in the expansion; the coefficients of these eigenfunctions squared being the time-dependent probabilities that the molecule would be found in these rotational states if the perturbation were suddenly removed. From these rotational states, the transitions to the nearby vibrational levels take place with much smaller probability. Under the influence of the perturbation, the transient internal energy surges back and forth between the various rotation-vibration states, certain states on occasion being at maximum while others are at nodal points. As the perturbation recedes, some of this internal energy flows back into the kinetic-energy mode, leaving the molecule with a distribution of probabilities, smaller than at the peak of interaction, among the various unperturbed vibration-rotation states. The transitions to other vibrational states will generally occur as given by small perturbation theory, but the rotational amplitudes will wander around the ladder of available states both in the initial vibrational state before transition amplitudes have changed appreciably to the final state, and also in the final vibrational state after the transition amplitudes in these states have grown appreciably. Since rotational changes will both climb and descend the ladder under the perturbation influence, we are able to get by with the approximate solutions where the two effects are decoupled. However, the strong dependence of the Fourier transforms on the value of the circular frequency ω suggests that the most frequent path of transition will be where ω is minimized; namely, where the rotational state is demoted to lower levels in the transition process, though it may subsequently be promoted to a distribution of rotational levels in the upper state.

This wandering around in the various rotational states during the impulse should be particularly noticed in the V-V type transitions important in laser gasdynamics. Thus, the full solution to the collision induced vibrational transition problem awaits the solution to the collision induced rotational transition problem, a solution that has not yet been satisfactorily accomplished.

APPENDIX 6A

VIBRATION-ROTATION TRANSITION OVERLAP INTEGRALS

The overlap integrals γ (Eq. (6.90)) are evaluated using rigid-rotator, harmonic oscillator wavefunctions

$$\psi_{v\ell m}(\rho,\theta,\phi) = Y_{\ell m}(\theta,\phi)\psi_v(\rho - \rho_e) \tag{6.A1}$$

where ψ_v is the normalized harmonic-oscillator wave function and $Y_{\ell m}$ is the usual spherical harmonic function. Then γ may be expressed

$$\gamma(v,\ell,m;v + \Delta v,\ell + \Delta\ell,m + \Delta m) = I_1(\Delta v)I_2(\Delta\ell,\Delta m) \tag{6.A2}$$

where

$$I_1(\Delta v) = \frac{\delta^2}{\sinh\,\delta}\int_0^\infty \psi^*_{v+\Delta v}\,\frac{\rho - \rho_e}{2L}\,\psi_v\rho\,d\rho \tag{6.A3}$$

$$I_2(\Delta\ell,\Delta m) = \int Y^*_{\ell+\Delta\ell,m+\Delta m}\left(\sin^2\theta\cos^2\phi + \frac{\delta^2}{6}\sin^4\theta\cos^4\phi\right)Y_{\ell m}\,d\Omega \tag{6.A4}$$

The integration of (6.A4) extends over all elements of the solid angle $d\Omega$.

The integral I_1 is easily found by usual methods, and it is nonzero only where $\Delta v = \pm 1$

$$I_1(\pm 1) = \frac{\delta^2}{\sinh\,\delta}\left(\frac{v + \frac{1}{2} \pm \frac{1}{2}}{8\mu\omega L^2/\hbar}\right)^{1/2} \tag{6.A5}$$

An elegant way to evaluate I_2 is to expand the perturbation in terms of spherical-harmonic functions. Then I_2 is the sum of integrals of triple products $Y^*_{\ell'm'}Y_{\ell''m''}Y_{\ell m}$ which are given in terms of Clebsch-Gordon coefficients (ref. 30). However, we will sketch the derivation in terms of commonly known relations between the associated Legendre functions.

I_2 can be expressed

$$I_2 = \frac{C^m_\ell C^{m'}_{\ell'}}{2\pi}\left(\int_0^{2\pi} e^{i(m-m')\phi}\cos^2\phi\,d\phi\int_0^\pi P^{m'}_{\ell'}(\cos\theta)P^m_\ell(\cos\theta)\sin^3\theta\,d\theta\right.$$

$$\left. + \frac{\delta^2}{6}\int_0^{2\pi} e^{i(m-m')\phi}\cos^4\phi\,d\phi\int_0^\pi P^{m'}_{\ell'}(\cos\theta)P^m_\ell(\cos\theta)\sin^5\theta\,d\theta\right) \tag{6.A6}$$

where C_ℓ^m and $C_{\ell'}^{m'}$ are the usual normalizing constants

$$C_\ell^m = \left[\frac{(2\ell + 1)(\ell - m)!}{2(\ell+m)!}\right]^{1/2} \tag{6.A7}$$

and m is understood here to represent the absolute magnitude of the magnetic quantum number.

Ultimately, we are interested in the limiting values of I_2 when $\ell >> 1$, and it simplifies the algebra enormously if we use limiting forms for the recursion relations between associated Legendre functions right from the beginning, rather than use the exact recursion relations and then take the limit at the end. The results are the same in either case. The limiting recursion relations are

$$xP_\ell^m(x) \xrightarrow[\ell>>1]{} \frac{1}{2\ell}\left[(\ell - m)P_{\ell+1}^m(x) + (\ell + m)P_{\ell-1}^m(x)\right] \tag{6.A8}$$

$$(1 - x^2)^{1/2}P_\ell^m(x) \xrightarrow[\ell>>1]{} \frac{1}{2\ell}\left[(\ell + m)^2P_{\ell-1}^{m-1}(x) - (\ell - m)^2P_{\ell+1}^{m-1}(x)\right] \tag{6.A9}$$

$$(1 - x^2)^{1/2}P_\ell^m(x) \xrightarrow[\ell>>1]{} \frac{1}{2\ell}\left[P_{\ell+1}^{m+1}(x) - P_{\ell-1}^{m+1}(x)\right] \tag{6.A10}$$

When these are used with the orthogonality relation

$$\int_{-1}^{1}[P_\ell^m(x)]^2dx = \left(\frac{1}{C_\ell^m}\right)^2 \tag{6.A11}$$

the integrals $I_2(\Delta\ell, \Delta m)$ become

$$I_2(0,0) = \frac{1}{4}\frac{\ell^2 + m^2}{\ell^2} + \frac{\delta^2}{128}\frac{3\ell^4 + 2\ell^2m^2 + 3m^4}{\ell^4} \tag{6.A12}$$

$$I_2(0,\pm2) = -\frac{1}{8}\frac{\ell^2 - m^2}{\ell^2} - \frac{\delta^2}{64}\frac{\ell^4 - m^4}{\ell^4} \tag{6.A13}$$

$$I_2(0,\pm4) = \frac{3\delta^2}{768}\frac{(\ell^2 - m^2)^2}{\ell^4} \tag{6.A14}$$

$$I_2(\pm2,0) = -\frac{1}{8}\frac{\ell^2 - m^2}{\ell^2} - \frac{\delta^2}{64}\frac{\ell^4 - m^4}{\ell^4} \tag{6.A15}$$

$$I_2(\pm2,\pm2) = \frac{1}{16}\frac{(\ell + m)^2}{\ell^2} + \frac{\delta^2}{96}\frac{(\ell + m)^2(\ell^2 - \ell m + m^2)}{\ell^4} \tag{6.A16}$$

$$I_2(\pm2,\mp2) = \frac{1}{16}\frac{(\ell - m)^2}{\ell^2} + \frac{\delta^2}{96}\frac{(\ell - m)^2(\ell^2 + \ell m + m^2)}{\ell^4} \tag{6.A17}$$

$$I_2(\pm2,\pm4) = -\frac{\delta^2}{384}\frac{(\ell + m)^2(\ell^2 - m^2)}{\ell^4} \tag{6.A18}$$

$$I_2(\pm 2,\mp 4) = -\frac{\delta^2}{384}\frac{(\ell - m)^2(\ell^2 - m^2)}{\ell^4} \tag{6.A19}$$

$$I_2(\pm 4,0) = \frac{3\delta^2}{768}\frac{(\ell^2 - m^2)^2}{\ell^4} \tag{6.A20}$$

$$I_2(\pm 4,\pm 2) = -\frac{\delta^2}{384}\frac{(\ell + m)^2(\ell^2 - m^2)}{\ell^4} \tag{6.A21}$$

$$I_2(\pm 4,\mp 2) = -\frac{\delta^2}{384}\frac{(\ell - m)^2(\ell^2 - m^2)}{\ell^4} \tag{6.A22}$$

$$I_2(\pm 4,\pm 4) = \frac{\delta^2}{1536}\frac{(\ell + m)^4}{\ell^4} \tag{6.A23}$$

$$I_2(\pm 4,\mp 4) = \frac{\delta^2}{1536}\frac{(\ell - m)^4}{\ell^4} \tag{6.A24}$$

For all other values of $\Delta\ell$ and Δm, I_2 vanishes, so the selection rules for the assumed perturbation are $\Delta\ell = 0, \pm 2, \pm 4$; $\Delta m = 0, \pm 2, \pm 4$. Next, the $I_2^2(\Delta\ell, \Delta m)$ are averaged over all $2\ell + 1$ initial values of m to get the total value $I_2^2(\Delta\ell)$ for a given change in angular momentum,

$$I_2^2(\Delta\ell) = \frac{1}{2\ell + 1}\sum_m\sum_{\Delta m} I_2^2(\Delta\ell,\Delta m) \tag{6.A25}$$

Recall that m signifies here the absolute value of magnetic quantum number, but there are $2\ell + 1$ terms. To terms of first order in ℓ, the average value of m^n is

$$\langle m^n \rangle \xrightarrow[\ell >> 1]{} \frac{\ell^n}{n + 1} \tag{6.A26}$$

and the averages given by Eq. (6.A25) become

$$I_2^2(0) = \frac{2}{15} + \frac{\delta^2}{35} + \frac{\delta^4}{630} \tag{6.A27}$$

$$I_2^2(\pm 2) = \frac{1}{30} + \frac{\delta^2}{105} + \frac{2\delta^4}{2835} \tag{6.A28}$$

$$I_2^2(\pm 4) = \frac{\delta^4}{22680} \tag{6.A29}$$

If the next-order term in the expansion of the perturbation had been included in Eq. (6.85) it would contribute nothing to terms of order δ^0 and δ^2 in the integrals I_2; it would increase the terms of order δ^4, but by less than a factor of 2. For realistic values of δ^2 (≤ 6), the major contribution comes from the terms of order δ^2 and lower, and we conclude that for real molecules the dominant rotational changes coupled to the vibrational transitions are $\Delta\ell = 0, \pm 2$.

The matric elements γ^2 have been evaluated here for rigid-rotator wavefunctions, while symmetric-top wavefunctions should be used, strictly speaking, for diatomic molecules with electronic states other than $^1\Sigma$. However, the projection of electron

spin and orbital momenta along the internuclear axis is rarely more than 3/2 quantum units in molecules of interest, so at high rotational quantum numbers ℓ, the coupling of electronic momenta perturbs the rigid-rotator wavefunctions only a small amount. Accordingly, we apply the above matrix elements to diatomic molecules in general.

APPENDIX 6B

COLLISION PERTURBATION FOURIER TRANSFORMS

The Fourier transform used when nonadiabatic collision effects are considered is

$$F = \omega \int_{-\infty}^{\infty} \operatorname{sech}^2(at) e^{(i\omega+b)t} dt \tag{6.B1}$$

A contour integration about the pole at $t = i\pi/2a$, along the real axis $t = x$ from $-\infty$ to $+\infty$ and back along $t = x + i\pi/a$, yields

$$[1 - e^{(i\pi b/a)-(\pi\omega/a)}] \frac{F}{\omega} = 2\pi i \operatorname{Res}\left(\frac{i\pi}{2a}\right) \tag{6.B2}$$

The residue at $i\pi/2a$ is

$$\operatorname{Res}\left(\frac{i\pi}{2a}\right) = \frac{b + i\omega}{a^2} e^{(i\pi b/2a)-(\pi\omega/2a)} \tag{6.B3}$$

and the dimensionless Fourier transform is thus

$$F = \left(\frac{\pi\omega}{a^2}\right)(\omega - ib)\operatorname{csch}\left(\frac{\pi\omega - i\pi b}{2a}\right) \tag{6.B4}$$

In the limit $(\omega/a) >> 1$, the modulus squared of this transform becomes

$$|F|^2 = 4\pi^2 \left(\frac{\omega}{a}\right)^4 e^{-\pi\omega/a}\left(1 + \frac{b^2}{\omega^2}\right) \tag{6.B5}$$

The factor $(1 + b^2/\omega^2)$ represents the correction to the usual adiabatic collision transition probability due to the asymmetrical factor e^{bt} in the impulse function. In addition, transforms of the type

$$F = \omega \int_{-\infty}^{\infty} [1 + \alpha(at)^2 + \beta(at)^4]\operatorname{sech}^2 at\, e^{i\omega t} dt \tag{6.B6}$$

are required for analysis of nonadiabatic-elastic collisions involving interactions between the vibrational and kinetic-energy modes. Define the function F_n

$$F_n = \int_{-\infty}^{\infty} t^n \operatorname{sech}^2(at) e^{i\omega t} dt \tag{6.B7}$$

where n is an integer. Again, perform the same contour integration along $t = x$ and back along $t = x + i\pi/a$:

$$\int_{-\infty}^{\infty} \frac{x^n e^{i\omega x} dx}{\cosh^2 ax} + \int_{\infty}^{-\infty} \frac{(x + i\pi/a)^n e^{i\omega x - (\pi\omega/a)}}{\cosh^2(ax + i\pi)} dx = 2\pi i \operatorname{Res}_n \tag{6.B8}$$

From Eq. (6.B8) we obtain

$$F_n(1 - e^{-\pi\omega/a}) + e^{-\pi\omega/a} n \frac{i\pi}{a} F_{n-1} + \frac{1}{2} n(n-1)\left(\frac{i\pi}{a}\right)^2 F_{n-2} + \ldots = 2\pi i \, \mathrm{Res}_n \tag{6.B9}$$

where Res_n is the residue of $t^n \mathrm{sech}^2(at) e^{i\omega t}$ at $i\pi/2a$,

$$\mathrm{Res}_n = \left(\frac{\pi\omega}{2a} + n\right)\left(\frac{i\pi}{2a}\right)^{n-1} \frac{e^{-\pi\omega/2a}}{a^2} \tag{6.B10}$$

In the limit as $(\omega/a) >> 1$,

$$F_n \xrightarrow[(\omega/a)>>1]{} \frac{4}{a}\left(\frac{i\pi}{2a}\right)^n \left(\frac{\pi\omega}{2a}\right) e^{-\pi\omega/2a} \tag{6.B11}$$

and the total Fourier transform given by Eq. (6.B6) then becomes

$$F \xrightarrow[(\omega/a)>>1]{} 2\pi\left(\frac{\omega}{a}\right)^2 e^{-\pi\omega/2a}\left(1 - \frac{\pi^2\alpha}{4} + \frac{\pi^4\beta}{16}\right) \tag{6.B12}$$

The square of the last term in brackets represents the correction to the usual adiabatic-elastic collision transition probability, required when the energy transiently stored in the vibrational modes is included in the conserved collision energy.

APPENDIX 6C

VIBRATIONAL ENERGY AND ITS DERIVATIVES AT THE COLLISION TURNING POINT

Consider a diatomic molecule subject to the perturbation

$$U = U_e + (\text{grad } U)_e \, y \qquad (6.C1)$$

where $y = (\rho - \rho_e)$, the oscillator coordinate. The amplitude y of a classical oscillator subject to this perturbation is found using Green's function. Starting from rest, y at any time t is

$$y = \int_{-\infty}^{t} \frac{(\text{grad } U)_e \sin \omega(t - \xi)}{\mu\omega} \, d\xi$$

The maximum amplitude Y may thus be expressed as

$$Y = \left| \int_{-\infty}^{t} \frac{(\text{grad } U)_e}{\mu\omega} \, e^{i\omega t} dt \right| \qquad (6.C2)$$

The net amount of vibrational energy excited is, in units of $\hbar\omega$

$$\varepsilon = \frac{\Delta E}{\hbar\omega} = \frac{\mu\omega^2 Y^2}{2\hbar\omega} = \frac{1}{2\mu\hbar\omega} \left| \int_{-\infty}^{t} (\text{grad } U)_e \, e^{i\omega t} dt \right|^2 \qquad (6.C3)$$

This classical result is exactly the same as the quantum probability of transition $0 \leftrightarrow 1$ given by small perturbation theory,

$$\varepsilon = P_{01} = \left| \frac{1}{\hbar} \int_{-\infty}^{t} H_{01} \, e^{i\omega t} dt \right|^2 \qquad (6.C4)$$

where H_{01} is the harmonic oscillator matrix element

$$H_{01} = \langle \psi_1^* | U | \psi_0 \rangle = \left(\frac{\hbar}{2\mu\omega} \right)^{1/2} (\text{grad } U)_e \qquad (6.C5)$$

When the transition probability becomes too large for small perturbation methods to apply, Kerner's solutions of Schroedinger's equation are used. The probability of transition $m \to n$ due to a forcing function acting on a harmonic oscillator is found to be

$$P_{mn} = \frac{e^{-\varepsilon} \, \varepsilon^{n+m}}{n!} \, m! n! S_{mn}^2(\varepsilon) \qquad (6.C6)$$

where the polynomial S_{mn} is

$$S_{mn}(\epsilon) = \sum_{j=0}^{m<n} \frac{(-1)^j \epsilon^{-j}}{(n-j)!\,j!\,(m-j)!} \tag{6.C7}$$

For present purposes, transitions from the ground state are of interest:

$$P_{on} = \frac{\epsilon^n e^{-\epsilon}}{n!} \tag{6.C8}$$

Note that P_{o1} reduces to the usual small perturbation result (Eq. (6.C4)) when ϵ is small. Also the sum of all P_{on} is unity as it should be. The total energy in all vibrational modes is

$$V = \hbar\omega \sum_{n=0}^{\infty} nP_{on} = \hbar\omega\, e^{-\epsilon} \sum_{n=1}^{\infty} \frac{\epsilon^n}{(n-1)!} = \hbar\omega\epsilon \tag{6.C9}$$

Where the interaction potential is exponential, and the molecule is homonuclear, so that $m_1 = 2\mu$

$$\text{grad } U = \frac{U}{2L}$$

and Eq. (6.C9) can be expressed as

$$\epsilon = \frac{V(t)}{\hbar\omega} = \left| \frac{\gamma_{o1}}{\hbar} \int_{-\infty}^{t} U_e(t) e^{i\omega t} dt \right|^2 \tag{6.C10}$$

which is the result used in Eq. (6.169). Hereafter, we shall drop the subscripts on γ and U for convenience.

The vibrational energy at $t = 0$ is

$$V_o = \frac{\gamma^2\omega}{\hbar} \left(\left| \int_{-\infty}^{o} U \cos \omega t \, dt \right|^2 + \left| \int_{-\infty}^{o} U \sin \omega t \, dt \right|^2 \right) \tag{6.C11}$$

The first integral on the right is negligibly small compared with the second. The latter can be treated by repeated integration by parts to give

$$\int_{-\infty}^{o} U \sin \omega t \, dt = -\frac{U_o}{\omega} + \frac{\ddot{U}_o}{\omega^3} - \frac{(d^4U/dt^4)_o}{\omega^5} + \cdots \tag{6.C12}$$

$$\simeq -\frac{U_o}{\omega}$$

where we have used the fact that U and all its derivatives vanish at $|t| = \infty$. Thus, to terms of first order in ω^{-1},

$$V_o = \frac{\gamma^2 U_o^2}{\hbar\omega} \tag{6.C13}$$

The derivatives of V at $t = 0$ are obtained by differentiation of Eq. (6.C10). The cosine transform of U and all odd derivatives of U at $t = 0$ are taken to vanish,

$$\int_{-\infty}^{\infty} U \cos \omega t \, dt = \dot{U}_o = \left(\frac{d^3U}{dt^3}\right)_o = 0 \tag{6.C14}$$

which is equivalent to neglect of asymmetrical terms in U and V. Then the results are:

$$\dot{V}_o = \left(\frac{d^2V}{dt^2}\right)_o = \left(\frac{d^3V}{dt^3}\right)_o = 0 \tag{6.C15}$$

$$\left(\frac{d^4V}{dt^4}\right)_o = \frac{\gamma^2\omega}{\hbar} U_o \ddot{U}_o \tag{6.C16}$$

The vibrational energy at the turning point is seen to vary essentially at t^4. These results are valid for any impulse function $U(t)$ where the duration of impulse is long compared with ω^{-1}, provided only that U varies exponentially with distance between the collision partners. Similar relations obtain in the more general case, only U is then replaced by (2L grad U).

REFERENCES

1. Landau, L.; and Teller, E.: Theory of Sound Dispersion. Phys. Zeits. d. Sowjetunion, vol. 10, no. 1, 1936, pp. 34-43.

2. V. Blackman, Vibrational Relaxation in Oxygen and Nitrogen. J. Fluid Mech., vol. 1, 1956, pp. 61-85.

3. Millikan, R. C.; and White, D. R.: Vibrational Energy Exchange Between N_2 and CO. The Vibrational Relaxation of Nitrogen. J. Chem. Phys., vol. 39, July 1963, pp. 98-101.

4. Millikan, R. C.; and White, D. R.: Systematics of Vibrational Relaxation. J. Chem. Phys., vol. 39, Dec. 15, 1963, pp. 3209-3213.

5. Appleton, J. P.; and Steinberg, M.: Vacuum-Ultraviolet Absorption of Shock-Heated Vibrationally Excited Nitrogen. J. Chem. Phys., vol. 46, Feb. 15, 1967, pp. 1521-1529.

6. Bethe, H. A.; and Teller, E.: Deviations from Thermal Equilibrium in Shock Waves. Aberdeen Proving Ground Rept. X-117, 1945.

7. Schwartz, R. N.; Slawsky, Z. I.; and Herzfeld, K. F.: Calculation of Vibrational Relaxation Times in Gases. J. Chem. Phys., vol. 20, Oct. 1952, pp. 1591-1599.

8. Zener, C.: Low Velocity Inelastic Collisions. Phys. Rev., vol. 38, July 15, 1931, pp. 277-281; Proc. Cambridge Phil. Soc., vol. 29, 1933, p. 136.

9. Jackson, J. M.; and Mott, N. F.: Energy Exchange Between Inert Gas Atoms and a Solid Surface. Proc. Roy. Soc. (London), vol. A137, Sept. 1, 1932, pp. 703-717.

10. Schwartz, R. N.; and Herzfeld, K. F.: Vibrational Relaxation Times in Gases (Three-Dimensional Treatment). J. Chem. Phys., vol. 22, 1954, pp. 767-773.

11. Mott, N. F.; and Massey, H. S. W.: The Theory of Atomic Collisions Approximate Methods. Clarendon, Oxford, England, 1949, 2nd ed., chap. VIII, sec. 5, for slow slow collisions. The Method of Distorted Waves. pp. 144-145.

12. Takayanagi, T.: On the Inelastic Collision Between Molecules. I. Progr. Theoret. Phys. Japan, vol. 8, July 1952, pp. 111-117.

13. Rapp, D.: Complete Classical Theory of Vibrational Energy Exchange. J. Chem. Phys., vol. 32, 1960, pp. 735-737.

14. Rossini, F. D.: Thermodynamics and Physics of Matter. Princeton U. Press, Princeton, N.J., 1955.

15. Rapp, D.; and Sharp, T. E.: Vibrational Energy Transfer in Molecular Collisions Involving Large Transition Probabilities. J. Chem. Phys., vol. 38, June 1963, pp. 2641-2648.

16. Sharp, T. E.; and Rapp, D.: Evaluation of Approximations Used in the Calculation of Excitation by Collision. I. Vibrational Excitation of Molecules. J. Chem. Phys., vol. 43, Aug. 1965, pp. 1233-1244.

17. Rapp, D.; and Englander-Golden, P.: Resonant and Near-Resonant Vibrational-Vibrational Energy Transfer Between Molecules in Collisions. J. Chem. Phys., vol. 40, Jan. 1964, pp. 573-575.

18. Kerner, E. H.: Note on the Forced and Damped Oscillator in Quantum Mechanics. Can. J. Phys., vol. 36, Mar. 1958, pp. 371-377.

19. Treanor, C. E.: Vibrational Energy Transfer in High-Energy Collisions. J. Chem. Phys., vol. 43, July 1965, pp. 532-538; Transition Probabilities for the Forced Harmonic Oscillator. J. Chem. Phys., vol. 44, Mar. 1966, pp. 2220-2221

20. Rapp, D.; and Kassal, T.: The Theory of Vibrational Energy Transfer Between Simple Molecules in Nonreactive Collisions. Chem. Rev., vol. 69, Feb. 1969, pp. 61-102.

21. Parker, J. G.: Rotational and Vibrational Relaxation in Diatomic Gases. Phys. Fluids, vol. 2, July-Aug. 1959, pp. 449-462.

22. Shin, H. K.: "Steric Factor" in Vibrational-Translation Energy Transfer. J. Chem. Phys., vol. 46, May 1967, pp. 3688-3690.

23. Mies, F. H.: Critical Examination of Vibrational Energy-Transfer Theory. J. Chem. Phys., vol. 42, Apr. 1965, pp. 2709-2720.

24. Stallcop, J. R.: Semiclassical Vibration-Rotation Transition Probabilities for Motion in Molecular State Averaged Potentials. Chem. Phys. Lett., vol. 12, Dec. 1971, pp. 30-34.

25. Hansen, C. F.; and Pearson, W. E.: Three-Dimensional Model of Collision-Induced Vibrational Transitions in Homonuclear Diatomic Molecules. J. Chem. Phys., vol. 53, Nov. 1, 1970, pp. 3557-3567.

26. Stallcop, J. R.: Corrections to Vibrational Transition Probabilities Calculated from a Three-Dimensional Model. J. Chem. Phys., vol. 56, May 1, 1972, pp. 4505-4512.

27. Meador, W. E.: The Interactions Between Nitrogen and Oxygen Molecules. NASA TR R-68, 1960.

28. Hansen, C. E.; and Pearson, W. E.: Semiclassical Theory of Vibrational Excitation for Diatomic Molecules with Conserved Collision Energy. J. Chem. Phys., vol. 54, Feb. 15, 1971, pp. 1539-1546.

29. Appleton, J. P.: Shock-Tube Study of the Vibrational Relaxation of Nitrogen Using Vacuum-Ultraviolet Light Absorption. J. Chem. Phys., vol. 47, Nov. 1, 1967, pp. 3231-3240.

30. Rose, M. E.: Elementary Theory of Angular Momentum. Wiley, New York, 1957.

CHAPTER VII COLLISION-INDUCED ROTATIONAL EXCITATION

7.1 SUMMARY

The close-coupled set of equations that describe rotational excitation by collision perturbation are the same as used previously to describe vibrational excitation. However, in this case the small perturbation methods fail and a large number of accessible states lie within kT of one another so that reaction paths from initial state n to final state j can go through a multiplicity of intermediate states, such as $n \to k \to \ell \to m \to \ldots \to j$. This renders even high-speed computer solutions very costly except at very low temperatures, where somewhat fewer levels need to be included in the coupled set. Nevertheless, a few steps in the problem can be carried forward analytically to give some physical insight into the character of the solutions. In particular, the sudden approximation is useful wherever the collision time is very short compared with the transition time ω^{-1}, and a series expansion of the solution is then possible in analytic form. Such solutions are illustrated by carrying out the integrals for cross section and rate coefficient for first- and second-order terms, but recognizing that additional terms, which greatly increase the complexity, must be included for convergence to the correct answer for most cases of practical importance. Some numerical integrations of the close-coupled set of rotational transition equations are given, using a severely truncated form of the interaction potential, to show the character of the precise solutions that can be provided, in principle, by high-speed computers. The effort to perform the precise solutions will be warranted once quantum chemistry methods have provided realistic interaction potentials.

7.2 INTRODUCTION

Collision-induced rotational transitions are important for a number of reasons. As we saw in the last chapter, rotational transitions are needed for a complete solution of the vibrational excitation problem; they are important in establishing population inversions in molecular gas lasers; they affect ultrasonic absorption and dispersion, transport properties of gases, and the shifting and broadening of spectral lines; and in astrophysics they contribute to the cooling of interstellar gas and possible maser action in such gas. The complete formalism for the equations which need to be solved has been laid out by Takayanagi more than a decade ago; his two review articles on the theory of rotational and vibrational transitions in molecular collisions (refs. 1 and 2) are still current. Unfortunately, the formalism has been of little help to engineers who needed quantitative estimates of the transition rates, because small perturbation methods which lead to analytic expressions are inaccurate, and the more exact solutions by numerical methods required excessive computing time. Takayanagi and others have studied approximate methods such as the Distorted Wave method (ref. 3) and the Modified Wave Number method (refs. 1 and 2), but the only method which seems capable of good accuracy is the close-coupling method which is a direct numerical solution of the set of Eqs. (6.28) derived in the last chapter. These equations are truncated at a finite number of rotational states, which may need to be much larger than the number of rotational states finally excited by the collision. The collision energy may be transiently stored in some of the high-lying rotational states during the course of the collision, just as in the upper vibrational states as discussed in the last chapter, and the set of equations must include all the

states which are excited to an appreciable extent during the collision. This method required so much computer time that only a few simple calculations have been performed until recently. Takayanagi (ref. 4) studied the rotational relaxation in HD-HD collisions at low temperature (20 to 40 K) where only the $J = 0$ and 1 levels needed to be considered; he calculated the number of collisions Z needed to relax the gas to equilibrium and found $Z = 25$ at 20 K and $Z = 19$ at 40 K; this result is within a factor of about 2 compared with experimental results, $Z = 10$, from sound absorption measurements by Prangsma et al. (ref. 5). Itikawa and Takayanagi (ref. 6) obtained better agreement for HD-He collisions, but the interaction potentials used are rather uncertain, so the agreement may be somewhat fortuitous. Three major factors have limited the enthusiasm for performing extensive calculations of rotational excitation (1) the excessive computer time required, (2) the lack of accurate knowledge about interaction potentials, and (3) the lack of accurate experimental data with which to validate the calculations. With respect to the latter, rotational excitation cannot be observed directly with molecular beam methods because the beam densities are far too low for any kind of spectroscopic emission or absorption measurement, even with laser light sources. However, one type of beam measurement can be made quite accurately, the excitation of rotation by electron impact. The electron scattering and energy are measured, and the specific rotational state excited is deduced from conservation of energy. For this reason, the most work is currently being done on electron impact excitation of rotations, both experimentally and theoretically.

In view of the embryonic state of the problem at present, we will discuss only a few specific numerical results, but first we will examine the nature of the close-coupled set of equations which need to be solved, in order to learn something about the general form their solution must take. Some of the recent numerical work follows the complete quantum formalism laid out by Takayanagi in which the incoming particle is treated as a sum of partial waves, each wave representing one unit of angular momentum with respect to the relative motion between the two collision partners. The problem with this approach is that several hundreds of these partial waves may need to be included before the solution converges to the correct value of the cross section. In other words, the cross sections are large enough so that for heavy particles and realistic collision velocities a very large number of quantum angular momentum units is involved at the larger miss distances. The problem is not as severe for the light-weight electrons, of course, which is why calculations involving these collision partners are more tractable. For present purposes, we will limit ourselves to the semiclassical model for conceptual simplification, and withhold remarks about the full quantum approach until chapter X, where the scattering of these partial waves will be discussed.

7.3 SEMICLASSICAL CLOSE-COUPLING METHOD

The coupled set of equations which describe rotational excitation by collision perturbation are just the same set derived in the last chapter to describe vibrational transitions by perturbation (Eq. 6.28)

$$\dot{a}_k = -\frac{i}{\hbar}\sum_{n=1}^{L} a_n U_{nk}\,, \quad k = 1, 2, \ldots L \tag{7.1}$$

The matrix elements U_{nk} are

$$U_{nk} = \langle Y_k | H' | Y_n \rangle \, e^{i(\omega_n - \omega_k)t} \qquad (7.2)$$

where Y_k and Y_n are the eigenfunctions of states k and n with energy eigenvalues $\hbar\omega_k$ and $\hbar\omega_n$, respectively, and H' is the time-dependent collision perturbation potential. For the rotational problem of interest here, the eigenfunctions Y_k will be taken as the rigid-rotator, spherical-harmonic wave functions $Y_{\ell_k}^{m_k}$, where ℓ_k and m_k are, respectively, the quantum numbers giving the angular momentum of the rotator and its projection on the z axis for the state k in units of $\hbar$.

The quantity H' in the semiclassical model is the time-dependent perturbation determined by the classical collision trajectory. This is a reasonably good approximation if the colliding particles are massive enough to have, at the velocities of interest, a quantum wavelength short compared with the distance of appreciable potential change. This condition is typically satisfied for molecular collisions of interest, except for electron collisions which need to be treated by a full quantum treatment; that is, the translational wave function must then be included as part of the interaction matrix elements. The main problem with the semiclassical method is that it is awkward to allow for conservation of angular momentum and total energy during the collision event, though this can be done approximately by the expansions about the point of closest approach as for the vibrational transitions considered in chapter VI.

The square of the amplitudes a_k represent the probability that at any time t the system will be represented by the steady state eigenfunction Y_k with energy $\hbar\omega_k$, if the perturbation were to be removed at that time. The system starts out with unit probability in some initial state, and a characteristic of the solutions to Eq. (7.2) is that total probability is conserved

$$\sum_{k=1}^{L} a_k^* a_k = 1 \qquad (7.3)$$

The equations are truncated at some total number of states L, which might represent the total number of vibrational-rotational levels up to the dissociation limit in a complete solution, for example. In practical terms, the number of levels is usually truncated at the number which are appreciably excited during the course of the collision event, in order to reduce the computation time required. At very low temperatures, where the collisions are very low energy, a two level approximation may provide reasonably good answers; the two level approximation was used by Takayanagi (ref. 4) and Itikawa and Takayanagi (ref. 6) to calculate rotational excitation of HD at gas temperatures from 20 K to 40 K, for example. At higher temperatures, it may prove necessary to include the order of a hundred levels of a typical rotational excitation problem.

The general character of the solutions can be appreciated from inspection of Kerner's solution for large perturbation vibrational transitions of harmonic oscillators (chapter VI). These analytic solutions are the same as obtained from numerical solutions of the coupled set of equations. The imaginary coefficients in the differential equations, (7.1), establishes a 90° phase charge between the amplitude components a_k and the time derivatives $\dot{a}_k$, which in turn assures the conservation of probability, Eq. (7.3), and results in components of the probability vector which

exhibit maxima and nodes as a function of time (see figs. 6.5(a-c)). The probabilities are, in effect, surging back and forth between the various available levels during the course of the perturbation event, and the final distribution of the probability among the steady-state levels is highly dependent on the duration of the perturbation as well as its magnitude. Of course, Kerner's solutions apply only to a harmonic oscillator case where the perturbation is linear in the oscillator coordinate, but the general character of the solutions will be the same for any set of levels and any time-dependent perturbation function. This is well illustrated in the two-level approximation, where analytic solutions are possible.

7.4 TWO-LEVEL APPROXIMATION

In the two-level approximation, the coupled set of equations reduce to

$$\dot{a}_1 = -iV(t)(a_1 + U\, e^{i\omega_o t}\, a_2) \tag{7.4}$$

$$\dot{a}_2 = -iV(t)(U\, e^{-i\omega_o t}\, a_1 + a_2) \tag{7.5}$$

where

$$\omega_o = (E_2 - E_1)/\hbar\,, \quad V(t) = U_{11} = U_{22}$$

and

$$UV(t) = U_{12} = U_{21}$$

Let

$$b_k = a_k \exp\left[i \int V(t)dt\right] \tag{7.6}$$

Since $b_k^* b_k = a_k^* a_k$, we may transform the equations to the amplitudes b_k and solve for these quantities.

$$\dot{a}_k = \dot{b}_k \exp\left[-i \int V(t)dt\right] - a_k iV(t) \tag{7.7}$$

$$\dot{b}_1 = -iV(t)U \exp(i\omega_o t)a_2 \exp\left(i \int V\, dt\right) = -iV(t)U \exp(i\omega_o t)b_2 \tag{7.8}$$

$$\dot{b}_2 = -iV(t)U \exp(-i\omega_o t)a_1 \exp\left(i \int V\, dt\right) = -iV(t)U \exp(-i\omega_o t)b_1 \tag{7.9}$$

The solution can be carried forward for arbitrary $V(t)$, but to illustrate the form of the solution we consider the case where the perturbation $V(t)$ is a rectangular pulse. Differentiate Eqs. (7.8) and (7.9) with respect to time and let $U^2V^2 = C^2$, to obtain

$$\ddot{b}_1 - i\omega_o \dot{b}_1 + C^2 b_1 = 0 \tag{7.10}$$

$$\ddot{b}_2 + i\omega_o \dot{b}_2 + C^2 b_2 = 0 \tag{7.11}$$

Solutions to these equations are

$$b_1 = e^{i\omega_1 t} \tag{7.12}$$

$$b_2 = e^{i\omega_2 t} \tag{7.13}$$

where

$$\omega_1 = \frac{\omega_o \pm \sqrt{\omega_o^2 + 4C^2}}{2} \tag{7.14}$$

$$\omega_2 = \frac{-\omega_o \pm \sqrt{\omega_o^2 + 4C^2}}{2} \tag{7.15}$$

Thus, a general solution for b_1 and b_2 is

$$b_1 = e^{i\omega_o t/2}(A_1\, e^{i\omega_p t} + B_1\, e^{-i\omega_p t}) \tag{7.16}$$

$$b_2 = e^{-i\omega_o t/2}(A_2\, e^{i\omega_p t} + B_2\, e^{-i\omega_p t}) \tag{7.17}$$

where

$$\omega_p = \sqrt{\left(\frac{\omega_o}{2}\right)^2 + C^2} \tag{7.18}$$

Now to satisfy this initial condition where the rotator is known to be in level 1 before the start of the impulse at $t = 0$

$$b_1(0) = 1 = A_1 + B_1 \tag{7.19}$$

$$b_1(0) = 0 = i\left[\left(\frac{\omega_o}{2} + \omega_p\right)A_1 + \left(\frac{\omega_o}{2} - \omega_p\right)B_1\right] \tag{7.20}$$

$$b_2(0) = 0 = A_2 + B_2 \tag{7.21}$$

$$\dot{b}_2(0) = -iC = -i\left[\left(\frac{\omega_o}{2} - \omega_p\right)A_2 + \left(\frac{\omega_o}{2} + \omega_p\right)B_2\right] \tag{7.22}$$

we require that

$$A_1 = \frac{1}{2} - \frac{\omega_o}{4\omega_p}, \quad B_1 = \frac{1}{2} + \frac{\omega_o}{4\omega_p} \tag{7.23}$$

$$A_2 = -B_2 = -\frac{C}{2\omega} \tag{7.24}$$

The solutions, Eqs. (7.16) and (7.17) can thus be expressed

$$b_1 = e^{i\omega_o t/2}\left(\cos \omega_p t - \frac{i\omega_o}{2\omega_p} \sin \omega_p t\right) \tag{7.25}$$

$$b_2 = -e^{-i\omega_o t/2}\left(- \frac{iC}{\omega_p} \sin \omega_p t\right) \tag{7.26}$$

Exercise 7.1: Show that the two-level solutions given by Eqs. (7.25) and (7.26) satisfy the conservation of probability

$$b_1 b_1^* + b_2 b_2^* = 1$$

Two limiting cases will be of interest. If $C >> \omega_o$, that is, the perturbation is very strong

$$\omega_p \to C\left[1 + \frac{1}{2}\left(\frac{\omega_o}{2C}\right)^2 + \ldots\right] \simeq C \tag{7.27}$$

$$b_1^2 \xrightarrow[C>>\omega_o]{} \cos^2 Ct \tag{7.28}$$

$$b_2^2 \xrightarrow[C>>\omega_o]{} \sin^2 Ct \tag{7.29}$$

The rotator surges back and forth with a high frequency C/π. On the other hand if $C << \omega_o$, that is, the perturbation is very weak

$$\omega_p \to \frac{\omega_o}{2}\left[1 + \frac{1}{2}\left(\frac{2C}{\omega}\right)^2 + \ldots\right] \simeq \frac{\omega_o}{2}$$

$$b_1^2 \xrightarrow[\omega_o>>C]{} \cos^2 \frac{\omega_o t}{2} + \sin^2 \frac{\omega_o t}{2} \simeq 1$$

$$b_2^2 \xrightarrow[\omega_o>>C]{} \left(\frac{2C}{\omega_o}\right)^2 \sin^2 \frac{\omega_o t}{2}$$

In this case the upper state is never very highly populated, but a small amount of energy flows in and out of this rotational state with the frequency $\omega_o/2\pi$.

Solutions can be carried forward for a general impulse shape; the solutions for w_1 and w_2 then become complex numbers with factors such as $(\dot{C}/C)$ in the imaginary part. In this case the solutions are also damped and thus have the character of a damped oscillation between levels. Such two-level approximations are not very realistic in most practical situations however, so we need not develop them further here; our interest in this approximation has been mainly to develop a feeling for the characteristics of solutions to the set of coupled equations. Next, we will look at expressions for these solutions which are series expansions in powers of h^{-1}.

7.5 SERIES EXPANSIONS OF SOLUTIONS TO THE CLOSE-COUPLED SET OF EQUATIONS

In the small perturbation approximation, the value of the coefficient a_n, where n is the initial state, is simply taken to be a constant, $a_n = 1$. All other coefficients a_k are taken to vanish in the first approximation. Then, the set of differential Eqs. (7.1) are uncoupled

$$\dot{a}_k = -\frac{i}{\hbar} U_{nk} e^{i(\omega_n - \omega_k)t}, \quad k = 1, 2, 3, \ldots \tag{7.30}$$

for which the solutions are simply

$$a_n = 1 - \frac{i}{\hbar} \int_{-\infty}^{t} U_{nn}\, dt \tag{7.31a}$$

$$a_k = -\frac{i}{\hbar} \int_{-\infty}^{t} U_{nk} e^{i(\omega_n - \omega_k)t}\, dt \tag{7.31b}$$

The total probability is not conserved in this approximation, but does remain close to unity if I_{nk} defined as the Fourier transform integrals of U_{nk}, are all small

$$I_{nk} = \int_{-\infty}^{t} U_{nk} e^{i(\omega_n - \omega_k)t}\, dt \tag{7.32a}$$

$$a_n a_n^* = 1 + \frac{I_{nn}^2}{\hbar^2} \tag{7.32b}$$

$$a_k a_k^* = \frac{I_{nk}^2}{\hbar^2} \tag{7.32c}$$

$$P = \sum_j a_j a_j^* = 1 + \frac{1}{\hbar^2} \sum_k I_{nk}^2 \neq 1 \tag{7.33}$$

The probability will, however, be conserved if we retain all terms of order $\hbar^{-2}$ in the expressions for $a_n a_n^*$. For conciseness in notation let

$$V_{jk} = U_{jk} e^{i(\omega_j - \omega_k)t} \tag{7.34}$$

The solutions for the coefficients a_k may then be expressed exactly

$$\ell n\, a_n = -\frac{i}{\hbar} \int_{-\infty}^{t} V_{nn}\, dt - \frac{i}{\hbar} \sum_{k \neq n} \int_{-\infty}^{t} \frac{a_k(t)}{a_n(t)} V_{nk}\, dt \tag{7.35a}$$

$$a_k = -\frac{i}{\hbar}\int_{-\infty}^{t} a_n(t)V_{nk}\,dt - \frac{i}{\hbar}\sum_{j\neq n}\int_{-\infty}^{t} a_j(t)V_{jk}\,dt \qquad (7.35b)$$

Now inserting the first-order approximations in the right-hand side of Eq. (7.35a) and (7.35b)

$$\ln a_n = -\frac{i}{\hbar}\int_{-\infty}^{t} V_{nn}(t')dt' - \frac{1}{\hbar^2}\sum_{k\neq n}\int_{-\infty}^{t} V_{nk}(t')\int_{-\infty}^{t'} V_{nk}(t'')dt''\,dt' + \ldots \qquad (7.36a)$$

$$a_k = -\frac{i}{\hbar}\int_{-\infty}^{t} V_{nk}(t')dt' + \ldots \qquad (7.36b)$$

The double integrals of Eq. (7.36a) are easily evaluated

$$\int_{-\infty}^{t}\left[\int_{-\infty}^{t'} V_{nk}(t'')dt''\right]V_{nk}(t')dt' = \int_{-\infty}^{t} I_{nk}(t')\frac{dI_{nk}}{dt'}\,dt'$$

$$= \frac{I_{nk}^2(t')}{2}\Bigg|_{-\infty}^{t} = \frac{I_{nk}^2(t)}{2} \qquad (7.37)$$

Then

$$\ln a_n = -\frac{i}{\hbar}I_{nn} - \frac{1}{\hbar^2}\sum_{k\neq n}\frac{I_{nk}^2}{2} + \ldots \qquad (7.38a)$$

$$a_n = 1 - \frac{i}{\hbar}I_{nn} - \frac{1}{\hbar^2}\sum_{k\neq n}\frac{I_{nk}^2}{2} - \frac{I_{nn}^2}{2\hbar^2} + \mathcal{O}\left(\frac{1}{\hbar^3}\right) + \ldots \qquad (7.38b)$$

$$a_k = -\frac{i}{\hbar}I_{nk} + \mathcal{O}\left(\frac{1}{\hbar^2}\right) + \ldots \qquad (7.38c)$$

Now the absolute values of the squares of the coefficients a_k are, to order $\hbar^{-2}$

$$a_n a_n^* = 1 - \frac{1}{\hbar^2}\sum_{k} I_{nk}^2 + \frac{1}{\hbar^2}I_{nn}^2 + \ldots = 1 - \frac{1}{\hbar^2}\sum_{k\neq n} I_{nk}^2 + \ldots \qquad (7.39a)$$

$$a_k a_k^* = \frac{I_{nk}^2}{\hbar^2} \qquad (7.39b)$$

The probability is thus conserved to order $\hbar^{-2}$

$$\sum_k a_k a_k^* = 1 - \frac{1}{\hbar^2}\sum_{k\neq n} I_{nk}^2 + \frac{1}{\hbar^2}\sum_{k\neq n} I_{nk}^2 + \ldots = 1 + \mathcal{O}(\hbar^{-3}) \tag{7.40}$$

The expansion can of course be continued to higher order terms. For example

$$a_k = -\frac{i}{\hbar}\int_{-\infty}^{t} V_{nk}(t')dt' - \frac{1}{\hbar^2}\int_{-\infty}^{t}\int_{-\infty}^{t'} V_{nn}(t')V_{nk}(t'')dt''\,dt'$$

$$-\frac{1}{\hbar^2}\sum_{j\neq n}\int_{-\infty}^{t}\int_{-\infty}^{t'} V_{jk}(t')V_{jk}(t'')dt''\,dt' + \mathcal{O}(\hbar^{-3}) \tag{7.41}$$

$$\frac{a_k}{a_n} = a_k + \frac{1}{\hbar^2}\int_{-\infty}^{t}\int_{-\infty}^{t'} V_{nk}(t')V_{nn}(t'')dt''\,dt' + \mathcal{O}(\hbar^{-3}) \tag{7.42}$$

$$\ell n\, a_n = -\frac{i}{\hbar}\int_{-\infty}^{t} V_{nn}(t')dt' - \frac{1}{\hbar^2}\sum_{k\neq n}\int_{-\infty}^{t}\int_{-\infty}^{t'} V_{nk}(t')V_{nk}(t'')dt''\,dt'$$

$$+\frac{1}{\hbar^3}\sum_{k\neq n}\sum_{j\neq n}\int_{-\infty}^{t}\int_{-\infty}^{t'}\int_{-\infty}^{t''} V_{nk}(t')V_{jk}(t'')V_{jk}(t''')dt'''\,dt''\,dt' + \mathcal{O}(\hbar^{-4}) \tag{7.43}$$

The variables of integration are designated t', t", t'", etc., to call attention to the fact that they are dummy variables and that the true functional variable is the upper limit of the last integral to be performed. As long as the perturbation functions are all the same, the nested integrals may be evaluated exactly by repeated application of the result in Eq. (7.37).

$$\int_{-\infty}^{t}\int_{-\infty}^{t_1}\cdots\int_{-\infty}^{t_q} V_{nk}(t_q)V_{nk}(t_{q-1})\ldots V_{nk}(t_1)dt_q\,dt_{q-1}\ldots dt_1 = \frac{I_{nk}^q(t)}{q!} \tag{7.44}$$

However, where the perturbation functions are different, the general result is not so simply expressed. An approximation known as the sudden approximation is often used at this point, where the perturbation is treated as a delta function in time. The physical interpretation of this approximation is that the impulse duration is very short compared with the period of transition between any two steady states, that is

$$(\omega_n - \omega_k) << \frac{1}{\tau_c} \tag{7.45}$$

where τ_c is the effective duration of the collision perturbation. This is a reasonably good approximation for high-temperature collisions when the adjacent states are close together, e.g., in high temperature excitation of low-lying rotational states. However, the approximation becomes poorer as the values of $\Delta\omega$ become larger, as they do for upper rotational states where the energy increases as $\ell(\ell+1)$ — approximately the square of the rotational quantum number ℓ.

Wherever the sudden approximation is justified, the nested integrals can be evaluated simply

$$\int_{-\infty}^{t}\int_{-\infty}^{t'-} V_{nj}(t')V_{nk}(t'')dt''\,dt' = \frac{I_{nj}I_{nk}}{2} \tag{7.46a}$$

$$\int_{-\infty}^{t}\cdots\int_{-\infty}^{t_{q-1}} V_1(t_1)V_2(t_2)\cdots V_q(t_q)dt_1\,dt_2\cdots dt_q = \frac{I_1I_2\cdots I_q}{q!} \tag{7.46b}$$

Problem 7.2a: Consider the rectangular perturbation impulses

$$V_{nk} = V_o\,, \quad -\varepsilon < t < \varepsilon$$
$$= 0\,, \quad \varepsilon < |t|$$

show that if

$$I_{nk}(t) = \int_{-\infty}^{t} V_{nk}(t')dt'$$

the nested integral is given by

$$\int_{-\infty}^{t}\int_{-\infty}^{t'} V_{nk}(t')V_{nk}(t'')dt''\,dt' = \frac{I_{nk}^2}{2}$$

Problem 7.2b: Consider rectangular perturbation impulses such that

$$V_{nj} = V_o\,, \quad V_{k\ell} = W_o\,, \quad |t| < \varepsilon$$
$$= 0\,, \quad = 0\,, \quad \varepsilon < |t|$$

show that if we define the single integral

$$I_{jk}(t) = \int_{-\infty}^{t} V_{jk}(t')dt'$$

the double integral is given by

$$\int_{-\infty}^{t}\int_{-\infty}^{t'} V_{nj}(t')V_{k\ell}(t'')dt''\,dt' = \frac{I_{nj}I_{k\ell}}{2}$$

Problem 7.3: Consider a triple-nested integral of rectangular functions $v_i(t)$ with different half widths ϵ_i and different heights V_{i0}

$$\int_{-\infty}^{t}\int_{-\infty}^{t'}\int_{-\infty}^{t''} v_1(t')v_2(t'')v_3(t''')dt'''\,dt''\,dt'$$

where

$$\begin{aligned} v_1(t) &= V_{10}, & |t| &< \epsilon_1 \\ &= 0 & \epsilon_1 &< |t| \\ v_2(t) &= V_{20} & |t| &< \epsilon_2 \\ &= 0 & \epsilon_2 &< |t| \\ v_3(t) &= V_{30} & |t| &< \epsilon_3 \\ &= 0 & \epsilon_3 &< |t| \end{aligned}$$

show that as t becomes greater than the largest half width, the nested integral may be expressed

$$\frac{V_{10}V_{20}V_{30}2^3\epsilon_1\epsilon_2\epsilon_3}{6} \quad \text{or} \quad \frac{I_1I_2I_3}{6}$$

where

$$I_i = \int_{-\infty}^{t} v_i(t')dt'$$

Using the sudden approximation to evaluate the nested integrals, one obtains the expansions

$$a_{j\neq n} = -\frac{i}{\hbar}I_{nj} - \frac{1}{2\hbar^2}\sum_k I_{nk}I_{kj} + \frac{1}{6\hbar^3}\sum_k\sum_\ell I_{nk}I_{k\ell}I_{\ell j} + \frac{1}{24\hbar^4}\sum_k\sum_\ell\sum_m I_{nk}I_{k\ell}I_{\ell m}I_{mj} + \ldots \mathcal{O}(\hbar^{-5}) \qquad (7.47)$$

$$a_n = 1 - \frac{i}{\hbar}I_{nn} - \frac{1}{2\hbar^2}\sum_k I_{nk}^2 + \frac{i}{6\hbar^3}\sum_k\sum_\ell I_{nk}I_{k\ell}I_{\ell n} + \frac{1}{24\hbar^4}\sum_k\sum_\ell\sum_m I_{nk}I_{k\ell}I_{\ell m}I_{mn} + \ldots \mathcal{O}(\hbar^{-5}) \qquad (7.48)$$

Now evaluate the absolute squares of these coefficients to order $\hbar^{-4}$

$$\begin{aligned} a_j a_j^* &= \left(\frac{I_{nj}}{\hbar} - \frac{1}{6\hbar^3}\sum_k\sum_\ell I_{nk}I_{k\ell}I_{\ell j}\right)^2 + \frac{1}{4\hbar^4}\left(\sum_k I_{nk}I_{kj}\right)^2 + \ldots \\ &= \frac{I_{nj}^2}{\hbar^2} - \frac{1}{3\hbar^4}\sum_k\sum_\ell I_{nk}I_{k\ell}I_{\ell j}I_{nj} + \frac{1}{4\hbar^4}\sum_k\sum_\ell I_{nk}I_{kj}I_{n\ell}I_{\ell j} \\ &\quad + \ldots \mathcal{O}(\hbar^{-6}) \end{aligned} \qquad (7.49)$$

$$a_n a_n^* = \left(1 - \frac{1}{2\hbar^2}\sum_j I_{nj}^2 + \frac{1}{24\hbar^4}\sum_j\sum_k\sum_\ell I_{nj}I_{jk}I_{k\ell}I_{\ell n}\right)^2$$

$$+\left(\frac{I_{nn}}{\hbar} - \frac{1}{6\hbar^3}\sum_j\sum_k I_{nj}I_{jk}I_{kn}\right)^2 + \ldots$$

$$= 1 - \frac{1}{\hbar^2}\sum_{j\neq n} I_{nj}^2 + \frac{1}{12\hbar^4}\sum_j\sum_k\sum_\ell I_{nj}I_{jk}I_{k\ell}I_{\ell n} + \frac{3}{12\hbar^4}\sum_k\sum_\ell I_{nk}^2 I_{n\ell}^2$$

$$- \frac{4}{12\hbar^4}\sum_k\sum_\ell I_{nk}I_{k\ell}I_{\ell n}I_{nn} + \ldots \mathcal{O}(\hbar^{-6}) \qquad (7.50)$$

Now sum over all $a_j a_j^*$

$$\sum_{j\neq n} a_j a_j^* = \frac{1}{\hbar^2}\sum_{j\neq n} I_{nj}^2 - \frac{4}{12\hbar^4}\sum_{j\neq n}\sum_k\sum_\ell I_{nk}I_{k\ell}I_{\ell j}I_{nj}$$

$$+ \frac{3}{12\hbar^4}\sum_{j\neq n}\sum_k\sum_\ell I_{nk}I_{kj}I_{n\ell}I_{\ell j} + \ldots \mathcal{O}(\hbar^{-6}) \qquad (7.51)$$

The terms of order $\hbar^{-2}$ in $a_n a_n^*$ and $\Sigma a_j a_j^*$ obviously add up to zero as before. With a little rearrangement of the indices of summation (which are dummy indices) the terms of order $\hbar^{-4}$ are found to cancel as well. For example,

$$\sum_j\sum_k\sum_\ell I_{nk}I_{kj}I_{n\ell}I_{\ell j} = \sum_j\sum_k\sum_\ell I_{nj}I_{jk}I_{k\ell}I_{\ell n} \qquad (7.52)$$

Thus,

$$\sum_{j\neq n}\sum_k\sum_\ell I_{nk}I_{kj}I_{n\ell}I_{\ell j} + \sum_k\sum_\ell I_{nk}^2 I_{n\ell}^2 = \sum_j\sum_k\sum_\ell I_{nj}I_{jk}I_{k\ell}I_{\ell n} \qquad (7.53)$$

$$-\sum_{j\neq n}\sum_k\sum_\ell I_{nk}I_{k\ell}I_{\ell j}I_{nj} - \sum_k\sum_\ell I_{nk}I_{k\ell}I_{\ell n}I_{nn} = -\sum_j\sum_k\sum_\ell I_{nj}I_{jk}I_{k\ell}I_{\ell n} \qquad (7.54)$$

where the summations extend over all levels including the initial level subscript n, unless indicated otherwise. The higher-order terms will also cancel when the expansions are carried further, and probability is thus conserved to each order of approximation.

$$\sum_k a_k a_k^* = 1 \qquad (7.55)$$

Conservation of probability does not prove the accuracy of the separate transition probabilities, of course; one must carry the expansion to the point where it converges in each case of interest. In cases where the sudden approximation is not reliable, one would need to evaluate multiple integrals instead of the simple product of single integrals (see Eq. (7.46b)).

Problem 7.4: Derive the expansions for a_j and a_n given by Eqs. (7.47) and (7.48). A relatively direct method is to use successive approximation in the exact relations of Eqs. (7.35a) and (7.35b).

7.6 CALCULATION OF ROTATIONAL TRANSITIONS WITH THE SUDDEN APPROXIMATION

The solutions of rotational transition probabilities with high-speed digital computers usually are performed by direct numerical integration of the coupled set of equations (7.1). This may consume excessive amounts of computer time when a large number of equations need to be included, as they do when a large number of coefficients a_j transiently take on sizable values during the course of a collision event. This occurs whenever a large number of energy states are accessible with energy spacing less than kT, which is the case for the typical rotation excitation problem. However, one can also proceed to use a computer to evaluate expansions such as Eqs. (7.47) and (7.48). These expansions can be expressed in terms of nested multiple integrals Eq. (7.46), and in principle, these integrals could be evaluated numerically with a computer without resorting to the sudden approximation. However, the amount of computer time required to evaluate such multiple integrals is hopelessly excessive, and the expansion-type solutions are, therefore, always evaluated using the sudden approximation.

Stallcop (ref. 7) carries forward the sudden approximation expansions to an analytic result for the cross sections for transition from rotational state j to j', using a linear-trajectory approximation for the classical interaction impulse. The linear-trajectory approximation is rather reasonable because the rotational transitions are promoted more effectively by the large number of weak interaction collisions, with large impact parameter b, where the trajectory is reasonably linear, than by the much smaller number of strong interaction collisions with small impact parameter b, where the trajectory is strongly deflected. Stallcop (ref. 7) also shows that the sudden approximation is justified for collision velocities the order of 10^5 cm/sec and rotational temperatures the order of 300 K for typical diatomic molecules and appropriate interaction potentials. The analytic expressions are rather complex, but the method of approach is straightforward and may be summarized as follows:

The first and key step is to express the collision interaction potential as a series expansion of terms that are separable in the collision variables (miss distance b, collision velocity u, and time t) and the molecular axis angular coordinates (θ and ϕ). Stallcop (ref. 8) shows that the total transition probability cannot depend on the coordinate system chosen, a fact that corresponds with our natural intuition. We will choose collision coordinates as shown in figure 6.3, but other choices are certainly permissible; the choice should be made to simplify the solution as far as possible. The interaction potential may, after some manipulation, be expressed in the form

$$U(\theta,\phi,b,u,t) = \sum_{L} \sum_{M=-L}^{L} u_{LM}(b,u,t) Y_{LM}(\theta,\phi) \tag{7.56}$$

where $Y_{LM}(\theta,\phi)$ is the normalized spherical harmonic function, and $u_{LM}(b,u,t)$ is the coefficient for each term in the summation over the various angular momentum values L and their projections M on the designated polar axis direction. For rigid rotator wave functions $Y_{\ell m}$ and $Y_{\ell' m'}$, corresponding to a transition from state ℓm to state $\ell' m'$, the integrals of Eq. (7.32a), which are factors in the terms of the sudden approximation expansion, are given by

$$I^{LM}_{\ell m \ell' m'}(b,u) = \left\langle Y_{\ell m}(\theta,\phi) Y_{LM}(\theta,\phi) Y_{\ell' m'}(\theta,\phi) \right\rangle \int_{-\infty}^{\infty} u_{LM}(b,u,t) e^{i\omega_{\ell\ell'} t}\, dt \tag{7.57}$$

The first factor is the so-called Wigner-3j coefficient or more commonly the Clebsch-Gordon coefficient, an integral average over all coordinates of three spherical harmonic functions

$$C^{LM}_{\ell m \ell' m'} = \begin{pmatrix} \ell \ell' L \\ m m' M \end{pmatrix} = \left\langle Y_{\ell m} Y_{LM} Y_{\ell' m'} \right\rangle \tag{7.58}$$

These coefficients are rather complex expressions of the indices ℓ, m, ℓ', m', L, and M

$$C^{LM}_{\ell m \ell' m'} = \left[\frac{(L+\ell-\ell')!(L-\ell+\ell')!(\ell+\ell'-L)!(L+M)!(L-M)!(2L+1)}{(L+\ell+\ell'+1)!(\ell-m)!(\ell+m)!(\ell'-m')!(\ell'+m')!} \right]^{1/2}$$

$$\times \sum_{k} \frac{(-1)^{k+\ell'+m'}}{} \frac{(L+\ell'+m-k)!(\ell-m+k)!}{(L-\ell+\ell'-k)!(L+M-k)!k!(k+\ell-1'-m)!} \tag{7.59}$$

These are derived by Wigner (ref. 9), they are discussed by Landau and Lifshitz (ref. 10) and by most advanced quantum texts, and they have been tabulated for a number of values of ℓ, ℓ' and L by Edmonds (ref. 11). The second expression of Eq. (7.58) is the notation used by Edmonds. The summation over the integers k in Eq. (7.59) is a summation over values from $\ell' - \ell + M$ or 0, whichever is greater, to $L + M$ or $L - \ell + \ell'$, whichever is smaller. The coefficients are very symmetrical, though as Landau and Lifshitz (ref. 10) point out, this is difficult to recognize because one cannot explicitly calculate the sum in Eq. (7.59). One can see at once that $M = -(m_1 + m_2)$ is one requirement for a finite coefficient, so only those terms in the expansion need be retained for a given transition.

The second term on the right side of Eq. (7.57) is just the Fourier transform of the expansion coefficient u_{LM}

$$F^{\ell\ell'}_{LM}(b,u) = \int_{-\infty}^{\infty} u_{LM}(b,u,t) e^{i\omega_{\ell\ell'} t}\, dt \tag{7.60}$$

where the circular frequency $\omega_{\ell\ell'}$ is

$$\omega_{\ell\ell'} = [\ell'(\ell'+1) - \ell(\ell+1)] \frac{\hbar}{2I} \tag{7.61}$$

Note that if this transform varies appreciably from the simple integral over the impulse

$$F_{LM}^{\ell\ell'}(b,u) \simeq \int_{-\infty}^{\infty} u_{LM}(b,u,t)dt \tag{7.60a}$$

then the sudden approximation is beginning to deteriorate for the calculation of that particular transition. In other words, the impulse time which determines the width in time of the coefficient u_{LM} must be short compared with the inverse frequency $\omega_{\ell\ell'}^{-1}$.

$$\tau \simeq \frac{1}{u_{LM}(b,u,0)} \int_{-\infty}^{\infty} u_{LM}(b,u,t)dt << \omega_{\ell\ell'}^{-1} \tag{7.62}$$

Note that the integrals have been performed over all time from $-\infty$ to $+\infty$, since we are mainly interested in the final result after the collision event is completed. If one is interested in the time variation of the perturbed wave function during the collision, then the upper limits of these integrals are all taken as t, of course.

At this point, the elements of the sudden approximation integrals have been determined as a product of a numerical Clebsch-Gordon coefficient and a Fourier transform which is a function of miss distance b and collision velocity u

$$I_{\ell m\ell' m'}^{LM}(b,u) = C_{\ell m\ell' m'}^{LM} F_{LM}^{\ell\ell'}(b,u) \tag{7.63}$$

The total integral of Eq. (7.32a) is, of course, the sum over all terms in the expansion of the interaction potential, Eq. (7.56)

$$I_{\ell m\ell' m'}(b,u) = \sum_{L} \sum_{M} I_{\ell m\ell' m'}^{LM} \tag{7.64}$$

Once the coefficients $a_{\ell m\ell' m}$ are calculated with the results above inserted into Eqs. (7.47) and (7.48), the transition probabilities are simply

$$P_{\ell m\ell' m'}(b,u) = a_{\ell m\ell' m'} a_{\ell m\ell' m'}^{*} \tag{7.65}$$

Usually, one is interested only in the total transition probability from a given rotational level ℓ to another level ℓ'. In this case we may sum over all initial values of the quantum number m, giving each of them equal weight in the collision event, and also sum over all final values of m'.

$$P_{\ell\ell'} = \frac{1}{2\ell + 1} \sum_{m} \sum_{m'} P_{\ell m\ell' m'} \tag{7.66}$$

To recapitulate some of the previous results in chapter II on collision cross section $S(u)$ and rate coefficient $\alpha(T)$, these are given by the integrals

$$S(u) = \int_{0}^{\infty} P(b,u) 2\pi b \, db \tag{7.67}$$

$$\alpha(T) = \frac{\bar{u}}{s}\int_0^\infty S(x)x\, e^{-x}\, dx\ , \quad x = \frac{mu^2}{2kT} \tag{7.68}$$

7.7 ILLUSTRATION OF CALCULATION METHODS USING EXPONENTIAL INTERACTION POTENTIAL

To illustrate the calculation procedures and to provide some approximate expectations about the rotational transition probabilities, we may use the same potential derived for the vibrational transition calculations in chapter VI, Eq. (6.83). Figure 6.4 defines the coordinate system used. The molecule is treated as a rigid rotator in this case so that terms in $y - y_e$ vanish.

$$U = U_o\, e^{-(r-\sigma/L)}[\cosh(\delta \sin\theta\cos\phi) + \chi\delta \sin\theta \sin\phi \sinh(\delta \sin\theta\cos\phi) + \ldots] \tag{7.69}$$

Where r and x are functions of t, σ is the distance of closest approach, L is the characteristic scale length of the exponential interaction, and δ is $y_e/2L$, a constant that is the order of unity. Expanding to terms of first order

$$U = U_o\, e^{-(r-\sigma/L)}\left[1 + \frac{\delta^2}{2}\sin^2\theta\cos^2\phi + \chi(t)\delta^2 \sin^2\theta\cos\phi\sin\phi + \ldots\right] \tag{7.70}$$

As in chapter VI, we expand about the turning point at $t = 0$ and fit the first and second derivatives that obtain there

$$e^{-(r-\sigma/L)} = \operatorname{sech}^2 at \tag{7.71}$$

where

$$a^2 = \frac{\ddot{r}_o}{2L} = \left(\frac{u}{2L}\right)^2\left[1 - (1-\varepsilon)\left(1 - \frac{2L}{\sigma}\right)\right] \tag{7.72}$$

$$\varepsilon = \frac{2U_o}{mu^2} \tag{7.73}$$

and

$$\chi(t) \simeq \frac{u_o t}{\sigma} = \frac{u}{\sigma}(1-\varepsilon)^{1/2}t \tag{7.74}$$

The first term in the perturbation potential of Eq. (7.70) will produce only elastic scattering, no rotational transitions. The second term will produce finite matrix elements only for transitions $\ell' = \ell$, $\ell \pm 2$ and $m' = m$, $m \pm 2$; where ℓ' and m' are the final quantum numbers. The third term will produce the same transitions in ℓ and m except that $m' = m$ results in a vanishing matrix element. The evaluation of the averages over the angular coordinates, which result in these selection rules,

$$C_{\ell m \ell' m'} = \left\langle Y_{\ell m}(\theta,\phi) \middle| \sin^2\theta \cos^2\phi \middle| Y_{\ell' m'}(\theta,\phi) \right\rangle \tag{7.75}$$

$$D_{\ell m \ell' m'} = \left\langle Y_{\ell m}(\theta,\phi) \middle| \sin^2\theta \cos\phi \sin\phi \middle| Y_{\ell' m'}(\theta,\phi) \right\rangle \tag{7.76}$$

are worked out in appendix 7A. Higher-order transitions will, of course, result from higher-order terms in the expansion of the potential. However, it is not clear that real potentials are exactly exponential anyway, so the significance of higher-order terms is somewhat moot. In order to keep our illustrative example uncluttered, we shall assume that the effective potential is given by the truncation of Eq. (7.70) at the first three terms.

One can, however, see that continuing the expansion of Eq. (7.70) will result in even powers of $\sin\theta$ so that only transitions involving an even integer change in rotational quantum number ℓ will occur, unless other interaction terms are involved. This is in agreement with experimental observations on the collision invariance of ortho and para states of diatomic molecules, unless some catalyst such as a paramagnetic molecule is introduced which creates relatively strong magnetic dipole interactions during the collision, for example. For collisions between diamagnetic molecules we expect potentials of the form of Eq. (7.69) to be a reasonable approximation. From Stallcop's results (ref. 7) one can show that $\ell' = \ell \pm 2$ are at least expected to be the strongest transition, though the higher-order transitions are not totally negligible. Note that $\ell' = \ell$ transitions are elastic since the rotational energy depends only on ℓ. The elastic collisions resulting in $\ell' = \ell$ and $m' = m \pm 2$ are interesting, as they have produced a flip of the molecule's angular momentum vector in space with no change in energy. The integrals needed to calculate the transition amplitudes from Eqs. (7.47) and (7.48) are now

$$I_{\ell m \ell' m'} = \frac{U_o \delta^2}{2}\left[C_{\ell m \ell' m'} \int_{-\infty}^{\infty} \operatorname{sech}^2 at\, e^{i\omega_{\ell\ell'}t}\, dt \right.$$

$$\left. + D_{\ell m \ell' m'} \frac{2u}{\sigma}(1-\varepsilon)^{1/2} \int_{-\infty}^{\infty} t \operatorname{sech}^2 at\, e^{i\omega_{\ell\ell'}t}\, dt \right] \tag{7.77}$$

For rotational transitions where the sudden approximation is valid, the ratio $\omega/a << 1$, unlike a typical vibrational transition in chapter VI where this ratio was assumed to be large compared with unity. In the present case the Fourier transforms are approximately

$$\int_{-\infty}^{\infty} \operatorname{sech}^2 at\, e^{i\omega_{\ell\ell'}t}\, dt \simeq \int_{-\infty}^{\infty} \operatorname{sech}^2 at\, dt = \frac{1}{a}\tanh at \Big|_{-\infty}^{\infty} = \frac{2}{a} \tag{7.78}$$

$$\int_{-\infty}^{\infty} t \operatorname{sech}^2 at\, e^{i\omega_{\ell\ell'}t}\, dt \simeq \int_{-\infty}^{\infty} t \operatorname{sech}^2 at\, dt = 0 \tag{7.79}$$

The contribution of the third term in Eq. (7.70) is negligible because $\chi(t)\exp[-r - \sigma/L)]$ is an odd function of time. Thus, to first order

$$I_{\ell m \ell' m'} \simeq \frac{U_o \delta^2}{a} C_{\ell m \ell' m'} - \tag{7.80}$$

At this point all the elements necessary for calculation of the sudden approximation expansions for the probability amplitudes are at hand. First the factors $I_{\ell m \ell' m'}$ are multiplied together and summed as required in Eqs. (7.47) and (7.48); next the real terms are all added together and squared and similarly, the imaginary terms are added together and squared. Finally these squared sums are added together to obtain the transition probability. For example, Eq. (7.47) gives to terms of order $\hbar^{-4}$

$$P_{\ell m \ell' m'} = a^2_{\ell' m'} = \frac{I^2_{\ell m \ell' m'}}{\hbar^2} + \frac{1}{4\hbar^4}\left(\sum_{\ell'' m''} I_{\ell m \ell'' m''} I_{\ell'' m'' \ell' m'}\right)^2$$

$$- \frac{1}{3\hbar^4}\left(I_{\ell m \ell' m'} \sum_{\ell'' m''} \sum_{\ell''' m'''} I_{\ell m \ell'' m''} I_{\ell'' m'' \ell''' m'''} I_{\ell''' m''' \ell' m'}\right) + \ldots \mathcal{O}(\hbar^{-6}) \tag{7.81}$$

One can see that this expansion rapidly gets beyond the bounds of convenient analytic expression and becomes a job for machine computation. Nevertheless, it is useful to carry the analytic approximations this far before resorting to machine computation, as this greatly economizes the machine usage.

The first order term in Eq. (7.81) is the same expression as given by the small perturbation solution and is hardly adequate for typical collisions that promote rotations in diatomic gases. Nevertheless it will be a useful illustration of method to follow through the integrations of the first term of Eq. (7.81) over the range of impact parameters to get an expression for the cross section, and finally over the range of velocities to get an expression for rate coefficient.

$$P_{\ell m \ell' m'} = \frac{\delta^4 C^2_{\ell m \ell' m'}}{\hbar^2} \frac{U^2_o(b,u)}{a^2(b,u)} + \ldots \tag{7.82}$$

We will define P_o as the function of velocity u given by the first term of Eq. (7.82) when the miss distance $b = 0$

$$P_o = \frac{\delta^4 C^2_{\ell m \ell' m'}}{\hbar^2} \frac{E^2}{a^2_o(u)} \tag{7.83}$$

then the ratio

$$\frac{P}{P_o} = \varepsilon^2 \left(\frac{a_o}{a}\right)^2 + \ldots \tag{7.84}$$

From equation (6.87)

$$\varepsilon^2 \left(\frac{a_o}{a}\right)^2 = \frac{\varepsilon^2}{1 - (1 - \varepsilon)\left(1 - \frac{2L}{\sigma}\right)} = \frac{\varepsilon}{1 + \frac{2L}{\sigma}\frac{1 - \varepsilon}{\varepsilon}} \tag{7.85}$$

The element of differential cross section is given in terms of ε, the fraction of the collision energy transformed to potential energy at the point of closest approach, by Eq. (6.95)

$$2\pi b\, db = -\pi\sigma^2\left(1 + \frac{2L}{\sigma}\frac{1 - \varepsilon}{\varepsilon}\right) d\varepsilon \tag{7.86}$$

The total cross section thus becomes

$$S = P_o \int_o^\infty \frac{P}{P_o}\, 2\pi b\, db = P_o \int_o^1 (\pi\sigma^2\varepsilon + \ldots) d\varepsilon \tag{7.87}$$

The distance of closest approach is also a function of ε which is troublesome in the integration because it goes to ∞ as ε approaches zero. However, the strongest interactions occur where ε is near unity, so we expand the weakly varying function σ about this point.

$$\sigma = \sigma_o\left(1 - \frac{L}{\sigma_o} \ln \varepsilon\right) \simeq \sigma_o\left[1 + \frac{L}{\sigma_o}(1 - \varepsilon) + \ldots\right] \tag{7.88}$$

Then the cross section expression becomes

$$S = \pi\sigma_o^2 P_o \int_o^1 \left\{\left[1 + \frac{2L}{\sigma_o}(1 - \varepsilon)\right]\varepsilon + \ldots\right\} d\varepsilon$$

$$= \frac{\pi\sigma_o^2 P_o}{2}\left(1 + \frac{2L}{3\sigma_o}\right) + \ldots \simeq \frac{\pi\sigma_o^2 P_o}{2} \tag{7.89}$$

The quantity P_o is proportional to the first power of collision energy E or in other words to u^2

$$P_o = \frac{\delta^4 C^2_{\ell m \ell' m'}}{\hbar^2}\frac{(mu^2/2)^2}{(u/2L)^2} = \left(\frac{\delta^4 C^2_{\ell m \ell' m'}}{\hbar^2}\right) m^2 u^2 L^2 \tag{7.90}$$

The distance of closest approach at $b = 0$ may be expressed

$$\sigma_o = L \ln \frac{\bar{A}}{E} = L \ln \frac{2\bar{A}}{mu^2} \tag{7.91}$$

where $\bar{A}$ is the spherically averaged constant in the exponential interaction potential given by Eq. (6.105a)

$$E = 2A \frac{\sinh \delta}{\delta} e^{-\sigma_o/L} = \bar{A}\, e^{-\sigma_o/L} \tag{7.92}$$

The factors P_o and σ_o are now expressed in terms of the variable x, which is $mu^2/2kT$

$$P_o(x) = \left(2\delta^4 \frac{mL^2kT}{\hbar^2} C^2_{\ell m \ell' m'}\right) x = B\left(\frac{mL^2kT}{\hbar^2}\right) x \tag{7.93}$$

where the dimensionless constant B is defined by the right most equality of Eq. (7.93)

$$\sigma_o = L\, \ell n(\bar{A}/xkT) \tag{7.94}$$

Then the rate coefficient is

$$\alpha_{\ell m \ell' m'} = \frac{\bar{u}}{s} \int_{x^*}^{\infty} S(x) x\, e^{-x}\, dx$$

$$= \frac{\bar{u}}{s} \frac{\pi B}{2} \frac{mL^2kT}{\hbar^2} \int_{x^*}^{\infty} \left\{ \left[L^2 \left(\ell n \frac{\bar{A}}{xkT} \right)^2 + \frac{2L^2}{3} \left(\ell n \frac{\bar{A}}{xkT} \right) \right] x + \ldots \right\} x\, e^{-x}\, dx \tag{7.95}$$

The threshold value of x occurs where the collision energy equals the change in rotational energy

$$x^* = \frac{\hbar \omega_{\ell \ell'}}{kT} = [\ell'(\ell' + 1) - \ell(\ell + 1)] \frac{\hbar}{2IkT} \tag{7.96}$$

The slowly varying logarithmic factors can, to a good approximation, be equated to their value at x^* and pulled outside the integral

$$\alpha_{\ell m \ell' m'} = \frac{\bar{u}}{s} \pi \sigma_o^{*2} \left(1 + \frac{2}{3} \frac{L}{\sigma_o^*}\right) \frac{B}{2} \frac{mL^2kT}{\hbar^2} \int_{x^*}^{\infty} (x^2 + \ldots) e^{-x}\, dx \tag{7.97}$$

where

$$\sigma_o^* = L\, \ell n \frac{\bar{A}}{\hbar \omega_{\ell \ell'}} \tag{7.94a}$$

Normally, x^* or $\hbar\omega_{\ell\ell'}/kT \ll 1$ and $\bar{A}/\hbar\omega_{\ell\ell'} \gg 1$, so to a good approximation the first term in the sudden approximation expansion gives for the rate coefficient,

$$\alpha_{\ell m \ell' m'} \simeq \frac{\bar{u}}{s} \pi \sigma_o^{*2} B \frac{mL^2kT}{\hbar^2} e^{-x^*} \tag{7.97a}$$

Observe that Eq. (7.97a) is an Arrhenius relation with a pre-exponential factor that varies as $T^{3/2}$.

To carry the expansions one step further, we will shorten the notation and let a single index j, k, ℓ, and n denote the states with quantum numbers (ℓ',m'), (ℓ",m"), (ℓ'",m'"), and (ℓ,m) respectively. The sums over indices j, k, ℓ, or n must be recognized as double sums over all values of ℓ and m considered in the set of coupled states for which the matrix elements are finite. From Eq. (7.81)

$$P = \frac{I_{nj}^2}{\hbar^2}\left[1 + \frac{1}{4\hbar^2}\left(\frac{\sum_k I_{nk}I_{kj}}{I_{nj}}\right)^2 - \frac{1}{3\hbar^2}\left(\sum_k\sum_\ell \frac{I_{nk}I_{k\ell}I_{\ell j}}{I_{nj}}\right) + \ldots \mathcal{O}(\hbar^{-4})\right] \quad (7.98)$$

where P is understood to be the probability of transition from initial state n to state j

$$\frac{P}{P_o} = \left(\frac{U_o(b)a_o}{U_o(0)a}\right)^2\left\{1 - \frac{G}{\hbar^2}\left(\frac{U_o(0)}{a_o}\right)^2\left[1 - \left(\frac{U_o(b)a_o}{U_o(0)a}\right)^2\right] + \ldots \mathcal{O}(\hbar^{-4})\right\} \quad (7.99)$$

where the constant G is defined by

$$G = \frac{\delta^4}{4}\left(\sum_k \frac{C_{nk}C_{kj}}{C_{nj}}\right)^2 - \frac{\delta^4}{3}\sum_k\sum_\ell \frac{C_{nk}C_{k\ell}C_{\ell j}}{C_{nj}} \quad (7.100)$$

The following relations are used

$$\left(\frac{U_o(b)a_o}{U_o(0)a}\right)^2 = \left(\varepsilon\,\frac{a_o}{a}\right)^2 = \frac{\varepsilon}{1 + \frac{2L}{\sigma}\left(\frac{1-\varepsilon}{\varepsilon}\right)} \quad (7.101)$$

$$\left(\frac{U_o(0)}{a_o}\right)^2 = \frac{m^2u^2L^2}{\hbar^2} \quad (7.102)$$

So the cross section may be expressed

$$S = \pi\sigma_o^2 P_o \int_o^1 \left[1 + \frac{2L}{\sigma_o}(1-\varepsilon) + \ldots\right]\left[1 - \frac{Gm^2u^2L^2}{\hbar^2}\left(1 + \frac{2L}{\sigma_o}\right)(1-\varepsilon) + \ldots \varepsilon\right] d\varepsilon \quad (7.103)$$

Neglecting terms of order $(1-\varepsilon)L/\sigma_o$, one obtains

$$S = \pi\sigma_o^2 P_o \int_o^1 \left\{1 + \left[\frac{2L}{\sigma_o} - \frac{Gm^2u^2L^2}{\hbar^2}\left(1 + \frac{2L}{\sigma_o}\right)\right](1-\varepsilon) + \ldots\right\}\varepsilon\, d\varepsilon$$

$$= \frac{\pi\sigma_o^2 P_o}{2}\left\{1 + \frac{1}{3}\left[\frac{2L}{\sigma_o} - \frac{Gm^2u^2L^2}{\hbar^2}\left(1 + \frac{2L}{\sigma_o}\right)\right] + \ldots\right\}$$

$$= \pi\sigma_o^2 B\,\frac{mL^2kTx}{2\hbar^2}\left\{\left(1 + \frac{2L}{3\sigma_o}\right) - G\left(1 + \frac{2L}{\sigma_o}\right)\frac{mL^2kTx}{3\hbar^2} + \ldots\right\} \quad (7.104)$$

the same result as Eq. (7.89) plus an additional term. This may now be integrated over all x to obtain the rate coefficient, again letting $\sigma_o = \sigma_o^*$ and pulling it outside the integral

$$\alpha = \frac{\bar{u}}{s} \pi \sigma_o^{*2} B \frac{mL^2kT}{\hbar^2} \int_{x^*}^{\infty} \left[\left(1 + \frac{2L}{3\sigma_o}\right) \frac{x}{2} - G\left(1 + \frac{2L}{\sigma_o}\right) \frac{mL^2kT}{\hbar^2} \frac{x^2}{6} + \cdots \right] x\, e^{-x}\, dx$$

$$\approx \frac{\bar{u}}{s} \pi \sigma_o^{*2} B \frac{mL^2kT}{\hbar^2} \left(1 - \frac{GmL^2kT}{\hbar^2} + \cdots\right) e^{-x^*} \qquad (7.105)$$

One can anticipate that the higher-order terms will be expressible in terms of a constant coefficient, such as B and G, that are determined by the size of the matrix element averages over the molecular axis angular coordinates, and higher powers of the dimensionless quantity $mL^2kT/\hbar^2$. For typical values of interest in molecular collisions of diatomic molecules, $m \sim 25\times10^{-24}$ gm and $L \sim 2\times10^{-9}$ cm,

$$\frac{mL^2kT}{\hbar^2} \sim 0.014\ T \qquad (7.106)$$

Thus, this factor does not promote convergence of the expansion until temperatures are well below 100 K.

The first constant B represents those transitions which occur directly from state n to the final state j. The constant G includes the effect of transitions which have, during the course of the collision, surged from state n to k and then from state k to j and also some transitions that have followed a path $n \to k \to \ell \to j$. Coefficients of higher-order terms will represent transition paths through a still larger number of states that are accessible in accordance with the perturbation selection rules. Although the multistep transitions are far less probable than a single step transition, there are many different paths when a large number of levels are accessible. Thus, the sum over all paths, given by the multiple sums in equations such as (7.47) and (7.48), can total to a value comparable with the much more probable single step transitions.

7.8 NUMERICAL INTEGRATION OF THE CLOSE-COUPLED SET OF ROTATIONAL PERTURBATION EQUATIONS

The calculation of the completed set of coupled equations for rotational transitions of a diatomic molecule, with realistic collision interaction potentials, is a formidable task both for the programmer and for the computer. However, we can appreciate all the essential qualitative features of these solutions, by examining some calculations for a very simple single-term potential function, which is the first term in the expansion of the exponential interaction, and by truncating the number of available rotational levels.

To recapitulate our previous results, the equations we need to solve have the form:

$$\dot{a}_k = -\frac{i}{\hbar}\sum_n a_n U_{nk} , \quad k = 1, 2, 3, \ldots . \tag{7.107a}$$

where the matrix elements U_{nk} are

$$U_{nk} = \left\langle Y_k H' Y_n \right\rangle e^{i(\omega_n - \omega_k)t} \tag{7.107b}$$

The rotator wave functions Y_k will be taken to be the rigid rotator spherical harmonic wave functions Y_ℓ^m, where ℓ is the rotator's angular momentum quantum number and m is the azimuthal quantum number for the projection of this momentum on the z-axis. The transition probabilities we seek are just the complex squares of the amplitudes starting from a given initial state $\langle \ell m \rangle$ and ending in the state $\langle \ell' m' \rangle$

$$P_{\ell m}^{\ell' m'} = a_{\ell m, \ell' m'} a^*_{\ell m, \ell' m'} \tag{7.108}$$

These probabilities must all sum to unity for every initial state, of course

$$\sum_{\ell' m'=0}^{L} \sum_{m'=-\ell'}^{\ell'} P_{\ell m}^{\ell' m'} = 1 \tag{7.109}$$

where L is the limiting rotational state imposed naturally by dissociation of the molecule, or artificially by truncating the number of equations at some level sufficiently high that still higher levels are not involved in the transitions of interest. We shall use a limit of $L = 40$ in the examples to follow.

Generally we are most interested in the total transition probability from initial rotational level ℓ to another level ℓ' and do not concern ourselves with the distribution over azimuthal quantum states m. Thus, we sum over all initial values of m, giving them equal weighting in the collision event, and also sum over all final values of m'

$$P_{\ell\ell'} = \frac{1}{2\ell + 1} \sum_{m=-\ell}^{\ell} \sum_{m'=-\ell'}^{\ell'} P_{\ell m}^{\ell' m'} \tag{7.110}$$

For purposes of illustrating the method we assume a highly oversimplified perturbation function

$$H' = H_o(t)\sin^2\theta\cos^2\phi \tag{7.111}$$

This is just the first term of the expansion of the exponential perturbation which leads to rotational transitions (Eq. 7.70). The advantage in using this truncated potential is that we then need consider only transitions $\ell' = \ell, \ell \pm 2$ and $m' = m, m \pm 2$, which enormously simplifies the programming and shortens the calculations. In a real collision, higher-order transitions will take place, just as in Kerner's treatment of the vibrational transitions discussed in chapter VI. However, the $\ell \pm 2$ transitions are no doubt the most probable for real collision perturbations if the collision energy is not too large, because they represent the effect of the leading term in the perturbation and also because they involve the smallest energy changes.

Two different functions will be considered for the time-dependent part of the perturbation; the first is just a square pulse

$$H_o(t) = E, \quad \text{a constant for} \quad 0 < t \leq \tau \tag{7.112}$$

which allows us to see the effect of different pulse lengths on the results; the second is a more realistically shaped pulse

$$H_o(t) = E\,\mathrm{sech}^2(at) \tag{7.113}$$

which is a pulse with width about $2/a$. We shall wish to apply this analysis to some levels where the rotational quantum number ℓ is small; therefore we use the exact perturbation integrals developed in appendix 7A which are valid for arbitrary values of ℓ and m, rather than the limiting values valid for large ℓ such as developed for rotation coupled vibration transitions in chapter VI.

For the sample calculations the value of $B/\hbar$ has been taken equal $0.27\ \mu\mu\mathrm{sec}^{-1}$, which corresponds to the rotational constant for the O_2 molecule ($B = 1.44\ \mathrm{cm}^{-1}$). Collision energies $E/\hbar$ equal 5, 50, and 500 $\mu\mu\mathrm{sec}^{-1}$ have been chosen, corresponding to collinear collision energies of about 1/300, 1/30, and 1/3 eV, respectively. Of course, these values represent the perturbation at closest approach, so the results also apply to the case of higher energy collisions that are glancing. These energies are the mean collision energies at temperatures about 30 K, 300 K, and 3000 K. However, recall that collisions with the tail of the Maxwell-Boltzmann distribution may be more effective in promoting transitions than collisions with molecules having the average velocity. For example, vibrations are already excited to about one-half their equilibrium value in gases at the characteristic vibrational temperature, yet at this temperature the average collision is just reaching the threshold of zero transition probability.

Figures 7.1(a), (b), (c) show results for rotational transitions of a diatomic rotator as a function of collision time, where the rotator is subject to constant perturbations of 5, 50, and 500 $\mu\mu\mathrm{sec}^{-1}$, respectively. The initial rotational state is $\ell = 4$, $m = 0$ for all these examples. Incidentally, initial values of $m = 2$ and 4 give slightly different results; corresponding to the classical notion that the collision-induced rotations should depend on initial geometry to some extent.

However, initial values of $m = \pm 2$ or $m = \pm 4$ give exactly the same result, as they should, due to the symmetry of these geometric configurations.

The lowest perturbation in figure 7.1(a) corresponds to cryogenic gas collisions. The initial state $\ell = 4$ is reduced only about 10%, with about 5% each going to the adjacent states $\ell = 6$ and $\ell = 2$. If the perturbation lasts long enough, the probabilities periodically surge back and forth just as we found in the two-state approximation; however, there is a slow but continual drain to the higher rotational states that would eventually result in a more or less homogeneous distribution of rotational states if the perturbation were to continue indefinitely. The $\ell = 2$ states are actually populated more readily than the $\ell = 6$ states because a smaller energy difference exists between initial and final states; however, a larger degeneracy of $\ell = 6$ states exists than for $\ell = 2$, so in total the higher rotational states are populated a bit ahead of the lower rotational states.

Figure 7.1(b) shows the results for a normal temperature level of collision perturbation. The calculation has been deliberately prolonged beyond the usual collision duration just to show the surging of probability back and forth between states. The periodic pattern is a complex one because it is the result of superposition of

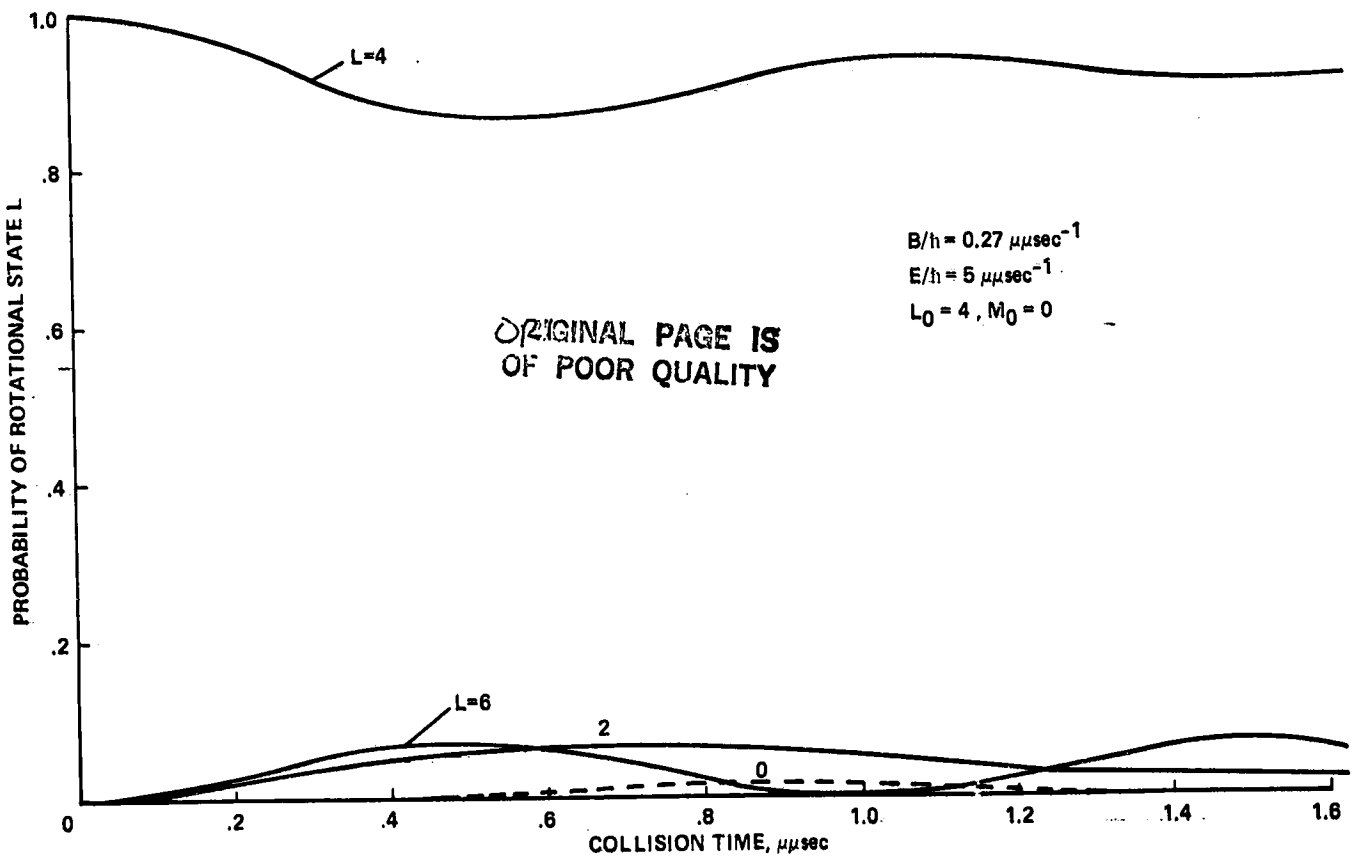

(a) $E/\hbar = 5\ \mu\text{sec}^{-1}$.

Figure 7.1- Rotational transitions as a function of collision time for a constant perturbation.

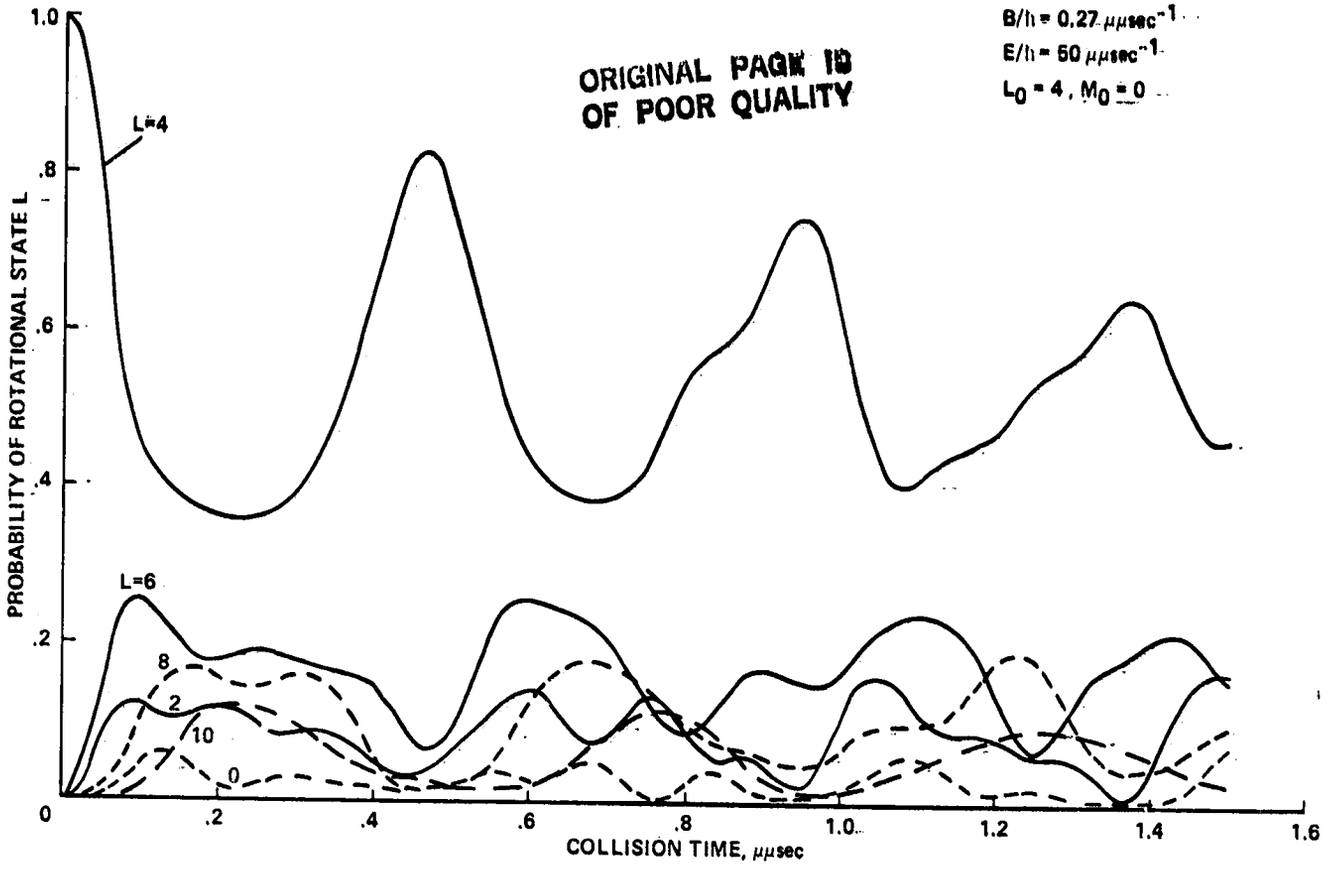

(b) $E/\hbar = 50\ \mu\text{sec}^{-1}$.

Figure 7.1- Continued.

different characteristic frequencies between each set of adjacent rotational states. At this level of perturbation the initial state $\ell = 4$ is immediately depopulated about 40% on the average, with the adjacent states picking up about 10 to 15% each, and the next states picking up about 5% each.

Finally, figure 7.1(c) shows results for rather high energy collisions (1/3 eV head-on collision, or a 1 eV collision with $\varepsilon = 33\%$, the fraction of kinetic energy transformed to potential at closest approach, for example). Here, the initial state $\ell = 4$ is immediately reduced to about 15% probability, and the probabilities of the adjacent levels (shown only to $\ell = 8$) become more or less homogenized with superposed ripple frequencies.

These results are reasonably consistent with the experience of shock tube experimenters that at normal temperature about 10 collisions are required to achieve a more or less equilibrium Boltzmann distribution of rotational states, whereas, at elevated temperatures that occur in moderately strong shock waves a single collision is almost sufficient to achieve equilibrium. On the other hand, at the low temperatures that occur in a supersonic expansion, the order of a hundred collisions or more may be required to achieve rotational equilibrium.

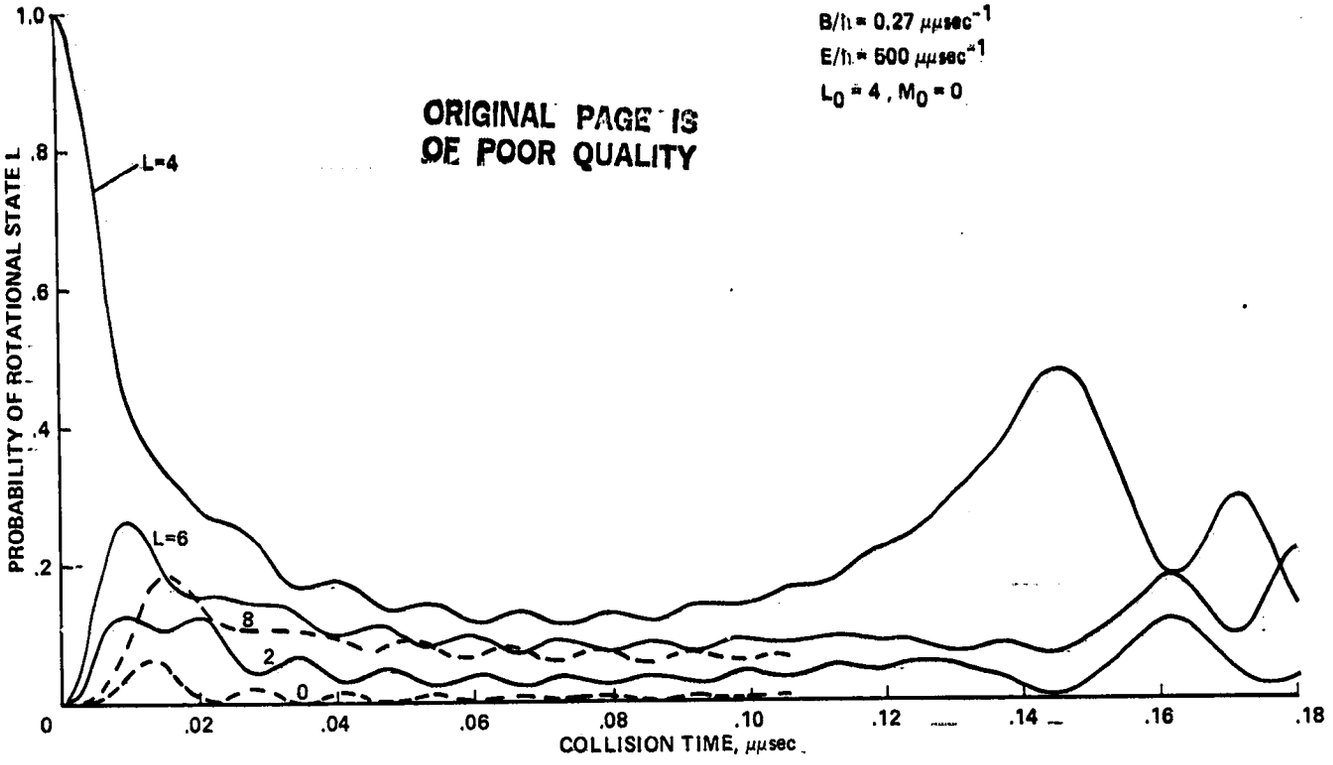

(c) $E/\hbar = 500\ \mu\mu sec^{-1}$.

Figure 7.1-- Concluded.

Next, consider the effect of using a realistic collision-pulse shape. For the reduced mass appropriate to an $Ar-O_2$ collision, the mean collision velocity $\bar{u}$ relative to the center of mass is about 6×10^4 cm/sec at usual temperatures. If the characteristic perturbation potential length L is the order of 0.3 Å, as found in chapter VI for vibration transitions, the mean collision time $2L/\bar{u}$ is the order of 0.1 μμsec. Recall that several different interaction potentials between collision partners are generally possible, depending on how the electron spin vectors happen to add up during the collision event, and that the vibrational transitions are heavily weighted by the interactions that occur along the steepest possible interaction potential. Thus, some interactions may promote purely rotational transitions where the characteristic perturbation potential length is double the above value, or perhaps even more. Thus, the mean collision times of interest may be 0.2 μμsec or more. This is all for room temperature collisions. If the temperatures are reduced by a factor of 10 to about 30 K, the collision times are increased by $\sqrt{10}$; if the temperatures are increased a factor of 10 to about 3000 K, the collision times are decreased by $\sqrt{10}$.

Figure 7.2(a) shows the rotational transitions produced from an initial state $\ell = 4$, $m = 0$ when the collision pulse is $E/\hbar = 50\ \mu\mu sec^{-1}\ sech^2(t/0.1\ \mu\mu sec)$. This pulse has an effective width just about 0.2 μμsec. The results are almost the same as for the constant perturbation pulse shown in figure 7.1(b) if that perturbation were terminated at 0.2 μμsec. The principal difference is that the time scale is stretched out a bit in the beginning and again at the end of the pulse, and the probabilities all tail off asymptotically to constant values rather than terminating with a discontinuity in the slope as they would for a finite square-pulse. In figure 7.2(b) the

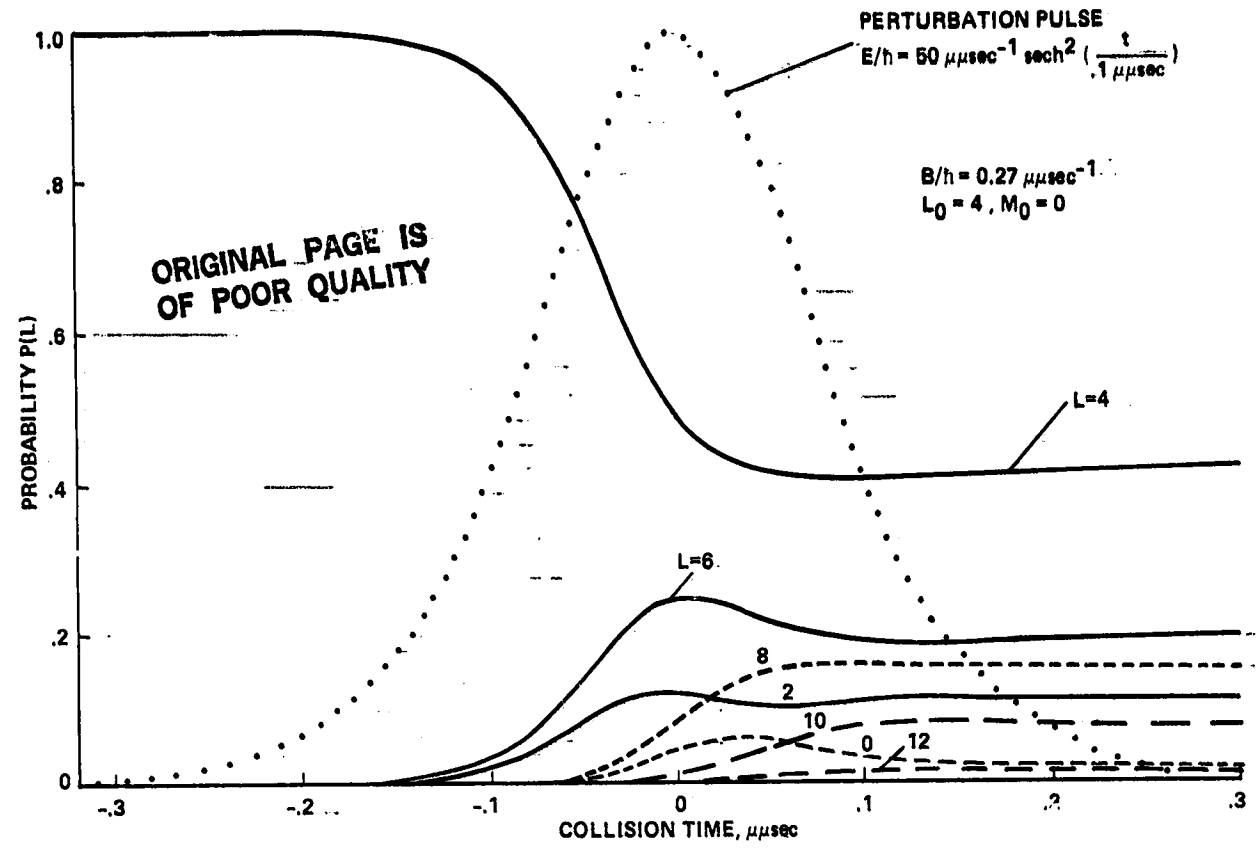

(a) About 0.2 μμsec duration.

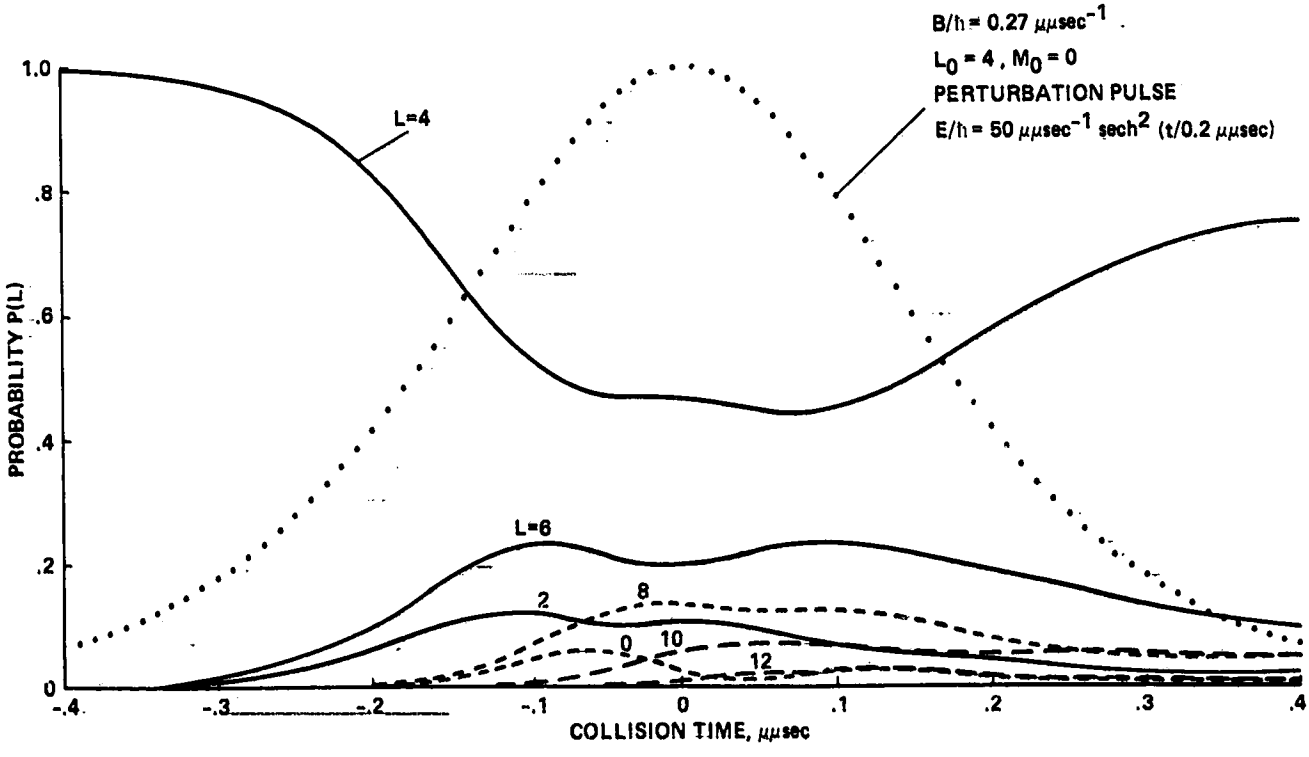

(b) About 0.4 μμsec duration.

Figure 7.2- Rotational transitions for a collision-like perturbation pulse.

pulse width has been doubled. In this case, some probability amplitude surges back into the initial state $\ell = 4$ at the end of the collision, just as for a square pulse terminated at 0.4 μμsec in figure 7.1(b).

The collisions with such a low rotational state as $\ell = 4$ are rather atypical at normal temperature; the average rotational level is given by

$$\ell(\ell + 1) = kT/B$$

which gives $\ell \sim 27$ for normal temperatures and $B = 1.44\ cm^{-1}$. At large ℓ, a larger number of rotational levels are required for the close coupled set of equations used. In the present case we have truncated this set at $L = 40$. A calculation for initial $\ell = 20$, $m = 0$ is shown in figure 7.3 for a collision-like pulse of 0.2 μμsec duration. The principal difference compared with the calculation of 7.2(a) for the same strength and duration collision pulse is that the collision is more adiabatic; the initial state $\ell = 20$ loses only about 30% of its probability and recovers to lose only 15% at the finish of the collision event, whereas the initial state $\ell = 4$ lost 60% of its probability. This occurs because the energy spacing to adjacent levels is significantly larger for the higher rotational state, about 25 times larger for the two cases considered here. This increases the frequency $\omega_{\ell\ell'}$ in the Fourier transform $\langle \text{sech}^2(at)\exp(i\omega_{\ell\ell'}t)\rangle$ (see Eq. (7.77)) and makes the

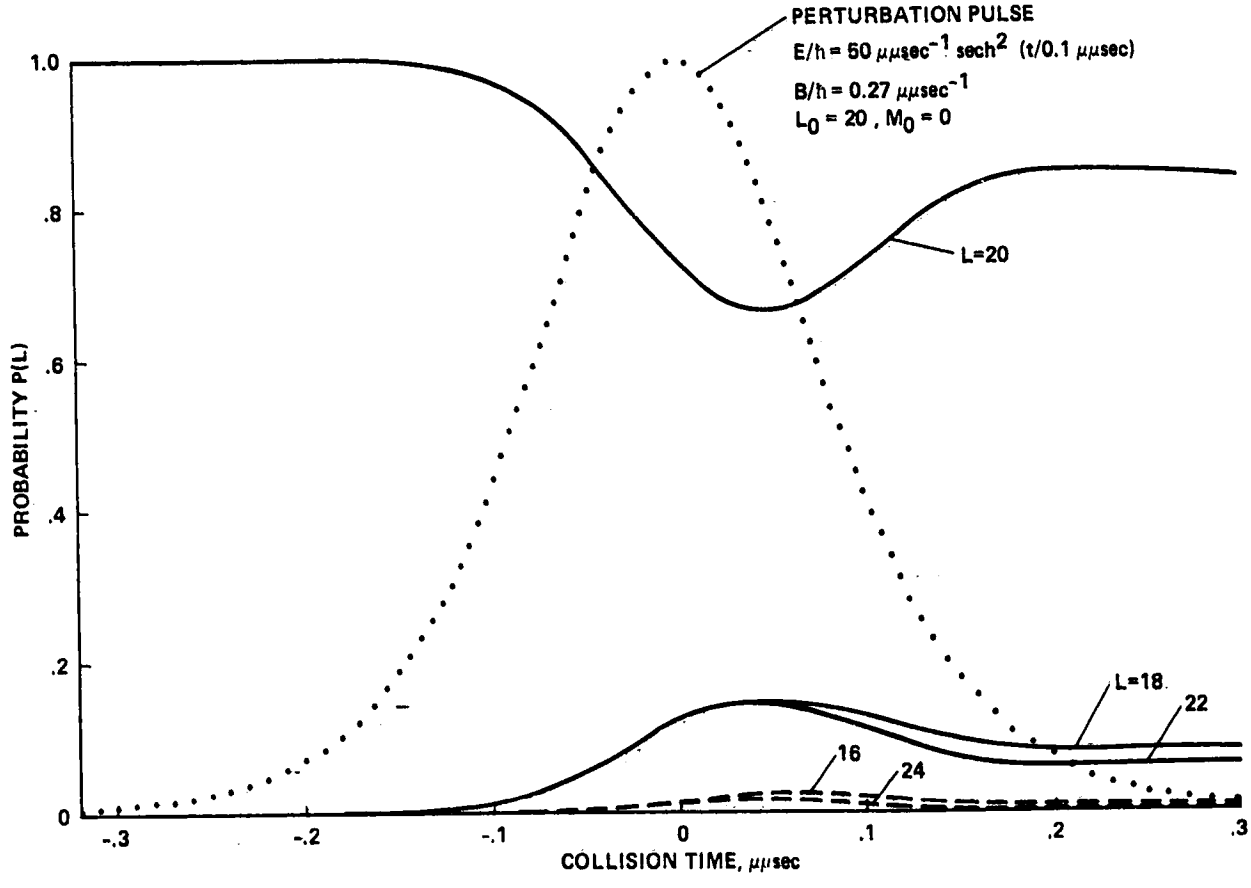

Figure 7.3- Rotation transitions from the initial state $L = 20$ for a 0.2 μμsec collision impulse.

collision more adiabatic. In fact, the step size chosen in the numerical integrations performed by the computer is determined primarily by the maximum value of $\omega_{\ell\ell'}$ that is needed for the calculation at hand. We wish the time increment Δt to be small compared with the period of rotation $B\ell(\ell + 1)/\hbar$

$$\Delta t \simeq 0.01\ \hbar/B\ell(\ell + 1)$$

This would give a numerical step every 3.6° on the rotational time scale. For $B/\hbar = 0.27\ \mu\text{sec}^{-1}$ this requires $\Delta t \sim 0.002\ \mu\text{sec}$ for $\ell = 4$ and $\Delta t \sim 0.0001\ \mu\text{sec}$ for $\ell = 20$. Actually the requirement is not quite as severe as this; the frequency that establishes the acceptable time increment is $\omega_{\ell\ell'}$, the difference between the rotational period of the initial and final states. For most of the numerical integrations shown in the figures of this chapter $\Delta t = 0.0001\ \mu\text{sec}$ was used. Small but not significant differences were observed when $\Delta t = 0.001$ was used.

Still stronger collisions are shown in figures 7.4(a) and 7.4(b) where peak collision energies are 500 and 1500 μsec^{-1}, respectively, corresponding to head-on collisions at about 1/3 eV and 1 eV, respectively. For these cases, we have also chosen very short pulse durations corresponding to interaction along a very steep potential of $L \sim 0.3$ Å and relative collision velocities about 3×10^5 cm/sec. These might thus represent those collision interactions which are most effective in producing vibrational excitation with the coupled rotations as discussed in chapter VI. We see that these strong collisions spread out the rotational state populations on both

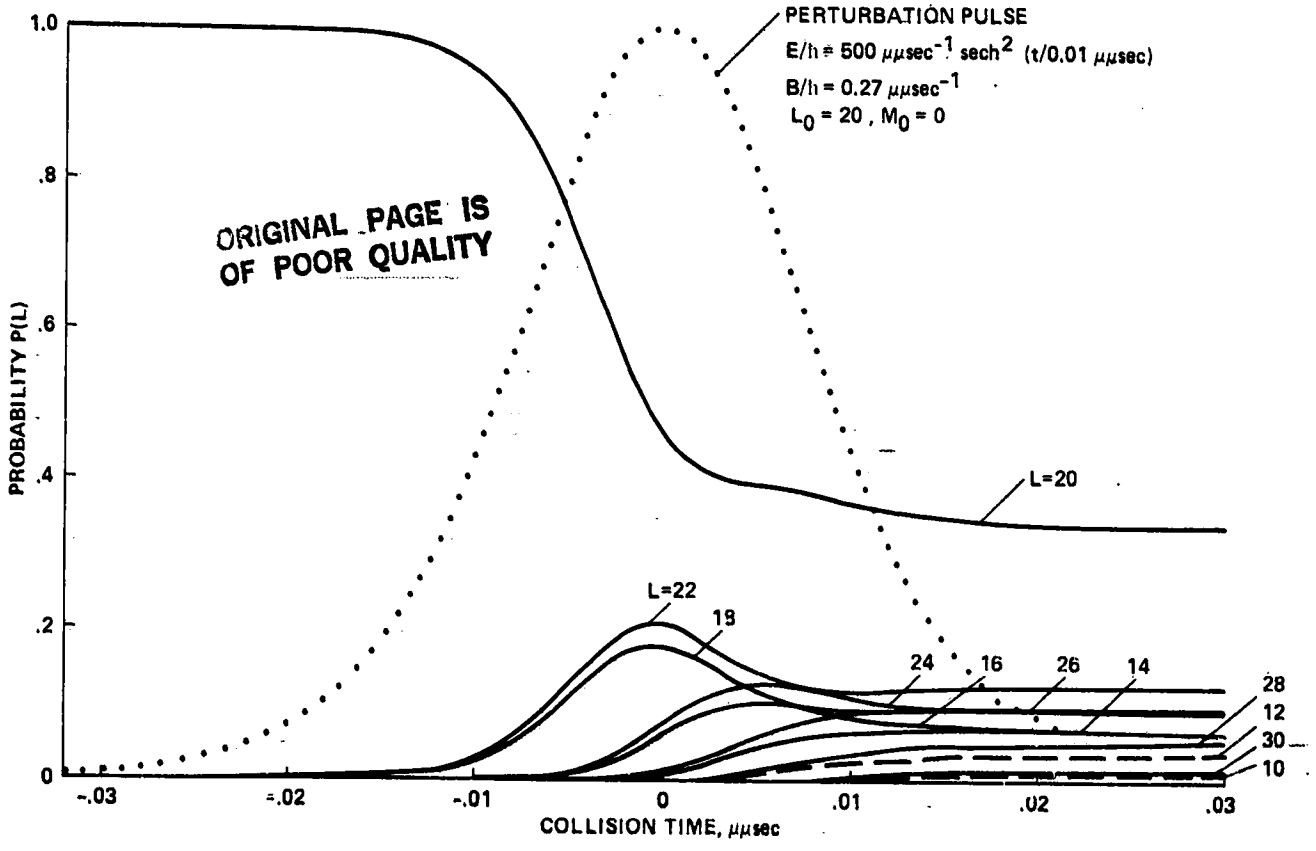

(a) $E/\hbar = 500\ \mu\text{sec}^{-1}$.

Figure 7.4- Rotational transitions from $L = 20$ for collision perturbation pulse.

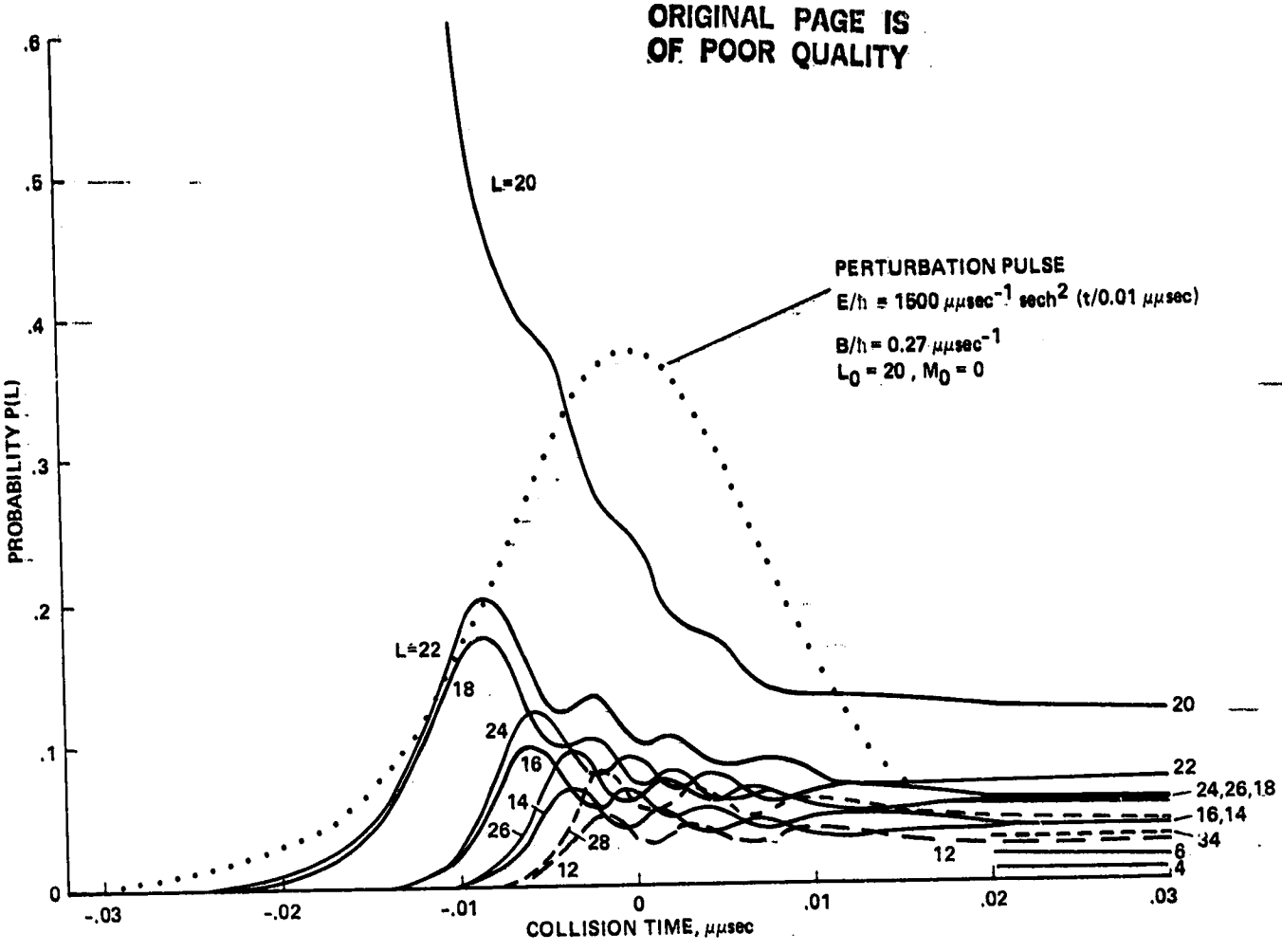

(b) $E/\hbar = 1500\ \mu\mu sec^{-1}$.

Figure 7.4- Concluded.

sides of the initial state rather effectively. Actually, higher-order terms would no doubt be important in the perturbation for these collisions, giving direct multiple jump transitions, so the homogenization would be even more complete than indicated by our simple model. This suggests that a reasonable approximation for the coupled vibration-rotation transition might be to assume an equilibrium-like distribution of rotational states produced by each and every collision.

7.9 CONCLUDING REMARKS

Solutions for rotational collision excitation are found to be exceedingly lengthy because of the large number of rotational states involved and because the rotational energy spacing is small compared with kT, or the average collision energy, for most cases of practical importance. Thus, solutions cannot practically be carried to completion analytically even though the formalism for the expansion of solutions using the sudden approximation is available; the first-order approximation in these expansions is not very accurate quantitatively, though it does give

qualitative insight to the problem. Numerical integrations of the close-coupled set of equations can now be performed with high-speed computers to give accurate answers for collision-induced rotational transitions if realistic molecular interaction potentials are known. Some sample calculations using a severely truncated form of interaction potential show the character that these solutions will have. Fully realistic interaction potentials would require retention of many more terms leading to multiple rotational quantum jumps. Although the software development and computing time required for these more exact calculations is very large — it could be done; however, it will be worth doing only when reliable interaction potentials become available. Quantum chemistry computations may very well provide reasonable approximations to these interaction potentials in the near future.

APPENDIX 7A

EVALUATION OF MATRIX ELEMENTS $\left\langle Y_{\ell'}^{-m'} \middle| \sin^2\theta \cos^2\phi \middle| Y_{\ell}^{m} \right\rangle$

In the collision of a diatomic molecule with an inert particle having exponential-like repulsive interaction potentials between atomic centers, the strongest rotational transitions are expected to result from a perturbation term proportional to $\sin^2\theta \cos^2\phi$. Thus, we need to evaluate the matrix elements

$$I_{\ell m \ell' m'} = \left\langle Y_{\ell'}^{-m'} \middle| \sin^2\theta \cos^2\phi \middle| Y_{\ell}^{m} \right\rangle \tag{A7.1}$$

where, for the case of a rigid rotator, the rotational wave function is

$$Y_{\ell}^{\pm m} = \frac{e^{\pm im\phi}}{\sqrt{2\pi}} C_{\ell m} P_{\ell}^{m}(\cos\theta) \tag{A7.2}$$

$$C_{\ell m} = \left[\frac{(2\ell+1)(\ell-m)!}{2(\ell+m)!}\right]^{1/2} \tag{A7.3}$$

and ℓ and m are the total angular momentum and azimuthal angular momentum quantum numbers, respectively. Note that m has been taken as the absolute value of the latter quantum number, and that both positive and negative rotations are allowed for in the wave function of Eq. (A7.2). The integrals over ϕ are the easiest to evaluate. Let $k = (m' - m)$

Case I)

If $k = 0$, that is $m' = m$

$$\frac{1}{2\pi}\int_0^{2\pi} \cos^2\phi \, d\phi = \frac{1}{2} \tag{A7.4}$$

Case II)

If $k = \pm 2$, that is $m' = m + 2$ and $m - 2$, respectively

$$\frac{1}{2\pi}\int_0^{2\pi} \cos^2\phi \, e^{\pm 2i\phi} \, d\phi = \frac{1}{2\pi}\int_0^{2\pi} \left(\frac{1}{2}\cos 2\phi + \frac{1}{2}\right)\cos 2\phi \, d\phi$$

$$= \frac{1}{4\pi}\int_0^{2\pi} \cos^2 2\phi \, d\phi = \frac{1}{4} \tag{A7.5}$$

For all other values of k the integral vanishes

$$\frac{1}{2\pi}\int_0^{2\pi} \cos^2\phi\, e^{ik\phi}\, d\phi = \frac{1}{2\pi}\int_0^{2\pi}\left(\frac{1}{2}\cos 2\phi + \frac{1}{2}\right)\cos k\phi\, d\phi$$

$$= \frac{1}{4\pi}\int_0^{2\pi} \cos 2\phi \cos k\phi\, d\phi$$

$$= \frac{1}{4\pi}\left|\frac{\sin(2-k)x}{2(2-k)} + \frac{\sin(2+k)x}{2(2+k)}\right|_0^{2\pi} = 0. \qquad \text{(A7.6)}$$

To evaluate the integrals over θ, the following two recursion relations between Legendre polynomials are used:

$$(2\ell+1)\sin\theta\, P_\ell^m = P_{\ell+1}^{m+1} - P_{\ell-1}^{m+1} \qquad \text{(A7.7)}$$

$$(2\ell+1)\sin\theta\, P_\ell^m = (\ell+m)(\ell+m-1)P_{\ell-1}^{m-1} - (\ell-m+1)(\ell-m+2)P_{\ell+1}^{m-1} \qquad \text{(A7.8)}$$

Case 1) $m' = m$

$$I = \frac{1}{2}\frac{C_{\ell m}C_{\ell' m'}}{(2\ell+1)(2\ell'+1)}\int_0^{\pi}(P_{\ell+1}^{m+1} - P_{\ell-1}^{m+1})(P_{\ell'+1}^{m+1} - P_{\ell'-1}^{m+1})\sin\theta\, d\theta \qquad \text{(A7.9)}$$

There exist just 3 possibilities leading to finite integrals, namely $\ell' = \ell$, $\ell+2$, and $\ell-2$. The integral vanishes for all other cases because of the orthogonality between associated Legendre polynomials having the same value of m.

For $\ell' = \ell$, one obtains for $I(\Delta\ell, \Delta m)$

$$I(0,0) = \frac{C_{\ell m}^2}{2(2\ell+1)^2}\left\{\int_0^{\pi}(P_{\ell+1}^{m+1})^2\sin\theta\, d\theta + \int_0^{\pi}(P_{\ell-1}^{m+1})^2\sin\theta\, d\theta\right\}$$

$$= \frac{C_{\ell m}^2}{2(2\ell+1)^2}\left(C_{\ell+1,m+1}^{-2} + C_{\ell-1,m+1}^{-2}\right)$$

$$= \frac{(\ell-m)!}{4(2\ell+1)(\ell+m)!}\left[\frac{2(\ell+m+2)!}{(2\ell+3)(\ell-m)!} + \frac{2(\ell+m)!}{(2\ell-1)(\ell-m-2)!}\right]$$

$$= \frac{1}{2(2\ell+1)}\left[\frac{(\ell+m+2)(\ell+m+1)}{2\ell+3} + \frac{(\ell-m)(\ell-m-1)}{2\ell-1}\right] \qquad \text{(A7.10)}$$

Next if $\ell' = \ell + 2$,

$$I(2,0) = -\frac{C_{\ell m} C_{\ell+2,m}}{2(2\ell+1)(2\ell+5)} \int_0^{\pi} (P_{\ell+1}^{m+1})^2 \sin\theta \, d\theta$$

$$= -\frac{1}{2}\sqrt{\frac{(\ell-m)!(\ell-m+2)!}{2(2\ell+1)(\ell+m)!2(2\ell+5)(\ell+m+2)!}} \cdot \frac{2(\ell+m+2)!}{(2\ell+3)(\ell-m)!}$$

$$= -\frac{1}{2(2\ell+3)}\sqrt{\frac{(\ell-m+1)(\ell-m+2)(\ell+m+1)(\ell+m+2)}{(2\ell+1)(2\ell+5)}} \qquad \text{(A7.11)}$$

Similarly if $\ell' = \ell - 2$

$$I(-2,0) = -\frac{C_{\ell m} C_{\ell-2,m}}{2(2\ell+1)(2\ell-3)} \int_0^{\pi} (P_{\ell-1}^{m+1})^2 \sin\theta \, d\theta$$

$$= -\frac{1}{2}\sqrt{\frac{(\ell-m)!(\ell-m+2)!}{2(2\ell+1)(\ell+m)!2(2\ell-3)(\ell+m-2)!}} \cdot \frac{2(\ell+m)!}{(2\ell-1)(\ell-m-2)!}$$

$$= -\frac{1}{2(2\ell-1)}\sqrt{\frac{(\ell-m)(\ell-m-1)(\ell+m)(\ell+m-1)}{(2\ell+1)(2\ell-3)}} \qquad \text{(A7.12)}$$

Case II) $m' = m + 2$

Expand the integrand with the following recursion relations

$$(2\ell+1)\sin\theta \, P_\ell^m = P_{\ell+1}^{m+1} - P_{\ell-1}^{m+1} \qquad \text{(A7.7a)}$$

$$(2\ell'+1)\sin\theta \, P_{\ell'}^{m+2} = (\ell'+m+2)(\ell'+m+1)P_{\ell'-1}^{m+1} - (\ell'-m-1)(\ell'-m)P_{\ell'+1}^{m+1} \qquad \text{(A7.8a)}$$

Then if $\ell' = \ell$

$$I(0,2) = -\frac{1}{4}\frac{C_{\ell m}C_{\ell,m+2}}{(2\ell+1)^2}\left[\int_0^\pi (\ell-m-1)(\ell-m)(P_{\ell+1}^{m+1})^2 \sin\theta\, d\theta + \int_0^\pi (\ell+m+2)(\ell+m+1)(P_{\ell-1}^{m+1})^2 \sin\theta\, d\theta\right]$$

$$= -\frac{1}{4(2\ell+1)}\sqrt{\frac{(\ell-m)!(\ell-m-2)!}{2(\ell+m)!2(\ell+m+2)!}}\left[(\ell-m-1)(\ell-m)\frac{2(\ell+m+2)!}{(2\ell+3)(\ell-m)!} + (\ell+m+2)(\ell+m+1)\frac{2(\ell+m)!}{(2\ell-1)(\ell-m-2)!}\right]$$

$$= -\frac{1}{4(2\ell+1)}\left(\frac{1}{2\ell+3}+\frac{1}{2\ell-1}\right)\sqrt{(\ell+m+1)(\ell+m+2)(\ell-m)(\ell-m-1)} \qquad \text{(A7.13)}$$

If $\ell' = \ell + 2$

$$I(2,2) = \frac{1}{4}\frac{C_{\ell m}C_{\ell+2,m+2}}{(2\ell+1)(2\ell+5)}\int_0^\pi (\ell+m+4)(\ell+m+3)(P_{\ell+1}^{m+1})^2 \sin\theta\, d\theta$$

$$= \frac{1}{4}\sqrt{\frac{(\ell-m)!(\ell-m)!}{2(2\ell+1)(\ell+m)!2(2\ell+5)(\ell+m+4)!}}(\ell+m+4)(\ell+m+3)\frac{2(\ell+m+2)!}{(2\ell+3)(\ell-m)!}$$

$$= \frac{1}{4(2\ell+3)}\sqrt{\frac{(\ell+m+4)(\ell+m+3)(\ell+m+2)(\ell+m+1)}{(2\ell+1)(2\ell+5)}} \qquad \text{(A7.14)}$$

and if $\ell' = \ell - 2$

$$I(-2,2) = \frac{1}{4}\frac{C_{\ell m}C_{\ell-2,m+2}}{(2\ell+1)(2\ell-3)}\int_0^\pi (\ell-m-3)(\ell-m-2)(P_{\ell-1}^{m+1})^2 \sin\theta\, d\theta$$

$$= \frac{1}{4}\sqrt{\frac{(\ell-m)!(\ell-m-4)!}{2(2\ell+1)(\ell+m)!2(2\ell-3)(\ell+m)!}}(\ell-m-3)(\ell-m-2)\frac{2(\ell+m)!}{(2\ell-1)(\ell-m-2)!}$$

$$= \frac{1}{4(2\ell-1)}\sqrt{\frac{(\ell-m)(\ell-m-1)(\ell-m-2)(\ell-m-3)}{(2\ell+1)(2\ell-3)}} \qquad \text{(A7.15)}$$

Case II) $m' = m - 2$

Now expand the integrand with the following recursion relations

$$(2\ell + 1)\sin\theta\, P_\ell^m = (\ell + m)(\ell + m - 1)P_{\ell-1}^{m-1} - (\ell - m + 1)(\ell - m + 2)P_{\ell+1}^{m-1} \qquad \text{(A7.7b)}$$

$$(2\ell' + 1)\sin\theta\, P_{\ell'}^{m-2} = P_{\ell'+1}^{m-1} - P_{\ell'-1}^{m-1} \qquad \text{(A7.8b)}$$

Then following the same procedures as above, when $\ell' = \ell$

$$I(0,-2) = -\frac{1}{4(2\ell + 1)}\left(\frac{1}{2\ell + 3} + \frac{1}{2\ell - 1}\right)\sqrt{(\ell - m + 2)(\ell - m + 1)(\ell + m)(\ell + m - 1)} \qquad \text{(A7.16)}$$

when $\ell' = \ell + 2$

$$I(2,-2) = \frac{1}{4(2\ell + 3)}\sqrt{\frac{(\ell - m + 4)(\ell - m + 3)(\ell - m + 2)(\ell - m + 1)}{(2\ell + 1)(2\ell + 5)}} \qquad \text{(A7.17)}$$

and when $\ell' = \ell - 2$

$$I(-2,-2) = \frac{1}{4(2\ell - 1)}\sqrt{\frac{(\ell + m - 3)(\ell + m - 2)(\ell + m - 1)(\ell + m)}{(2\ell + 1)(2\ell - 3)}} \qquad \text{(A7.18)}$$

A somewhat more symmetrical formalism is evident if we define $\bar{\ell} = (\ell + \ell')/2$ and $\bar{m} = (m + m')/2$, that is the values of ℓ and m averaged over initial and final states. Then for $\ell' = \ell$

$$I(0,0) = \frac{1}{2(2\ell + 1)}\left[\frac{(\ell + m + 2)(\ell + m + 1)}{2\ell + 3} + \frac{(\ell - m)(\ell - m - 1)}{2\ell - 1}\right] \qquad \text{(A7.19)}$$

$$I(0,2) = I(0,-2) = -\frac{1}{4(2\ell + 1)}\left(\frac{1}{2\ell + 3} + \frac{1}{2\ell - 1}\right)\sqrt{(\ell + \bar{m})(\ell + \bar{m} + 1)(\ell - \bar{m})(\ell - \bar{m} + 1)} \qquad \text{(A7.20)}$$

Such transitions are of course elastic and contribute to elastic scattering, along with the contribution provided by the first term in the interaction potential. The inelastic scattering matrix elements are those for $\ell' = \ell \pm 2$

$$I(2,0) = I(-2,0) = \frac{1}{2(2\bar{\ell} + 1)}\sqrt{\frac{(\bar{\ell} + m)(\bar{\ell} + m + 1)(\bar{\ell} - m)(\bar{\ell} - m + 1)}{(2\bar{\ell} - 1)(2\bar{\ell} + 3)}} \qquad \text{(A7.21)}$$

$$I(2,2) = I(-2,-2) = \frac{1}{4(2\bar{\ell} + 1)}\sqrt{\frac{(\bar{\ell} + \bar{m} + 2)(\bar{\ell} + \bar{m} + 1)(\bar{\ell} + \bar{m})(\bar{\ell} + \bar{m} - 1)}{(2\bar{\ell} - 1)(2\bar{\ell} + 3)}} \qquad \text{(A7.22)}$$

$$I(2,-2) = I(-2,2) = \frac{1}{4(2\bar{\ell} + 1)}\sqrt{\frac{(\bar{\ell} - \bar{m} + 2)(\bar{\ell} - \bar{m} + 1)(\bar{\ell} - \bar{m})(\bar{\ell} - \bar{m} - 1)}{(2\bar{\ell} - 1)(2\bar{\ell} + 3)}} \qquad \text{(A7.23)}$$

REFERENCES

1. Takayanagi, K.: Vibrational and Rotational Transitions in Molecular Collisions. Prog. Theo. Phys. Suppl., vol. 25, 1963, pp. 1-98.

2. Takayanagi, K.: Adv. Atom. Mol. Phys., vol. 1, 1965, p. 149.

3. Curtiss, C. F.; and Bernstein, R. B.: Molecular Collisions. IX. Restricted Distorted-Wave Approximation for Rotational Excitation and Scattering of Diatomic Molecules. J. Chem. Phys., vol. 50, Feb. 1969, pp. 1168-1176.

4. Takayanagi, K.: Rotational Relaxation of HD. Institute of Space and Aeronautical Science, U. of Tokyo, Report 467, July 1971.

5. Prangsma, G. J.; Heemskerk, J. P. J.; Knaap, H. F. P.; and Beenakker, J. J. M.: Rotational Relaxation of HD below 40K. Physica, vol. 50, Dec. 7, 1970, pp. 433-443.

6. Itikawa, Y.; and Takayanagi, K.: Rotational Transitions in the HD Molecule in Low Energy HD-He Collisions. J. Phys. Soc., Japan, vol. 32, June 1972, pp. 1605-1611.

7. Stallcop, J. R.: Inelastic Scattering in Atom-Molecule Collisions. I. Rotational Transitions in the Sudden Approximation. J. Chem. Phys., vol. 61, Dec. 15, 1974, pp. 5085-5097.

8. Stallcop, J. R.: Orientational Invariance of the Rotational Transition Probability in the Sudden Approximation. Chem. Phys., vol. 5, Sept. 1974, pp. 456-463.

9. Wigner, E.: Gruppentheorie und ihre Anwendung auf die Quantenmechanik der Atomspektren. Vieweg, Brunswick, 1931. (A reference on p. 332, Landau and Lifshitz, Quantum Mechanics Nonrelativistic Theory, vol. 3 of Course on Theoretical Physics, Pergamon Press, London, 1958.)

10. Landau, L. D.; and Lifshitz, E. M.: Quantum Mechanics, Nonrelativistic Theory. Pergamon Press and Addison-Wesley Publishing Co., 1958.

11. Edmonds, A. R.: Angular Momentum in Quantum Mechanics. Princeton U. Press, Princeton, N.J., 1957.

CHAPTER VIII TRANSITIONS AT POTENTIAL SURFACE CROSSINGS

8.1 SUMMARY

The interaction between close-lying eigenstates is analyzed to show the form of potential curves that occur in a region of "potential crossing." Potentials of like symmetry are found to avoid crossing; potentials of different symmetry may very nearly cross. The Landau-Zener-Steuckelberg method of evaluating the probability of transition from one potential surface to the other is derived as a function of the collision velocity. In spite of severe limitations in the assumptions of the Landau-Zener method that would seem to invalidate it for most conditions of interest, the method is found to give reasonably good results that agree with experiment, at least for simple charge exchange type reactions. This is partly due to the fact that inaccuracies in the transition probability are somewhat mitigated, in performing the integrations to obtain collision cross section and the rate coefficient. The theoretical cross sections do, however, fall off as $E^{-1/2}$ rather than as E^{-1}, as generally observed in high-collision energy experiments.

8.2 INTRODUCTION

In the previous two chapters, the excitation of rotations and vibrations has been considered without invoking the concept of a potential crossing at which the transition occurs. This was possible because analytic expressions for the rotational and vibrational wave functions were known with good accuracy, and the electronic wave functions were assumed to be undisturbed in the collisions leading to these transitions. However, when electronic excitation, atom exchange, or ionization reactions are considered, the electronic wave functions are changed. If these functions were known in detail, we could proceed to solve perturbation transition problems in a manner similar to the rotational and vibrational excitation problems; that is, the perturbation function would be used to evaluate the transition matrix elements involved in solutions to a closed-coupled set of differential equations. Electronic wave functions are actually being evaluated with fairly good accuracy with large digital computers at the present time, at least for diatomic molecules, and eventually reaction rate problems may be solved in this way using the computer. However, for most engineering needs the electronic wave functions of multielectron systems are not available at present; even when they become available, they involve so many coordinate variables that evaluation of the matrix elements will be exceedingly time consuming. For present purposes then, we are interested in developing some analytic approximations that are useful guides to the functional relationships involved and that may be useful later in developing reasonably economical computer solutions to the problem.

Since the electronic wave functions of multielectron systems are not generally available, the interaction potentials between such systems are not calculable from fundamental principles either. However, many of the attractive potential curves are known with good accuracy from spectroscopic data, a few points on repulsive potentials are also available from spectroscopic data, and some average potential interactions are available from scattering measurements and from measurements of transport properties of gases such as viscosity, thermal conductivity, mass diffusion, or electrical conductivity. For present purposes we will assume that the interaction potential functions are known and proceed with solutions from this premise, but it should be

recognized that in actual engineering practice the results are of limited application because precise interaction potentials are not generally available.

8.3 POTENTIAL SURFACE CROSSING

Frequently two potential surfaces come very close to one another or even appear to cross one another, depending on the symmetries of the electronic wave functions involved. This situation is illustrated in figure 8.1, where the potentials of two colliding particles in the ground state, A + B, and in an excited electronic state, A + B*, are shown. Theoretically the potentials can cross one another only where they apply to different symmetry states; if they are for the same symmetry, a coupling interaction occurs which splits the potentials apart as diagrammed in figure 8.2.

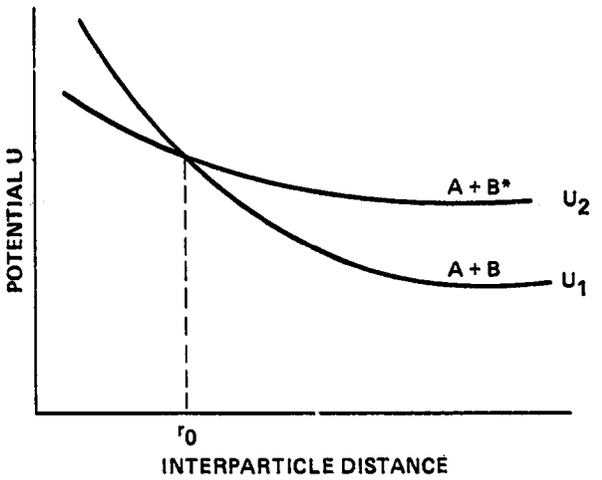

Figure 8.1- Crossing between potential surfaces as a function of interparticle distance neglecting coupling interaction.

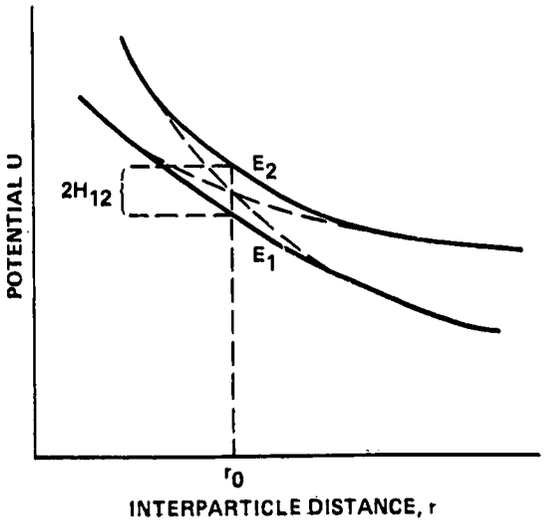

Figure 8.2- Potential surfaces in the region of strong coupling interaction.

Before considering the motion of the colliding particles along the two potential surfaces, we need to consider the effect of coupling between the two electronic states at some fixed distance r. If the motion of the two nuclear particles is relatively slow, the electronic states will have time to relax to their steady state values at each position. This model of the collision process is known as the Born-Oppenheimer approximation. It is generally a good approximation for the collision between two heavy molecules at the kinetic velocities that obtain near threshold of most reactions. It is often not a good approximation for electron impact processes; for this case a sudden approximation will generally give better results. The concept of a potential surface loses its validity anyway when the Born-Oppenheimer approximation breaks down, for the potential represents the combined nuclear repulsions and electronic interaction energy for the collision pair.

The solutions for transition are needed primarily in the region of the crossing point, where it will often be sufficient to use a two-level approximation and neglect all other excited electronic states. Let the Hamiltonian operator be expressed as the sum

$$\tilde{H} = \tilde{H}_o + \tilde{H}' \qquad (8.1)$$

where H_o contains the dominant terms that determine the electronic eigenfunction away from the crossing point, and H' represents the effect of the interaction between states that becomes sizable only in the region near the crossing point r_o. We will not look for the form of this coupling perturbation in detail, but presumably it represents effects such as magnetic quadrupole interactions, or angular momentum coupling, or other higher order terms in the exact Hamiltonian that can be neglected with good approximation whenever the eigenvalues for the two states are far apart. Let ϕ_1 and ϕ_2 be orthonormal eigenfunctions of the operator H_o that represent good approximations to the true wavefunctions away from the crossing point

$$\tilde{H}_o\phi_1 = \varepsilon_1\phi_1 \tag{8.2a}$$

$$\tilde{H}_o\phi_2 = \varepsilon_2\phi_2 \tag{8.2b}$$

The potential energies U_1 and U_2 represent the total electronic energy; these may be obtained approximately by operating on ϕ_1 and ϕ_2 with the exact Hamiltonian, then multiplying by ϕ_1^* and ϕ_2^*, respectively, and finally averaging over all space

$$U_1 = \left\langle \phi_1^*\tilde{H}\phi_1 \right\rangle = \left\langle \phi_1^*\tilde{H}_o\phi_1 \right\rangle + \left\langle \phi_1^*\tilde{H}'\phi_1 \right\rangle = \varepsilon_1 + H_{11} \tag{8.3a}$$

$$U_2 = \left\langle \phi_2^*\tilde{H}\phi_2 \right\rangle = \left\langle \phi_2^*\tilde{H}_o\phi_2 \right\rangle + \left\langle \phi_2^*H'\phi_2 \right\rangle = \varepsilon_2 + H_{22} \tag{8.3b}$$

where H_{ij} are defined as the perturbation matrix elements

$$H_{ij} = \left\langle \phi_i^*\tilde{H}'\phi_j \right\rangle \tag{8.4}$$

Now in the region of the crossing point let the wave function be a linear combination of ϕ_1 and ϕ_2

$$\psi = a_1\phi_1 + a_2\phi_2 \tag{8.5}$$

Substituting this wave function in the exact steady state Schroedinger equation yields

$$(\tilde{H}_o + \tilde{H}')\psi = E(a_1\phi_1 + a_2\phi_2) = a_1\varepsilon_1\phi_1 + a_2\varepsilon_2\phi_2 + a_1\tilde{H}'\phi_1 + a_2\tilde{H}'\phi_2 \tag{8.6}$$

Multiply Eq. (8.6) first by ϕ_1^* and average over all space, and again by ϕ_2^* and average overall space, to get a set of two simultaneous equations to solve for the constants a_1 and a_2

$$(\varepsilon_1 - E)a_1 + a_1H_{11} + a_2H_{12} = 0 \tag{8.7a}$$

$$(\varepsilon_2 - E)a_2 + a_1H_{21} + a_2H_{22} = 0 \tag{8.7b}$$

with the perturbation matrix elements H_{ij} again defined by Eq. (8.4). The allowed energy levels E can be obtained without actually solving for the constants a_1 and a_2, since the set of Eqs. (8.7a) and (8.7b) have solutions if and only if the matrix equation

$$\begin{vmatrix} \varepsilon_1 + H_{11} - E & H_{12} \\ H_{21} & \varepsilon_2 + H_{22} - E \end{vmatrix} = 0 \tag{8.8}$$

is satisfied. The two roots of this determinant are

$$E = \frac{1}{2}\left[(\varepsilon_1 + H_{11}) + (\varepsilon_2 + H_{22})\right] \pm \frac{1}{2}\sqrt{\left[(\varepsilon_1 + H_{11}) - (\varepsilon_2 + H_{22})\right]^2 + 4H_{12}H_{21}} \tag{8.9}$$

the operator H is Hermitian so H_{12} equals H_{21} and Eq. (8.9) may be expressed

$$E = \frac{1}{2}(U_1 + U_2) \pm \frac{1}{2}\sqrt{(U_1 - U_2)^2 + 4H_{12}^2} \tag{8.10}$$

Far from the crossing point H_{12} is small compared with $|U_1 - U_2|$ and the solution reduces to

$$E \xrightarrow[r \neq r_o]{} \frac{1}{2}(U_1 + U_2) \pm \frac{1}{2}(U_1 - U_2) = U_1 \text{ or } U_2 \tag{8.11a}$$

In the neighborhood of r_o, $U_1 \simeq U_2$ and the solution reduces to

$$E \xrightarrow[r \simeq r_o]{} \frac{1}{2}(U_1 + U_2) \pm H_{12} \tag{8.11b}$$

Thus, the potentials are split apart by the coupling effect and do not cross one another, as shown in figure 8.2, and the perturbation matrix element H_{12} represents one-half the energy of separation at the point of closest approach. The potential surfaces are prevented from crossing one another by the coupling perturbation, but the strongest transitions will occur at the distance where the closest eigenvalues and the strongest coupling occur. Of course, if the symmetry of the two wave functions ϕ_1 and ϕ_2 is different in a way not affected by the perturbation H', then the perturbation matrix elements H_{12} vanish and the potentials U_1 and U_2 are allowed to cross one another.

Experimentally, spectroscopists observe that strongest coupling occurs when the two electronic wave functions have the same symmetry type, and that negligible coupling occurs when the wave functions have different symmetry. This gives rise to the so-called noncrossing rule, namely: potential surfaces for molecular wave functions having the same symmetry do not cross. In reality there is no doubt always some coupling produced by small higher-order terms in the Hamiltonian which are normally negligible, but when the symmetry types are different the perturbation matrix element H_{12} is so small that for all practical purposes the potential surfaces may be treated as though they actually cross. On the other hand when the electronic wave functions have the same symmetry, the matrix elements H_{12} can become quite large and the spectroscopist often deduces potentials with rather irregular shapes as a result.

The spectroscopist only observes effects of potential surface crossing when at least one of the surfaces represents a bound state and therefore gives rise to an observable vibration-rotation spectrum. If the two potentials represent different electronic symmetry types, the effect is as shown in figure 8.3(a): the vibrational energy levels may be broadened in the region near the crossing, even to the point of

being unrecognizable in a relatively weak spectrum, but above and below the crossing the vibrational levels will be relatively sharp and occur at the normal levels for an harmonic oscillator with appropriate corrections for anharmonic potential shape. As we shall find later, the nuclear motions for the upper vibrational states proceed as though the potential surface is unbroken, whenever H_{12} is exceedingly small. When the coupling interaction is large, as shown for potentials of the same symmetry type in figure 8.3(b), the spectrum is quite different. As long as the internuclear motions are not too high velocity, the electronic eigenfunctions adjust adiabatically to stay on their initial potential surface. The vibrational levels of the lower surface will be truncated near the maximum produced in this surface; the upper levels of this truncated set may be somewhat broadened as a result of tunneling through the barrier. The upper surface typically results in a tightly bound state with a narrow, steep potential that gives rise to a widely spaced vibration levels. Occasionally crossing between two bound state potentials are observed; these may give rise to some rather strange looking potential surfaces (refs. 1 and 2).

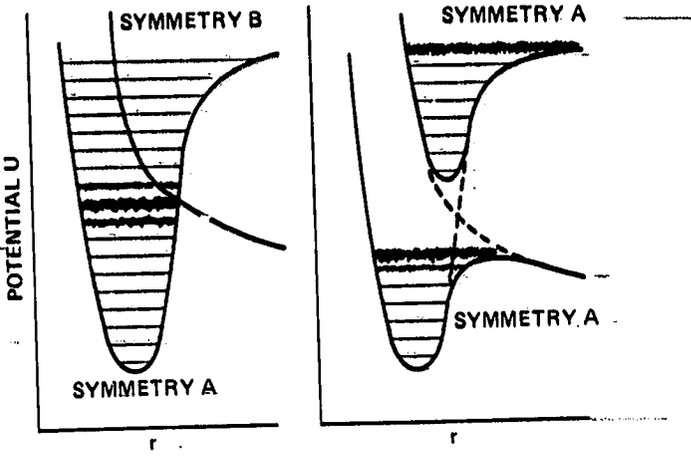

a) DIFFERENT SYMMETRY TYPES b) SAME SYMMETRY TYPES

Figure 8.3- Typical effects of potential surface crossing on observed vibrational energy levels.

As an example of the case shown in figure 8.3(a), the CℓO molecule, which is an important species in upper atmosphere reactions is found to have very diffuse vibrational levels around the 7th and 8th levels of the $A^2\pi$ state of the molecule; this is observed by the spectroscopist looking at the $A^2\pi \rightarrow X^2\pi$ band system of CℓO. Presumably a repulsive potential crosses near these levels; although the symmetry of the repulsive potential is not known, it is presumably different than the $^2\pi$ state, since the vibrational levels above the 8th are observed with relative sharp eigenvalues again, so the crossing perturbation must be modest. An example of the stronger perturbation between like symmetries is given by the $B^1\Sigma^+(\sigma \rightarrow 3A)$ and $^1\Sigma(\pi - \pi^*)$ states of CO. Application of the rule that potentials of like symmetry do not cross led spectroscopist A. G. Gaydon (ref. 2) to predict the correct values for dissociation energy of both CO and N_2 long before more direct experimental evidence was available, while most other spectroscopists favored lower values that seemed consistent with extrapolation of vibrational level spacing to a lower limit. Thus, the noncrossing rule is now well established as a practical and useful guide to the interpretation of spectra.

8.4 TIME-DEPENDENT SOLUTIONS

When the nuclear centers are moving, the wave functions ϕ_1 and ϕ_2 are functions of both the electronic coordinates q and the internuclear distance r. The latter is time-dependent, so we now need to solve the time-dependent Schroedinger equation

$$i\hbar \frac{\partial \psi}{\partial t} = \tilde{H}\psi \qquad (8.12)$$

The wave function ψ is assumed to be the two-state approximation

$$\psi = a_1(t)\phi_1(r,q)\exp\left(-\frac{1}{\hbar}\int_{-\infty}^{t} H_{11}dt\right) + a_2(t)\phi_2(r,q)\exp\left(-\frac{i}{\hbar}\int_{-\infty}^{t} H_{22}dt\right) \tag{8.13}$$

The coefficients a_1 and a_2 that were constant in the last section are now functions of time, as are the wave functions ϕ_1 and ϕ_2 and the perturbation matrix elements H_{11}, H_{12}, and H_{22}.

Substituting Eq. (8.13) in (8.12), one obtains

$$\exp\left(-\frac{i}{\hbar}\int_{-\infty}^{t} H_{11}dt\right)\left(i\hbar\dot{a}_1 + a_1H_{11} + i\hbar a\frac{d}{dt}\right)\phi_1$$

$$+ \exp\left(-\frac{i}{\hbar}\int_{-\infty}^{t} H_{22}dt\right)\left(i\hbar\dot{a}_2 + a_2H_{22} + i\hbar a_2\frac{d}{dt}\right)\phi_2$$

$$= \exp\left(-\frac{i}{\hbar}\int_{-\infty}^{t} H_{11}dt\right)a_1\tilde{H}\phi_1 + \exp\left(-\frac{i}{\hbar}\int_{-\infty}^{t} H_{22}dt\right)a_2\tilde{H}\phi_2 \tag{8.14}$$

Now multiply first by $\phi_1^* = \exp[(i/\hbar)\int_{\infty}^{t} H_{11}dt]$ and average over all space, then by $\phi_2^* = \exp[(i/\hbar)\int_{\infty}^{t} H_{22}dt]$ and average over all space, to obtain the coupled equations

$$\dot{a}_1 = -\left\langle\phi_1^*\frac{d}{dt}\phi_1\right\rangle a_1 - \left\langle\phi_1^*\frac{d}{dt}\phi_2\right\rangle a_2\, e^{-i\Delta} - \frac{i}{\hbar}H_{12}a_2\, e^{-i\Delta} \tag{8.15a}$$

$$\dot{a}_2 = -\left\langle\phi_2^*\frac{d}{dt}\phi_2\right\rangle a_2 - \left\langle\phi_2^*\frac{d}{dt}\phi_1\right\rangle a_1\, e^{-i\Delta} - \frac{i}{\hbar}H_{12}a_1\, e^{i\Delta} \tag{8.15b}$$

$$\Delta = \frac{1}{\hbar}\int_{-\infty}^{t}(H_{22} - H_{11})dt \tag{8.16}$$

The matrix elements now represent the average of the total Hamiltonian operator

$$H_{ij} = \left\langle\phi_i^*\tilde{H}\phi_j\right\rangle \tag{8.17}$$

rather than the averages of the perturbation $\tilde{H}'$ as in Eq. (8.4). The elements H_{12} are, however, the same as before

$$H_{12} = \left\langle\phi_2^*\tilde{H}_o\phi_1\right\rangle + \left\langle\phi_2^*\tilde{H}'\phi_1\right\rangle = \left\langle\phi_2^*\tilde{H}'\phi_1\right\rangle = \left\langle\phi_1^*\tilde{H}'\phi_2\right\rangle \tag{8.18}$$

while the elements H_{11} and H_{22} are just the unperturbed U_1 and U_2 respectively,

$$H_{11} = U_1 \tag{8.19a}$$

$$H_{22} = U_2 \tag{8.19b}$$

at least to the level of the Born-Oppenheimer approximation.

Note that Eqs. (8.15a) and (8.15b) indicate that motion of the nuclei can produce electronic transitions even if H_{12} vanishes. For example, in the straight line

trajectory shown in figure 8.4, an approximation that becomes valid in the limit of very small interaction,

$$z = ut \qquad \frac{d}{dt} = u\left(\frac{\partial}{\partial r} + \frac{1}{r}\frac{\partial}{\partial \theta}\right)$$

$$\left\langle \phi_i^* \frac{d}{dt} \phi_j \right\rangle = u\left(\left\langle \phi_i^* \frac{\partial}{\partial r} \phi_j \right\rangle + \left\langle \phi_i^* \frac{1}{r}\frac{\partial}{\partial \theta} \phi_j \right\rangle\right) \tag{8.20}$$

where the z axis has been defined to be parallel with the relative velocity vector $\vec{u}$. Transitions among states of the same symmetry (e.g., $\Sigma \to \Sigma$, $\pi \to \pi$, etc., in the case of two atom or diatomic molecule collisions) are promoted by the first term on the right side of Eq. (8.20); transitions among states of different symmetry (e.g., $\Sigma \to \pi$, $\pi \to \Delta$, etc.) are promoted by the second term.

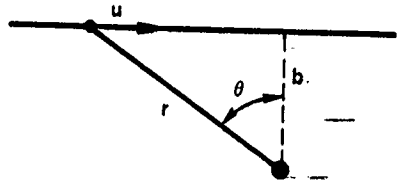

Figure 8.4- Straight line collision trajectory coordinates.

8.5 LANDAU-ZENER TRANSITION PROBABILITY

The basic quantum treatment of transition probability at a potential crossing, or near crossing, was worked out as far back as 1932 by Landau (ref. 3), Zener (ref. 4), and Stueckelberg (ref. 5). Reviews of the method have been given by Eyring, Walter, and Kimball (ref. 6) and by Geltman (ref. 7), among others. The method has not been widely applied to calculation of specific reaction rates because it depends on knowledge of the potential shapes (H_{11} and H_{22}) and the perturbation separation between potentials, H_{12}, at the crossing point. Normally these quantities have been unavailable, particularly in the case of repulsive potentials which are of higher degeneracy and therefore of greatest influence in collision problems. Most of our reliable information on specific potentials is presently limited to the lower-degeneracy, attractive-potential situations where the spectroscopist can observe a rotational-vibrational spectrum and deduce the potential turning points at each observed eigenvalue of energy using the Rydberg-Klein-Reese method. (See chapter V of ref. 8 for a review of this method of determining potentials.) In spite of this limitation on the practical applications of the Landau-Zener transition probability, the derivation will be worthwhile to follow because it gives a good insight into the physical processes that occur during reaction; moreover, accurate potentials, including the repulsive states, are now being computed by numerical solutions of Schroedinger's equation using large expansions of the wave functions into basis sets such as Slater type electronic orbitals or Gaussian orbitals (refs. 9 and 10). The one quantity that will be difficult to assess accurately even with high speed computers is the perturbation interaction H_{12}; however, in time this quantity will probably also become known for specific cases of interest. For these reasons then it should be profitable to follow the Landau-Zener derivation in some detail.

The Landau-Zener method assumes that the nuclear motion terms are small compared with the coupling interaction terms, in which case the coupled set of differential Eq. (8.15) reduce to

$$\dot{a}_1 = -\frac{i}{\hbar} a_2 H_{12} e^{-i\Delta} \tag{8.21a}$$

$$\dot{a}_2 = -\frac{i}{\hbar} a_1 H_{12} e^{i\Delta} \qquad (8.21b)$$

Differentiate (8.21b) to obtain

$$\ddot{a}_2 = -\frac{i}{\hbar}\left[H_{12}\dot{a}_1 + \dot{H}_{12}a_1 + \frac{i}{\hbar} H_{12}(H_{22} - H_{11})a_1\right] e^{i\Delta} \qquad (8.22)$$

and eliminate $\dot{a}_1$ and a_1 with the help of Eqs. (8.21a) and (8.21b)

$$\ddot{a}_2 = -\left[\frac{\dot{H}_{12}}{H_{12}} + \frac{i}{\hbar}(H_{22} - H_{11})\right]\dot{a}_2 + \frac{H_{12}^2}{\hbar^2} a_2 = 0 \qquad (8.23)$$

Now assume that the major contribution to the transition probability takes place in a very small region near the crossing point so that the difference $H_{22} - H_{11}$ is a linear function of r and therefore of t

$$H_{22} - H_{11} \simeq \alpha\hbar t + \ldots$$

$$\alpha = \frac{1}{\hbar}\frac{d}{dt}(H_{22} - H_{11}) \qquad (8.24)$$

where t is taken to be zero at the crossing point. Also the difference $2H_{12}$ between the adiabatic potentials E_2 and E_1 (fig. 8.2) is assumed approximately constant

$$H_{12} \simeq \beta\hbar\,, \quad \dot{H}_{12} \simeq 0 \qquad (8.25)$$

Then the differential Eq. (8.23) becomes

$$\ddot{a}_2 - i\alpha t\dot{a}_2 + \beta^2 a_2 = 0 \qquad (8.26)$$

Equation (8.26) is transformed by replacing the independent variable t with the complex variable z

$$z = \alpha^{1/2} e^{i\pi/4} t = \alpha^{1/2}\left(\frac{1}{\sqrt{2}} + \frac{i}{\sqrt{2}}\right) t \qquad (8.27)$$

and the dependent variable a with the dependent variable b

$$b = a\, e^{-z^2/4} \qquad (8.28)$$

With these transformations one obtains

$$\dot{a} = \alpha^{1/2} e^{i\pi/4}\left(\frac{db}{dz} + \frac{z}{2} b\right) e^{z^2/4} \qquad (8.29a)$$

$$-i\alpha t\dot{a} = -i\alpha z\left(\frac{db}{dz} + \frac{z}{2} b\right) e^{z^2/4} \qquad (8.29b)$$

$$\ddot{a} = i\alpha\left[\frac{d^2b}{dz^2} + z\frac{db}{dz} + \left(\frac{1}{2} + \frac{z^2}{4}\right)b\right] e^{z^2/4} \qquad (8.29c)$$

and the differential Eq. (8.26) becomes

$$\frac{d^2b}{dz^2} + \left(n + \frac{1}{2} - \frac{z^2}{4}\right) b = 0 \tag{8.30}$$

where the quantity n is the complex number

$$n = -\frac{i\beta^2}{\alpha} \tag{8.31}$$

For the moment we will assume that the transition occurs in the direction which makes α positive. Later we will return to consider negative α. Equation (8.30) is Weber's equation, and the solutions are the parabolic cylindrical functions $D_n(z)$, $D_{-n-1}(iz)$ defined in Whittaker and Watson (ref. 11). We shall only need be concerned with the asymptotic behavior of these functions since the transition probability will be obtained from the solution at $t = +\infty$, and the initial conditions will be related to the solution at $t = -\infty$, with $t = 0$ defined as the time the collision system reaches the potential crossing point. The leading term of the parabolic cylindrical functions in the expansion in inverse powers of z is given by Whittaker and Watson (ref. 11),

$$D_n(z) \xrightarrow[|z|\to\infty]{} z^n\, e^{-z^2/4} \quad , \quad -\frac{3\pi}{4} < \arg z < \frac{3\pi}{4} \tag{8.32a}$$

$$\longrightarrow z^n\, e^{-z^2/4} - \frac{\sqrt{2\pi}}{\Gamma(-n)}\, e^{i\pi n}\, z^{-n-1}\, e^{z^2/4} \quad , \quad \frac{\pi}{4} < \arg z < \frac{5\pi}{4} \tag{8.32b}$$

$$\longrightarrow z^n\, e^{-z^2/4} - \frac{\sqrt{2\pi}}{\Gamma(-n)}\, e^{-i\pi n}\, z^{-n-1}\, e^{z^2/4} \quad , \quad -\frac{5\pi}{4} < \arg z < -\frac{\pi}{4} \tag{8.32c}$$

The arguments of the complex quantities z, iz, and z^2 are immediately observed from the following relations

$$\left.\begin{aligned} z = (\alpha^{1/2}\, e^{i\pi/4})t &= -|z|e^{i\pi/4} = |z|e^{-i3\pi/4} && t < 0 \\ &= |z|e^{i\pi/4} && t > 0 \\ iz = i|z|e^{-i3\pi/4} &= |z|e^{-i\pi/4} && t < 0 \\ = i|z|e^{i\pi/4} &= |z|e^{i3\pi/4} && t > 0 \\ z^2 = |z|^2\, e^{i\pi/2} &= i|z|^2 && \text{all } t \end{aligned}\right\} \tag{8.33}$$

Now the asymptotic value $D_n(z)$ is

$$D_n(z) \xrightarrow[t\to-\infty]{} (|z|e^{-i3\pi/4})^{-i\beta^2/\alpha}\, e^{-i|z|^2/4}$$

$$\longrightarrow e^{-z\pi\beta^2/4\alpha}|z|^{-i\beta^2/\alpha}\, e^{-i|z|^2/4} \tag{8.34}$$

thus, the absolute magnitude of $D_n(z)$ is in the limit $t = -\infty$

$$|D_n(z)| \xrightarrow[t\to-\infty]{} e^{-3\pi\beta^2/4\alpha} \tag{8.35}$$

Note that any real number (such as $|z|$) raised to the ith power has the magnitude of unity.

The general solution for the coefficient b in Eq. (8.30), a second order differential equation, may be expressed as a linear combination of any two independent parabolic cylindrical functions, such as $D_n(z)$ and $D_{-n-1}(iz)$, with coefficients determined to fit the boundary conditions. In the present derivation we will define the first coefficient b of interest to be the one having vanishing probability at $t = -\infty$; in this case the coefficient of $D_n(z)$ must vanish, since this function has a finite limit at $t = -\infty$ as given by Eq. (8.35). However, the function $D_{-n-1}(iz)$ is observed to vanish at $t = -\infty$

$$\begin{aligned} D_{-n-1}(iz) &\xrightarrow[t\to-\infty]{} (iz)^{-(n+1)} e^{z^2/4} \\ &\longrightarrow (|z|e^{-i\pi/4})^{(i\beta^2/\alpha)-1}\ e^{i|z|^2/4} \\ &\longrightarrow \frac{e^{\pi\beta^2/4\alpha}}{|z|}\left[\frac{|z|^{i\beta^2/\alpha}\ e^{i|z|^2/4}}{e^{-i\pi/4}}\right] \end{aligned} \tag{8.36}$$

Thus, the absolute magnitude of $D_{-n-1}(iz)$ vanishes at $t = -\infty$

$$|D_{-n-1}(iz)| \xrightarrow[t=-\infty]{} \frac{e^{\pi\beta^2/4\alpha}}{|z|} = 0 \tag{8.37}$$

Define a_2 as the channel with zero initial probability, then a_2 can be expressed

$$a_2 = b_2\, e^{z^2/4} = AD_{-n-1}(iz)e^{z^2/4} \tag{8.38}$$

where A is a constant coefficient which will be determined by the boundary condition that $|a_1(t = -\infty)| = 1$.

From Eq. (8.21b)

$$a_1 = \frac{i\hbar\, e^{-i\Delta}}{H_{12}}\,\dot{a}_2 = \frac{i\, e^{-i\Delta}}{\beta}\,\frac{dz}{dt}\,\frac{da_2}{dz} \tag{8.39}$$

From Eqs. (8.38) and (8.27)

$$\frac{da_2}{dz} = \left(\frac{db_2}{dz} + \frac{z}{2}\,b_2\right) e^{z^2/4} \tag{8.40a}$$

$$\frac{dz}{dt} = \alpha^{1/2}\ e^{i\pi/4} \tag{8.40b}$$

Thus

$$a_1 = A\, e^{(i\pi/4)-i\Delta}\left(\frac{\alpha^{1/2}}{\beta}\right)\left[\frac{d}{d(iz)} D_{-n-1}(iz) - \frac{iz}{2} D_{-n-1}(iz)\right]e^{z^2/4} \tag{8.41}$$

The bracketed factor in Eq. (8.41) can be expressed in terms of $D_{-n}(iz)$ using a recursion relation proven by Whittaker and Watson (ref. 11)

$$\frac{d}{dz} D_n(z) + \frac{z}{2} D_n(z) - nD_{n-1}(z) = 0 \tag{8.42a}$$

which is equivalent to

$$\frac{d}{dz} D_n(z) - \frac{z}{2} D_n(z) = -D_{n+1}(z) \tag{8.42b}$$

$$\frac{d}{d(iz)} D_{-n-1}(iz) - \frac{iz}{2} D_{-n-1}(iz) = -D_{-n}(iz) \tag{8.42c}$$

Consequently, a_1 may be expressed

$$a_1 = \frac{\alpha^{1/2}}{\beta} AD_{-n}(iz)e^{z^2/4+(i\pi/4)-i\Delta} \tag{8.43}$$

The magnitude of this quantity must equal unity at $t = -\infty$

$$D_{-n}(iz) \xrightarrow[t=-\infty]{} (iz)^{-n}\, e^{z^2/4}$$

$$\longrightarrow (|z|e^{-i\pi/4})^{i\beta^2/\alpha}\, e^{i|z|^2/4}$$

$$\longrightarrow e^{\pi\beta^2/4\alpha}|z|^{i\beta^2/\alpha}\, e^{i|z|^2/4} \tag{8.44}$$

$$|D_{-n}(iz)| \longrightarrow e^{\pi\beta^2/4\alpha} \tag{8.45}$$

Thus

$$|A| = \frac{|\beta|}{\alpha^{1/2}}\, e^{-\pi\beta^2/4\alpha} \tag{8.46}$$

Now the probability of transition from potential surface U_1 to potential surface U_2 is given by

$$P = \lim_{t\to\infty} |a_2|^2 = A^2 \lim_{t\to\infty} |D_{-n-1}(iz)|^2$$

$$= \frac{\beta^2}{\alpha}\, e^{-\pi\beta^2/2\alpha} \lim_{t\to\infty} |D_{-n-1}(iz)|^2 \tag{8.47}$$

For $t > 0$, $(iz) = |z|e^{i3\pi/4}$, so the argument of iz is between $\pi/4$ and $5\pi/4$ in this limit. Consequently, the asymptotic form of $D_n(z)$ given by Eq. (8.32b) must be used.

$$D_{-n-1}(iz) = (iz)^{-(n+1)} e^{z^2/4} - \frac{\sqrt{2\pi}}{\Gamma(n+1)} e^{-(n+1)\pi i}(iz)^n e^{-z^2/4} \tag{8.48}$$

The first term on the right side of (8.48) vanishes at $t = \infty$ just as in Eq. (8.37), because of the factor $|z|^{-1}$ that is present. The $\Gamma(n+1)$ is evaluated from a relation (ref. 12) between $\Gamma(iy)$ and the sinh πy

$$|\Gamma(iy)|^2 = \frac{\pi}{y \sinh \pi y} \tag{8.49}$$

Thus

$$|\Gamma(n+1)|^2 = |n\Gamma(n)|^2 = \left(\frac{-i\beta}{\alpha}\right)^2 \frac{\pi}{\left(\frac{-\beta^2}{\alpha}\right) \sinh \pi \left(\frac{-\beta^2}{\alpha}\right)} = \frac{-\pi \left(\frac{\beta^2}{\alpha}\right)}{\sinh \pi \left(\frac{\beta^2}{\alpha}\right)} \tag{8.50}$$

$$|D_{-n-1}(iz)|^2 = \frac{2\pi \sinh \frac{\pi\beta^2}{\alpha}}{\pi\beta^2/\alpha} \left| e^{-i\pi-(\pi\beta^2/\alpha)} |z|^{-i\beta^2/\alpha} (e^{i3\pi/4})^{-i\beta^2/\alpha} e^{-i|z|^2/4} \right|^2$$

$$= \frac{2 \sinh \pi\beta^2/\alpha}{\beta^2/\alpha} |e^{-\pi\beta^2/4\alpha}|^2 \tag{8.51}$$

Finally, the probability of transition is

$$P = A^2 \lim |D_{-n-1}(iz)|^2$$

$$= \left(\frac{\beta^2}{\alpha}\right) e^{-\pi\beta^2/2\alpha} \left(\frac{\alpha}{\beta^2}\right) (e^{\pi\beta^2/\alpha} - e^{-\pi\beta^2/\alpha}) e^{-\pi\beta^2/2\alpha}$$

$$= 1 - e^{-2\pi\beta^2/\alpha} \tag{8.52a}$$

Recall that in the definition of the complex constant n, Eq. (8.31), α was taken to be positive by defining the collision event so that H_{22} was initially less than H_{11}

$$\alpha = \frac{1}{\hbar} \frac{d}{dt} (H_{22} - H_{11}) \tag{8.53}$$

However, where the inverse transition is considered, the differential is observed to be invariant under time reversal ($z \to -z$). Thus, one can conclude that transition probability is independent of the direction of traverse through the crossing point, and the time reversed case provides the solution where α is negative. Therefore, in general, the transition probability of Eq. (8.52a) is given by

$$P = 1 - e^{-2\pi\beta^2/|\alpha|} \tag{8.52b}$$

Equation (8.52b) is still only the probability of transition for one traverse of the potential crossing; in a collision event where $E > E^*$, the potential at the

C-3

crossing point, two traverses take place, one in the ingoing direction and the other in the reverse direction. By conservation of probability, the factor S

$$S = e^{-2\pi\beta^2/|\alpha|} \tag{8.52c}$$

represents the probability that transition does not occur in a single crossing. Thus the total probability of transition in a single collision event is

$$P_{1\to 2} = S(1 - S) + (1 - S)S = 2S(1 - S)$$

$$= 2\, e^{-2\pi\beta^2/|\alpha|}\left(1 - e^{-2\pi\beta^2/|\alpha|}\right) \tag{8.54}$$

This is the result known as the Landau-Zener-Stueckelberg transition probability.

8.6 LIMITATIONS OF LANDAU-ZENER METHOD

The Landau-Zener method has some rather severe limitations when the consequences of the assumptions involved are examined critically. This problem has been discussed by Bates (ref. 13) and more recently by Thorson, Pelos, and Boorstein (ref. 14), with the conclusion that the method is clearly not rigorous in most collisions of practical interest. Without going into great detail, the method fails at very low energy because the trajectory of the collisions has been treated semiclassically, and near threshold, where the velocity at the crossing point nearly vanishes, the wavelength of the collision partner's kinetic motion becomes long compared with the characteristic length of potential change — a situation where the classical trajectory obviously breaks down. Again at high-collision energies the effective width of the reaction zone Δ_r increases, as shown by Bates (ref. 13).

$$\Delta_r \simeq \frac{4\pi u_o \hbar}{\left|\frac{d}{dr}(H_{11} - H_{22})\right|} \tag{8.55}$$

Thus, at very high velocity u_o, the assumptions of constant H_{12} and linear $H_{11} - H_{22}$ are unwarranted. Moreover, the reaction zone may reach farther than the classical turning point of the trajectory, in which case taking the limit at $t = +\infty$ gives too large a transition probability. Finally, the 2-state model has limitations; in typical collisions there is a multiplicity of potential crossings with several excited state potentials close enough to demand an expansion of the wave functions into a linear combination of all nearby states, and with reaction zones that may overlap one another. Such a situation is shown schematically in figure 8.5, where the collision particles have incomplete multielectron outer shells that give rise to a wide range of possible spin and angular momentum combinations, many with multiple degeneracy. Interactions between multiple degenerate states will give rise to a multiplicity of close-lying levels near the crossing point; thus, reaction proceeds by a complex reaction path that may take many different routes through the maze of potential crossings. One consequence of this large multiplicity of crossing points is that one of them is bound to occur near the energy difference between the final state and initial state systems, shown as E^* in figure 8.5 for the transition from $A + B$ to $A + B^*$. Two such crossing points near the threshold of E^* are indicated in the figure by the circled intersections, but in actual practice even more might be operative. The figure shows 4 interaction potentials for the lower state, which is the

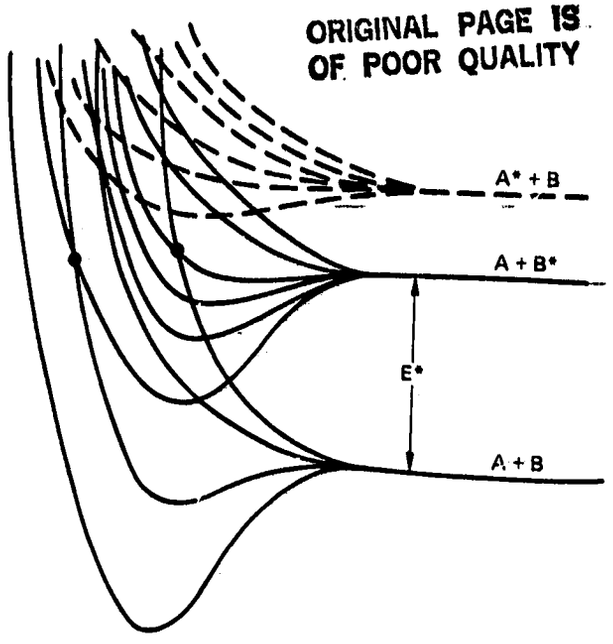

Figure 8.5- Schematic diagram of typical multiple interaction potential crossings that occur for multielectron collision particles that have large degeneracy.

case for two ground state nitrogen atoms, for example, having three unpaired p-electrons each in the outer shell which may add spins to give $^1\Sigma$, $^3\Sigma$, $^5\Sigma$, and $^7\Sigma$ states. The latter two are repulsive where most of the spins are additive and the Pauli exclusion principle operates to prevent these electrons from occupying the same quantum cell in phase space. The $^1\Sigma$ and $^3\Sigma$ states are attractive for the reason that the paired spin electrons can occupy the same cell in phase space, and these set up a resonance as they transfer from one nuclear center to the other during collision, leading to a lower total energy and therefore, a binding. However, other atoms in typical gases, such as O and C, have greater multiplicity yet, as do the excited state species where the spin pairing possibilities become still more numerous as additional cells in phase space are opened up to the electrons and leave unfilled quantum cells in the lower eigenstates. Thus, the final transition probability observed experimentally usually involves much more than a single potential crossing point, and the reader can readily appreciate the difficulty in making meaningful comparisons between experiment and calculations.

D. R. Bates (ref. 13) makes comparisons between Landau-Zener calculations and some qualitatively correct transition probabilities for charge exchange between collision partners like $H^- + Na^+$, $H^+ + Al^{++}$, $He + Be^{+++}$, etc., where the transition occurs between two s-states. The results are shown in figure 8.6. Bates concludes that the Landau-Zener probability is not highly accurate, since even in this favorable case of s-s transitions the probability peaks more closely to threshold than it should.

Hasted (ref. 15) summarizes quantum calculations of charge exchange process made prior to 1964 (refs. 16-18), and the experimental studies of curve crossing charge exchange processes that were conducted also before that time (refs. 19 and 20). Hasted concludes that the Landau-Zener formula is reasonably consistent with the data provided that $\log_{10} H_{12}$ is a smoothly varying function of $(r_c)^{-1}$. Figure 8.7 shows the empirical curve for H_{12} that provides agreement between the experiments and theory, and also the calculated values of H_{12} which existed. The calculated H_{12} are seen to scatter reasonably closely about the empirical curve.

More recently, Moseley, Olson, and Peterson (ref. 21) compared Landau-Zener results with a number of ion-ion mutual neutralization experiments. For simple atom-atom systems the reaction approximates a series of single potential crossings well removed from one another, and in this case the Landau-Zener method gives reasonably good results, as shown in table 8.1. However, Moseley et al. point out that the Landau-Zener model cannot predict the detailed structure that is observed in the $H^+ + H^-$ case, for example. In these comparisons, interaction matrix elements H_{12} were determined semi-empirically. The molecular ion reactions are more complicated due to the large multiplicity of crossings that occur in this case, somewhat as

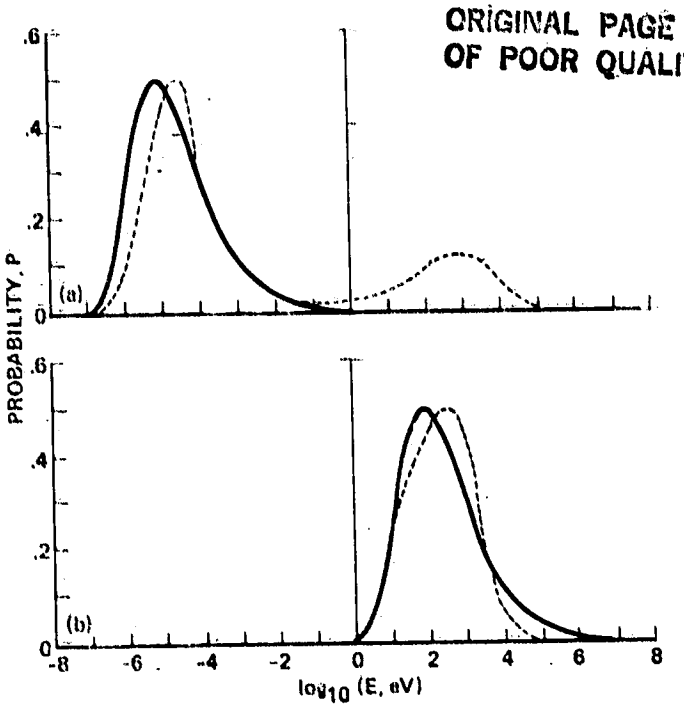

Figure 8.6- Probability P of charge transfer for s-s transitions; calculated from Landau-Zener formula; qualitative corrected result. In (a) Z_c is large and in (b) Z_c is moderate or small in sense described in text.

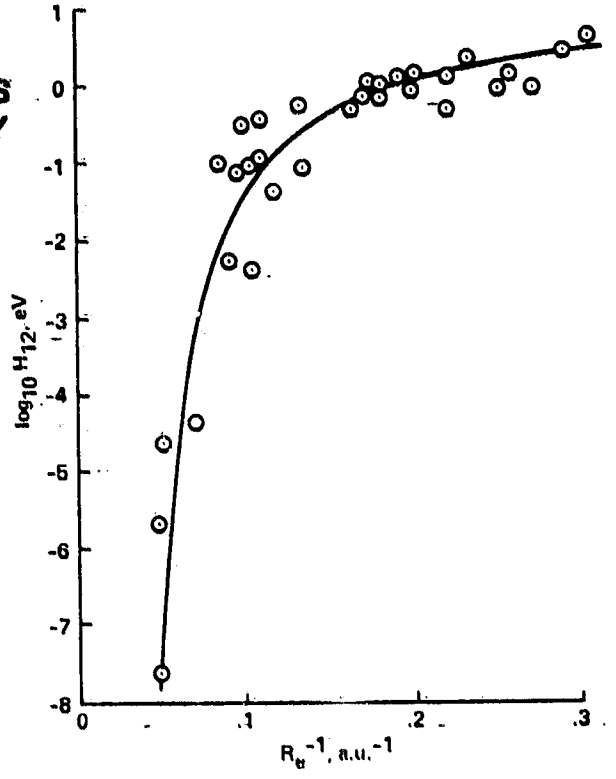

Figure 8.7- $H_{12}(R_c^{-1})$ function appropriate to the calculation of Landau-Zener transition probabilities.

suggested by figure 8.5. Olson (ref. 22) develops a so-called "absorbing-sphere-model," which is based on the Landau-Zener approximation, to account for this situation. Olson's method gives reasonably good results for molecular ion-molecular ion charge exchange reactions as shown in table 8.2. Here, "reasonably good" means an agreement within factors of about 3, that is, good from the viewpoint of engineering applications, though from a purely scientific viewpoint one could certainly desire more. In actual practice the inaccuracies in the transition probabilities will be considerably mitigated in the integrations performed to obtain the cross sections and rate coefficients, provided the probability has something like the correct shape near its maximum.

TABLE 8.1- REACTION RATE COEFFICIENTS AT 300 K — ATOMIC IONS, α(300 K) IN 10^{-7} CM^3/SEC

System	Experimental	Theoretical
$H^+ + H^-$	3.9 ± 2.1	1.5 4.0 1.2
$N^+ + O^-$	2.6 ± 0.8	1.8
$O^+ + O^-$	2.7 ± 1.3	1.1 .8
$Na^+ + O^-$	2.1 ± 1.0	.7
$He^+ + H^-$	---	5.7 7.3
$He^+ + D^-$	---	4.7 5.7

TABLE 8.2- REACTION RATE COEFFICIENTS AT 300 K — MOLECULAR IONS, α(300 K) IN 10^{-7} CM^3/SEC

System	Experimental	Theoretical
$H_2^+ + D^-$	4.7 ± 1.5	8.5 ± 2.1
$N_2^+ + O^-$	---	2.0 ± 0.6
$NO^+ + O^-$	4.9 ± 2.0	1.9 ± 0.6
$O_2^+ + O^-$	1.0 ± 0.4	1.9 ± 0.5
$N_2^+ + O_2^-$	1.6 ± 0.5	2.5 ± 0.8
$NO^+ + O_2^-$	5.8 ± 1.0	2.4 ± 0.8
$O_2^+ + O_2^-$	4.2 ± 1.3 1.0 ± 0.1	2.4 ± 0.8
$N_2^+ + NO_2^-$	1.3 ± 0.5	1.3 ± 0.3
$NO^+ + NO_2^-$	5.1 ± 1.5 2.1 ± 0.6 1.75 ± 0.6	1.2 ± 0.3
$O_2^+ + NO_2^-$	4.1 ± 1.3	1.2 ± 0.3
$NO^+ + NO_3^-$	8.1 ± 2.3 0.34 ± 0.12	1.1 ± 0.3
$O_2^+ + NO_3^-$	1.3 ± 0.4	1.0 ± 0.2

Thus, in spite of all the uncertainties in the Landau-Zener method it does provide some useful results. It approaches the correct limits at both very high and very low velocity in a qualitative way, and is expected to give the best quantitative results near its maximum. It will be instructive to carry forward the single crossing point transition probability to the calculation of cross section and rate coefficient to find the functional forms predicted for these quantities.

8.7 CROSS SECTIONS DERIVED FROM LANDAU-ZENER RESULTS

The quantity β in Eq. (8.54) is just a constant, while the quantity α may be expressed

$$\alpha = \frac{1}{\hbar} \left| \frac{dr}{dt} \frac{d}{dr} (H_{22} - H_{11}) \right|_{r_c} \tag{8.56}$$

The derivative (dr/dt) is obtained from the classical equation of motion

$$\left(\frac{dr}{dt}\right)_{r_c} = u \sqrt{1 - \frac{b^2}{r_c^2} - \frac{V(r_c)}{E}} \tag{8.57}$$

where r_c is, of course, the crossing point internuclear distance and $V(r_c)$ is the interaction potential at that point. The collision energy $(mu^2/2)$ is E and the miss distance is b. In the straight-line trajectory approximation, $V(r)$ is merely set equal to zero.

The total collision transition probability may now be expressed

$$P_{1,2}(b,u) = 2 \exp\left[-\frac{\gamma}{u}\left(a^2 - \frac{b^2}{r_c^2}\right)^{-1/2}\right]\left\{1 - \exp\left[-\frac{\gamma}{u}\left(a^2 - \frac{b^2}{r_c^2}\right)^{-1/2}\right]\right\} \tag{8.58}$$

where the factor γ is a constant related to separation and slopes of the potential functions at the crossing,

$$\gamma = \frac{2\pi H_{12}^2}{\hbar\left|\frac{d}{dr}(H_{22} - H_{11})\right|_{r_c}} \tag{8.59}$$

and the factor a is a function of initial velocity u only

$$a^2 = 1 - \frac{2V(r_c)}{mu^2} \tag{8.60}$$

The cross section is now obtained by integrating over the miss distance b.

$$S(u) = 2\pi \int_0^{ar_c} P_{12} b \, db = 4\pi \int_0^{ar_c} \left\{\exp\left[-\frac{\gamma}{u}\left(a^2 - \frac{b^2}{r_c^2}\right)^{-1/2}\right] - \exp\left[-\frac{2\gamma}{u}\left(a^2 - \frac{b^2}{r_c^2}\right)^{-1/2}\right]\right\} b \, db \tag{8.61}$$

The upper limit is the value of b where the collision just reaches the crossing point. Now transform the variable of integration to

$$y = \left(1 - \frac{b^2}{a^2 r_c^2}\right)^{-1/2}, \quad 1 < y < \infty \tag{8.62}$$

$$dy = -\frac{1}{2}\left(1 - \frac{b^2}{a^2 r_c^2}\right)^{-3/2}\left(\frac{-2b \, db}{a^2 r_c^2}\right) = \frac{y^3}{a^2 r_c^2} b \, db \tag{8.63}$$

Then

$$S(u) = 4\pi a^2 r_c^2 \int_{1/a}^{\infty} (e^{-\gamma y/au} - e^{-2\gamma y/au}) \frac{dy}{y^3}$$

$$= 4\pi a^2 r_c^2 \left[E_3\left(\frac{\gamma}{au}\right) - E_3\left(\frac{2\gamma}{au}\right)\right] \tag{8.64}$$

where

$$E_3(x) = \int_1^\infty \frac{e^{-xy}}{y^3}\, dy = x^2\Gamma(-2,x) \tag{8.65}$$

and $\Gamma(-2,x)$ is an incomplete gamma function. In the limit as x becomes very large (ref. 12)

$$\Gamma(-2,x) \xrightarrow[x\to\infty]{} \frac{e^{-x}}{x^3}\left(1 - \frac{3}{x} + \frac{12}{x^2} - \cdots\right) \tag{8.66}$$

Thus, at low velocities the cross section becomes

$$S(u) \xrightarrow[(\gamma/au)\to\infty]{} 4\pi a^2 r_c^2 \left(\frac{au}{\gamma}\right) e^{-\gamma/au} \tag{8.67}$$

For very high velocities the transition probability is evaluated in the limit as γ/au becomes small

$$P_{12}(b,u) = 2\exp\left[-\frac{\gamma}{au}\left(1 - \frac{b^2}{a^2 r_c^2}\right)^{-1/2}\right]\left\{1 - \exp\left[-\frac{\gamma}{au}\left(1 - \frac{b^2}{a^2 r_c^2}\right)^{-1/2}\right]\right\}$$

$$\xrightarrow[(\gamma/au)\to 0]{} \frac{2\gamma}{au}\left(1 - \frac{b^2}{a^2 r_c^2}\right)^{-1/2} \tag{8.68}$$

and the cross section then becomes

$$S(u) = \frac{4\pi\gamma}{au}\int_0^{ar_c} \frac{b\, db}{\left(1 - \frac{b^2}{a^2 r_c^2}\right)^{1/2}} = 2\pi\left(\frac{\gamma}{au}\right) a^2 r_c^2 \int_0^1 \frac{dx}{x^{1/2}}$$

$$= 4\pi\left(\frac{\gamma}{au}\right) a^2 r_c^2$$

$$= S_o\left(\frac{a\gamma}{u}\right) \tag{8.69}$$

Note that in this limit the quantity $a = (1 - Vc/E)^{1/2}$ remains close to unity, and that the cross section then varies as u^{-1} or $E^{-1/2}$, a result in disagreement with experimental observation for most reactions; the cross section generally decreases as E^{-1} for large collision energy. However, as we found in chapter II, this does not influence the rate coefficient very much, as that quantity depends primarily on the behavior of the cross section near threshold.

The rate coefficient integral can be performed exactly for the high velocity limit cross section.

$$S(x) = \frac{\gamma a}{u}(4\pi r_c^2) = \frac{\gamma a}{u} S_o$$

where

$$a = \left(1 - \frac{x^*}{x}\right)^{1/2}$$

$$u = \left(\frac{2kT}{m}\right)^{1/2} x^{1/2}$$

$$\alpha = \frac{\bar{u} S_o \gamma}{s} \int_{x^*}^{\infty} \frac{x\, e^{-x}\, dx}{\left(\frac{2kT}{m}\right)^{1/2} x^{1/2}} = \left(\frac{4}{\pi}\right)^{1/2} \frac{S_o \gamma}{x} \int_{x^*}^{\infty} (x - x^*)^{1/2}\, e^{-x}\, dx$$

$$= \left(\frac{4}{\pi}\right)^{1/2} \frac{S_o \gamma}{s} e^{-x^*} \int_0^{\infty} y^{1/2}\, e^{-y}\, dy = \frac{S_o \gamma}{s} e^{-x^*} \qquad (8.70)$$

The rate coefficient in this approximation is the cross section swept out by the internuclear distance at the crossing point multiplied by the characteristic crossing velocity γ, where the probability of transition is near its maximum, and by the Arrhenius factor $\exp(-x^*)$.

Problem 8.1: Show that P_{12} given by the Landau-Zener method is a maximum and equal one-half when the crossing velocity is $(\gamma/\ln 2)$. What is P_{12} when the crossing velocity is exactly γ?

Problem 8.2: Consider a pure, homogeneous gas composed of particles of mass 28 amu (atomic mass unit) which have just two interaction potentials between the particles, a ground state interaction U_1 and an excited state U_2.

$$U_1 = A\, e^{-\alpha r} \quad , \quad A = 100 \text{ eV} \, , \quad \alpha^{-1} = 1 \text{ Å}$$

$$U_2 = B\, e^{-\beta r} + E_o \, , \quad B = 5 \text{ eV} \, , \quad \beta^{-1} = 1 \text{ Å} \, , \quad E_o = 5 \text{ eV}$$

Assume the perturbation interaction at the crossing point is $H_{12} = 0.1$ eV.

a) Find the crossing point r_o in Å, the activation energy E^* in eV, and the cross section coefficient $S_o = 4\pi r_o^2$ in cm^2. Graphical solution or successive approximation may be used.

b) Find the temperature T in K where the mean gas velocity $\bar{u}$ equals γ.

c) What is the threshold velocity, u^* in cm/sec where the crossing point is just reached in head-on collision ($b = 0$)?

d) Calculate and plot the transition probability for a single collision (i.e., incoming and outgoing crossing at r_o) for velocities from 0 to 20×10^5 cm/sec.

e) Calculate the cross section ratio S/S_o from both the low velocity limit formula and the high velocity limit formula. How do the results compare?

f) Calculate and plot the rate coefficient α, given by the high velocity limit cross section, as a function of T from 300 to 30,000 K.

8.8 CONCLUDING REMARKS

The Landau-Zener method of evaluating transition probability at a potential curve crossing has been derived, and although the method is recognized to have a number of deficiencies in terms of the approximations involved, it gives results that agree reasonably well with experimental observations on a number of charge exchange reactions that occur in atomic ion collisions. The method has also been used for cases of molecular ion collision charge transfer, where a more complex set of curve-crossing transition points is involved. The calculations and experiment agree within factors of about 3, not too exciting from a scientific viewpoint but certainly adequate for some engineering applications. In general, the Landau-Zener transition seems to increase too rapidly near threshold, and falls off too slowly at high-collision energy, as $E^{-1/2}$ rather than E^{-1} as usually observed. Nevertheless, the transition probability goes to the correct limits of zero at very low and high collision energies, and is expected to be most accurate near the maximum values where the largest contributions to the cross section and rate coefficient integrals will occur. Much of the inaccuracy in the transition probability is mitigated in these integrations, so the cross sections and rate coefficients are somewhat more reliable than might at first be expected from an analysis of limitations in the assumptions involved in the Landau-Zener method.

REFERENCES

1. Herzberg, G.: Molecular Spectra and Molecular Structure. I. Spectra of Diatomic Molecules. D. Van Nostrand, 1950.

2. Gaydon, A. G.: Dissociation Energies and Spectra of Diatomic Molecules. Dover Publications, N.Y., 1950.

3. Landau, L.: Phys. Z. Sow., vol. 1, 1932, p. 88; ibid, vol. 2, 1932, p. 46.

4. Zener, C.: Non-Adiabatic Crossing of Energy Levels. Proc. Roy. Soc., vol. A137, Sept. 1, 1932, pp. 696-702; Interchange of Vibrational and Translational Energy. Proc. Cambridge Phil. Soc., vol. 29, Jan. 31, 1933, pp. 136-141.

5. Stueckelberg, E. C. G.: Theory of Inelastic Collisions Between Atoms. Helv. Phys. Acta, vol. 5, 1932, pp. 369-423.

6. Eyring, H.; Walter, J.; and Kimball, G. E.: Quantum Chemistry. John Wiley and Sons, N.Y., 1944.

7. Geltman, : Topics in Atomic Collision Theory. Academic Press, N.Y., 1964, pp. 217-222.

8. Hansen, C. F.: Molecular Physics of Equilibrium Gases, A Handbook for Engineers. NASA SP-3096, 1976.

9. Schaefer, H. F.: The Electronic Structure of Atoms and Molecules. A Survey of Rigorous Quantum Mechanical Results. Addison-Wesley, Reading, Mass., 1972.

10. Schaefer, H. F., ed.: Modern Theoretical Chemistry II. Ab Initio Methods. Plenum Press, 1977.

11. Whittaker, E. T.; and Watson, G. N.: A Course of Modern Analysis. Cambridge U. Press, England, 1958.

12. Abromovitz, M.; and Stegun, I. E., eds.: Handbook of Mathematical Functions. NBS Applied Math Series 55, June 1964.

13. Bates, D. R.: Collisions Involving the Crossing of Potential Energy Curves. Proc. Roy. Soc., vol. A257, Aug. 23, 1960, pp. 22-31.

14. Thorson, W. R.; Pelos, J. B.; and Boorstein, S. A.: Studies of the Potential Curve Crossing Problem. I. Analysis of Stueckleberg's Method. Phys. Rev., vol. 4A, Sept. 1971, pp. 1052-1066.

15. Hasted, J. B.: Physics of Atom Collision. Butterworths, Washington, D.C., 1964.

16. Dalgarno, A.: Inelastic Heavy-Particle Collisions Involving the Crossing of Potential Energy Curves. II: Charge Transfer from H Atoms to Al^{3+}, B^{2+}, Li^{2+}, and Al^{2+}. Proc. Phys. Soc. Lond, vol. A67, Nov. 1, 1954, pp. 1010-1017.

17. Bates, D. R.; and Moiseiwitsch, B. L.: Inelastic Heavy Particle Collisions Involving the Crossing of Potential Energy Curves. I: Charge Transfer from H Atoms to Bi^{2+}, Si^{2+}, and Mg^{2+} Ions. Proc. Phys. Soc. Lond., vol. A67, Sept. 1, 1954, pp. 805-812

18. Bates, D. R.; and Boyd, T. J. M.: Inelastic Heavy Particle Collisions Involving the Crossing of Potential Energy Curves. IV: Ionic Recombination. Proc. Phys. Soc., Lond., vol. A69, Dec. 1, 1956, pp. 910-916.

19. Hasted, J. B.; Phil, D.; and Smith, R. A.: The Detachment of Electrons from Negative Ions. Proc. Roy Soc., vol. A235, May 8, 1956, pp. 349-353.

20. Hasted, J. B.; and Chong, A. Y. J.: Electron Capture Processes for Multiply Charged Ions. Proc. Phys. Soc. Lond., vol. 80, Aug. 1, 1962, pp. 441-449.

21. Moseley, J. T.; Olson, R. E.; and Peterson, J. R.: Ion-Ion Mutual Neutralization. In Case Studies in Atomic Physics, North Holland Publishing Co., Amsterdam, vol. 5, 1975, pp. 1-45.

22. Olson, R. E.: Absorbing-Sphere Model for Calculating Ion-Ion Recombination Total Cross Sections. J. Chem. Phys., vol. 56, Mar. 15, 1972, pp. 2979-2984.

CHAPTER IX CLASSICAL REACTION SYSTEMS ON A SINGLE POTENTIAL SURFACE

9.1 SUMMARY

The reactions that occur exclusively on a single potential surface are treated as a system of classical particles following the Hamilton equations of motion. Hamilton's equations can be integrated to any desired degree of accuracy, but good approximations for the potential surface are not available in most cases, so this fact has blocked the full application of the method, except for a few illustrative examples that give some useful qualitative ideas about classical type reaction systems. Approximate potentials are developed assuming that the total potential is merely the superposition of two-electron exchange terms, which are obtained by fitting experimental data for two-body interactions; these are the LEPS (London-Eyring-Polyani-Sato) potentials, which are found to be very sensitive to the approximations used to account for the effects of two-electron overlap integrals. A still more empirical method of obtaining potential surfaces is to smoothly piece together functions that are known to fit observed experimental vibrational spectra for the isolated two-body pairs; the Cℓ - O - O potential is cited as an example of this procedure and the results are used to evaluate the probable activation energy and temperature dependence of the $ClO + O \rightarrow Cl + O_2$ reaction-rate coefficient.

9.2 INTRODUCTION

In chapter VIII the transitions that occur at the crossing or near-crossing of two potential surfaces were considered. If the perturbation interaction energy H_{12} is large there is very little probability of transition between the lower state and the upper state. The lower state of interest will generally be the lowest or ground state of electronic energy; the "ground state" is by definition that eigenstate that everywhere exhibits the lowest-lying electronic energy and therefore the lowest-lying potential surface. This situation was diagrammed for a one-dimensional, two-body type collision in figure 8.3(b). In this case, the collision takes place adiabatically along the lowest lying potential surface, and transitions to the upper surface are so improbable they may be ignored.

A typical two-body ground state potential that results from a crossing type of interaction with a large coupling perturbation between two states with different electronic configuration, but with the same symmetry, is redrawn in figure 9.1. The widely removed excited potential surface is shown by the dashed line at the top of the figure. The position of the maximum in the potential at r_m is approximately the distance of the potential crossing r_c considered in the last chapter. Two different states for the atomic pair exists in the sense that all situations with $r > r_m$ or with kinetic energy $E > E_m$ are free states, whereas a bound diatomic state with vibrational and rotational energy exists if $r < r_m$ and $E < E_m$. A collision that occurs with energy $E < E_m$ can make a transition from the free state to the bound state by the so-called "quantum tunneling" effect. The wave function, though it decreases in an exponential manner across the potential barrier where $E_m > E$, is nevertheless finite on the other side of the barrier, and a finite transition probability results from collision. However, this quantum tunneling effect is negligible in most cases of practical interest in gas-phase collisions; it becomes important only where the potential barrier is extremely narrow, such as a thin oxide layer deposited on a metal or semiconductor surface. For our purposes here, it will be

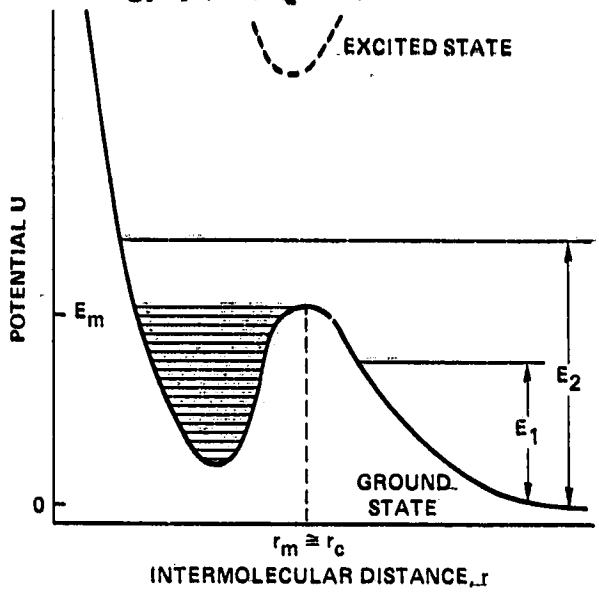

Figure 9.1- Ground state potential surface for two particle collision with a maximum produced by large interactive coupling between two states with different electronic configuration but same symmetry.

adequate to treat such collisions classically and the collisions with $E < E_m$ merely cause scattering in this approximation.

If the collision occurs with kinetic energy $E > E_m$, the bound state configuration has a short lifetime — for head-on collision the duration is about one vibrational period, but for a finite miss distance b, the two atoms may orbit one another several times, particularly when E is not much greater than E_m. However, the result is unstable in time unless a third body takes part in the collision to carry away the excess kinetic energy and drop the atom pair into one of the stable bound rotational-vibrational states shown in figure 9.1. Thus, adiabatic potential surface trajectories lead to a recognizable or interesting chemical-like reaction only where three or more nuclear centers participate in the collision, and the potential surface becomes multidimensional. The following discussion will be concerned with those three particle reactions which can be described with a single adiabatic potential surface; these are typically association-dissociation reactions such as

$$A + B + C \rightleftharpoons AB + C \tag{9.1}$$

and atom exchange reactions such as

$$A + BC \rightleftharpoons AB + C \tag{9.2}$$

For these reactions the potential surface is three-dimensional. A possible set of coordinates is shown in figure 9.2(a): the three internuclear distances R_{ab}, R_{bc}, and R_{ca}. Other coordinate systems are of course possible, such as the distances R_{bc} and R_{ca} being replaced by $R_{\overline{ab}-c}$ the distance from atom c to the center of mass of atoms A and B; the spherical angle coordinates θ and γ are then used to give the direction of the R_{ab} vector with respect to the vector $R_{\overline{ab}-c}$. Alternatively, an angle such as ϕ_{abc} could be used to replace R_{ac}.

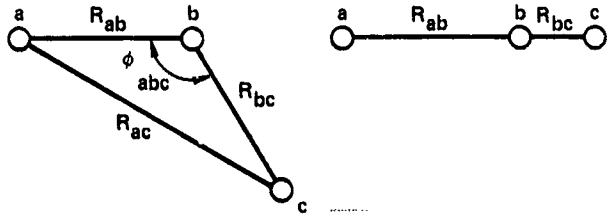

a) GENERAL 3-DIMENSIONAL COLLISION CASE

b) COLLINEAR COLLISION CASE

Figure 9.2- Coordinates for 3-body collision.

Potential surfaces in three or more dimensions are hard to visualize, so typically the two-dimensional surface used to describe a collinear collision, with coordinate configuration as shown in figure 9.2(b), is used to describe the dynamics of three-body reactive collision. One should always bear in mind that these collinear collisions are atypical, and do not

duplicate all features of a typical or average collision. With this caution in mind, the two-dimensional potential surfaces for collinear three-body collision can be useful as aids to understanding and physical visualization of the problem.

The two-dimensional figure which was used to describe collision between two particles with a spherical interaction potential, figure 9.1, exhibited a simple hump or maximum which can be related to the activation energy. On the surface used to describe collinear collision between three particles, the hump becomes a three-dimensional saddle point. The height of the saddle point is the activation energy, and the path of steepest descent (or maximum gradient) across the saddle point is known as the reaction path. Physically, the reaction path represents a kind of average of the most probable trajectories leading to reaction. The path of maximum positive curvature at the saddle point is orthogonal to the reaction path, and the curvature of this path is a measure of the width of the saddle point. The width and height of the saddle point are the most important parameters to duplicate in any approximate potential surface used to assess the rate coefficient. When the collision is not collinear, the potential is a function of three independent variables and the saddle point in the potential becomes a four-dimensional figure. One may visualize this situation by thinking of the three-dimensional saddle point with a barrier height and thickness along the reaction path and width at the pass which continually change as a function of the fourth independent coordinate, which might be the angle ϕ_{abc} shown in figure 9.2(a), for example. The trajectories over this surface are computed numerically, and in this case the lack of a visualizable model is not a handicap to the computer; the only limit on the number of nuclear centers and therefore on the number of dimensions that can be involved is the practical one of available computer speed, size, and calculation cost.

The reaction-rate problem is solved in three steps. First, the adiabatic potential must be determined either approximately or with more exact quantum wave-function expansions; the barrier height and width parameters should be most closely duplicated. Next a multiplicity of trajectories over this surface are calculated, starting from suitably weighted initial conditions. A statistical determination of the fraction of collisions which lead to chemical reaction for a given miss distance and velocity is then computed and used as the value of the transition probability in the cross-section integral. Finally, the reaction-rate coefficient is a Boltzmann-averaged cross section, just as discussed in previous chapters.

9.3 ADIABATIC POTENTIAL SURFACES

The really crucial part of the adiabatic reaction-rate problem is the determination of the potential surface with sufficient accuracy. Once this is done, the numerical solutions of collision trajectories and the statistical averaging procedures may be tedious and time consuming on the computer, but they are relatively straightforward and can be performed to any required degree of accuracy. Unfortunately, very few potential surfaces are known accurately at the present time, even with modern quantum chemistry computing methods available. Thus, approximations are widely used and are usually based on the methods for approximating potential surfaces developed by London, Eyring, and Polyani (ref. 1). These approximate potentials are called LEP potentials. Sato (ref. 2) introduced a semi-empirical correction for the LEP potential which allows the model potential, called the LEPS potential, to better fit experimental results and also provides a smoother potential surface that is believed to be more realistic. However, it should be kept in mind that none of these potential

surfaces are truly precise. Parr and Truhlar (ref. 3) have given a critical review of the LEPS type potentials and point out that the calculated reaction barrier heights are pathologically oversensitive to the approximations used. This occurs because the final potential is a balance of very large repulsive and attractive (positive and negative) integrals. Thus, even though the separate integrals can be obtained quite accurately by modern quantum calculations, the final balance is very sensitive to residual uncertainties.

In spite of its defects, the LEPS-type potential has been very useful in evaluating the nature and the functional form of potential for adiabatic collision type reaction. Often the coefficients in the semi-empirical Sato type approximation can be adjusted to give reasonably satisfactory agreement with experiment. For this reason, the derivation of the potential for a simple three-electron system will be followed to illustrate the general method. This is precisely the potential needed for a three-body hydrogen exchange reaction

$$H_a + H_bH_c \rightarrow H_aH_b + H_c \qquad (9.3)$$

and is similar to the potentials used for hydrogen halides. Electronically, the ground state of the seven electron outer shell of the halogen behaves something like a single electron.

The starting approximation is the assumption that all three-center interaction integrals are negligible compared with the two-center integrals. This is indeed generally true, but since the final result is the difference between competing positive and negative terms, it is not certain that neglect of three-center interaction integrals is quantitatively justifiable. No doubt, the reason the approximation works as well as it does is because the positive and negative three-center terms also tend to neutralize one another. At any rate, the approximation is very appealing because the two-center interactions are known quite accurately in many cases from experimental spectroscopy, and these interactions can now be calculated with about equal precision. Thus, we consider first the energy of a two-center, two-electron system with exchange, and subsequently sum all the two-center interactions to get a total potential for a three-, four-, or more body system.

9.4 TWO-CENTER, TWO-ELECTRON SYSTEM POTENTIALS

The contribution of spin momentum to energy will be neglected for systems of light atoms; then the Hamiltonian operator can be simply expressed as a function of only the spatial coordinates of electrons 1 and 2 and of the two nuclear centers a and b. Where the two nuclear centers are hydrogen, the Hamiltonian operator becomes

$$\hat{H} = \hat{H}_1 + \hat{H}_2 + \hat{H}' + \frac{1}{R_{ab}} \qquad (9.4)$$

where $\hat{H}_1$ is an operator involving coordinates of electron 1 only and $\hat{H}'$ is an operator involving coordinates of both electrons. For example

$$\left.\begin{aligned} \tilde{H}_1 &= -\frac{\nabla_1^2}{2} - \frac{1}{R_{a_1}} - \frac{1}{R_{b_1}} \\ \tilde{H}_2 &= -\frac{\nabla_2^2}{2} - \frac{1}{R_{b_2}} - \frac{1}{R_{a_2}} \\ \tilde{H}' &= \frac{1}{R_{12}} \end{aligned}\right\} \qquad (9.5)$$

is one possible grouping of the operator terms. The energies are given in Hartrees (e^2/a_o) and the distances R_{ij} between particles i and j are given in Bohr units (a_o). The distance R_{ab} between nuclear centers is treated as a constant in the Born-Oppenheimer approximation, where the nuclear motions are regarded as fixed compared with the very rapid electron motions. Thus, the term $1/R_{ab}$ can be separated from the rest of the Hamiltonian and simply added again to the final energy to account for the repulsion between nuclear centers; there is no need to complicate the calculations by carrying this term through all the wave function integrals. The problem is to determine with perturbation methods the total energy for each value of R_{ab} selected.

A logical expansion of the wave function ψ would be in eigenfunctions of the operators $\tilde{H}_1$ and $\tilde{H}_2$

$$\left.\begin{aligned} \tilde{H}_1\phi(1) &= E_o\phi(1) \\ H_2\phi(2) &= E_o\phi(2) \end{aligned}\right\} \qquad (9.6)$$

where the function $\phi(i)$ is just the ground-state eigenfunction for the H_2^+ ion in the coordinates of electron i and E_o is the corresponding energy; E_o is known very accurately as a function of R_{ab} for the H_2^+ ion and very good analytic approximations for the wave function of this ion are known. This expansion would constitute a full molecular orbital (MO) treatment for the H_2 molecule. However, a linear combination of atomic orbitals (LCAO approximation) is found to give a much better result than the MO treatment, so it is more common to group the operator terms as a series of atomic Hamiltonian operators (refs. 4-6). Slater's text (ref. 6), for example, breaks down the Hamiltonian in a different but totally equivalent form

$$\left.\begin{aligned} \tilde{H}_1 &= -\frac{\nabla_1^2}{2} - \frac{1}{R_{a_1}} \\ \tilde{H}_2 &= -\frac{\nabla_2^2}{2} - \frac{1}{R_{b_2}} \\ \tilde{H}' &= \frac{1}{R_{12}} + \frac{1}{R_{ab}} - \frac{1}{R_{b_1}} - \frac{1}{R_{a_2}} \end{aligned}\right\} \qquad (9.5a)$$

Note that the constant term $1/R_{ab}$ has been carried along as part of the perturbation $\tilde{H}'$.

At this point some form must be chosen for the wave function, and we should keep in mind that any form chosen is necessarily an approximation; therefore, the resulting potential is also only an approximation. A rather good approximation for the H_2^+ ion eigenfunction has the form

$$\phi_i = u_a(i) + u_b(i) \tag{9.7}$$

where $u_a(i)$ is a function of the coordinates of electron i centered on atom a, and $u_b(i)$ is the same function centered on atom b. The function ϕ_i is then a molecular orbital, and the product of $\phi_1\phi_2$ gives a full molecular orbital form for the wave function ψ.

$$\psi = \phi_1\phi_2 = u_a(1)u_b(2) + u_b(1)u_a(2) + u_a(1)u_a(2) + u_b(1)u_b(2) \tag{9.8}$$

However, this wave function is found not to give good results, because the third and fourth terms in this sum have both electrons about the same center, and these really represent the higher energy ionic state H^+H^- rather than the ground state of H_2 which we seek. London found that a much better wave function was obtained by dropping these terms, and most of the modern development of molecular wave functions has concentrated on the LCAO form.

$$^1\psi = u_a(1)u_b(2) + u_b(1)u_a(2) \tag{9.9a}$$

Since this ground-state wave function is symmetrical with respect to the spatial coordinates, the spin eigenfunction for the two electrons involved must be asymmetric, in order to satisfy the Pauli principle that the total wave function be asymmetric with respect to exchange of any two electrons. Thus, the spins are paired, with a total spin of zero, and the function $^1\psi$ is a singlet. We will also be concerned with the triplet wave function $^3\psi$ that results when the spin eigenfunction is symmetric, that is, the spins are said to be unpaired and the total spin is one; in this case the function must be spatially asymmetric to satisfy the Pauli principle

$$^3\psi = u_a(1)u_b(2) - u_b(1)u_a(2) \tag{9.9b}$$

The exact nature of the functions u_a and u_b has not been specified. However, we are merely concerned now with the functional form of the potential, not with the numerical results of calculations (which are still somewhat approximate); we want to fit this form to experimental two-body interaction potentials, and then use these results to deduce the multibody potential.

Using the relations of Eq. (9.6), one obtains

$$\tilde{H}\psi = (2E_o + \tilde{H}')[u_a(1)u_b(2) \pm u_b(1)u_a(2)] \tag{9.10}$$

where the (+) sign represents the singlet state and the (-) sign represents the triplet.

The value of E_o represents the lowest energy for $\tilde{H}_1$ and $\tilde{H}_2$ operating on the functions ϕ_a and ϕ_b. The integrated value of ψ^2 is needed for normalization; that is, the integrated probability of the system over all possible electron configurations must be unity. If the functions u_a and u_b are normalized

$$\langle \psi^2 \rangle = \langle u_a^2(1) u_b^2(1) \rangle \pm 2 \langle u_a(1) u_b(1) u_a(2) u_b(2) \rangle + \langle u_b^2(1) u_a^2(2) \rangle = 2(1 \pm S^2) \tag{9.11}$$

where S is defined as the overlap integral

$$S = \langle u_a(1) u_b(1) \rangle = \langle u_a(2) u_b(2) \rangle \tag{9.12}$$

To obtain the average total energy of the system given by this wave function, multiply Eq. (9.10) by ψ, integrate over both electron spaces, and divide by the normalization constant

$$E = \frac{\langle \psi \tilde{H} \psi \rangle}{\langle \psi^2 \rangle} = 2E_o + \frac{K}{1 \pm S^2} \mp \frac{J}{1 \pm S^2} + \frac{1}{R_{ab}} \tag{9.13}$$

where the Coulomb integral K and the exchange integral J are defined, respectively, by

$$K = \langle u_a^2(1) \tilde{H}' u_b^2(2) \rangle \tag{9.14}$$

$$J = - \langle u_a(1) u_b(1) \tilde{H}' u_a(2) u_b(2) \rangle \tag{9.15}$$

The signs of K and J are chosen so that both are normally positive quantities.

The Coulomb integral derives its name because in the atomic structure problem, where the perturbation is simply $(1/R_{12})$, this integral represents the average Coulomb repulsion between the charge distribution $u_a^2(1)$ and the charge distribution $u_b^2(2)$. In the present case where $\tilde{H}'$ may contain other terms, the interpretation is not so physically simple; however, the name "Coulomb integral" is retained for any integral of this type. The exchange integral derives its name because these terms appear in the energy only when the form chosen for the wave function gives equal probability to all configurations where two identical electrons are exchanged, as in Eqs. (9.9a and b). The exchange terms are necessary to theoretically model the observed splitting between states with different total electron spins, in this case the difference between singlet and triplet energy levels.

Perhaps the simplest choice for u_a and u_b that qualitatively duplicates the features of the H_2 potential is two hydrogen-like wave functions with variational parameter Z

$$u_a(i) = \left(\frac{Z}{\pi}\right)^{1/2} e^{-ZR_{ai}}$$

$$u_b(j) = \left(\frac{Z}{\pi}\right)^{1/2} e^{-ZR_{bj}} \tag{9.16}$$

In this approximation $E_o = -Z^2/2$ and the integrals S, K, and J can all be performed analytically. (See, for example, Slater's text "Quantum Theory of Molecules and Solids (ref. 6).) Note that Slater's nomenclature is somewhat different than used here; the energy units are in Rydbergs or $(e^2/2a_o)$, and J is used for Coulomb integral and K for exchange integral. In Slater's notation, our $K = H_o - (2/R)$ or $2J + J'$ while our $(-J) = H_1 - (2S^2/R)$ or $2KS + K'$.

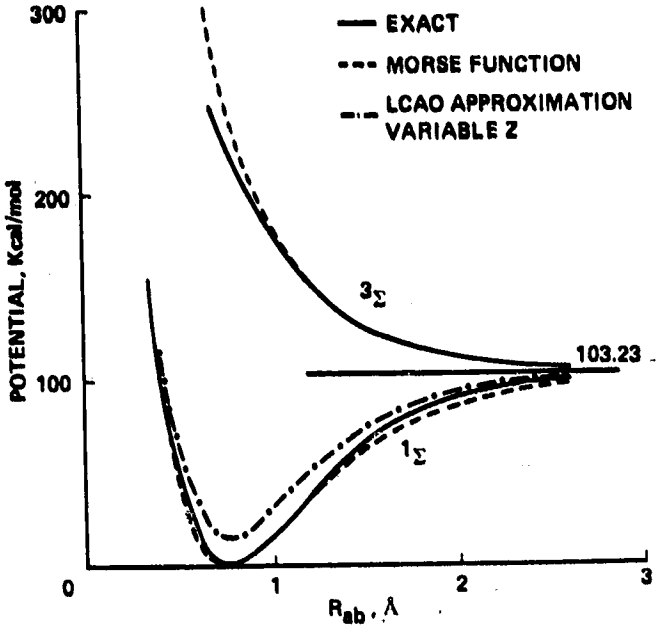

Figure 9.3- H_2 potential functions.

The H_2 potential calculated using the functions of Eq. (9.16) is shown in figure 9.3 as the LCAO approximation with variable Z. The exact potential is shown by the solid line, and one can see that the approximate model potential does have the correct qualitative shape with the minimum at the proper distance, $R_{ab} \simeq 0.74$ Å, but the potential minimum is about 15 Kcal/mol above the correct value. A slightly better result can be obtained using polarized wave functions (for example, mixing some p-orbitals with the s-orbitals) but the only way the model can closely approach the true potential is when it includes terms in R_{12} which correlate electron positions such that the two electrons tend to avoid one another; this enormously complicates the algebra of the problem.

For the purpose of computing three-body interaction potentials, it is convenient to use experimentally determined Morse potentials which fit both the observed vibrational energy levels near the bottom of the potential, and the observed dissociation energy. For the singlet state then the Morse function approximation, with the totally dissociated state taken as the zero energy level, is

$$U_1 \simeq D(e^{-2x} - 2\,e^{-x}) \tag{9.17}$$

where $x = (\hbar\omega/2D)^{1/2}(r - r_e)$, ω is the vibrational circular frequency, r is distance between atoms (i.e., R_{ab}) and r_e is the equilibrium value of r at the potential minimum. Sato (ref. 2) noted that the triplet state potential is approximately

$$U_3 \simeq \frac{D}{2}(e^{-2x} + 2\,e^{-x}) \tag{9.18}$$

These Morse potentials are shown in figure 9.3 and one sees that they are reasonably good approximations; the singlet potential U_1 approaches its asymptotic value a little too slowly as R_{ab} is increased, whereas the triplet potential U_3 becomes somewhat too large at small values of R_{ab}.

At large separation (large R_{ab}) the overlap integral is very small, and to a first approximation S has often been neglected; the form of the potential given by Eq. (9.13) is then expressed

$$U_1 = Q - J \tag{9.19}$$

$$U_3 = Q + J \tag{9.20}$$

where Q represents $2E_o + K + (1/R_{ab})$. If we now equate (9.17) and (9.19) and also (9.18) and (9.20), the expressions for Q and J which correspond with the Morse potential are

$$Q = \frac{D}{4}\,(3\,e^{-2x} - 2\,e^{-x}) \tag{9.21}$$

$$J = -\frac{D}{4}(e^{-2x} - 6\,e^{-x}) \tag{9.22}$$

However, these potentials are found not to duplicate experimental activation energies very well, and sometimes lead to strange looking humps and ridges in three-body potential surfaces. Sato (ref. 2) proposed that the trouble was primarily due to the neglect of the overlap integral, and he corrected this in an approximate, semi-empirical way but letting S^2 be a constant value chosen to best fit the experimental observations.

$$U_1 = \frac{Q - J}{1 + S^2} = D(e^{-2x} - 2\,e^{-x}) \tag{9.23}$$

$$U_3 = \frac{Q + J}{1 - S^2} = \frac{D}{2}\,(e^{-2x} + 2\,e^{-x}) \tag{9.24}$$

Solving for Q and J we obtain

$$Q = \frac{D}{4}\,(3\,e^{-2x} - 2\,e^{-x}) + \frac{S^2 D}{4}\,(e^{-2x} - 6\,e^{-x}) \tag{9.25}$$

$$J = \frac{D}{4}\,(6\,e^{-x} - e^{-2x}) + \frac{S^2 D}{4}\,(2\,e^{-x} - 3\,e^{-2x}) \tag{9.26}$$

The quantity S^2 is denoted by k in Sato's papers; values of S^2 the order of 0.2 seem to give reasonable results for the H_3 interaction, but this value changes for other systems. Note that Sato's correction is still an approximation; the real values of S^2 are not constant but vary from 0 at large R_{ab} to 1 at vanishing R_{ab}.

Potentials involving heavier atoms than hydrogen are treated in the same way; the Morse function potentials are available for many diatomic pairs, and in any case modern computational quantum methods can be used to obtain two-body potentials quite accurately. Halogens can be treated in a manner similar to the hydrogens because the 7 electron shell behaves electronically much like a single (1s) electron; two ground state atoms combine to give a singlet attractive state and a triplet repulsive state. Atoms like oxygen and nitrogen are somewhat different; as they approach another atom the electron spins can add up in a number of different ways, leading to a multiplicity of potential interaction surfaces (see Meador (ref. 7), e.g.). However, as an empirical stratagem these atoms have sometimes been treated by the same formalism.

9.5 MULTIPLE-ATOM POTENTIALS

London (ref. 8) developed the expression for multiple atom interactions using the approximation that all multiple center integrals could be neglected in comparison with the two-center integrals; in other words, the total potential is simply the linear sum of two-electron interactions. One can indeed argue that these multiple center integrals are much smaller than the two-center integrals; however, as we have seen, the final potential is the resulting balance of large positive and negative integrals, so the influence of these smaller three-center integrals could be

significant. London's approximation is valid to the extent that these three-center integrals are also a series of both positive and negative values that will balance out to a much smaller residual, just as the two-center integrals do. London's model allows the electrons to interchange between all the different pair bonds with equal probability. London works out the equation for a four-electron, four-center system; for the system of three H-like atoms of present interest, this reduces to:

$$E_{abc} = Q_{ab} + Q_{bc} + Q_{ca} - \frac{1}{\sqrt{2}} [(J_{ab} - J_{bc})^2 + (J_{ac} - J_{bc})^2 + (J_{ca} - J_{ab})^2]^{1/2} \quad (9.27)$$

where the values of Q_{ij} and J_{ij} can be obtained from the Morse potentials for the diatomic pairs as outlined in the previous section. The differences between the exchange integrals J_{ij} occur because in a three-electron system, two of the electrons must have the same spin while the third electron will have opposed spin (at least in the ground state configuration), so each electron must have a bond pairing with one of the remaining electrons, and an antibond pairing with the other, as shown in Eq. (9.27).

Eyring and Polyani based their LEP potentials on Eq. (9.27) using values of Q_{ij} and J_{ij} derived from the Morse functions by neglecting the overlap integral S^2. These potentials typically do not give a reasonable value of the potential barrier height according to the experimentally known activation energies for reaction. Thus, Sato (ref. 2) was led to modify this equation with an empirical constant k, which represents a sort of average of all the overlap integrals (S^2_{ab}, S^2_{bc}, S^2_{ac}) at the distances where the reaction barrier exits.

$$E_{abc} = \frac{1}{1 + k} \left\{ Q_{ab} + Q_{bc} + Q_{ac} - \frac{1}{2} [(J_{ab} - J_{ac})^2 + (J_{bc} - J_{ba})^2 + (J_{ca} - J_{cb})^2]^{1/2} \right\} \quad (9.27a)$$

In the present treatment, we introduce this correction in the evaluation of the Q_{ij} and the J_{ij} as shown in Eqs. (9.25) and (9.26), so we automatically get Sato's result using these values in Eq. (9.27).

To illustrate these potentials, some calculations for H-H-H potentials are shown in the potential contour plots of figures 9.4(a), (b), (c), and (d). Figure 9.4(a) shows the LEP potential, which is obtained when $S^2 = 0$, for a collinear configuration. The reference level of potential has here been adjusted so that the H_2 molecule has zero potential at the bottom of its well. Thus, when $R_1 = 0.74$ Å and $R_2 \to \infty$, U = 51.6 Kcal/mol, the energy of the free H atom, or one-half the dissociation energy of H_2. The same value occurs when $R_1 \to \infty$ and $R_2 = 0.74$ Å, of course. When both R_1 and R_2 become large, the potential is a broad level plane with the energy of three separate H atoms, i.e., 154.8 Kcal/mol. Between the two valleys is a barrier opposing the exchange of one H atom for another in the triatomic collision. This barrier is 22.1 Kcal/mol, much too high to agree with the experimental value of activation energy, which is 7.5 ± 1 Kcal/mol (ref. 9).

Figure 9.4(b) shows the potential when $S^2 = 0.1$ is chosen. The barrier height has been reduced to 12 Kcal/mol, still too high to agree with experimental activation energy. Figure 9.4(c) shows the results when $S^2 = 0.2$. Now the barrier height is 2.8 Kcal/mol, which is perhaps a little too low. The activation energy is actually larger than this barrier height because collisions are not collinear in general, and the activation energy is an average of the minimum energy required for collisions occurring at all angles, which lead the system from one valley across the barrier to the next valley. The barrier height increases as the angle of incidence is increased;

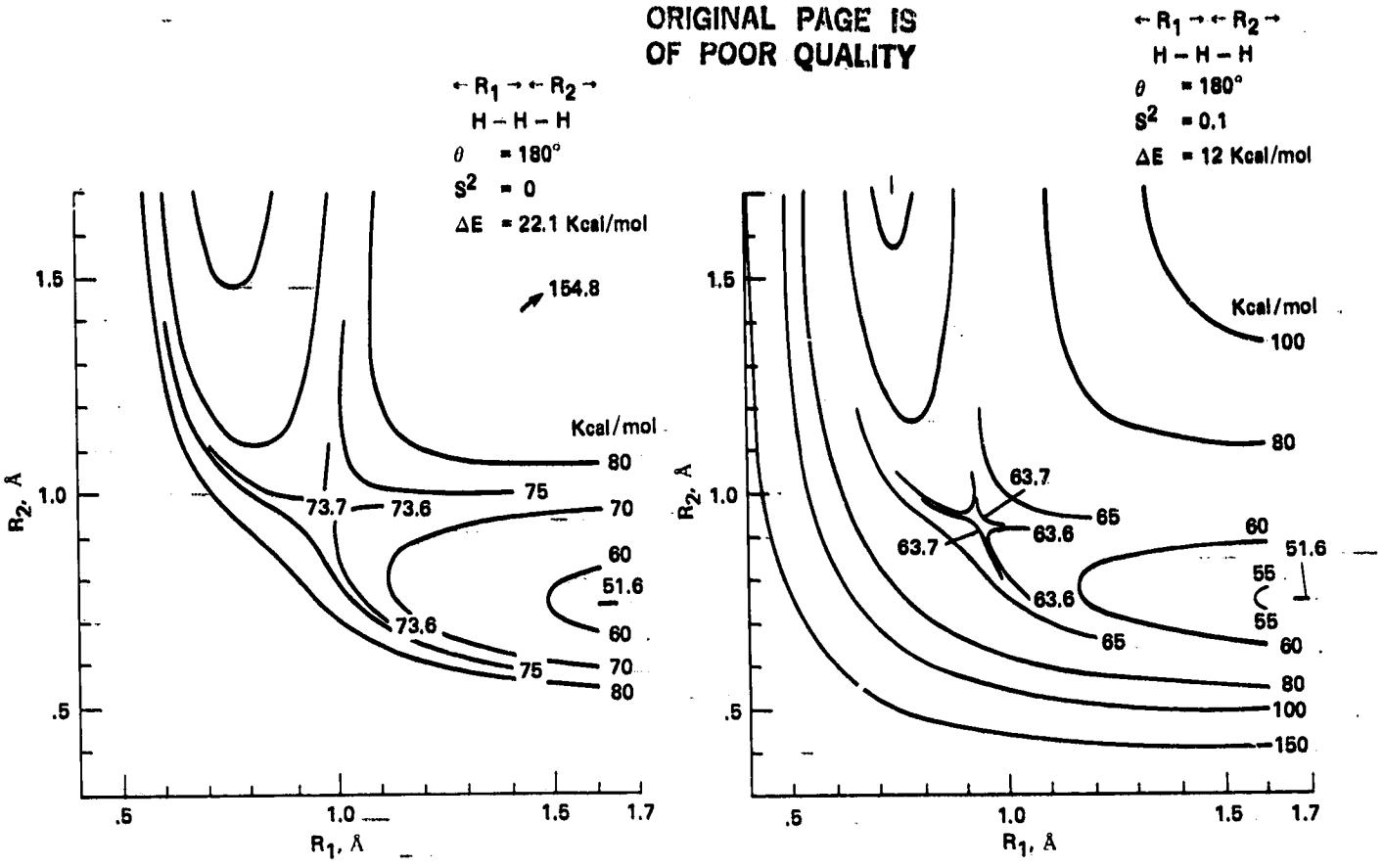

(a) $S^2 = 0$, $\theta = 180°$.

(b) $S^2 = 0.1$, $\theta = 180°$.

Figure 9.4- H_2 potential.

as figure 9.4(d) shows, the barrier height with $S^2 = 0.2$ has increased to 20.2 Kcal/mol at 90° angle. Practically no atom exchanges will occur at normal temperatures with this large a barrier; the reaction will occur only for configurations clustered in a small cone around $\theta = 180°$. However, the effective activation energy will be a statistical average of the reactions that do occur within this cone of angles. Sato[2] concludes that $S^2 = 0.18$, with a collinear barrier about 5.4 Kcal/mol gives a reasonable fit to the experimental evidence.

9.6 DYNAMICS OF ADIABATIC CHEMICAL REACTION

The dynamics of the three-body hydrogen exchange reaction have been analyzed by Karplus, Porter, and Sharma leading to values for the reaction cross section and the rate coefficient (ref. 10). A more typical reaction, because it is exothermic, is the collision-induced exchange of F for one of the hydrogens in H_2

$$F + H_2 \rightarrow HF + H \qquad (9.28)$$

The dynamics for this reaction have been worked out by Jaffe and Anderson (ref. 11), with some follow-on analysis by Jaffe, Henry, and Anderson (ref. 12). The potential energy surface for a collinear collision configuration is shown in figure 9.5; a

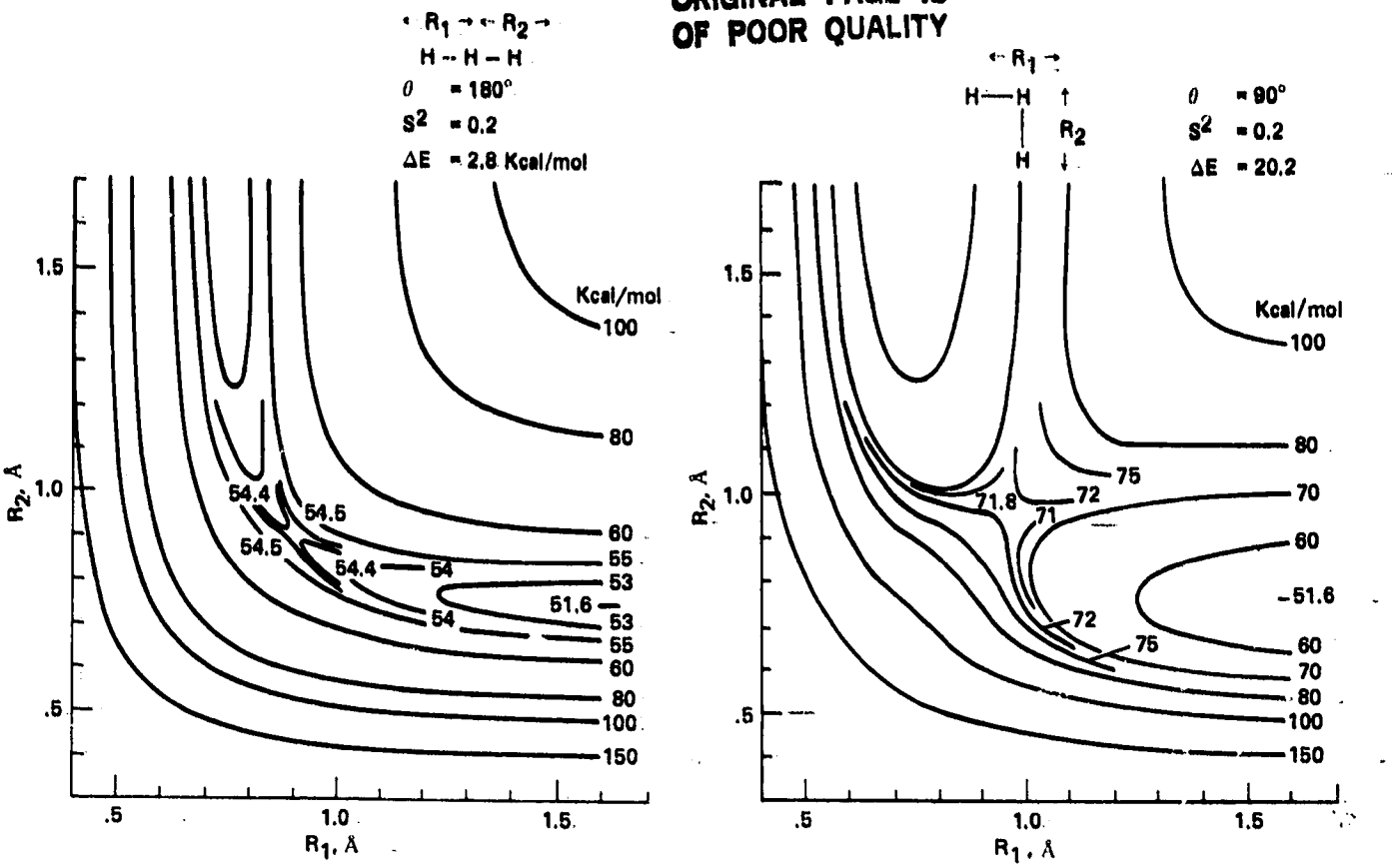

(c) $S^2 = 0.2$, $\theta = 180°$.

(d) $S^2 = 0.2$, $\theta = 90°$.

Figure 9.4- Concluded.

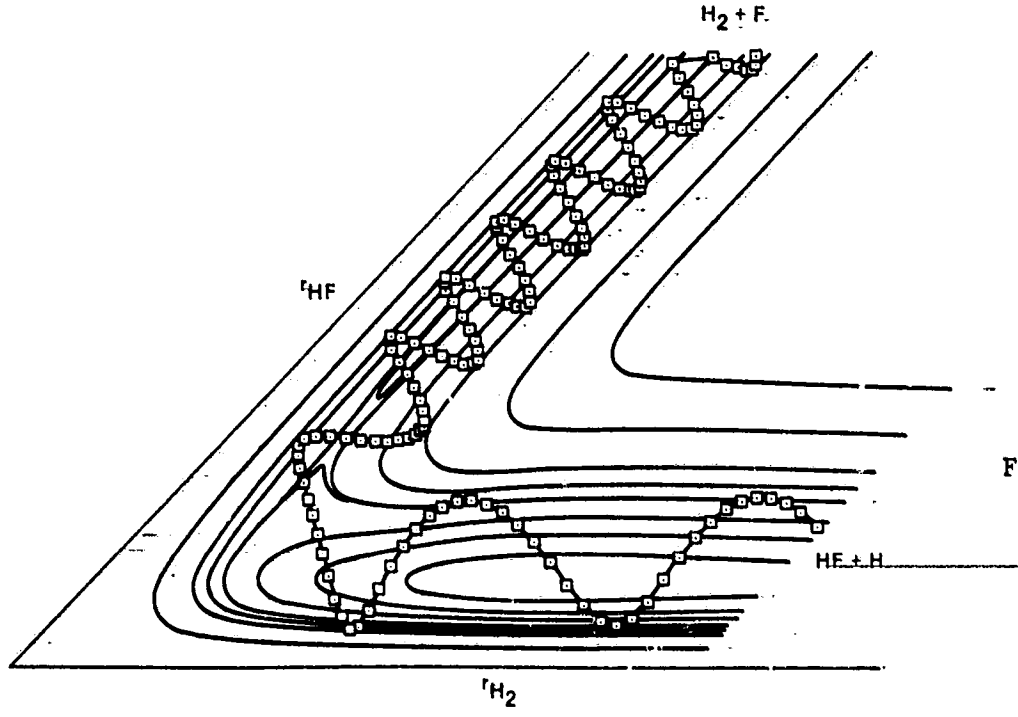

Figure 9.5- LEP potential surface for F + H + H with a trajectory starting from H_2 vibrational level v = 1 and collision energy of 2.0 Kcal/mol.

typical trajectory between the reactant and product states calculated by Jaffe (ref. 12) is also shown on the figure. The trajectory calculation is a step by step numerical solution of Hamilton's canonical equations of motion in which the derivatives of the Hamiltonian with respect to coordinates are calculated using the analytical approximation for the potential given by Eqs. 9.27, 9.21, and 9.22. (The Sato correction was not used here.) The derivatives of the Hamiltonian with respect to the conjugate momenta are very simple analytic functions, namely p/μ, where μ is the appropriate reduced mass. The angle between the coordinate axii in figure 9.5 has been chosen to give the vibrational displacements a direction normal to the coordinates that results when the cross product terms in kinetic energy are eliminated by coordinate transformation.

$$T = \mu_1 \dot{R}_{HH}^2 + \mu_2 \dot{R}_{HF}^2 + \mu_3 \dot{R}_{HH} \dot{R}_{HF} + \mu(\dot{x}^2 + \dot{y}^2) \qquad (9.29)$$

This transformation is used merely to help us visualize the motion on the potential surface more realistically; the computer really doesn't care what coordinate system is used.

The initial coordinates for the F + H_2 interaction are illustrated in figure 9.6. The fluorine atom is given an initial momentum P relative to the center of mass of the H_2 molecule with an impact parameter (miss distance) b; the latter plus the initial rotational energy of the H_2 establishes the total angular momentum of the system. The initial position of the H_2 molecule is specified by any two of the direction cosines, α, β, or γ. Alternate coordinated systems are possible, of course. Hamilton's equations of motion are then integrated step by step to obtain the trajectory of the system over the potential surface, subject to the constraints that both total energy and total angular momentum are conserved. A fixed numerical step size is not very efficient; one desires to use as few steps as possible to hasten the integration, but a small enough step size to ensure accuracy. Thus, the step size should be chosen to vary inversely with the potential surface gradient. Various algorithms for nonlinear extrapolation are helpful in increasing the step size that can be tolerated for a given accuracy.

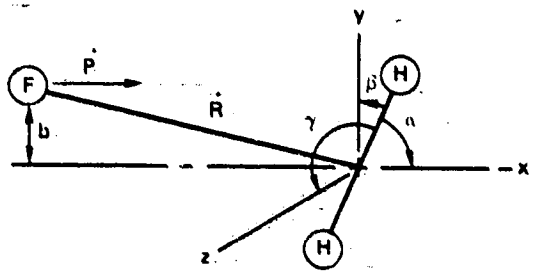

Figure 9.6- Initial coordinates for calculation of fluorine, hydrogen-molecule dynamics.

The initial momentum P, the impact parameter b, the initial vibrational and rotational quantum numbers v and J of the H_2 molecule, are typically chosen by a random number generator, and the trajectory that results is then weighted by the proper temperature-dependent statistical probability parameter p; P, v, and J are weighted according to the Maxwell-Boltzmann distribution, while b is weighted as b^2 to give equal probability per unit cross-section area

$$pdb^2 e^{-[P^2/2\mu + v\hbar\omega + BJ(J+1)]/kT} = b^2 e^{-(E+E_{vJ})/kT} \qquad (9.30)$$

where E is the translational energy of the system, and E_{vJ} is the vibration-rotation energy of the H_2 molecule. The miss distance b is constrained to some

maximum value $b_{max} = (S/\pi)^{1/2}$, where S is the total collision cross section discussed in earlier chapters. Also, P, v, and J are usually restricted to some maximum value that is very improbable at the temperatures of interest; often v and J are fixed at a given value so the results obtained apply to a single initial state of the H_2 molecule.

Each trajectory calculated can be either reactive (HF + H or F + H + H are formed) or nonreactive (F and H_2 remain stable). For exothermic reactions the heat of reaction channeled into HF vibration and rotation can be determined by an analysis of the final coordinates and momenta obtained. The total reaction cross section is given, for fixed values of initial translational energy E and rotation-vibration state v, J

$$S_r = \lim_{N\to\infty} \pi b_m^2 \frac{N_r(E,v,J)}{N(E,v,J)} \tag{9.31}$$

where N is the total number of trajectories calculated and N_r is the number that are reactive. These cross sections are then substituted in the usual collision theory expression to compute the rate constant $\alpha(T)$.

$$\alpha(T) = Q_{vJ}^{-1}(\pi\mu_{F,H_2})^{-1/2}\left(\frac{2}{kT}\right)^{3/2}\left(\sum_{v,J}(2J+1)e^{-E_{vJ}/kT}\right)\int S_r\, e^{-E/kT}\, E\, dE \tag{9.32}$$

where Q_{vJ} is the vibration rotation partition function of H_2.

Typically, to get a good statistical average cross section S, one must calculate the order of 500 trajectories for each set of initial E, v, and J; then one must calculate enough values for S to obtain a decent integral over the energies in Eq. (9.32) for the rate coefficient $\alpha(T)$. This all adds up to a large amount of computer time, so one can appreciate that the effort becomes worthwhile only when some reasonably reliable estimates for the potential surface are found.

Because of the large amount of computer time required, there is a search for schemes that may shorten this approach. In particular, one would like to avoid computing all the nonreactive trajectories and concentrate only on those initial conditions that lead to reaction, and then the reaction probability is the ratio of the number of these initial conditions to the total number of all possible initial conditions, a ratio which can again be determined by statistical weighting. One method of doing this is to consider the system in phase space with the Gibbs canonical distribution of phase, then assume a surface which divides phase space into "reactant" and "product" regions. If the system consists of N atoms, phase space has 6N-6 degrees of freedom (3-coordinates and 3-conjugate momenta for each atom less the 3 coordinates and 3-momenta describing the center of mass) and the dividing surface is (6N-7) dimensional. (In the case of the present three-body F + H_2 reaction, phase space has 12 degrees of freedom and the dividing surface is 11-dimensional). A schematic representation of this phase space and the dividing surface S is shown in figure 9.7. Each reactive trajectory must cross S at least once, so we can choose initial conditions close to S and with the proper trajectory to assure that the system will cross. The problem is that many nonreactive systems may also cross S; these will then double back and recross the surface to end up on the reactant side. Also, some reactive systems may cross more than once. Thus, the phase space-sampling method can only provide an upper bound on the rate constant, and the trick is to attempt to devise surfaces S that will minimize this upper bound.

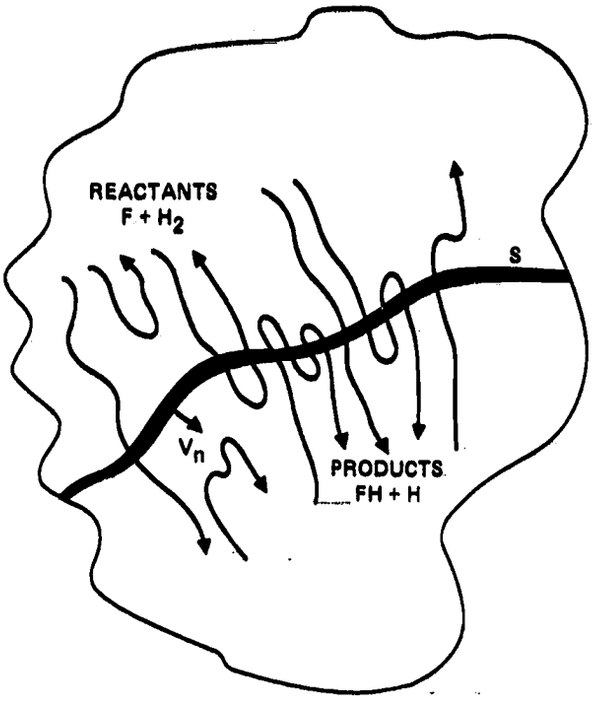

Figure 9.7- Schematic representation of a (6N-6) dimensional phase space with (6N-7) dimensional surface dividing reactants from products.

The phase space sampling approach to the calculation of reaction rates was first outlined by Wigner (ref. 13) as long ago as 1937, but the development of the modern numerical computer was required to really make use of the method quantitatively. To summarize Wigner's method, the reaction rate in the forward direction for a two-body collision, for example, is the number of systems crossing the surface S in one direction per unit time, provided that the surface is chosen so no system crosses more than once. The forward rate constant for the three-body system is

$$\alpha = \frac{-(dn_1/dt)}{n_1 n_2 n_3} = \frac{-(dn_2/dt)}{n_1 n_2 n_3} = \frac{-(dn_3/dt)}{n_1 n_2 n_3} \qquad (9.33)$$

where n_1, n_2, and n_3 are the number density of molecules of type 1, 2, and 3, respectively, and (dn_i/dt) are the number of atoms of type i used up each second by reaction, or in other words the probability that a single system will cross the surface S in unit time multiplied by the total number of systems per unit volume. All atoms are assumed to stay in the ground state of electronic excitation and the nuclear motions are assumed classical. Wigner chooses a trial surface where the energy H_o of the product molecule is a constant, namely, the dissociation energy of the molecule. This surface is, in general, a function of all the coordinates q_i and their conjugate momenta p_i,

$$H_o = H_o(p_i, q_i) \qquad (9.34)$$

Thus, the time derivative can be expressed

$$\frac{dH_o}{dt} = \sum_i \left(\frac{\partial H_o}{\partial q_i} \frac{\partial q_i}{\partial t} + \frac{\partial H_o}{\partial p_i} \frac{\partial p_i}{\partial t} \right) \tag{9.34a}$$

If H represents the total Hamiltonian

$$\dot{q}_i = \frac{\partial H}{\partial p_i} , \quad \dot{p}_i = - \frac{\partial H}{\partial q_i} \tag{9.35}$$

Thus, Eq. (9.34) can be expressed

$$\frac{dH_o}{dt} = \sum_i \left(\frac{\partial H_o}{\partial q_i} \frac{\partial H}{\partial p_i} - \frac{\partial H_o}{\partial p_i} \frac{\partial H}{\partial q_i} \right)$$

$$= \sum_i \left[\frac{\partial H_o}{\partial q_i} \frac{\partial (H - H_o)}{\partial p_i} - \frac{\partial H_o}{\partial p_i} \frac{\partial (H - H_o)}{\partial q_i} \right] \tag{9.36}$$

Those systems cross the H surface per unit time which are closer than $(dH_o/dt)/|\text{grad } H_o|$ if (dH_o/dt) is less than zero. At equilibrium, the density of systems in phase space is the Gibb's canonical distribution

$$\rho = e^{(\psi - H)/kT} \tag{9.37}$$

so the probability of finding the system in a given volume element of phase space is proportional to $\exp(-H/kT)$. Then the number of systems which disappear per unit time is

$$-\left(\frac{dn_i}{dt}\right) = \frac{n_1 n_2 n_3 \int \frac{dH_o/dt}{|\text{grad } H_o|} e^{-H/kT} \, d\sigma}{\int e^{-H/kT} \, dp_1 \ldots dq_n} \tag{9.38}$$

where $d\sigma$ is an element of the surface H_o and the integral is restricted to the portion where $(dH_o/dt) < 0$. The denominator is just the classical partition function Q, and the ratio of the two integrals is the probability that the system finds itself in that region of phase space where it will cross the H_o surface in unit time. Comparing Eqs. (9.33) and (9.38), one obtains an expression for the rate coefficient.

$$\alpha = \frac{1}{Q} \int_{(dH_o/dt)<0} \frac{(dH_o/dt)}{|\text{grad } H_o|} e^{-H/kT} \, d\sigma \tag{9.39}$$

At this point Wigner defines the integral $I(E)$

$$I(E) = -\int\cdots\int_{H_o<E} \frac{dH_o}{dt} e^{-H/kT}\, dq_1\, dq_2\, dq_3 \ldots \tag{9.40}$$

and further stipulates that the coordinate system q_i be rotated so that q_1 is normal to the surface and orthogonal to the remaining q_i lying in the surface H_o. Thus

$$dq_1 = \frac{dH_o}{\text{grad } H_o} \tag{9.41}$$

and Eq. (9.40) can be expressed

$$I(E) = \int_o^E\int \frac{dH_o/dt}{\text{grad } H_o} e^{-H/kT}\, d\sigma\, dH_o \tag{9.42}$$

The derivative of $I(E)$ with respect to E is just the inner integral of Eq. (9.42)

$$\frac{dI}{dE} = \int \frac{dH_o/dt}{\text{grad } H_o} e^{-H_o/kT}\, d\sigma \tag{9.43}$$

If the surface integral is limited to that part where $(dH_o/dt) < 0$ and is evaluated at $E = 0$, the rate coefficient of Eq. (9.39) can be expressed.

$$\alpha = \frac{1}{Q}\left(\frac{dI(E)}{dE}\right)_{E=0} \tag{9.44}$$

The dissociation energy H_o is given in terms of the phase-space coordinates of the product molecule

$$H_o = \frac{p^2}{2m} + V_o(r) \tag{9.45}$$

where r is the distance between the two atoms of the molecule, p is the momentum of these two atoms relative to their center of mass, and $V_o(r)$ is the unperturbed vibrational potential energy of this molecule, in other words H_o is just the minimum total rotation-vibration energy of a dissociating product molecule when the collision partner is far away. This is obviously a surface which must be crossed by every associating system, but of course this surface may be recrossed again before the perturbing collision partner is out of range. The difference between the total energy and H_o is then

$$H - H_o = \frac{P^2}{2M} + \frac{p_3^2}{2\mu} + (V - V_o) \tag{9.46}$$

where M is the total mass of the system and P is the momentum of the center of mass, p_3 is the momentum of the collision partner relative to the center of mass of the associating pair and μ is the reduced mass for this collision, and finally

$(V - V_o)$ is the potential perturbation felt by the associating pair upon approach of the collision partner. Thus, the derivatives of H_o and $H - H_o$ are

$$\frac{\partial H_o}{\partial \vec{q}} = \text{grad } V_o \qquad \frac{\partial H_o}{\partial \vec{p}} = \frac{\vec{p}}{m}$$

$$\frac{\partial (H - H_o)}{\partial \vec{p}} = 0 \qquad \frac{\partial (H - H_o)}{\partial \vec{q}} = \text{grad}(V - V_o)$$

and all other derivatives of H_o vanish. Note that each of these vector derivatives corresponds to three terms in the Poisson bracket expression for $(\partial H_o/dt)$, Eq. (9.36).

$$\frac{dH_o}{dt} = -\frac{\vec{p}}{m} \text{grad}(V - V_o) \tag{9.47}$$

The integrations can be carried forward analytically for this simple choice of H_o, and Keck has refined this somewhat by choosing a surface that takes into account the rotational barrier and also requires that the collision partner come within a certain distance of the associating pair; Keck uses this latter distance as a variational parameter to minimize the recombination rate coefficient. However, the choice of surfaces which can be handled analytically is rather limited, whereas we need not bother to find the optimum surface for the computer calculations; a simple surface like Wigner's choice of H_o will suffice because the computer can count the number of systems that recross this surface and then correct the calculated crossing rate. This means, of course, that the trajectory must be computed until it is far enough from the surface that there exists a negligible probability the system will return and recross the surface. Note that the trajectories starting at S must also be followed backward in time, to make sure whether the system has not already crossed the dividing surface. In practice, this is not a difficult choice to program into the computer; the collision partner is merely required to recede from the associated pair and be at a distance where it perturbs the system negligibly. Thus, the advantage of the phase space-sampling scheme is that a reasonable choice of surface S will assure that most of the systems sampled will be reactive, and the system trajectory in phase space need be followed a relatively short distance, both of which greatly reduce the computing time required. The disadvantage of this approach is that the sample chosen will not correspond to any given initial state; however the sample should correspond to a Boltzmann distribution of initial systems since the Gibb's distribution in phase, Eq. (9.37), is used as a weighting factor.

9.7 NONHYDROGEN LIKE POTENTIALS

Not all potentials can be well described by the LEPS model, which has been derived for the case where all the atom pairs in the system interact something like two H atoms. Halogens can be treated by the LEPS model because the 7-electron shell behaves electronically like a one-electron system; this means that only one bonding potential and one antibonding potential (the singlet and triplet potentials, respectively) occurs for this case, and these can be described by the London formula in terms of integrals like K and J. However, when one treats systems with atoms like O, N, C, S, etc., the situation grows more complex. These multiple electron systems interact along a multiplicity of potential surfaces depending upon

how the electron spin vectors add up. For example, two N atoms in the ground state have 3 p electrons each and can interact along four different potential surfaces, the $^1\Sigma$, $^3\Sigma$, $^5\Sigma$, and $^7\Sigma$ potentials. Meador (ref. 7) treats these with a London-like model in which the exchange integrals for the p electrons are allowed to take all possible combinations of pairing. In the case of O atoms, with four p-electrons each, the multiplicity of interaction potentials increases to 32. Also in systems where p-orbitals are occupied, these orbitals have directional characteristics and the minimum potentials generally occur in bent configurations rather than the linear configuration obtained for purely s-orbital electrons. These complications add to the uncertainty of the model potentials, so typically the potential surfaces are then generated by taking the spectroscopically observed interactions for all the atom pairs in isolation, and for the multiatom system also if it is stable, and fit these regions together with empirical smoothing functions. A case in point is the reaction

$$C\ell O + O \rightarrow C\ell + O_2 \tag{9.48}$$

treated in this way by Jaffe (ref. 14). This reaction is thought to be an important step in the chlorine-catalyzed destruction of O_3 in the earth's upper atmosphere. The measured reaction rates were conflicting at the time of Jaffe's paper; some upper atmosphere scientists had been led to conclude that the rate coefficient for Eq. (9.48) had no temperature dependence whatever, which is clearly unreasonable in view of the fact that a $T^{1/2}$ dependence must remain due to the collision rate between gas particles, even if there is no activation energy whatsoever (unless the cross section for reaction should decrease with increasing collision energy at the threshold of the reaction, which is an unlikely phenomenon). Jaffe's calculations were performed to help resolve this inconsistency, using an empirical potential energy surface constructed to fit experimental data for $C\ell O$, O_2, and $C\ell O_2$ molecules. Then smoothing functions used to join one potential region to the others allowed for a variation in the reaction barrier height, so this was systematically varied to give reasonable agreement with data. The usefulness of the calculation model lies in the fact that once its activation energy has been calibrated with experiment, it can then be used to get a probable temperature variation for the rate coefficient.

Figures 9.8(a), (b), and (c) show the smoothed potential surfaces used by Jaffe for the reactions of Eq. (9.48) for three different configurations representing the angles α between the vectors R (Cℓ - O) and R (O - O) of 90°, 110°, and 130°, respectively. The 110° angle gives the minimum potential barrier. Figure 9.9 shows one of the trajectories for a $C\ell O + O$ system traversing this potential surface. One observes the complex vibrational motions in the short-lived $C\ell O_2$ activated complex that eventually dissociates to the products $C\ell + O_2$.

An Arrhenius plot of the rate constant for the $C\ell O + O \rightarrow C\ell + O_2$ reaction is shown on figure 9.10. The solid lines are Jaffe's calculations for the reaction barriers of 0, 0.5, and 1.0 Kcal/mol. Jaffe concludes that a probable rate coefficient is

$$\alpha = 4.36\times10^{-11} \exp(-191/T) \text{ cm}^3/\text{molecule-sec} \tag{9.49}$$

This rate is consistent with the data of Basco and Dogra (ref. 15) and of Park (ref. 16), and in view of the uncertainties in the potential surface, it is reasonably consistent with the data of Freeman and Phillips (ref. 17). It is clearly lower than the remaining data by a factor of 2 to 3, though the activation energy deduced by Clyne and Nip (ref. 18) is about 0.6 Kcal/mol, reasonably consistent with Jaffe's 0.5 Kcal/mol. The experimental data comes from a wide variety of techniques; Park's

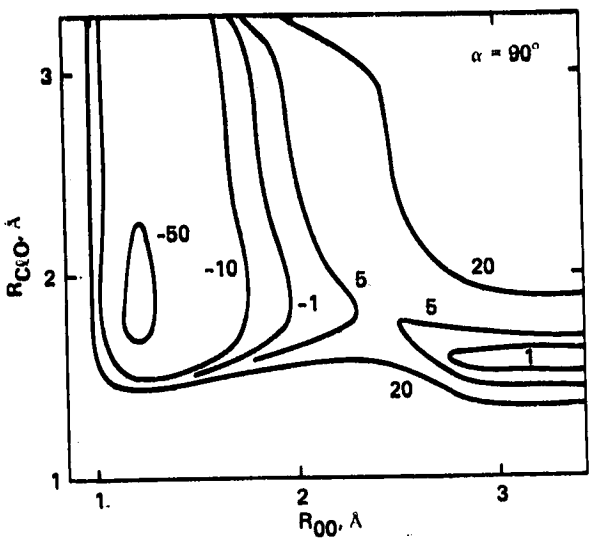

(a) α = 90°.

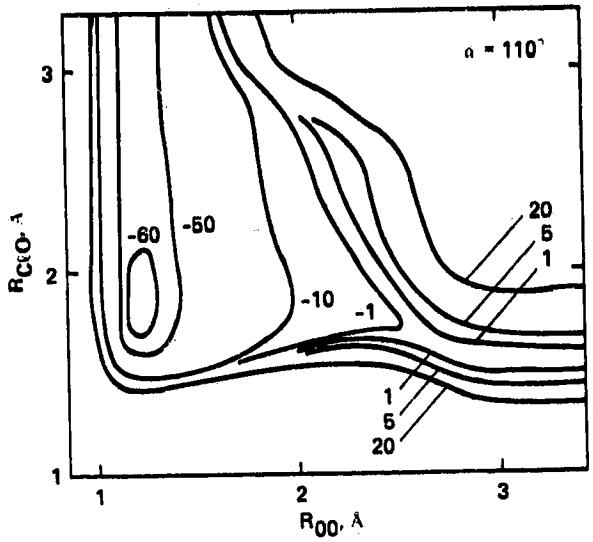

(b) α = 110°.

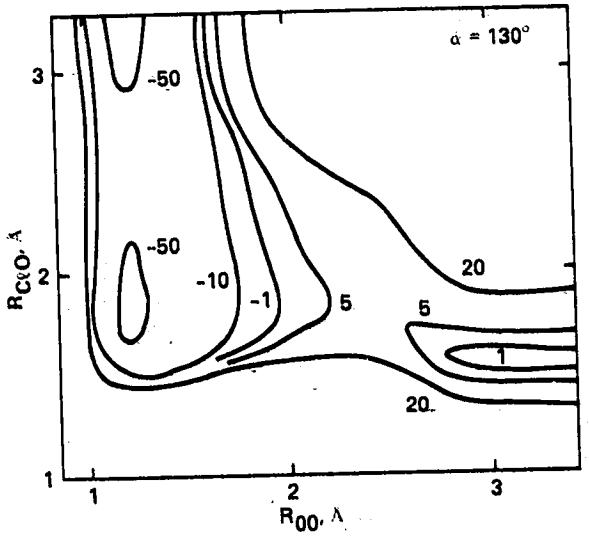

(c) α = 130°.

Figure 9.8- Ground state potential surfaces for Cℓ + O + O interaction for different angles α between R(Cℓ - O) and R(O - O) vectors.

high temperature data comes from a shock-tube measurement of the reaction rate in the endothermic direction, whereas the room temperature data come from flash photolysis and from microwave discharge techniques measuring the reaction in the exothermic direction. Thus, it is not at all surprising to find this much variation in the absolute value of the rate data (as we have seen in previous chapters, a factor of 2 to 3 scatter in data is typical, and each experimental technique also involves some uncertainties peculiar to itself). The calculations, together with experiment, do establish the temperature variation of the reaction within reasonable limits at the very least.

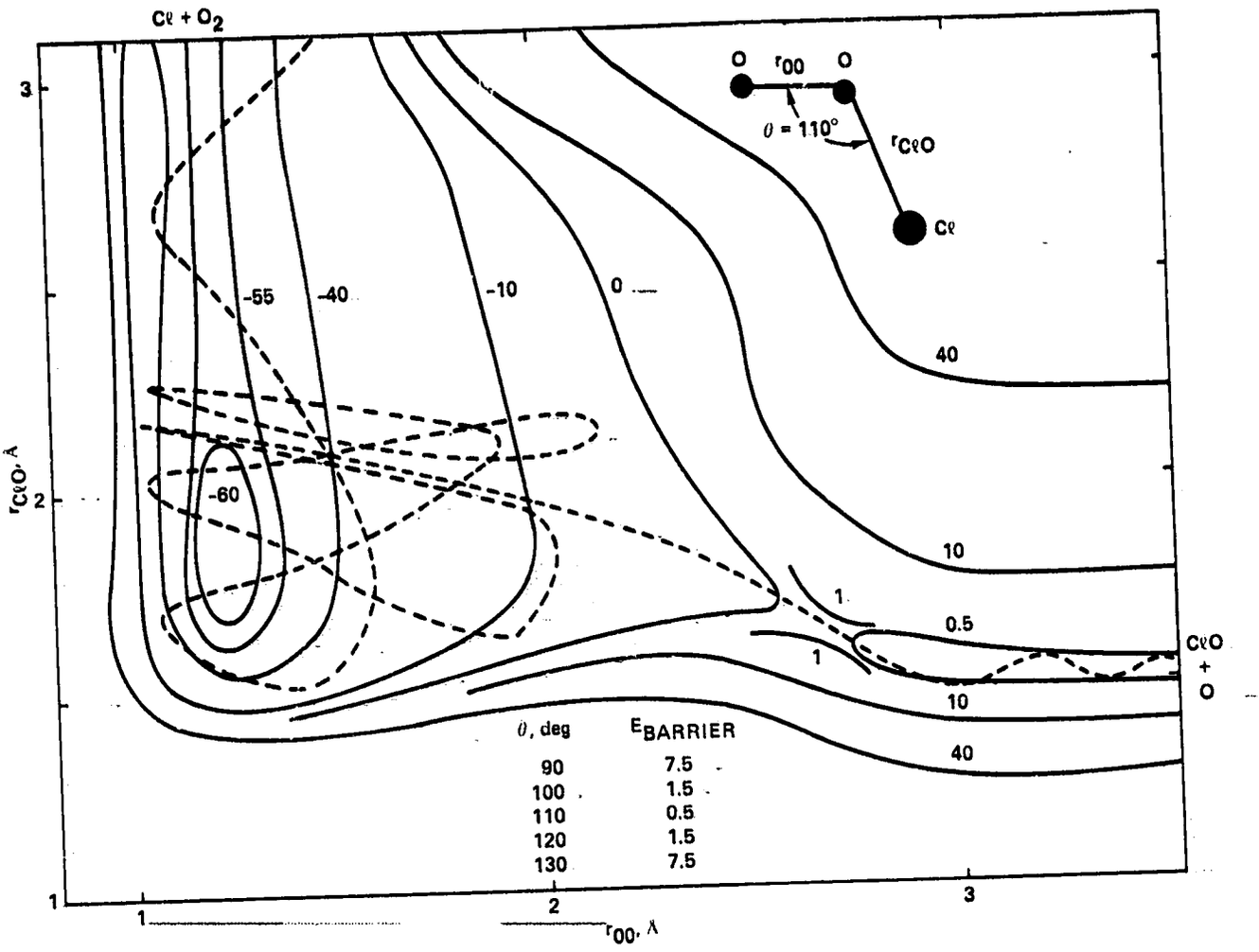

Figure 9.9- Ground state potential surface for CℓOO.

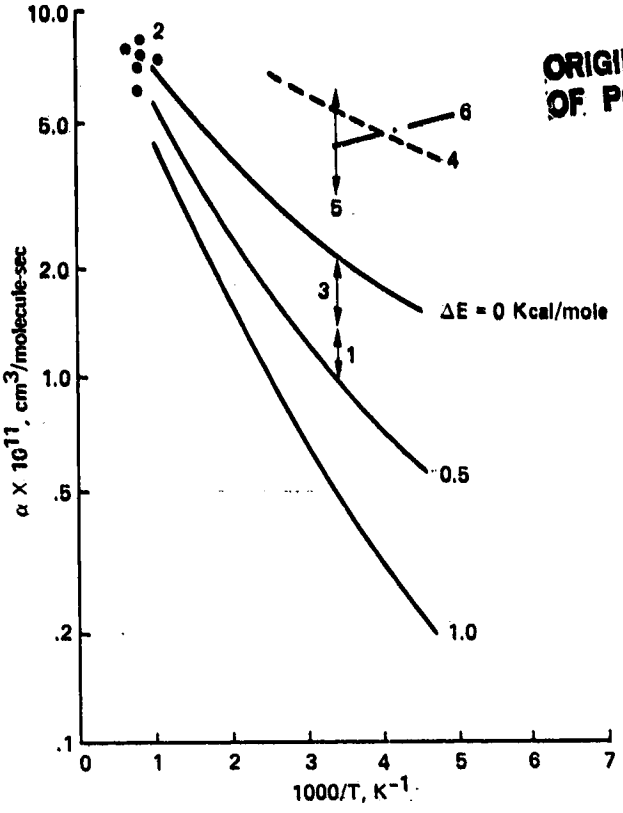

Figure 9.10- Arrhenius plot of rate constants for $C\ell O + O \rightarrow C\ell + O_2$. Solid curves are calculations of Jaffe (ref. 14). Data: ↕① Basco and Dogra (ref. 15), •② Park (ref. 16), ‡③ Freeman and Phillips (ref. 17), ---④ Clyne and Nip (ref. 18), ‡⑤ Bemand et al. (ref. 19), -·-⑥ Zahniser and Kaufman (ref. 20).

9.8 CONCLUDING REMARKS

For those cases where the ground state potential of a system is well below the energy of any excited state (so that transitions to the excited states can be ignored) and where all the reacting particles are heavy (i.e., no free electrons), the reacting system can usually be adequately treated as a classical system moving on a single potential surface. The numerical calculations of reaction trajectory can be made to any desired degree of accuracy, provided that a large, fast computer is available; the obstacle to accurate calculations of reaction rates is the uncertainty in approximations to the potential surfaces. The London-Eyring-Polyani-Sato (LEPS) potentials are reasonably good approximations for systems involving interactions only between hydrogen and halogen type atoms, but even for this case these potentials are very sensitive to the approximations used to account for the effect of the overlap integrals involved and spin-orbit coupling may be significant (ref. 21). For more electronically complex atoms the potentials used are expressions compounding harmonic or Morse potentials that fit the observed vibrational spectra of the isolated species. These potentials are faired into one another with purely empirical smoothing functions; the smoothing functions are adjusted until the resulting potential does not have any unlikely ridges or troughs and the reaction barrier is about equal to the observed activation energy. This procedure does allow one to at least extrapolate the experimental data with reasonable confidence to temperatures that are experimentally

inaccessible. This has been done, for example, in the case of the ClO + O reaction, believed to be important in the destruction of O_3 in the upper atmosphere, with results that at least tend to clarify the uncertainties. Aside from a few cases like this, and a few very instructive illustrative examples, the extreme labor and cost of performing the numerical calculations will be warranted only when reliable potentials become available. Modern quantum chemistry is rapidly approaching the capability to do this, although the problem will be a formidable one at this level of precision where multiple integrals and spin-orbit interactions will need to be taken into account.

REFERENCES

1. Glasstone, S.; Laidler, K. J.; and Eyring, H.: The Theory of Rate Processes. McGraw Hill, New York, 1941.

2. Sato, S.: On a New Method of Drawing the Potential Energy Surface. J. Chem. Phys., vol. 23, Mar. 1955, pp. 592-593; Potential Energy Surface of the System of Three Atoms. Ibid, vol. 23, Dec. 1955, p. 2465.

3. Parr, C. A.; and Truhlar, D. G.: Potential Energy Surfaces for Atom Transfer Reactions Involving Hydrogens and Halogens. J. Phys. Chem., vol. 75, June 1971, pp. 1844-1860.

4. Pauling, L.; and Wilson, E. B., Jr.: Introduction to Quantum Mechanics. McGraw Hill, New York, 1935.

5. Eyring, H.; Walter, J.; and Kimball, G. E.: Quantum Chemistry. John Wiley & Sons, New York, 1944.

6. Slater, J. C.: Electronic Structure of Molecules. In Quantum Theory of Molecules and Solids, vol. 1, McGraw Hill Co., New York, 1963.

7. Meador, W. E.: The Interaction Between Nitrogen and Oxygen Molecules. NASA TR R-68, 1960.

8. London, F.: Quantum Relations of Activation. Z. Electrochem., vol. 35, Sept. 1929, pp. 552-555.

9. Boato, G.; Careri, G.; Cimino, A., et al.: Homogeneous Exchange Reaction Between Hydrogen and Deuterium. J. Chem. Phys., vol. 24, April 1956, pp. 783-791.

10. Karplus, M.; Porter, R. N.; and Sharma, R. D.: Exchange Reactions with Activation Energy. I. Simple Barrier Potential for H, H_2. J. Chem. Phys., vol. 43, Nov. 1, 1965, pp. 3259-3287.

11. Jaffe, R. L.; and Anderson, J. B.: Classical Trajectory Analysis of the Reaction $F + H_2 \rightarrow HF + H^*$. J. Chem. Phys., vol. 54, Mar. 1, 1971, pp. 2224-2236.

12. Jaffe, R. L.; Henry, J. M.; and Anderson, J. B.: Variational Theory of Reaction Rates: Application to $F + H_2 \rightleftarrows HF + H$. J. Chem. Phys., vol. 59, Aug. 1, 1973, pp. 1128-1141.

13. Wigner, E.: Calculation of the Rate of Elementary Association Reactions. J. Chem. Phys., vol. 5, Sept. 1937, pp. 720-725.

14. Jaffe, R. L.: Calculated Rate Constants for the Reaction $C\ell O + O \rightarrow C\ell + O_2$ between 220 and 1000 K. Chem. Phys., vol. 40, July 1, 1979, pp. 185-206.

15. Basco, N.; and Dogra, S. K.: Reactions of Halogen Oxides Studied by Flash Photolysis II. The Flash Photolysis of Chlorine Monoxide and of the CℓO Free Radical. Proc. Roy. Soc. Lond., vol. A323, June 22, 1971, pp. 401-415.

16. Park, C.: Rates of Reactions $C\ell O + C\ell O \rightarrow C\ell_2 + O_2$ and $C\ell O + O \rightarrow C\ell + O_2$ at Elevated Temperatures. J. Phys. Chem., vol. 80, Mar. 11, 1976, pp. 565-571.

17. Freeman, G. C.; and Phillips, L. F.: Kinetics of Chlorine Oxide Reactions. I. The Reaction of Oxygen Atoms with $C\ell_2O$. J. Phys. Chem., vol. 72, Aug. 1968, pp. 3025-3028.

18. Clyne, M. A. A.; and Nip, W. S.: Reactions of Chlorine Oxide Radicals, Part 6 - The Reaction $O + C\ell O \rightarrow C\ell + O_2$ from 220 to 426 K. J. Chem. Soc. London, Faraday Trans. Part 1, Physical Chem., vol. 72, 1976, pp. 2211-2217.

19. Bemand, P. P.; Clyne, M. A. A.; and Watson, R. T., Jr.: Reactions of Chlorine Oxide Radicals. Part 4 - Rate Constants for the Reactions $C\ell + OC\ell O$, $O + OC\ell O$, $H + OC\ell O$, $NO + OC\ell O$, and $O + C\ell O$. J. Chem. Soc. London, Faraday Trans., Part 1, Physical Chem., vol. 69, 1973, pp. 1356-1374.

20. Zahniser, M. S.; and Kaufman, F.: Kinetics of the Reactions of $C\ell O$ with O and with NO*. J. Chem. Phys., vol. 66, Apr. 15, 1977, pp. 3673-3681.

21. Jaffe, R. L.; Morokuma, K.; and George, T. F.: Ab Initio and Semiempirical Study of Multiple Surfaces and their Analytic Continuation for Collinear $F(^2P_{3/2}, ^2P_{1/2}) + H_2 \rightarrow FH + H$. J. Chem. Phys., vol. 63, Oct. 15, 1975, pp. 3417-3424.

CHAPTER X QUANTUM SCATTERING THEORY

10.1 SUMMARY

The elements of quantum scattering theory are introduced and the relations between classical scattering parameters and the quantum scattering parameters are defined. The S-wave scattering from a spherical potential well is developed, which applies when the potential domain is small compared to the wavelength of the incident particle. The scattering amplitude is given in terms of the change in phase that is produced by the perturbing potential in the scattered particle's standing wave function. The cross section is derived for hard sphere scattering, and also for the Born approximation that applies when the potential is a small perturbation compared with the energy of the incident beam particle. Some examples are cited for the case of a slowly varying field where the WKB approximation can be used. Finally, the difference in scattering of like particles and of unlike particles due to symmetry considerations are discussed.

10.2 INTRODUCTION

Quantum scattering theory has, up to the present time, been primarily applied to elastic scattering problems rather than to reactive scattering, at least so far as quantitative results are concerned. However, the theory does contain the elements of a rigorous approach to reaction processes, and with the application of large, high-speed computers to the problem, this approach may ultimately provide useful numerical results. Therefore, it seems appropriate in a text on reaction processes to include some discussion of quantum scattering theory.

The number of publications on elastic scattering alone is enormous and it would be impossible to include here all the viewpoints presented. However, in spite of all the approximations and variations in theoretical modeling that have appeared since then, the foundations of the theory have not really changed since the 1930s, and the classic text by Mott and Massey (ref. 1), first published in 1933 with a third edition published in 1965, remains among the best expositions of the fundamentals that can be found. More recent texts by Goldberger and Watson (ref. 2) and by Newton (ref. 3), and by Rodberg and Thaler (ref. 4) are particularly helpful. Scattering theory has historically been based on the time-independent stationary scattering states that are solutions to the steady-state Schroedinger equation obtained when the usual separation of time and spatial variables is assumed; the rigorous justification of this formalism came almost 30 years later with the development of the time-dependent theory, which is reviewed in a text by Taylor (ref. 5). The fundamentals most important in a numerical approach to scattering problems are stressed in a text by Smith (ref. 6). Stallcop (ref. 7) developed approximations in a form most useful for numerical calculations using computers. All of the above work is limited to elastic scattering.

Although quantum scattering theory can handle reactive collisions in principle, very little quantitative work on reactive collisions has been performed. Even if the theoretical model were developed, accurate potential surfaces are not available and it is not very economical to expend large amounts of computer time to solve problems in an approximate manner. However, recently Kupermann and his coworkers (refs. 8-10) have produced some of the first rigorous quantum solutions for simple reactive molecular systems, such as $H + H_2$. This work is no doubt a forerunner of other rigorous

reactive scattering solutions that will be forthcoming. However, as Kupermann points out, the computer time needed for these solutions is severe and becomes increasingly worse as the molecular weights and electron numbers increase; thus these rigorous solutions will for some time yet be limited to selected check-point calculations that can be used to evaluate the quality of approximate methods, such as those discussed in the preceding chapters.

The primary advantage gained in use of quantum scattering theory is that time-dependent trajectories are replaced with spatially dependent wave functions, a procedure which not only simplifies the calculation but also avoids the failure of some semiclassical methods to provide conservation of energy and angular momentum during the collision event. Since there are so few quantitative results of significance for engineering applications to serve as illustration, the primary purpose of this chapter will be to outline a concise review of the fundamental concepts involved in quantum scattering theory, that can help engineers follow the literature and intelligently apply such quantitative results as may be forthcoming. Most of these basic concepts can be illustrated by limiting the discussion to elastic scattering in spherically symmetric force fields and without concern for relativistic effects. The nonrelativistic model is a good approximation for most practical problems involving rate processes in gases below 20,000 K. Spherically averaging the potential field is a convenience that is not rigorous but which often provides approximately correct results for small molecules (2 to 3 atoms) provided they do not possess a large dipole moment. It may be noted that purely elastic scattering theory is useful in engineering evaluation of transport properties in gases.

Before beginning the discussion of quantum-scattering-theory proper, a few remarks about the correspondence principle will be appropriate. Classically, a force field that extends to infinity would give an infinite scattering cross section. However, quantum theory gives a finite value. The reason for this apparent departure from the correspondence principle is that in classical theory all deflections are counted, no matter how small, whereas in quantum theory only those deflections that exceed the limits of the uncertainty principle are counted. Experimentally, any apparatus has a finite resolving power so that only a finite cross section is ever measured. In principle, if the resolution of measurement is improved one could expect to approach the limiting value predicted by the quantum uncertainty principle.

The quantum and classical descriptions of scattering will agree at finite miss distances provided that: (1) the deBroglie wavelength of the motion of the reduced mass particle is much less than the distance of closest approach, and (2) the deflection of the particle is not obscured by the normal spread of the wave packet which describes the relative motion between the collision pair. In this sense, the correspondence principle is obeyed.

The uncertainty principle sets some real limits on the experimental resolution that can be achieved in molecular beam-type scattering measurements. If the beam axis is taken along the z-direction, then the uncertainty in one of the transverse directions x or y is given by

$$m \, \Delta u_y \, \Delta y > h \, . \tag{10.1}$$

where Δu_y is the uncertainty in velocity along the y coordinate and Δy the uncertainty in y coordinate position. The classical orbit concept is valid if the miss distance b is large compared with Δy

$$b >> \Delta y \simeq \frac{\hbar}{m\,\Delta u_y} \qquad (10.2)$$

The angle of spreading of the wave packet representing a beam particle is $\Delta u_y/u_o$, where u_o is the beam velocity, and the deflection angle θ, to be measurable, must be larger than this beam spreading.

$$\theta > \frac{\Delta u_y}{u_o} \simeq \frac{\hbar}{bmu_o} \qquad (10.3)$$

Classically, the deflection is given by a relation such as

$$\theta \simeq \frac{F_y \tau}{mu_o} \simeq \frac{(\text{grad } U)(b/r)\tau}{mu_o} \qquad (10.4)$$

where the duration of impact τ with $r \simeq b$ is the order of b/u_o

$$\theta b \simeq \frac{\text{grad } U\, b^2}{mu_o^2} \qquad (10.5)$$

Thus, if the intermolecular potential U falls off more rapidly than r^{-1} so that (grad U) falls off more rapidly than r^{-2}, the product θb will go to zero at large miss distance, and the cross section will approach a finite limit.

The coulomb potential is a special case of interest; this potential varies as r^{-1} and θb stays roughly constant at all miss distances b. Thus, the cross section for scattering in a Coulomb potential is infinite, and electron motion in a highly ionized plasma must be described as the result of simultaneous perturbations from many nearby neighbors rather than the result of just two-body collisions. The effect is rather well described by the simple Debye shielding model (see chapter 8, ref. 11).

Another problem of practical interest is the elastic scattering of an electron in the static field of any atom. If the perturbation of the atom by the electron is ignored, the potential energy a distance r from the center of the atom is

$$U(r) = -\frac{Ze^2}{r} + 4\pi e\left[\frac{1}{r}\int_o^r \rho(r)r^2\,dr + \int_r^\infty \rho(r)r\,dr\right] \qquad (10.6)$$

where $\rho(r)$ is the electron-charge density about the nucleus. The charge inside the shell r acts as though it is all concentrated at the center, whereas the potential associated with the charge outside the shell r is as though the charge is a layer of surface charge, or layers of concentric surface charge. The total potential is often approximated by an effective or screened nuclear charge

$$U(r) = -\frac{Z_p(r)e^2}{r} \qquad (10.7)$$

where Z_p falls off roughly exponentially with r in the limit of large r. Thus, a finite value of cross section results.

With just these simple concepts one can show that very high experimental resolution of scattering must be achieved to determine an accurate cross section. The leas demanding case is for an electron hitting a target molecule. For 1% accuracy in cros section, the experimenter must determine the scattering angle in laboratory coordinates within 11° if the electron kinetic energy is 1 eV, but within 2.3° at 100 eV, and within the difficult precision of 0.2° at 10,000 eV. For atomic projectiles, the requirements are much more severe. For a mere 10% accuracy in cross section for scattering of He by He, the scattering angle must be determined within 3.6° at 0.02 eV collision energy, and within 0.6° at 1 eV. The situation becomes even more difficult when more massive particles are involved. As a result, most of the experimental data that are available for comparison with scattering theory is limited to electron scattering, plus a lesser amount of proton and He^+ scattering, and most of this at higher energies than are useful for typical engineering applications. Neutra species beams are much harder to produce and collimate and detect, so that very littl data for neutral-neutral species scattering exist.

10.3 DEFINITIONS AND CLASSICAL THEORY

Consider a homogeneous beam of particles approaching a fixed sample of target gas. From the separation of the center of mass motion such as done in chapter 1, we know that the behavior of the two particles is like the behavior of a single hypothetical particle of reduced mass m interacting with a fixed center of force, or in other words interacting with a second particle of infinite mass. Measurements made in the laboratory coordinate system must be reduced to the center of mass coordinate system to compare with theory. For example, if θ_ℓ is the scattering angle observed for the beam particle in laboratory coordinates and θ is the scattering angle in center of mass coordinates, these are simply related by conservation of energy and momentum (refs. 12 and 13)

$$\tan \theta_\ell = \frac{\sin \theta}{\frac{m_1}{m_2} + \cos \theta} \tag{10.8}$$

where m_1 is the mass of the beam particle and m_2 is the mass of the target particle. Thus, if $m_1 << m_2$, as in the case of electrons bombarding atoms or molecules, $\theta \simeq \theta_\ell$. If the beam particles and target particles have the same weight, $m_1 = m_2$ and $\theta = 2\theta_\ell$. In all subsequent discussion, the collision system will be viewed as the particle of reduced mass in the fixed force field.

A portion of the beam molecules are deflected into an element of solid angle $d\omega$. Let $G\, d\omega$ be the fraction of the total beam passing through unit area which is scattered into the element of solid angle $d\omega$ (see fig. 10.1(a)). The coefficient G is known as the scattering coefficient. Generally, G will vary with direction

$$G\, d\omega = G(\theta,\phi)\sin\theta\, d\theta\, d\phi \tag{10.9}$$

If nu particles arrive per unit area per unit time, $nuG\, d\omega\, dt$ is the probable number that will be scattered in the interval dt and angular element $d\omega$. Thus, G has the dimensions cm^2/molecule-steradian.

Usually, we are interested in symmetrical scattering, as when spherically symmetric potentials are assumed, for example. Even where the molecules are polarized

we assume that the thermal motion randomizes all orientations so that the experiment is really responding to a sort of orientation-averaged intermolecular potential, which is again spherically symmetric. For such cases, the polar scattering coefficient, $F(\theta)$, is most useful

$$F(\theta)d\theta = 2\pi G(\theta)\sin\theta\, d\theta \qquad (10.10)$$

This is the fraction of the beam incident on a unit area which is scattered through an angular element $d\theta$ about θ. The total collision cross section S is

$$S = \int_0^{\pi} F(\theta)d\theta \qquad (10.11)$$

The polar scattering coefficient is related to the miss distance b, as shown in figure 10.1(b). The fraction of the beam which flows through the element of area $2\pi b\, db$ is assumed to all be scattered at the same angle, from θ to $\theta + d\theta$.

$$F(\theta)d\theta = 2\pi b(\theta)db \qquad (10.12)$$

Consequently, the polar scattering coefficient $F(\theta)$ may be defined

$$F(\theta) = 2\pi b\left|\frac{db}{d\theta}\right| \qquad (10.13a)$$

or alternatively the miss distance b may be defined

$$b = \frac{F(\theta)}{2\pi}\left|\frac{d\theta}{db}\right| \qquad (10.13b)$$

The absolute values in equations (10.13a) and (10.13b) indicate that it doesn't matter whether the deflection θ is positive or negative; in either case a given amount of energy and momentum has been transferred, and the mass flow has been impeded equally.

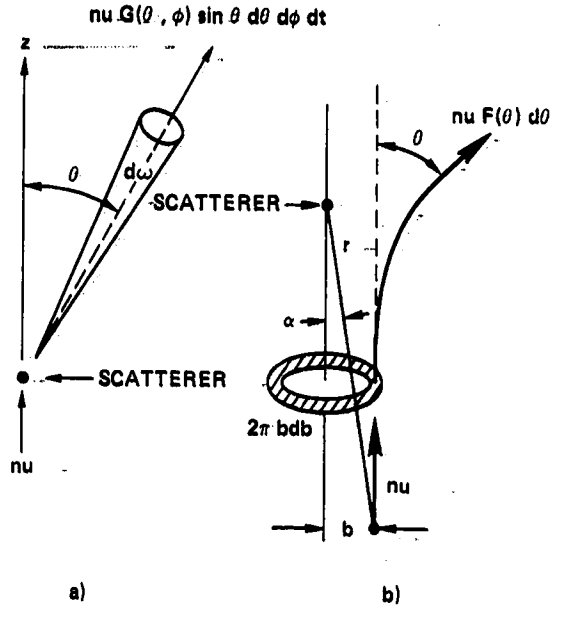

Figure 10.1- (a) Scattering coefficient $G(\theta,\phi)$. (b) Polar scattering coefficient $F(\theta)$.

Classically, the angle of deflection is simply obtained from conservation of angular momentum and energy

$$mr^2\dot{\alpha} = mub \qquad (10.14)$$

$$\frac{m}{2}(\dot{r}^2 + r^2\dot{\alpha}^2) + U(r) = \frac{mu^2}{2} \qquad (10.15)$$

where α is the angle between the z-axis, aligned with the velocity vector u, and the radius vector r between the scattering center and the incoming particle (see fig. 10.1(b)).

Solving for $d\alpha/dr$, one obtains

$$\frac{d\alpha}{dr} = \frac{\dot{\alpha}}{\dot{r}} = \frac{b}{r^2}\left(1 - \frac{2U}{mu^2} - \frac{b^2}{r^2}\right)^{-1/2} \qquad (10.16)$$

Since the path is symmetrical about r_o, the point of closest approach, the total increase in angle α during the collision is

$$\Delta\alpha = \pi - \theta = 2\int_{r_o}^{\infty} \frac{d\alpha}{dr}\, dr \qquad (10.17)$$

where the lower limit of this integral is given by

$$r_o^2 = b^2\left[1 - \frac{2U(r_o)}{mu^2}\right]^{-1} \qquad (10.18)$$

The angle of deflection θ is then

$$\theta = \pi - 2b\int_{r_o}^{\infty} \frac{dr}{r^2\{1 - [2U(r)/mu^2] - (b^2/r^2)\}^{1/2}} \qquad (10.19a)$$

which may be re-expressed in terms of the variable $x = r_o/r$

$$\theta = \pi - 2\int_{o}^{1} \frac{dx}{\{1 - [2U(r_o/x)/mu^2](r_o^2/b^2) - x^2\}^{1/2}} \qquad (10.19b)$$

As an example, the classical scattering coefficient for a hard sphere potential

$$U = \infty \quad r < r_o$$
$$= 0 \quad r_o < r \qquad (10.20)$$

becomes

$$\theta = \pi - 2\int_{o}^{1} \frac{dx}{[(r_o^2/b^2) - x^2]^{1/2}} = \pi - 2\arcsin\frac{b}{r_o} \qquad (10.21)$$

$$b = r_o \sin\frac{\pi - \theta}{2} = r_o \cos\frac{\theta}{2} \qquad (10.22)$$

$$\frac{db}{d\theta} = -\frac{r_o}{2}\sin\frac{\theta}{2} \qquad (10.23)$$

Thus, for hard spheres the polar scattering coefficient is

$$F(\theta) = 2\pi b \left|\frac{db}{d\theta}\right| = \frac{1}{2}\pi r_o^2 \sin\theta \tag{10.24}$$

and the scattering cross section is the constant

$$S = \int_o^\pi F(\theta)d\theta = \frac{\pi r_o^2}{2}\int_o^\pi \sin\theta\, d\theta = \pi r_o^2 \tag{10.25}$$

as it must be. In the case of a general potential $U(r)$, the cross section will then be a function of velocity u, of course. These classical definitions and results will be useful in interpretation of the physical meaning of the quantum scattering theory.

10.4 QUANTUM SCATTERING

In quantum theory the incident beam traveling along the z axis is represented by a plane wave function

$$\psi = C\, e^{i(kz-\omega t)} \tag{10.26}$$

where k is the wave number $2\pi/\lambda = p/\hbar = (2mE/\hbar)^{1/2}$. The circular frequency $\omega = 2\pi\nu = E/\hbar$. If the problem is formulated as a steady state one, then the factor $\exp(-i\omega t)$ is common to all the wave functions and may be disregarded.

The current density of the beam I is just the square of the wave function's amplitude multiplied by the beam velocity u, which is the beam particles' momentum p divided by the reduced mass m,

$$I = C^2 u = \frac{C^2 p}{m} \tag{10.27}$$

The total wave function is the sum of incident and scattered waves. The scattered wave should have the form of an outgoing spherical wave; at large r the amplitude falls as r^{-1} in order that current density falls as r^{-2}, and the total current of scattered particles is conserved.

$$\psi_s \sim \frac{C}{r} f(\theta) e^{ikr} \tag{10.28}$$

The coefficient $f(\theta)$ is called the scattering amplitude. The relation between $f(\theta)$ and $G(\theta)$ needs to be established, where G is considered a function of only θ because of spherical symmetry in the scattering potential. The radial current density at large r is,

$$u_o \frac{C^2 f^2}{r^2} dS = u_o C^2 f^2\, d\Omega = I f^2\, dr \tag{10.29}$$

Note that the assumption of elastic scattering has been used here, that is, the scattered beam velocity u_o is the same as the incident beam velocity. This

expression, Eq. (10.29), must equal the fraction of the incoming current which is scattered,

$$If^2(\theta)d\Omega = IG(\theta)d\Omega \tag{10.30}$$

Thus, the square of $f(\theta)$ is the same as the classical scattering coefficient. Note that it is unnecessary to know $\psi(r,\theta)$ completely to determine $G(\theta)$; only the asymptotic form need be known. One additional assumption here is that the incident beam does not pass through the surface element dS where the scattering is observed; in experimental situations collimation is always provided to minimize this mixing of incident and scattered beam flux.

To obtain $f(\theta)$ the time-independent wave equation for motion of a particle of reduced mass m and energy E in the potential field of a fixed scattering center is solved. The solution should have the asymptotic form

$$\psi \xrightarrow[r\to\infty]{} e^{ikz} + \frac{f(\theta)e^{ikr}}{r} \tag{10.31}$$

The steady-state Schroedinger equation with energy units of $\hbar^2/2ma_o^2$ and distance units of a_o takes a convenient, concise form

$$\nabla^2\psi + [k^2 - U(r)]\psi = 0 \tag{10.32}$$

As usual, separate the variables r and θ

$$\psi(r,\theta) = R(r)P(\theta) \tag{10.33}$$

Then the differential equation is separable into an equation for $R(r)$

$$\frac{1}{r^2}\frac{d}{dr}\left(r^2\frac{dR}{dr}\right) + \left[k^2 - U(r) - \frac{\ell(\ell+1)}{r^2}\right]R = 0 \tag{10.34}$$

and an equation for $P(\theta)$

$$\frac{1}{\sin\theta}\frac{d}{d\theta}\left(\sin\theta\frac{dP}{d\theta}\right) + \ell(\ell+1)P = 0 \tag{10.35}$$

Solutions to the Eq. (10.35) are just the Legendre polynomials $P_\ell(\cos\theta)$. Thus, the separated wave function of Eq. (10.33) may be expressed as a summation of these solutions

$$\psi(r,\theta) = \sum_{\ell=0}^{\infty} a_\ell P_\ell(\cos\theta)R_\ell(r) \tag{10.33a}$$

Each term in this sum is called a partial wave, representing that fraction of the incident beam which has angular momentum quantum number ℓ with respect to the scattering center

$$(mub)^2 = \ell(\ell+1)\hbar^2 \tag{10.36}$$

The coefficients a_ℓ represent the magnitude of the contribution to the scattering process furnished by each partial wave.

The radial wave functions $R_\ell(r)$ are solutions to Eq. (10.34). Usually $U(r)$ will always fall off faster than r^{-1} at large r and will not have a pole at the origin that is higher order than r^{-1}, for example, a decreasing exponential function of r which is often similar to realistic interaction potentials. Then let

$$R_\ell(r) = \frac{u_\ell\, e^{ikr}}{r} = \frac{g_\ell}{r} \tag{10.37}$$

Substituting Eq. (10.37) in (10.34), one obtains

$$\frac{d^2 g_\ell}{dr^2} + \left[k^2 - U(r) - \frac{\ell(\ell+1)}{r^2}\right] g_\ell = 0 \tag{10.38}$$

$$\frac{d^2 u_\ell}{dr^2} + 2ik\,\frac{du}{dr} - \left[U(r) + \frac{\ell(\ell+1)}{r^2}\right] u_\ell = 0 \tag{10.39}$$

For large r we expect $u(r)$ to be nearly constant, that is, the spherical wave must approach a plane wave. Then d^2u/dr^2 becomes negligible, and Eq. (10.39) becomes

$$2ik \int \frac{du}{u} \simeq \int_0^\infty \left[U(r) + \frac{\ell(\ell+1)}{r^2}\right] dr = 2ik\, \ln u \tag{10.40}$$

The integral converges if and only if $U(r)$ falls off faster than r^{-1}. When this integral converges rapidly, the assumption that u is a slowly varying function of r and that d^2u/dr^2 is negligible is well justified. Thus, an asymptotic form for $R(r)$ valid in such cases, is

$$R(r) \propto \frac{e^{ikr}}{r} \tag{10.41}$$

this can be expressed in the form

$$R(r) \propto \frac{1}{kr} \sin\left(kr - \frac{\ell\pi}{2} + \eta_\ell\right) \tag{10.42}$$

where η_ℓ is a constant for a given wave number k and $U(r)$, and is called the ℓth order phase shift. The term $-\ell\pi/2$ is added merely as a convention so that η_ℓ will be zero if $U(r)$ is zero.

Now to determine the constants a_ℓ in the expansion, the incoming plane wave is expanded in terms of partial waves

$$e^{ikz} = e^{ikr\cos\theta} = \sum_{\ell=0}^{\infty} (2\ell+1) i^\ell j_\ell(kr) P_\ell(\cos\theta) \tag{10.43}$$

The functions $j_\ell(kr)$ are the spherical Bessel functions of half-integer order

$$j_\ell(kr) = \left(\frac{\pi}{2kr}\right)^{1/2} J_{\ell+1/2}(kr) \tag{10.44}$$

The first few of these functions are

$$j_o = \frac{\sin(kr)}{kr} \tag{10.45a}$$

$$j_1 = \frac{\sin(kr)}{(kr)^2} - \frac{\cos(kr)}{(kr)} \tag{10.45b}$$

$$j_2 = \left[\frac{3}{(kr)^3} - \frac{1}{(kr)}\right]\sin(kr) - \frac{3}{(kr)^2}\cos(kr) \tag{10.45c}$$

and remaining functions may be evaluated with the recursion formula

$$j_{\ell+1} = \frac{2\ell + 1}{kr} j_\ell - j_{\ell-1} \tag{10.46}$$

For large r the asymptotic values of the spherical Bessel functions can be useful

$$j_\ell \xrightarrow[r\to\infty]{} \frac{1}{kr} \sin\left(kr - \frac{\ell\pi}{2}\right) \tag{10.47}$$

This asymptotic relation can be derived as follows. An expansion of Eq. (10.43) is made in terms of Legendre functions

$$e^{ikr\cos\theta} = \sum b_\ell j_\ell(r) P_\ell(\cos\theta) \tag{10.48}$$

Let $\cos\theta = t$, multiply both sides by P_ℓ and integrate from $\theta = 0$ to π or t from +1 to -1.

$$\int_{-1}^{1} e^{ikrt} P_\ell(t)dt = b_\ell j_\ell \int_{-1}^{1} P_\ell^2 \, dt = \frac{2b_\ell j_\ell(r)}{2\ell + 1} \tag{10.49}$$

Integrate by parts with $P_\ell(t) = u$ and $e^{ikrt}\, dt = dv$.

$$\int_{-1}^{1} e^{ikrt} P_\ell(t)dt = \frac{1}{ikr}\left|e^{ikrt} P_\ell(t)\right|_{-1}^{1} - \frac{1}{ikr}\int_{-1}^{1} e^{ikrt} \frac{dP_\ell}{dt} dt \tag{10.50}$$

The second term on the right of Eq. (10.50) is the order of r^{-2} for large r, so in the limit

$$\frac{2}{2\ell + 1} b_\ell j_\ell(r) \xrightarrow[r\to\infty]{} \frac{1}{ikr}\left|e^{ikrt} P_\ell(t)\right|_{-1}^{1} \tag{10.51}$$

A general property of the Legendre polynomial is

$$P_\ell(1) = 1 \tag{10.52a}$$

$$P_\ell(-1) = (-1)^\ell \tag{10.52b}$$

Thus, Eq. (10.51) becomes

$$\frac{2}{2\ell + 1} b_\ell j_\ell(r) \to \frac{2i^\ell}{kr} \sin\left(kr - \frac{\ell\pi}{2}\right) \tag{10.53}$$

Note that $\sin(kr - \ell\pi/2)$ becomes $\cos kr$ when ℓ is odd. The asymptotic form of the incident wave is thus

$$\psi_i = e^{ikz} \to \sum_\ell (2\ell + 1) i^\ell P_\ell(\cos\theta) \frac{\sin[kr - (\ell\pi/2)]}{kr} \tag{10.54}$$

The scattered wave is the total wave function given by Eqs. (10.33a) and (10.42), less the incident wave given by Eq. (10.54)

$$\psi_r = \sum_\ell \frac{P_\ell(\cos\theta)}{kr} \left[a_\ell \sin\left(kr - \frac{\ell\pi}{2} + \eta_\ell\right) - (2\ell + 1) i^\ell \sin\left(kr - \frac{\ell\pi}{2}\right)\right] \tag{10.55}$$

Substitute

$$\sin kr = \frac{e^{ikr} - e^{-ikr}}{2i}$$

and require that the term in e^{-ikr}/r must vanish, since this represents an incoming or spherical collapsing wave.

This boundary condition determines the values of the constant coefficients a_ℓ. The factors in brackets in the summation of Eq. (10.55) become

$$\left[a_\ell \sin\left(kr - \frac{\ell\pi}{2} + \eta_\ell\right) - (2\ell + 1) i^\ell \sin\left(kr - \frac{\ell\pi}{2}\right)\right]$$

$$= \frac{e^{i(kr - \ell\pi/2)}}{2i} [a_\ell e^{i\eta_\ell} - i^\ell(2\ell + 1)] - \frac{e^{-i(kr - \ell\pi/2)}}{2i} [a_\ell e^{-i\eta_\ell} - i^\ell(2\ell + 1)] \tag{10.56}$$

from which it is seen that

$$a_\ell = (2\ell + 1) i^\ell e^{i\eta_\ell} \tag{10.57}$$

The total wave function is thus

$$\psi = \sum_\ell (2\ell + 1) i^\ell e^{i\eta_\ell} P_\ell(\cos\theta) R_\ell(r) \tag{10.58}$$

and the effect of the scattering center has been to shift the phase of each of the partial waves by a different amount η_ℓ. The asymptotic expression for the scattered wave is

$$\psi_s = \sum_\ell \frac{P_\ell(\cos\theta)}{kr} \frac{e^{i(kr-\ell\pi/2)}}{2i} - (2\ell+1)i^\ell(e^{2i\eta_\ell} - 1) \tag{10.59}$$

The scattering amplitude $f(\theta)$ is, by comparison with Eq. (10.31)

$$f(\theta) = \frac{1}{2ik} \sum_\ell (2\ell+1)(e^{2i\eta_\ell} - 1)P_\ell(\cos\theta) \tag{10.60}$$

Note that $i^\ell \exp(-i\ell\pi/2)$ equals unity. The scattering amplitude is a complex function.

$$f(\theta) = A + iB \tag{10.61a}$$

$$A = \frac{1}{2k} \sum_\ell (2\ell+1)\sin 2\eta_\ell P_\ell(\cos\theta) \tag{10.61b}$$

$$B = \frac{1}{2k} \sum_\ell (2\ell+1)(1 - \cos 2\eta_\ell)P_\ell(\cos\theta) \tag{10.61c}$$

and the differential scattering coefficient is

$$G(\theta) = f^2(\theta) = A^2 + B^2 \tag{10.62}$$

Equation (10.60) may also be expressed

$$f(\theta) = \frac{1}{k} \sum_\ell (2\ell+1)e^{i\eta_\ell} \frac{e^{i\eta_\ell} - e^{-i\eta_\ell}}{2i} P_\ell(\cos\theta) \tag{10.63}$$

Thus

$$f^2(\theta) = \frac{1}{k^2}\left| \sum (2\ell+1)e^{i\eta_\ell} \sin\eta_\ell P_\ell(\cos\theta)\right|^2 \tag{10.64}$$

Integrate Eq. (10.64) over all solid angle to get the total cross section. Only those terms with $P_\ell^2(\cos\theta)$ survive this integration because of the orthogonality of Legendre polynomials, and the result is an expression for the total elastic scattering cross section.

$$S = \int_0^{2\pi}\int_0^{\pi} f^2(\theta)\sin\theta\, d\theta\, d\phi = \frac{4\pi}{k^2} \sum_\ell (2\ell+1)\sin^2\eta_\ell \tag{10.65}$$

All that remains is to evaluate the phase shift η_ℓ. At this point some approximation must always be made that is equivalent in one way or another to assuming a classical orbit, such as a straight line trajectory, and thus there is some question

whether the results are really more precise than the classical results, except that the quantum solutions have the wavelike character that is observed, whereas the classical solutions give a smoothed average result.

The most straightforward way to obtain the phase shifts η_ℓ, when the potential U(r) is known, is to numerically solve the Schroedinger equation of Eq. (10.38), and find the limiting value at large r.

$$R(r) = \frac{g(r)}{r} \xrightarrow[r\to\infty]{} \frac{1}{kr} \sin\left(kr - \frac{\ell\pi}{2} + \eta_\ell\right) \tag{10.66}$$

10.5 RELATION BETWEEN CLASSICAL IMPACT PARAMETER AND PARTIAL WAVES

Equation (10.36) equates the classical and quantum expressions for the angular momentum squared, and an impact parameter b_ℓ may be defined

$$b_\ell = \sqrt{\ell(\ell+1)}\,\frac{\hbar}{mu_o} = \sqrt{\ell(\ell+1)}\,\lambda_o = \frac{\sqrt{\ell(\ell+1)}}{k_o} \tag{10.67}$$

which represents a sort of mean miss distance for beam particles having the angular momentum $\ell\hbar$ with respect to the scattering center. The de Broglie wavelength of the beam particles is λ_o. The incident beam can be thought of as separated into partial waves entering tubular shells as shown in figure 10.2. The cross-section area for all shells containing the fraction of the beam with angular momentum less than or equal to $\ell\hbar$ is

$$S = \ell(\ell+1)\pi\lambda_o^2 \tag{10.68}$$

and the cross section for a single partial wave is

$$\frac{dS}{d\ell} = (2\ell+1)\pi\lambda_o^2 \tag{10.69}$$

This accounts for the weighting factor $(2\ell+1)$ which appears in the expansion of an incident wave into partial waves. The mean radius of the s-wave is zero, of the p-wave is $\sqrt{2}\lambda_o$, of the d-wave is $\sqrt{6}\lambda_o$, etc. A fairly good approximation for this mean radius is $(\ell+1/2)\lambda_o$. The outer radius of the tubular shell for a given ℓ may be taken as $(\ell+1)\lambda_o$.

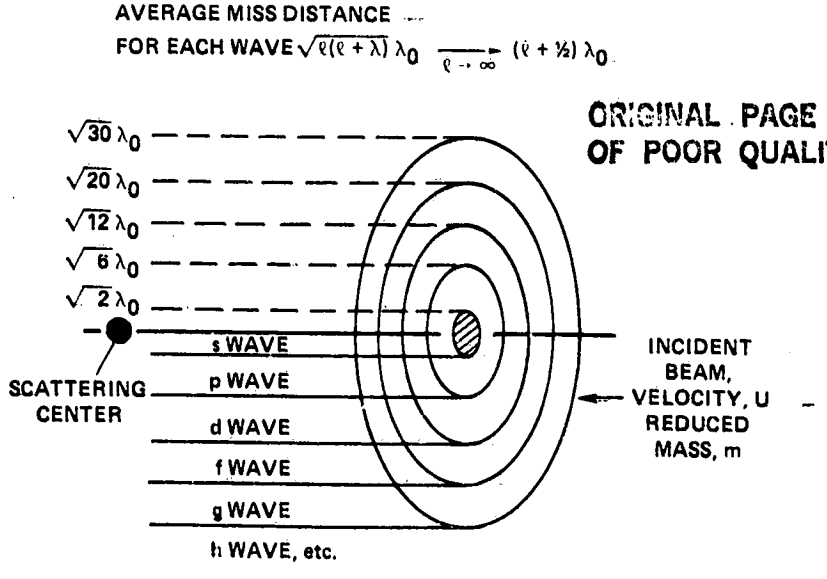

Figure 10.2- Partial waves of a molecular beam incident on a scattering center. $\lambda_o = \hbar/mu = 1/k_o$.

For heavy particles, λ_o is typically very small, at the collision velocities of interest, compared with the effective limits of realistic molecular scattering potentials; thus, a very large number of partial waves need to be included before the total effective cross section is accounted for. Only for the scattering of low velocity

electrons, where the momentum mu_o is small and λ_o is large, will a small number of partial waves suffice in a practical problem.

10.6 S-WAVE SCATTERING FROM A SPHERICAL POTENTIAL WELL

Consider the spherical potential well shown in figure 10.3

$$\begin{aligned} U(r) &= -U_o \ , \quad r < r_o \\ &= 0 \quad , \quad r_o < r \end{aligned} \tag{10.70}$$

for the case where r_o is smaller than the de Broglie wavelength λ_o. In this case only s-waves reach the potential well. Experimentally, s-wave scattering is often dominant in low velocity electron scattering. The total wave function for incident and scattered waves is then

$$\psi = e^{ik_o z} + f_o \frac{e^{ik_o r}}{r} \sim \frac{\sin k_o r}{k_o r} + f_o \frac{e^{ik_o r}}{r} \tag{10.71}$$

and the scattering amplitude f_o is

$$f_o = \frac{1}{2ik_o} (e^{2i\eta_o} - 1) \tag{10.72}$$

The asymptotic form of the total wave function is

$$\psi \sim \frac{e^{i\eta_o}}{k_o r} \sin(kr + \eta_o) \tag{10.73}$$

and the total elastic scattering cross section is

$$S = \frac{4\pi}{k_o^2} \sin^2 \eta_o \tag{10.74}$$

The phase angle η_o for the s-wave is evaluated from the solution of Eq. (10.38)

$$\frac{d^2 g}{dr^2} + [k_o^2 - U(r)]g = 0 \tag{10.75}$$

Inside the well, the solution which vanishes at the origin is

$$g = A \sin kr \tag{10.76}$$

where

$$k = \left[\frac{2m(E + U_o)}{\hbar}\right]^{1/2} \tag{10.77}$$

The wave function and its derivative outside the well are now matched to the wave-function inside the well.

$$\frac{e^{i\eta_o}}{k_o} \sin(k_o r_o + \eta_o) = A \sin kr_o \tag{10.78}$$

$$e^{i\eta_o} \cos(k_o r_o + \eta_o) = Ak \cos kr_o \tag{10.79}$$

Dividing Eq. (10.78) by (10.79), one obtains

$$\tan(k_o r_o + \eta_o) = \frac{k_o}{k} \tan kr_o \tag{10.80}$$

$$\eta_o = -k_o r_o + \arctan\left(\frac{k_o}{k} \tan kr_o\right)$$

$$= -\frac{\sqrt{2mE_o}}{\hbar} r_o + \arctan \frac{\tan \sqrt{2m(E_o + U_o)}(r_o/\hbar)}{1 + U_o/E_o} \tag{10.81}$$

Equation (10.81) gives the phase shift in terms of the incident beam energy E_o, the well depth U_o, and the well radius r_o.

The phase shift η_o vanishes as the velocity (and k_o) of the incident wave goes to zero, or as the potential U_o goes to zero; η_o represents the difference in phase outside the potential well compared with the wave solution in the limit of a vanishing potential. The total scattering cross section has a finite limit at zero velocity, however.

$$k_o r_o + \eta_o \simeq \frac{k_o}{k} \tan kr_o \tag{10.82}$$

$$S = \frac{4\pi}{k_o^2} \sin^2 \eta_o \simeq \frac{4\pi}{k_o^2} \left(\frac{k_o}{k} \tan kr_o - k_o r_o\right)^2$$

$$\simeq 4\pi r_o^2 \left(\frac{\tan kr_o}{kr_o} - 1\right)^2 \tag{10.83}$$

For values of $kr_o = \pi/2, 3\pi/2, 5\pi/2$, etc., the phase shift does not go to zero as k vanishes, and the cross section becomes infinite. This behavior is associated with the bound state energy levels that exist within the potential well.

Figure 10.3 shows the wave function $g(r)$, rather than $R(r)$, in order to have constant amplitude. The phase difference η_o is just k times the distance between crests. For attractive potentials the phase shift is positive; the incoming wave is drawn into the scattering center. Repulsive potentials lead to negative η_o and push the incoming wave away from the scattering center.

Typically the amplitude of the wave function $g(r)$ inside the well is small compared with the amplitude outside the well. This situation is usual when a short wavelength inside is to be joined to a long wavelength outside. In this case the scattering is called potential scattering, and the wave function $g(r)$ is qualitatively as shown at the top of figure 10.4. However, for certain values of the kinetic energy, or certain values of the radius r_o, the slope at the edge of the well is about zero and the inner and outer wavefunctions may be joined with about equal amplitude. The cross section then becomes very large and the scattering is called resonant scattering. Resonance is typically quite sharp and is not a large factor in atomic collisions, as it pertains to a very small portion of the total collision spectrum of velocities in a typical gas. Where the potential function extends a finite difference r_o greater than λ_o, the partial waves for which

$$r_o > \sqrt{\ell(\ell+1)}\,\lambda_o = \frac{\sqrt{\ell(\ell+1)}}{k_o}$$

will need to be included. Thus, the maximum value of ℓ which needs to be considered is about $r_o k_o$.

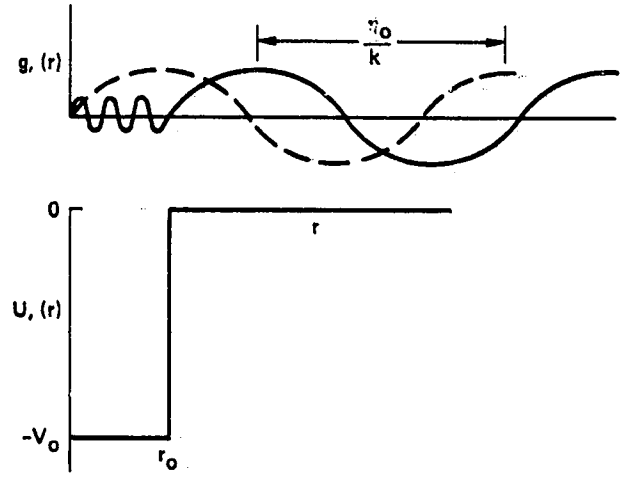

Figure 10.3- S-wave scattering from a spherical potential well. --- $g(r)$ wave for $U_o = 0$. —— $g(r)$ wave for $U_o \neq 0$.

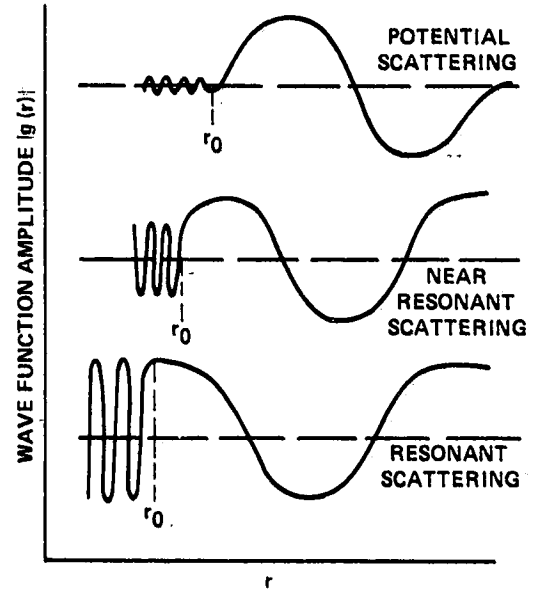

Figure 10.4- Amplitudes of $g(r)$ for potential scattering, near resonant scattering, and resonant scattering.

10.7 HARD SPHERE SCATTERING CROSS SECTION

For a hard sphere, the partial waves $R_\ell(r)$ must all vanish at the boundary $r = r_o$. From the asymptotic form of these functions given by Eq. (10.42)

$$\eta_\ell = \frac{\ell\pi}{2} - k_o r_o \qquad (10.84)$$

the total scattering cross section is approximately

$$S \simeq \frac{4\pi}{k_o^2} \sum_{\ell=0}^{k_o r_o} (2\ell + 1)\sin^2 \eta_\ell \tag{10.85}$$

where the upper limit of the summation is taken as $k_o r_o$. When a large number of partial waves is involved, the summation may be approximately evaluated as the integral

$$S = \frac{4\pi}{k_o^2} \int_o^{k_o r_o} (2\ell + 1)\left[\frac{1}{2} - \frac{1}{2}\cos(\ell\pi - 2k_o r_o)\right] d\ell$$

$$= \frac{2\pi}{k_o^2}\left|\ell^2 + \ell\right|_o^{k_o r_o} - \frac{2\pi}{k_o^2}\int_o^{k_o r_o} (2\ell + 1)\cos(\ell\pi - 2k_o r_o)\, d\ell$$

$$= 2\pi r_o^2\left[1 + \frac{1}{k_o r_o} - \frac{1}{k_o^2 r_o^2}\int_o^{k_o r_o} (2\ell + 1)(\cos \ell\pi \cos 2k_o r_o - \sin \ell\pi \sin 2k_o r_o)\, d\ell\right] \tag{10.86}$$

The integrals of $\ell \cos \ell\pi$ and $\ell \sin \ell\pi$ from 0 to kr_o all yield quantities that are the order of ℓ at the upper limit, that is $k_o r_o$. Thus, the total scattering cross section may be expressed

$$S \simeq 2\pi r_o^2\left[1 + \mathcal{O}\left(\frac{1}{k_o r_o}\right)\right] \tag{10.87}$$

which in the limit of large $k_o r_o$ becomes $2\pi r_o^2$ or just twice the classical scattering cross section, Eq. (10.25). If the differential scattering coefficient of Eq. (10.64) is plotted for a given value of k_o, one finds that this doubling of the classical cross section is due to a very large spike in scattering that occurs near $\theta = 0$, and that the differential scattering coefficient rapidly drops to a nearly constant value (for the hard sphere case) of $r_o^2/4$, the same as the classical value. The situation is sketched qualitatively in figure 10.5. The forward scattering given by quantum theory about $\theta = 0$ looks huge in terms of $f^2(\theta)$ as suggested by the broken vertical scale in figure 10.5. However, recall that this coefficient is weighted by $2\pi \sin \theta$ before integrating to get the cross section (see Eqs. (10.10) and 10.11)). The fraction of the beam which is forward scattered is just equal the fraction that is scattered throughout the remainder of the angular range. Thus, quantum scattering is just the classical result plus the forward scattering, except that the classical result for $f^2(\theta)$ gives a smoothly averaged value (constant in the case of hard spheres) which lacks the detailed structure given by the interference pattern of superimposed partial waves. Qualitatively, this same result is found for any steeply repulsive scattering potential; that is, except for the narrow peak of scattering in the forward direction, the classical result is a structureless average of the quantum result. For attractive potentials, resonances such as shown qualitatively in figure 10.4 are also possible; these provide narrow peaks in the differential scattering coefficients at selected values of k_o and θ which will be superimposed on the classical like or potential scattering background. Usually these peaks

are so narrow that for most engineering purposes, such as evaluating transport properties, they do not contribute very much to the total cross sections when averaged over a range of collision velocities.

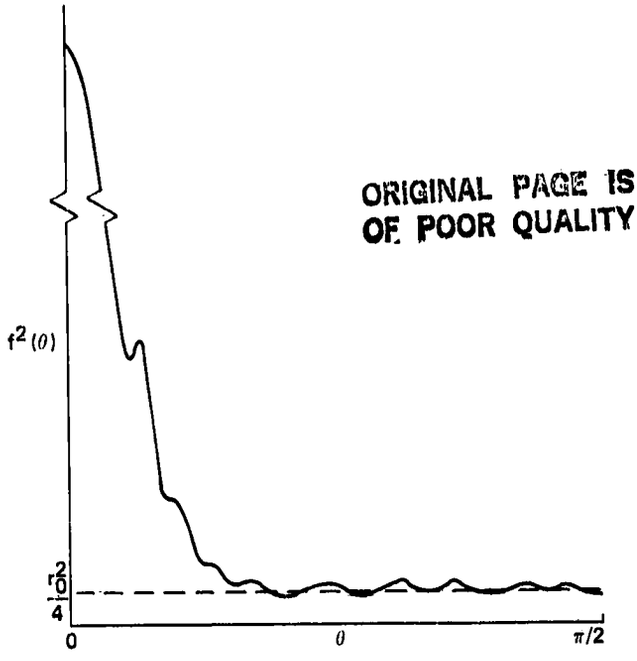

Figure 10.5- Differential scattering coefficient $f^2(\theta)$ for hard sphere scattering; —— quantum solution; --- classical solution.

10.8 BORN APPROXIMATION FOR CALCULATING PHASE SHIFTS

The Born approximation is one of the most used methods of evaluating partial wave shifts; it is valid in the limit where the collision energy is very large compared with the scattering potential. Unfortunately, this is not a realistically useful approximation for many engineering problems where low energy scattering is of importance; however, the Born approximation does give useful results for comparison with high energy molecular beam experiments. It also provides some useful insight into the scattering phenomenon. Since the scattering potential is defined to be very small, it is treated as a perturbation in this method. The Schroedinger equation may be expressed

$$\nabla^2\psi + k^2\psi = U(r)\psi \tag{10.88}$$

where $U(r)$ is a very small quantity and the wave function asymptotically approaches

$$\psi \rightarrow e^{ikz} + \frac{f(\theta)}{r} e^{ikr} \tag{10.89}$$

The scattering amplitude $f(\theta)$ will be very small in this case, however, and keeping only terms of first order on the right side of Eq. (10.88) results in

$$\nabla^2\psi + k^2\psi = U(r)e^{ikz} = F(x,y,z) \tag{10.90}$$

A solution to Eq. (10.90) is

$$\psi = G(x,y,z) - \frac{1}{4\pi}\iiint \frac{e^{ik|r - r'|}}{|r - r'|} F(x',y',z')dx'\ dy'\ dz' \qquad (10.91)$$

where the function G is any solution to the homogeneous part of Eq. (10.90)

$$\nabla^2 G + k^2 G = 0 \qquad (10.92)$$

and the second term can be shown to be a solution to the inhomogeneous equation using Green's theorem, which relates an outward flux over a surface to the production of that flux within the volume enclosed.

$$\int\left(\psi \frac{dK}{dn} - K \frac{d\psi}{dn}\right)dS = \int (\psi\nabla^2 K - K\nabla^2\psi)d\tau \qquad (10.93)$$

For the present problem the function K is

$$K = \frac{e^{ik|r - r'|}}{4\pi|r - r'|} \qquad (10.94)$$

By differentiating Eq. (10.94) one finds

$$\nabla^2 K = -k^2 K \qquad (10.95)$$

while from Eq. (10.90)

$$\nabla^2\psi = -k^2\psi + F \qquad (10.96)$$

Thus, the right-hand side of Eq. (10.93) is just

$$-\int(\psi k^2 K - Kk^2\psi \pm KF)d\tau = -\int KF\ d\tau \qquad (10.97)$$

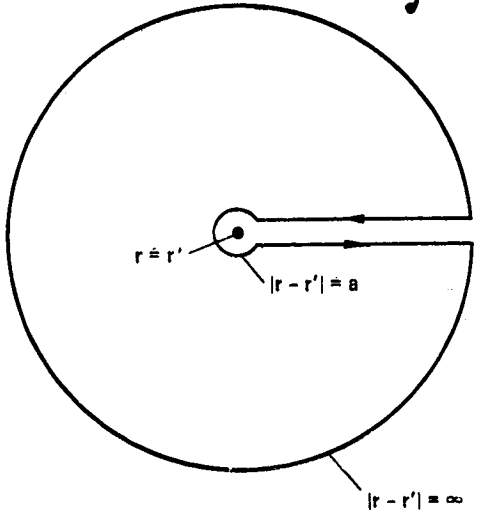

Figure 10.6- Contour integral for finding solution of the Schroedinger equation in the Born approximation using Green's theorem.

The integral on the left side of Eq. (10.93) can be performed over a surface about the singularity in K, that is, about the point $r = r'$. The surface integration path in the r-domain is shown in figure 10.6. The contribution over the outer surface vanishes as r becomes very large, approaching infinity, because both K and ψ vanish there; the contribution along the surface of variable r and back again cancel one another and contribute nothing to the total; only the contribution over the inner surface $r = a$ remains. As a goes to zero, the integral

$$\int_{r=a} K \frac{d\psi}{dn} dS \xrightarrow[a\to 0]{} 0 \qquad (10.98)$$

vanishes because $d\psi/dn$ is a finite constant within this small region, K varies as a^{-1}, but dS varies as a^2. However the integral

$$\int_{r=a} \frac{dK}{dn}\,\psi\,dS \to -\psi \int_{r=a} \frac{1}{4\pi|r - r'|^2}\,|r - r'|^2 d\Omega = -\psi \tag{10.99}$$

approaches a finite limit equal to $-\psi$. Thus

$$\psi = -\iiint KF\,d\tau \tag{10.100}$$

which is just the solution assumed in Eq. (10.91).

Now returning to the problem of evaluating $f(\theta)$, we note that r is the distance from the origin of the spherical scattering potential to the point where the solution for the scattered beam intensity is desired, with component z, while r' is the radius vector variable of integration with the component z' along the axis (see fig. 10.7). The solution for the wave function ψ is

$$\psi = e^{ikz} - \frac{1}{4\pi}\int \frac{e^{-ik(|\vec{r} - \vec{r}'| + z')}}{|r - r'|}\,U(r')d\tau' \tag{10.101}$$

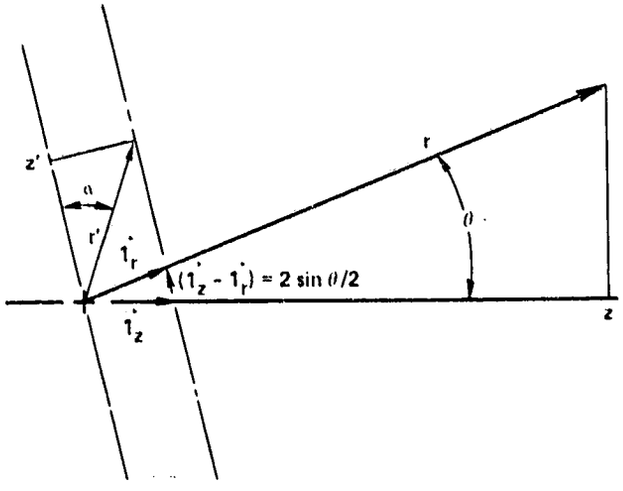

Figure 10.7- Coordinate transformation for the integration of Eq. (10.101).

For very large values of r compared with the effective range of the scattering potential

$$|\vec{r} - \vec{r}'| \simeq r - \vec{1}_r \cdot \vec{r}' + \mathcal{O}\left(\frac{1}{r^2}\right) \tag{10.102}$$

where $\vec{1}_r$ is a unit vector along the radius r. Thus

$$|\vec{r} - \vec{r}'| + z' \simeq r + (\vec{1}_z - \vec{1}_r) \cdot \vec{r}' + \ldots \tag{10.103}$$

where $\vec{1}_z$ is a unit vector along the z axis. The difference between these two unit vectors has a magnitude $2 \sin \theta/2$, and polar coordinates are chosen for the integration

$$d\tau' = r'^2 \, dr' \sin \alpha \, d\alpha \, d\phi$$

such that the axis of symmetry is in the direction of the difference vector $(\vec{1}_z - \vec{1}_r)$; or in other words the z' axis is parallel to $(\vec{1}_z - \vec{1}_r)$, figure 10.7.

$$(\vec{1}_z - \vec{1}_r) \cdot \vec{r}' = 2 \sin \frac{\theta}{2} r' \cos \alpha \qquad (10.104)$$

Using these definitions in Eq. (10.101), and keeping only terms of first order

$$\psi = e^{ikz} - \frac{e^{ikr}}{4\pi r} \int e^{2k \sin(\theta/2) r \cos \alpha} U(r) r^2 \, dr \sin \alpha \, d\alpha \, d\phi \qquad (10.105)$$

Comparing Eq. (10.105) with Eq. (10.89), we see that the scattering amplitude may be expressed,

$$f(\theta) = - \frac{1}{4\pi} \int e^{2k \sin(\theta/2) r \cos \alpha} U(r) r^2 \, dr \sin \alpha \, d\alpha \, d\phi \qquad (10.106)$$

The integration over ϕ contributes a factor of 2π, while the integral over α yields

$$\int_0^{\pi} e^{2k \sin(\theta/2) r \cos \alpha} \sin \alpha \, d\alpha = \frac{2 \sin[2kr \sin(\theta/2)]}{2kr \sin(\theta/2)} \qquad (10.107)$$

And a final expression for the Born approximation to $f(\theta)$ is

$$f(\theta) = - \int_0^{\infty} \frac{\sin[2kr \sin(\theta/2)]}{2kr \sin(\theta/2)} U(r) r^2 \, dr \qquad (10.108)$$

Recall that the energy $U(r)$ is expressed in units of $e^2/2a_o$ or $\hbar^2/2ma_o^2$, and the radius r in units of a_o in this derivation.

The Born approximation for coulomb scattering is obtained when

$$U(r) = \frac{2Z}{r} \qquad (10.109)$$

However when this potential is simply substituted in Eq. (10.108), a meaningless definite integral is obtained that does not converge to a constant.

$$f(\theta) = - \frac{Z}{k \sin(\theta/2)} \int_0^{\infty} \sin[2kr \sin(\theta/2)] dr \qquad (10.110)$$

Consequently, the potential is expressed as a screened potential

$$U(r) = \frac{2Z\, e^{-r/D}}{r} \tag{10.109a}$$

where the parameter D is the Debye shielding length, which physically represents the shielding of charge that always occurs in any plasma of finite density. For this shielded potential, the definite integral converges to a constant result even in the limit as D approaches infinity

$$\int_0^\infty \sin[2kr\,\sin(\theta/2)]e^{-r/D}\,dr = \frac{2k\,\sin(\theta/2)}{[2k\,\sin(\theta/2)]^2 + 1/D^2}$$

$$\xrightarrow[D\to\infty]{} \left(2k\,\sin\frac{\theta}{2}\right)^{-1} \tag{10.110a}$$

Thus, the scattering amplitude in the Born approximation is

$$f(\theta) = -\frac{Z}{2k^2\,\sin^2(\theta/2)} \tag{10.111}$$

and the polar scattering coefficient $F(\theta)$ is in units of a_o^2

$$F(\theta) = 2\pi\,\sin\theta f^2(\theta) = \frac{\pi Z^2\,\sin\theta}{2k^4\,\sin^4(\theta/2)} \tag{10.112}$$

The total cross section is of course

$$S = \int_0^\pi F(\theta)d\theta \tag{10.113}$$

A plot of $[\sin\theta/\sin^4(\theta/2)]$ is shown in figure 10.8. One can see the tremendous forward scattering spike caused by the long range small angle deflections. In any real situation, the Debye length D would have a finite value, of course, which would greatly reduce this forward spike.

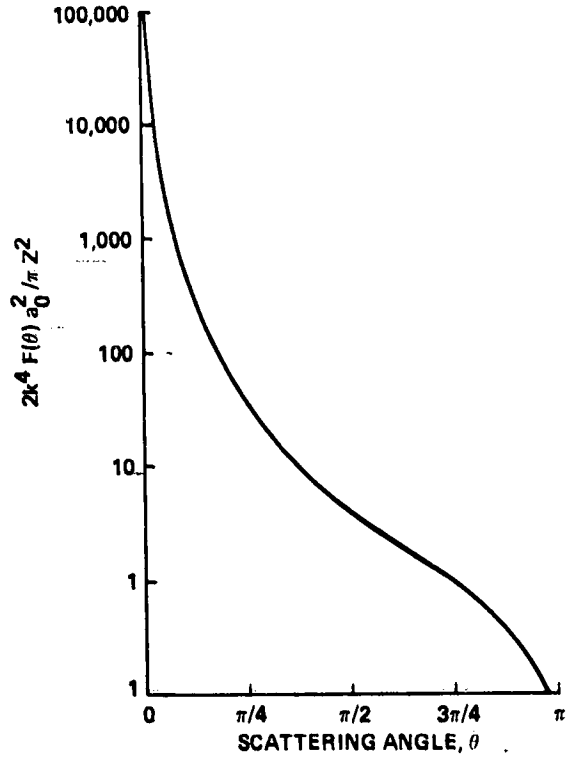

Figure 10.8- Born approximation to the polar scattering coefficient, $F(\theta)$, for the coulomb scattering potential, $2Z/r$.

10.9 PHASE SHIFTS IN A SLOWLY VARYING FIELD

Many practical problems are not adequately treated by the Born approximation, which is a small perturbation method. In chemical reactions the most important collisions occur near threshold where the perturbation potential may be very large compared with the collision kinetic energy; in this case other approximations must be developed. The most promising approach, from an engineer's point of view, seems to be a semiclassical approach such as outlined by Ford and Wheeler (refs. 14 and 15) and applied by Stallcop (ref. 7) for the calculation of elastic scattering cross sections for a class of spherical potential scattering centers with exponential repulsion and inverse 6th and 4th power attractions, in terms of the distance between centers. Possibly this method may some day be developed further to include nonelastic scattering or chemical reaction. Again, the work will become worthwhile when reliable potential functions become available; thus the accurate evaluation of multiatom potentials discussed in chapter 9 is really central to a large class of chemical reaction problems.

The semiclassical approach used by Ford and Wheeler is built upon an approximation developed by Jeffries (ref. 16) for the case where the potential $U(r)$ does not vary appreciably in a distance comparable with the wavelength. The WKB (Wenzel-Kramers-Brillouin) approximation is then used to obtain the phase shift (see, e.g., Goldberger and Watson (ref. 2)) by the so-called JWKB method

$$\eta \sim \eta_{JWKB} = \int_{r_c}^{\infty} [k(r) - k_o]dr - kr_c + \left(\ell + \frac{1}{2}\right)\frac{\pi}{2} \tag{10.114}$$

where k_o is the wave vector of the incident wave, r_c is the classical turning point or distance of closest approach, and $k(r)$ is the local wave number

$$k(r) = k_o \sqrt{1 - \frac{U(r)}{E} - \left(\frac{\ell + 1/2}{k_o r}\right)^2} \tag{10.115}$$

The approximation $\ell(\ell + 1) \simeq (\ell + 1/2)^2$ has been used in Eq. (10.115). The turning point r_c is the largest value of r which satisfies the equation

$$1 = \frac{U(r_c)}{E} + \left(\frac{\ell + 1/2}{k_o r_c}\right)^2 \tag{10.116}$$

that is, where the largest root in $k(r) = 0$ occurs. The phase shifts are related to the classical deflection angle of Eq. (10.19) by

$$2\frac{d\eta}{d\ell} = 0 \tag{10.117}$$

when the classical angular momentum for the miss distance b is equated to the quantum mechanical angular momentum for the ℓ partial wave

$$b = \left(\ell + \tfrac{1}{2}\right)k_o \tag{10.118}$$

For large values of ℓ where the scattering potential is small compared with the collision energy, $U(r)/E << 1$, a series expansion derived by Smith, Marchi, and Dedrick (ref. 17) is useful. Using an expansion of this type, Mason and Vanderslice (ref. 18) express the JWKB phase shift.

$$\eta = \frac{k_o}{2} \int_{b^2}^{\infty} F(z)(z - b^2)^{1/2} dz \qquad (10.119)$$

where

$$F(z) = \sum_{n=0}^{\infty} \frac{1}{\Gamma(n+2)} \frac{d^{n+1}}{dz^{n+1}} \left\{ z^n \left[\frac{U(z^{1/2})}{E} \right]^{n+1} \right\} \qquad (10.120)$$

For the special case where the potential falls off as the mth inverse power of r

$$U(r) = D \left(\frac{r_e}{r} \right)^m , \quad m \geq 2 \qquad (10.121)$$

the integration of Eq. (10.119) can be carried out analytically to give

$$\eta = \frac{\ell}{r} \sum_{n=0}^{\infty} \frac{\Gamma\left(\frac{n+1}{2} m - \frac{1}{2}\right)\Gamma\left(\frac{1}{2}\right)}{\Gamma(n+2)\Gamma\left(\frac{n+1}{2} m - n\right)} \left[-\frac{D}{E} \left(\frac{k_o r_e}{\ell} \right)^m \right]^{n+1} \qquad (10.122)$$

The series of Eq. (10.122) converges absolutely when

$$\frac{\left(\frac{m}{2}\right)^{m/2}}{\left(\frac{m}{2} - 1\right)^{(m/2)-1}} \left(\frac{k r_e}{\ell} \right)^m \frac{D}{E} < 1 \qquad (10.123)$$

For other potentials, the integrals generally need to be worked out numerically. For potentials with a maximum (such as fig. 9.1) the JWKB approximation for the phase shift becomes discontinuous when the collision energy E equals the barrier maximum, and it has doubtful accuracy for energies in this region. Stallcop works out an approximation to the phase shift which can be applied uniformly to energies in regions of both the potential maximum and the potential minimum. Using this approximation, Stallcop calculates the scattering of N^+ by N for four different interaction potentials shown on figure 10.9(a) which lead to ground state N and N^+; the resulting elastic scattering cross sections are shown in figure 10.9(b).

Many volumes would be required to describe in detail the multitude of approximations worked out for semiclassical elastic scattering, but the above examples will at least serve to indicate the general theoretical approach and the kind of modifications required to get approximate answers. In this era of modern numerical computers, the analytic approximations no longer hold as much importance; one can after all, numerically integrate Eq. (10.38) to find the asymptotic solution at large r to determine the phase shifts for a given interaction potential U(r). The really important

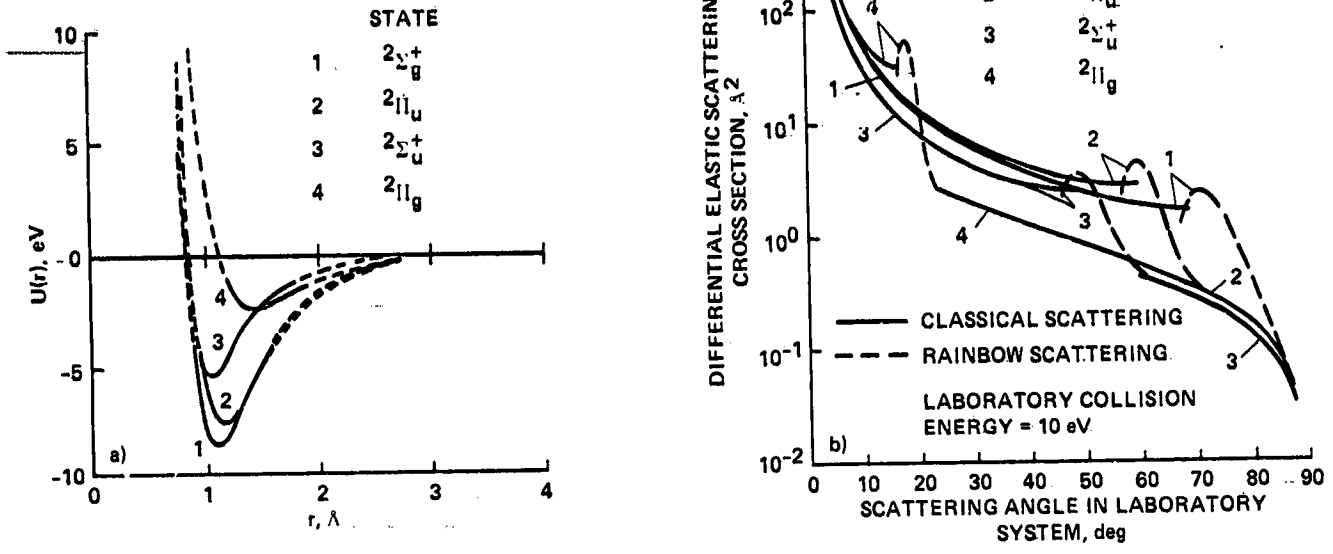

(a) Potential energy curves for N_2^+. (b) Differential cross section for the elastic scattering of N^+ by N in the laboratory system.

Figure 10.9- Example of elastic scattering cross sections obtained with the semiclassical JWKB approximation.

development, from the viewpoint of this book, would be to include inelastic effects to account for chemical-like reactive scattering.

10.10 SCATTERING OF LIKE PARTICLES

Up to this point we have been considering the scattering of unlike particles. If both particles are identical, it becomes impossible to distinguish whether the incident particle or the target particle is in the scattered wave. Consequently, the wave function ψ must be either symmetric or asymmetric with respect to exchange of the incident and target particles, depending upon whether the total spin is even or odd.

This interchange of particles is equivalent to a reversal of the radius vector; in the center of mass system this means that the angle θ becomes $\pi - \theta$ and z becomes $-z$. The spatial part of the wave function is thus

$$\psi = e^{ikz} \pm e^{-ikz} + \frac{e^{ikr}}{r}\left[f(\theta) \pm f(\pi - \theta)\right] \qquad (10.124)$$

where the (+) sign gives the symmetric function required when the total spin function is asymmetric, and the (-) sign gives the asymmetric function required by symmetric spin functions.

If the total spin function of the particles is asymmetric the intensity of the scattered wave is

$$I_s = |f(\theta) + f(\pi - \theta)|^2 \tag{10.125}$$

while if the total spin function is symmetric

$$I_a = |f(\theta) - f(\pi - \theta)|^2 \tag{10.126}$$

In classical theory the total intensity of the scattered wave is just

$$I_{classical} = f^2(\theta) + f^2(\pi - \theta) \tag{10.127a}$$

but in quantum theory this becomes the complex quantity

$$I_{quantum} = f(\theta)f^*(\theta) + f(\pi - \theta)f^*(\pi - \theta) \pm [f(\pi - \theta)f^*(\theta) + f(\theta)f^*(\pi - \theta)] \tag{10.127b}$$

In general there will exist a distribution of states and the total number of states is $(2S + 1)^2$, where S is the total spin of each collision partner. If S is half integral there will be $S(2S + 1)$ even total spin states and $(S + 1)(2S + 1)$ odd total spin states. These particles are Fermi-Dirac particles, and the total observed intensity of scattering for Fermi-Dirac particles is a weighted sum of symmetric and antisymmetric scattered waves.

$$I_{FD} = \frac{S + 1}{2S + 1} I_s + \frac{S}{2S + 1} I_a \tag{10.128}$$

On the other hand if the spin of each particle is integral, the particles are Bose-Einstein particles and the weighting factors are reversed; there are then $S(2S + 1)$ odd total spin functions and $(S + 1)(2S + 1)$ even total spin functions. The observed intensity of scattering of like bosons is

$$I_{BE} = \frac{S}{2S + 1} I_s + \frac{S + 1}{2S + 1} I_a \tag{10.129}$$

The differential cross section for scattering of distinguishable particles was

$$I(\theta) = \frac{1}{4k^2}\left|\sum_{\ell}(2\ell + 1)(e^{2i\eta_\ell} - 1)P_\ell(\cos\theta)\right|^2 \tag{10.130}$$

but for indistinguishable particles the cross section must be multiplied by 2, since the scattered waves representing the two collision parameters cannot be distinguished. However, only even or odd angular momentum states are involved in the sum, depending upon whether even or odd symmetry is required.

$$I_s(\theta) = \frac{1}{2k^2}\left|\sum_{\ell_{even}}(2\ell + 1)(e^{2i\eta_\ell} - 1)P_\ell(\cos\theta)\right|^2 \tag{10.131}$$

$$I_a(\theta) = \frac{1}{2k^2}\left|\sum_{\ell_{odd}}(2\ell + 1)(e^{2i\eta_\ell} - 1)P_\ell(\cos\theta)\right|^2 \tag{10.132}$$

10.11 CONCLUDING REMARKS

The foregoing discussion on quantum scattering theory has been included primarily to indicate to the engineering user the nature of this area of rate process theory development; the approach used in scattering theory will become really interesting as far as chemical-like rate processes in gas phase are concerned when it is able to incorporate inelastic scattering potentials and transitions between different potential surfaces. The primary interest in scattering theory now exists because it can explain some of the structure in scattered beam intensity as a function of scattering angle that is observed in relatively high energy molecular beam experiments. In addition to its extension to inelastic scattering, the theory also needs to include nonspherical potential scattering to really find full application to many practical problems.

REFERENCES

1. Mott, N. F.; and Massey, H. S. W.: Theory of Atomic Collisions. First ed. Clarendon Press, Oxford, 1933; Third ed., Oxford U. Press, London, 1965.

2. Goldberger, M. L.; and Watson, K. M.: Collision Theory. John Wiley and Sons, N.Y., 1964.

3. Newton, R. G.: Scattering Theory of Waves and Particles. McGraw Hill, N.Y., 1966.

4. Rodberg, L. S.; and Thaler, R. M.: Introduction to the Quantum Theory of Scattering. Academic Press, New York, 1967.

5. Taylor, J. R.: Scattering Theory: The Quantum Theory of Nonrelativistic Collisions. John Wiley and Sons, N.Y., 1972.

6. Smith, K.: The Calculation of Atomic Collision Processes. Wiley-Interscience, New York, 1971.

7. Stallcop, J. R.: Semiclassical Elastic Scattering Cross Sections for a Central Field Potential Function. NASA SP-3052, 1969.

8. Kuppermann, A.; Shatz, G. C.; and Baer, M.: Quantum Mechanical Reactive Scattering for Planar Atom Plus Diatom Systems I. Theory. J. Chem. Phys., vol. 65, Dec. 1, 1976, pp. 4596-4623.

9. Schatz, G. C.; and Kuppermann, A.: Quantum Mechanical Reactive Scattering for Planar Atom Plus Diatom Systems. II. Accurate Cross Sections for $H + H_2^*$. J. Chem. Phys., vol. 65, Dec. 1, 1976, pp. 4624-4641.

10. Schatz, G. C.; and Kuppermann, A.: Quantum Mechanical Reactive Scattering for Three-Dimensional Atom Plus Diatom Systems. I. Theory. J. Chem. Phys., vol. 65, Dec. 1, 1976, pp. 4642-4667.

11. Hansen, C. F.: Molecular Physics of Equilibrium Gases. NASA SP-3096, 1976.

12. Hasted, J. B.: Physics of Atomic Collisions. Butterworths, London, 1964.

13. McDaniel, E. W.: Collision Phenomena in Ionized Gases. John Wiley and Sons, New York, 1964.

14. Ford, K. W.; and Wheeler, J. A.: Semiclassical Description of Scattering. Ann. Phys., vol. 7, July 1959, pp. 259-286.

15. Ford, K. W.; and Wheeler, J. A.: Application of Semiclassical Scattering Analysis. Ann. Phys., vol. 7, July 1959, pp. 287-322.

16. Jeffreys, A.; and Jeffreys, B. S.: Methods of Mathematical Physics. First ed. Cambridge U. Press, London, 1946.

17. Smith, F. T.; Marchi, R. P.; and Dedrick, K. G.: Impact Expansions of Classical and Semiclassical Scattering. Phys. Rev., vol. 150, Oct. 7, 1966, pp. 79-92.

18. Mason, E. A.; and Vanderslice, J. T.: Elastic Scattering of Slow Ions in Gases. J. Chem. Phys., vol. 31, Sept. 1959, pp. 594-600.

★U.S. GOVERNMENT PRINTING OFFICE:1983-639-008/ 10 REGION NO. 4